Department of Energy

Washington, DC 20585

QA: N/A
DOCKET NUMBER 63-001

October 16, 2009

ATTN: Document Control Desk
John H. (Jack) Sulima, Project Manager
Project Management Branch Section B
Division of High-Level Waste Repository Safety
Office of Nuclear Material Safety and Safeguards
U.S. Nuclear Regulatory Commission
EBB-2B2
11545 Rockville Pike
Rockville, MD 20852-2738

YUCCA MOUNTAIN - REQUEST FOR ADDITIONAL INFORMATION - SAFETY EVALUATION REPORT, VOLUME 3 - POSTCLOSURE CHAPTER 2.2.1.3.4 - RADIONUCLIDE RELEASE RATES AND SOLUBILITY LIMITS, 4TH SET - (DEPARTMENT OF ENERGY'S SAFETY ANALYSIS REPORT SECTION 2.3.7)

Reference: Ltr, Sulima to Williams, dtd 9/28/2009, "Yucca Mountain – Request for Additional Information – Safety Evaluation Report, Volume 3 – Postclosure Chapter 2.2.1.3.4 – Radionuclide Release Rates and Solubility Limits, 4th Set – (Department of Energy's Safety Analysis Report Section 2.3.7)"

The purpose of this letter is to transmit the U.S. Department of Energy's (DOE) responses to the Requests for Additional Information (RAI) identified in the above-referenced letter. Each RAI response is provided as a separate enclosure.

Most of the DOE references cited in the RAI responses have previously been provided with the License Application (LA), the LA update, or as part of previous RAI responses. The references provided with previous RAI responses are identified within the enclosed response reference sections. The DOE references cited in the RAI responses, which have not been previously provided to the Nuclear Regulatory Commission, are included with this submittal.

There are no commitments in the enclosed RAI responses. If you have any questions regarding this letter, please contact me at (202) 586-9620, or by email to jeff.williams@rw.doe.gov.

Steven E Sombury (for)

Jeffrey R. Williams, Supervisor
Licensing Interactions Branch
Regulatory Affairs Division
Office of Technical Management

OTM: CJM-0033

NMSS25

Printed with soy ink on recycled paper

Enclosures (6):

1. Response to RAI Volume 3, Chapter 2.2.1.3.4, Set 4, Number 1
2. Response to RAI Volume 3, Chapter 2.2.1.3.4, Set 4, Number 2
3. Response to RAI Volume 3, Chapter 2.2.1.3.4, Set 4, Number 3
4. Mertz, C.J.; Finch, R.J.; Fortner, J.A.; Jerden, J.L., Jr.; Yifen, T.; Cunnane, J.C.; and Finn, P.A. 2003. *Characterization of Colloids Generated from Commercial Spent Nuclear Fuel Corrosion.* Activity Number: PAWTP30A. Argonne, Illinois: Argonne National Laboratory. ACC: MOL.20030422.0337.
5. SNL (Sandia National Laboratories) 2007. *EBS Radionuclide Transport Abstraction.* ANL-WIS-PA-000001 REV 03 ERD 02. Las Vegas, Nevada: Sandia National Laboratories. ACC: DOC.20090623.0001.
6. Wilson, C.N. 1990. *Results from NNWSI Series 3 Spent Fuel Dissolution Tests.* PNL-7170. Richland, Washington: Pacific Northwest Laboratory. ACC: NNA.19900329.0142.

cc w/encl:
J. C. Chen, NRC, Rockville, MD
J. R. Cuadrado, NRC, Rockville, MD
J. R. Davis, NRC, Rockville, MD
R. K. Johnson, NRC, Rockville, MD
A. S. Mohseni, NRC, Rockville, MD
N. K. Stablein, NRC, Rockville, MD
D. B. Spitzberg, NRC, Arlington, TX
J. D. Parrott, NRC, Las Vegas, NV
L. M. Willoughby, NRC, Las Vegas, NV
Jack Sulima, NRC, Rockville, MD
Christian Jacobs, NRC, Rockville, MD
Lola Gomez, NRC, Rockville, MD
W. C. Patrick, CNWRA, San Antonio, TX
Budhi Sagar, CNWRA, San Antonio, TX
Bob Brient, CNWRA, San Antonio, TX
Rod McCullum, NEI, Washington, DC
B. J. Garrick, NWTRB, Arlington, VA
Bruce Breslow, State of Nevada, Carson City, NV
Alan Kalt, Churchill County, Fallon, NV
Irene Navis, Clark County, Las Vegas, NV
Ed Mueller, Esmeralda County, Goldfield, NV
Ron Damele, Eureka County, Eureka, NV
Alisa Lembke, Inyo County, Independence, CA
Chuck Chapin, Lander County, Battle Mountain, NV
Connie Simkins, Lincoln County, Pioche, NV
Linda Mathias, Mineral County, Hawthorne, NV
Darrell Lacy, Nye County, Pahrump, NV
Jeff VanNeil, Nye County, Pahrump, NV
Joe Kennedy, Timbisha Shoshone Tribe, Death Valley, CA
Mike Simon, White Pine County, Ely, NV
K. W. Bell, California Energy Commission, Sacramento, CA
Barbara Byron, California Energy Commission, Sacramento, CA
Susan Durbin, California Attorney General's Office, Sacramento, CA
Charles Fitzpatrick, Egan, Fitzpatrick, Malsch, PLLC

RAI Volume 3, Chapter 2.2.1.3.4, Fourth Set, Number 1:

Explain why the igneous scenario TSPA model does not consider potential generation of greater quantities of waste form colloids in the igneous intrusive case, relative to the nominal case.

Basis: The response to RAI 3.2.2.1.3.4-1-002 and RAI 3.2.2.1.3.4-1-002 Supplemental Question explains that the igneous intrusive modeling case generally has generation of greater quantities of colloids than the nominal case because the igneous intrusion modeling case results in a higher rate of advection. The higher water volume from the higher rate of advection gives greater quantities of colloids at fixed concentrations in the aqueous phase.

Colloids could form in greater quantities for other reasons; for example:

1. Large settled particles of oxidized commercial and DOE spent nuclear fuels with a large total surface area could form, as summarized in the RAI responses. These oxidized particles could continue to dissolve (NRC 2008, page 8) at high rates in later seepage water due to their high total surface area. This further dissolution of oxidized spent fuel could result in the faster formation of stable phases such as schoepite in precipitates or colloids.

2. HLW glass could become altered by hydration in the early humid environments. The hydrated alteration layer will remain on the glass surface until contacted and transported by later seepage water [after BSC, 2004, p. 6-30]. This fast dissolution and transport of the alteration layer may result in the faster formation of stable crystalline phases such as smectite in precipitates or colloids.

3. There are considerable uncertainties in the interaction of waste form and dike, including chemical reactions of waste form with metals and basalt magma (SNL, 2007, 6.4.8.3.3). It is not clear how these interactions, and their likelihood, might affect colloid generation and colloid mass concentrations. The interacted phases may further dissolve and become more stable phases in precipitates or colloids.

Lastly, it is unclear how the colloid release model was stochastically treated in terms of the igneous event probability in the igneous scenario TSPA model.

1. RESPONSE

The igneous intrusion modeling case is not expected to create greater concentrations of colloidal actinides than the nominal modeling case. This explanation is based on process-level considerations, as previously discussed in the response to RAI 3.2.2.1.3.4-1-002, Supplemental Question, as well as on a discussion that considers the risk significance of the three possible mechanisms proposed in the current RAI. The risk-informed explanation compares the nominal/seismic case, which is called the seismic ground motion modeling case, with the igneous intrusion case. The seismic ground motion modeling case is the most risk-significant modeling case for the first 10,000 years, and is equal in risk significance to the igneous intrusion case at the peak of the post-10,000-year dose (SNL 2008, Figure 8.1-3[a]). Note that, as explained in Section 6.1.2 of the *Total System Performance Assessment Model /Analysis for the License Application* (TSPA-LA) report (SNL 2008), the nominal modeling case dose is not added into the total dose calculation because its probability is negligible; rather, nominal processes are part of the seismic ground motion modeling case. (Note: this response concentrates on plutonium because it is the most risk-significant colloidal actinide.)

1.1 SPENT FUEL COLLOIDS

The first scenario listed in the RAI postulates that colloids could be produced in larger quantities from fast dissolution of large settled particles of oxidized commercial spent nuclear fuel (SNF) and DOE-owned SNF. However, it is not expected that colloids will be produced in larger quantities for the following reasons:

(1) The state of the fuel, when water first flows through the waste package, will be similar for both the seismic ground motion modeling case (i.e., the nominal/seismic case) and the igneous intrusion modeling case (Section 1.1.1).

(2) Faster dissolution does not necessarily result in greater plutonium colloid concentrations in the bulk solution, because the majority of the plutonium remains in a residue layer at the reaction front (Section 1.1.2).

(3) The colloid model, and the associated aqueous colloid concentration range, are conservative (Section 1.1.3).

1.1.1 State of the Fuel at Time of First Water Flow

In the seismic ground motion modeling case, the packages are breached by stress corrosion cracks (that do not allow advective water flow) many thousands of years before they are breached by general corrosion patch openings (which do allow advection). The fuels are exposed to air and water vapor long enough to be converted to hydrated uranium (VI) minerals (dehydrated schoepite) before water flow is initiated. These minerals may exist as colloidal-sized particles initially, but will be converted into mats of crystals that are tens to hundreds of micrometers in length within a few years, as seen in drip tests by Wronkiewicz et al. (1992, Section 3.3), and as seen by Taylor et al. (1995) in air-steam mixtures that were moisture-saturated.

During an igneous event, the waste package is assumed to be fully breached, and the fuel will be exposed to temperatures of up to 1,150°C in the presence of magmatic gasses (SNL 2007a, p. 8-3). The temperature of the fuel will remain above 350°C for about eight months, during which time the fuel will oxidize (see Figure 1 of Ahn 1996a), forming a fine-grained powder. As the fuel cools and the relative humidity increases, the powder is expected to hydrate to a mat of crystalline uranium (VI) minerals much like that formed during vapor hydration of fuel pellets.

Once a mat of uranium (VI) mineral crystals forms over the degraded fuel, the mat and degraded fuel will provide abundant nucleation sites for the precipitation of actinides. Precipitation under the mat reduces the migration of actinides into the bulk solution, which limits the condensation of actinides into true colloids or onto pseudo-colloids in the bulk solution. In addition, the mat is expected to form a physical barrier, holding in particles of degrading fuel, thus limiting the importance of the intergranular dissolution dispersion process. The importance of the mat in holding in fuel particles was noted by Wronkiewicz et al. (1996) in the drip tests on UO_2 pellets, where three periods of reaction where observed. Period I was an incubation period of up to one year, characterized by low uranium release. Period II occurred between one and two years and had the highest and most variable uranium release rate, which was attributed to grain boundary corrosion and spallation of UO_{2+x} particles. Period III started after a mat of uranium (VI) crystals formed, and extended until the end of the 10 years reported. The uranium release rate decreased from a high of 15 mg/m^2 day to a more uniform 0.1 and 0.3 mg/m^2 day. The mat was not static, but underwent a paragenetic sequence, with uranyl-oxide hydrates converting to uranyl silicates, and finally to alkali and alkaline earth uranyl silicates as incoming groundwater added the necessary cations and silicate to the system.

In both the seismic ground motion and igneous intrusion modeling cases, when water first flows over the fuel, a mat of hydrated uranium (VI) minerals is expected to reduce but not eliminate the colloid releases from the degraded fuel. Ahn (1996b) lists several mechanisms for colloid formation: nucleation of intrinsic colloids, dispersion of reprecipitates, dispersion of fuel after intergranular dissolution, and pseudo-colloid formation. The mat is expected to limit the transport of supersaturated actinide solutions and particles of fuel or oxidized fuel into the bulk solution, thus reducing the nucleation of actinide intrinsic colloids, dispersion of fuel grains, and precipitation of actinides onto pseudo-colloids. The remaining processes of dispersion of reprecipitates from the mat and sorption onto pseudo-colloids in the bulk solution will continue to occur after the mat has formed and are the likely processes responsible for the actinide releases observed in the spent fuel drip tests (Mertz et al. 2003).

1.1.2 Plutonium Stays in Residue Layer

Faster dissolution does not necessarily result in greater plutonium colloid concentrations in the bulk solution. In vapor and high-drip tests on several commercial SNF samples, a plutonium-rich crypto-crystalline residue layer was found between the uranium (VI) alteration phases and the fuel (CRWMS M&O 2001, p. 34). Coupled with the plutonium fractional release rate that is less than 10^{-5} times the technetium fractional release rate, this suggests that the fluids at the UO_2 reaction front quickly become saturated with respect to plutonium-rich phases, which precipitate onto the UO_2 surface. This is expected, because plutonium is redox sensitive and would tend to precipitate in the reducing environment at the reacting fuel surface. Faster dissolution rates due

to higher oxidation state (for example U_3O_8) or larger surface area would not likely change this precipitation at the reaction front, which is reduced relative to the aerated bulk solution.

1.1.3 Colloid Model Is Conservative

The colloid model and the associated aqueous colloid concentration range are conservative. Both static immersion (Wilson 1990; SNL 2007b, Section 6.3.2.4) and drip (Mertz et al. 2003, Figure 4) tests show colloidal plutonium concentrations in the range of 10^{-12} to 10^{-6} molar (the drip data is for unfiltered plutonium, which is assumed to bound the colloidal plutonium concentration). These two types of tests are thought to be dominated by different colloid generation processes, condensation and dispersion respectively (as described in Ahn 1996b). For the static immersion tests, the colloidal plutonium was above 10^{-7}molar only in the early (33 days or less) test samples (SNL 2007b, Table 6-6a) when a mat of secondary phases had not yet formed. For the drip tests, plutonium concentrations above 10^{-8} molar plutonium were only found in leachates where fuel fragments were found (Mertz et al. 2003, Figures 5 and 6). Even after the fuel holders were changed, disrupting the alteration mat, the plutonium concentrations remained below 10^{-8} molar for the ATM 103 high drip rate tests and below 10^{-9} molar for the ATM 106 high drip rate tests. From this information, and the expectation that a mat of secondary phases will form over the degraded fuel, a log uniform distribution from 10^{-12} to 10^{-8} molar plutonium would be a reasonable distribution for the long-term total colloid concentration for all colloid types with attached plutonium. However, it was conservatively assumed that the plutonium concentrations from the above studies were solely from irreversible commercial SNF waste form colloids, and a more conservative range of 10^{-10} to 5×10^{-6} molar was chosen (SNL 2007b, Section 6.3.2.4).

In addition to the irreversible commercial SNF colloids, the colloid model also includes reversible pseudo-colloids in the waste form domain. The reversible waste form uranium mineral colloids (uranophane) (SNL 2007b, Table 6-10) and the reversible groundwater (smectite) colloids (SNL 2007b, Table 6-15) were modeled separately using actinide K_d distributions. The actinide K_d distributions for sorption onto the uranium mineral colloids are based on spent fuel experiments and some analogue studies (SNL 2007b, p. 6-31). The actinide K_d distributions for the smectite colloids are based on site-specific and literature data (SNL 2007b, Section 6.3.12.1). Thus, the colloid model includes all types of colloids that may occur in the waste form domain: irreversible waste form, reversible waste form, and pseudo-colloids.

1.2 HIGH-LEVEL WASTE (HLW) GLASS COLLOIDS

This section addresses the potentially faster formation of colloids and precipitates in the igneous intrusion modeling case. A similar risk-informed line of reasoning is applicable when comparing the igneous intrusion case to the seismic ground motion modeling case. In both cases, a significant alteration layer forms prior to the time of first contact by advective water flux. In the seismic ground motion modeling case, the waste package is breached and the glass is exposed to low-temperature vapor hydration long before advection is initiated, so a significant alteration layer is established prior to water flow. During an igneous event, the glass may re-melt (SNL 2007a, p. 6-229). During the slow cool-down period, crystalline phases are expected to

form instead of the glass phase, which was formed under rapid cooling conditions. Even if the heat of the intruded magma does not melt the glass, the raised temperature will lead to devitrification (BSC 2004, p. 6-48) and vapor hydration of any remaining glass surfaces. In either case, the surface of the waste will be crystalline. As water flows past these crystalline surfaces, fewer colloids will be generated than as water flows past fresh glass surfaces, as seen in glass intermittent flow tests reported by Bates et al. (1993). In these tests, the transuranic elements in the solutions flowing off of the fresh glass samples were 90% particulate, while that flowing off of the aged glass was estimated to be less than 25% particulate (Bates et al. 1993, p. 29). Therefore, it is believed that the colloid concentrations obtained from fresh glass immersion tests are bounding.

1.3 INTERACTION OF WASTE FORM AND DIKE

The TSPA has adopted a very conservative position to account for the uncertainties in the igneous intrusion modeling case, including those related to waste dissolution and colloid formation, by assuming that every waste package in the repository is completely compromised and provides no barrier to flow. In addition, in order to not underestimate the amount of water contacting each waste package, the TSPA conservatively assumes that every single waste package is contacted by the maximum amount of advecting water, an amount equal to the cross-sectional area of the drift (not the waste package) times the percolation flux. It is assumed that all waste forms are instantly degraded and their entire mass is contacted by this conservatively large flow rate of water. These significant conservatisms more than account for the uncertainties associated with the colloid concentration. Nevertheless, from a process perspective, interactions of the waste form with metals and basalt magma are likely to result in more stable phases and lower actinide content transported colloidally. For commercial SNF and DOE-owned SNF, if the waste forms react with metals or basalt, the resulting waste forms will react with air and water during the cool-down period. This would result in final waste forms at the time of water flow that are likely more stable than the original commercial SNF or DOE-owned SNF. More stable waste forms likely result in slower dissolution and slower release of actinides in colloidal form. For HLW glass, the igneous intrusion may melt the glass followed by slow cool-down, which may result in separation of the actinide oxides from the glass phase. If such separation occurs, these actinide oxides would form under conditions that would be conducive to crystalline formation and stability and thus less likely to be colloidal.

1.4 STOCHASTIC TREATMENT OF COLLOID RELEASE IN IGNEOUS INTRUSION MODELING CASE

The treatment of aleatory and epistemic uncertainties in the igneous intrusion modeling case are described in detail in Appendix J of the *Total System Performance Assessment Model/Analysis for the License Application* report (SNL 2008, Section J7). The consequences of igneous events (i.e., annual dose) are calculated by assuming an igneous event occurs, and then the expected consequence (i.e., the expected dose) is computed by integrating the annual dose with the uncertain number of igneous events during the time period under consideration (see also SNL 2008, Equation 6.1.2-16). This accounts for the igneous event probability. Because the colloid release model and the associated aqueous colloid concentrations are not temperature

dependent, and are the same for all modeling cases, there is no dependence of this model on igneous event time or probability.

1.5 SUMMARY

The potential generation of greater quantities of waste form colloids in the igneous intrusion case has been considered. However, the alteration of the waste forms that occurs before advective water flux initiates in the two most risk-significant modeling cases (the seismic ground motion and igneous intrusion modeling cases) would produce a crystalline layer that reduces the colloid generation rate. The spent fuel and glass waste form colloids models are based in part on experiments with fresh surfaces that had not formed a coherent alteration product layer. These colloid models are conservative for the most risk-significant modeling cases.

2. COMMITMENTS TO NRC

None.

3. DESCRIPTION OF PROPOSED LA CHANGE

None.

4. REFERENCES

Ahn, T.M. 1996a. *Dry Oxidation and Fracture of LWR Spent Fuels.* NUREG-1565. Washington, D.C.: U.S. Nuclear Regulatory Commission.

Ahn, T.M. 1996b. *Long-Term Kinetic Effects and Colloid Formations in Dissolution of LWR Spent Fuels.* NUREG-1564. Washington, D.C.: U.S. Nuclear Regulatory Commission.

Bates, J.K.; Bourcier, W.L.; Bradley, C.R.; Buck, E.C.; Cunnane, J.C.; Dietz, N.L.; Ebert, W.L.; Emery, J.W.; Ewing, R.C.; Feng, X.; Gerding, T.J.; Gong, M.; Hoh, J.C.; Li, H.; Mazer, J.J.; Morgan, L.E.; Newton, L.; Nielsen, J.K.; Phillips, B.L.; Tomozawa, M.; Wang, L.; and Wronkiewicz, D.J. 1993. *ANL Technical Support Program for DOE Environmental Restoration and Waste Management. Annual Report, October 1991-September 1992.* ANL-93/13. Argonne, Illinois: Argonne National Laboratory.

BSC (Bechtel SAIC Company) 2004. *Defense HLW Glass Degradation Model.* ANL-EBS-MD-000016 REV 02. Las Vegas, Nevada: Bechtel SAIC Company. ACC: DOC.20041020.0015.

CRWMS (Civilian Radioactive Waste Management System) M&O (Management and Operating Contractor) 2001. *Colloid-Associated Radionuclide Concentration Limits: ANL.* ANL-EBS-MD-000020 REV 00 ICN 01. Las Vegas, Nevada: CRWMS M&O. ACC: MOL.20010216.0003.

Mertz, C.J.; Finch, R.J.; Fortner, J.A.; Jerden, J.L., Jr.; Yifen, T.; Cunnane, J.C.; and Finn, P.A. 2003. *Characterization of Colloids Generated from Commercial Spent Nuclear Fuel Corrosion.* Activity Number: PAWTP30A. Argonne, Illinois: Argonne National Laboratory. ACC: MOL.20030422.0337.

NRC (U.S. Nuclear Regulatory Commission) 2008. *Dissolution Kinetics of Commercial Spent Nuclear Fuels in the Potential Yucca Mountain Environment.* NUREG-1914. Washington, DC: U.S. Nuclear Regulatory Commission.

SNL (Sandia National Laboratories) 2007a. *Dike/Drift Interactions.* MDL-MGR-GS-000005 REV 02. Las Vegas, Nevada: Sandia National Laboratories. ACC: DOC.20071009.0015.

SNL 2007b. *Waste Form and In-Drift Colloids-Associated Radionuclide Concentrations: Abstraction and Summary.* MDL-EBS-PA-000004 REV 03. Las Vegas, Nevada: Sandia National Laboratories. ACC: DOC.20071018.0019.[a]

SNL 2008. *Total System Performance Assessment Model /Analysis for the License Application.* MDL-WIS-PA-000005 REV 00 AD 01. Las Vegas, Nevada: Sandia National Laboratories. ACC: DOC.20080312.0001.

Taylor, P.; Wood, D.D.; and Owen, D.G. 1995. "Microstructures of Corrosion Films on UO_2 Fuel Oxidized in Air–Steam Mixtures at 225°C." *Journal of Nuclear Materials, 223,* (3), 316-320. New York, New York: Elsevier.

Wilson, C.N. 1990. *Results from NNWSI Series 3 Spent Fuel Dissolution Tests.* PNL-7170. Richland, Washington: Pacific Northwest Laboratory. ACC: NNA.19900329.0142.

Wronkiewicz, D.J.; Bates, J.K.; Gerding, T.J.; Veleckis, E.; and Tani, B.S. 1992. "Uranium Release and Secondary Phase Formation During Unsaturated Testing of UO2 at 90°C." *Journal of Nuclear Materials, 190,* 107-127. Amsterdam, The Netherlands: North-Holland Publishing Company.

Wronkiewicz, D.J.; Bates, J.K.; Wolf, S.F.; and Buck, E.C. 1996. "Ten-Year Results from Unsaturated Drip Tests with UO_2 at 90°C: Implications for the Corrosion of Spent Nuclear Fuel." *Journal of Nuclear Materials, 238,* (1), 78-95. Amsterdam, The Netherlands: North-Holland.

NOTE: [a]Provided as an enclosure to letter from Williams to Sulima dtd 02/17/2009. "Yucca Mountain – Request for Additional Information Re: License Application (Safety Analysis Report Section 2.1), Safety Evaluation Report Volume 3 – Postclosure Chapters 2.2.1.1 and 2.2.1.3.7 – Submittal of Department of Energy Reference Citations."

RAI Volume 3, Chapter 2.2.1.3.4, Fourth Set, Number 2:

Explain the basis for the range of stainless steel corrosion rates used to calculate corrosion product formation in the corrosion product domain (SNL, 2007a) and why this range does not lead to underestimated advective releases. Explain why the minimum and mean values of the lognormal distribution are reasonable during the performance assessment period.

Basis: The stainless steel corrosion rate is used in the EBS radionuclide transport abstraction to calculate the formation rate of corrosion products in the corrosion product domain. Greater accumulation of these corrosion products results in greater radionuclide sorption and pH buffering capacity; the limited pH range, in turn, affects radionuclide solubilities and colloid stability. (A different range of stainless steel corrosion rates is used in the in-package chemistry abstraction; this RAI does not address that particular range.)

For the stainless steel corrosion rate, DOE adopted a lognormal distribution ranging from 0.01 to 0.51 μm/yr for this rate (SNL, 2007a, page 6-94). The minimum value was based on the mean Alloy 22 corrosion rate and is higher than the lowest measured rates for stainless steel compiled by DOE (Aqueous Corrosion Rate AMR); this compilation reports values as low as 0.0007 μm/yr for 316L stainless steel in freshwater at 29.5°C. DOE acknowledged the possibility that they could be overestimating rates (and, therefore, corrosion product mass accumulation rates) for long time periods, during which corrosion rates could decrease, but concluded that the resulting higher modeled diffusive release rates would "tend to offset the overestimated retardation of radionuclides by sorption onto corrosion products. Thus, diffusive releases of radionuclides are not necessarily underestimated if corrosion rates are overestimated" (SNL, 2007a, page 6-94). It is not clear if this reasoning would apply also to conditions, such as in the igneous intrusion case and during general corrosion, under which advective releases far exceed diffusive releases. Staff needs to understand DOE's justification, under advective conditions, for adopting minimum and mean stainless steel corrosion rates that may overestimate the time-dependent availability of corrosion products in the corrosion product domain.

1. RESPONSE

The statement in the RAI that the data source used by DOE reports values lower than the minimum stainless steel corrosion rate specified in *EBS Radionuclide Transport Abstraction* (RTA) (SNL 2007a, p. 6-94) is explained. The mean corrosion rate is based on reasonable experimental data, as described in the cited DOE source, and the minimum rate is based on reasonable surrogate data. Included in this discussion is an analysis of the time dependence of the relevant stainless steel corrosion rate data reported in the cited DOE source and justification of the use of a constant value (sampled from a distribution) in the total system performance assessment (TSPA) calculations. Finally, the conservative nature of the waste-form mobilization

analysis and the associated availability of water at the waste form surfaces with respect to corrosion of stainless steel and formation of corrosion products is described.

1.1 MINIMUM STAINLESS STEEL CORROSION RATE

The RAI questions why the minimum corrosion rate for stainless steel of 0.01 μm/yr was adopted when the data source cited by the DOE (output DTN from BSC 2004) reports a minimum value of 0.0007 μm/yr for Stainless Steel Type 316 in fresh water at 29.5°C (BSC 2004, Table 4-3). This is explained in the RTA report on the page cited in this RAI (SNL 2007a, p. 6-94) as follows: "Longer term (up to 16 yr) data in DTN: MO0409SPAACRWP.000 [DIRS 172059] are not used because, as reported in the original reference (Southwell et al. 1976 [DIRS 100927], Tables 4, 5, and 6), no weight loss was measured, so the actual measured corrosion rates were zero."

The value in question (0.0007 μm/yr) is based on one of a series of measurements made on Stainless Steel Type 316 at 1, 2, 4, 8, and 16 years immersed in Gatun Lake (freshwater) in the Panama Canal Zone. As mentioned in footnote g of Table 4-3 and Section 4.1.3.1 of *Aqueous Corrosion Rates for Waste Package Materials* (BSC 2004), a measured weight loss of zero was actually reported in the original reference. Instead of using the actual weight loss, which was zero, the corrosion rate reported in the cited source (BSC 2004, Table 4-3) was computed using the "detection limit" (i.e., weighing precision) of the measurement equipment recorded by the original reference, 0.01 g. Thus, the corrosion rates reported in the source (BSC 2004, Table 4-3) for the Gatun Lake tests were computed simply from:

$$\text{Rate} = \frac{\text{detection limit}}{(\text{density})(\text{total sample surface area})(\text{elapsed time})}.$$

For example, the rate after 1 year is reported as (BSC 2004, Table 4-3):

$$\text{Rate}\ (@1\ \text{yr}) = \frac{(0.01\ \text{g})(10^4\ \mu\text{m/cm})}{(7.98\ \text{g/cm}^3)(1113.2\ \text{cm}^2)(1\ \text{yr})} = 0.0113\ \mu\text{m/yr}.$$

The rate at 16 years is reported as 1/16th of the one-year rate, or 0.0007 μm/yr. The variability in rates reported in the cited source (BSC 2004, Table 4-3) for the Gatun Lake tests results entirely from differences in the surface area of the test samples and the duration of the tests.

The fact that the original data source reported a weight loss of zero at all five immersion times for all Gatun Lake samples indicates that uncertainty exists in the measurements that is not adequately characterized simply by the detection limit reported in the cited source (BSC 2004). Since the original data source provides no additional information by which to characterize the uncertainty, the use of nonzero corrosion rates based on measurements of zero weight loss cannot be justified, so none of the Gatun Lake data is used to establish a range for the Stainless Steel Type 316 corrosion rate in the RTA report (SNL 2007a). All known relevant experimental data for corrosion of Stainless Steel Type 316 in fresh water based on nonzero measurements are summarized in Table 4-3 of *Aqueous Corrosion Rates for Waste Package Materials* (BSC 2004)

and listed in Table 4.1-1 of the RTA report (SNL 2007a), where the minimum corrosion rate is 0.037 μm/yr.

1.2 BASES FOR MEAN AND MINIMUM STAINLESS STEEL CORROSION RATES

The corrosion rate of stainless steel should decrease over time as a passive layer of corrosion products builds up on the surface and inhibits diffusion of oxygen and water vapor to the metal surface. To account for this, the lower bound on the range is set to 0.01 μm/yr instead of the measured minimum rate of 0.037 μm/yr. This lower bound value is the approximate mean corrosion rate of Alloy 22 at 75°C (SNL 2007b, Figure 6-26), which is known to corrode more slowly than Stainless Steel Type 316. A corrosion rate for Stainless Steel Type 316 that is lower than that of Alloy 22 is not justifiable in view of the measured corrosion rates for Stainless Steel Type 316 and Alloy 22, all of which show Stainless Steel Type 316 corroding faster than Alloy 22 at 75°C. Since the minimum value used is lower than any measured rate for stainless steel listed in Table 4.1-1 of the RTA report (SNL 2007a), it is a reasonable minimum value.

The mean corrosion rate for Stainless Steel Type 316, 0.267 μm/yr, is based on a statistical analysis of the corrosion rate data listed in Table 4.1-1 of the RTA report (SNL 2007a). This analysis is described in Appendix F of that report (SNL 2007a). Only those data listed in Table 4.1-1 of the RTA report (SNL 2007a) are used to compute the mean of the lognormal distribution. The mean value is shown in Figure 1 in relation to the measured data and the bounds developed in the RTA. Because the mean corrosion rate is based on a statistical analysis of all known relevant nonzero experimental data, as listed in Table 4.1-1 of the RTA report (SNL 2007a), it is a reasonable representation of stainless steel corrosion rate measurements.

While the corrosion rate would be expected to decrease over time in a static environment, the available data do not conclusively support such a trend. This may be due in large part to the slow rate of corrosion of Stainless Steel Type 316 in fresh water and the short duration of most tests. The time dependence of available data is shown in Figure 1, in which the data listed in Table 4.1-1 of the RTA report (SNL 2007a) are plotted. Data are grouped by temperature for each reference. Data reported for a particular temperature from any individual reference are not necessarily from a single sample measured over time, but are grouped together as a series of measurements over time based on the reference using the same material and experimental conditions to make the measurements. Figure 1 shows that only five sets of data can be considered to be time dependent, and data are available only at two times. Of the five sets of time-dependent data, two show the rate to be increasing over time, which contradicts the expected trend. Independent measurements seem to trend downward over time. However, extrapolating this trend from the maximum time measurement of 1.3 years to one million years is not a reasonable approach. The RTA, therefore, specifies a constant corrosion rate, sampled from a lognormal distribution bounded, as shown in Figure 1, between 0.01 μm/yr and 0.51 μm/yr. Furthermore, the use of a constant corrosion rate for Stainless Steel Type 316 is consistent with the rate calculated for Alloy 22, which is temperature dependent, but becomes effectively constant after about 100,000 years, once the temperatures inside the drift reach near ambient conditions (see, for example, SNL 2008, Figure L-4).

Further justification for the use of a constant corrosion rate is provided by the results of the TSPA model (SNL 2008). The RAI questions whether the corrosion rates used for Stainless Steel Type 316 in the TSPA model result in advective releases being underestimated. Such a result would be obtained if the mass of corrosion products were overestimated due to the corrosion rates being too high; if that were the case, then retardation of radionuclides by sorption onto an overestimated mass of corrosion products would cause releases to be underestimated under advective conditions. However, this is not the case, as described below for the igneous intrusion modeling case, where advective releases exceed the diffusive releases.

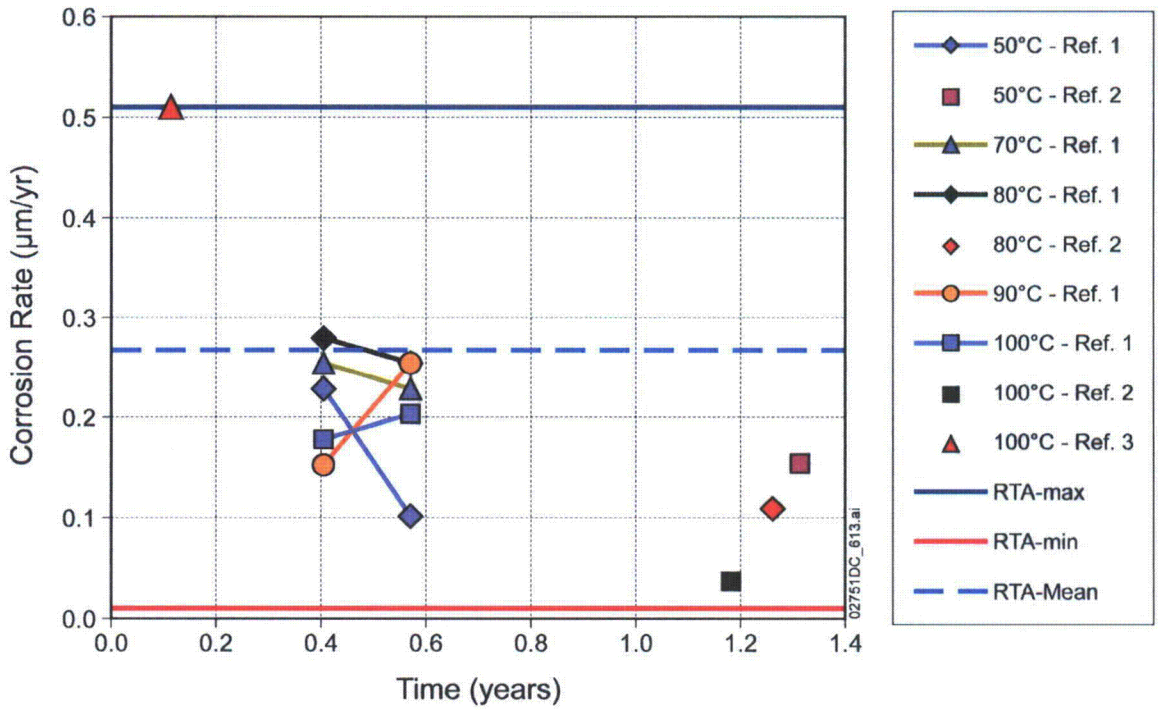

Source: BSC 2004, Table 4-3 footnotes. Ref. 1: Footnote d. Ref. 2: Footnote e. Ref. 3: Footnote f.

Figure 1. Time Dependence of Stainless Steel Type 316 Corrosion Rate Data Listed in RTA Report (SNL 2007a, Table 4.1-1)

In the igneous intrusion modeling case, the waste form is assumed to degrade instantaneously following the igneous event, and corrosion products begin to form at the same time. However, radionuclide mass is not available for advective and diffusive transport until the temperatures fall below 100°C. For the first 8,000 years after repository closure, the mean annual dose for the igneous intrusion modeling case is dominated by the rapidly transporting fission products ^{99}Tc and ^{129}I (SNL 2008, Figure 8.2-8a[a]), which are non-sorbing and, therefore, unaffected by the mass or rate of production of corrosion products (SNL 2008, Figure K6.3.1-10). After 8,000 years, the mean annual dose for this case is dominated by ^{239}Pu. However, the TSPA sensitivity analyses show that the release rate of dissolved ^{239}Pu from the Engineered Barrier System (EBS) to the unsaturated zone resulting from an igneous intrusion is relatively insensitive to the stainless steel corrosion rate (SNL 2008, Figures K6.3.1-7, K6.3.1-8, and K6.3.2-4).

Rather, the ^{239}Pu release rate is most sensitive to uncertainty in plutonium solubility limits and infiltration. The reason that the release rate of ^{239}Pu is insensitive to the stainless steel corrosion rate is that the sorption capacity of corrosion products is seldom fully occupied, as indicated by the results shown in Figure 2. The mean fraction of sorption capacity occupied is about 20% in the case shown, which is for an igneous intrusion occurring at 100 years in which advective releases dominate. Thus, even under advective conditions, a significant fraction of the corrosion product sorptive capacity is unoccupied. This implies that radionuclides are not excessively retarded, and that the mass of corrosion products resulting from the constant corrosion rates described above does not cause radionuclide releases to be underestimated.

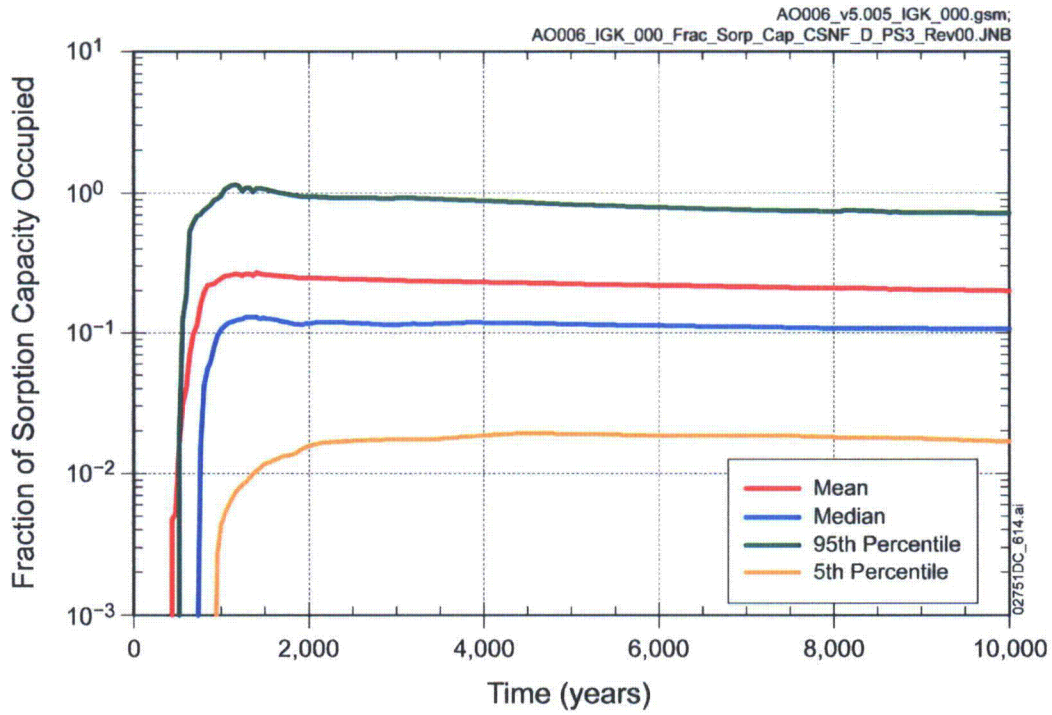

Source: Modified from SNL 2007a, ERD 02, Figure 1.

NOTE: In approximately 5% of the simulations in the TSPA, sorption of radionuclides onto steel corrosion products slightly exceeds the sorption capacity. This is due to over-prediction of K_d for uranium based on the abstraction implemented in TSPA for conditions when dissolved concentration of uranium is high ($>10^{-4}$ mol/L) and sorption sites per liter of water are low (< 4 mol-sites/L). A supplemental sorption model was developed and tested in a subset of the TSPA analyses to show that an improved regression fit for the sorption model has an insignificant impact on repository performance, i.e., on predicted dose (SNL 2007a, ERD 02, Section II).

Figure 2. Fraction of Sorption Capacity Occupied for Commercial Spent Nuclear Fuel Waste Packages in Percolation Subregion 3 Dripping Environments after an Igneous Intrusion at 100 Years

In the seismic ground motion modeling case, where general corrosion patches form and allow advective releases, the effect of corrosion rate is expected to be even smaller than that indicated for the igneous intrusion modeling case. This is because stress corrosion cracking from seismic events will occur much earlier than the general corrosion patches (SNL 2008, Figures 8.3-9[a](a)

and 8.3-11[a](a)) and allow the corrosion products to start forming, leading to relatively large build-up of sorption sites by the time the general corrosion patches appear and advective releases become important. As shown in *Total System Performance Assessment Model/Analysis for the License Application* (SNL 2008, Figure K.7.7.2-2), the expected dose is insensitive to uncertainty in steel corrosion rates and more sensitive to parameters that influence the waste package failure.

1.3 CONSERVATIVENESS OF CORROSION RATES

The stainless steel corrosion rates used in the TSPA, based on experimental measurements, are consistent with the conceptual model of corrosion used in the TSPA (SAR Section 2.3.7.12.3.2), wherein corrosion products tend to laminate and flake off the corroding metal surface, minimizing the thickness of corrosion products that might inhibit diffusion of water and oxygen to the metal surface, maintaining relatively high, early-time corrosion rates. This conceptual model provides for stainless steel waste package components degrading and failing quickly, thereby allowing water to access the waste form immediately after the waste package outer barrier is breached, conservatively overestimating degradation rates and releases of radionuclides (see the response to RAI 3.2.2.1.3.4.4-003).

Regarding sorption of radionuclides on steel corrosion products, sorption is only considered for iron oxides, even though other oxides/oxyhydroxides that can sorb radionuclides (such as oxyhydroxides of Ni, Cr, and Mn, etc.) will be present in the waste package. Thus, sorption of radionuclides on corrosion products is conservatively modeled by neglecting sorption on potentially available sorption sites on steel corrosion products other than iron oxides.

1.4 SUMMARY

The response is summarized as follows:

1. The minimum value of the corrosion rate for Stainless Steel Type 316 (0.0007 μm/yr) reported in Table 4-3 of *Aqueous Corrosion Rates for Waste Package Materials* (BSC 2004) is based on a measured weight loss of zero and therefore is not a valid measure of the minimum corrosion rate; rates reported in the source (BSC 2004) that are based on zero-weight-loss measurements are not used to determine the range of corrosion rates for Stainless Steel Type 316.

2. Use of a minimum corrosion rate of 0.01 μm/yr for Stainless Steel Type 316, equal to the mean corrosion rate of Alloy 22, is justified since all experimental rate measurements indicate that Alloy 22 corrodes more slowly than Stainless Steel Type 316.

   The mean corrosion rate for Stainless Steel Type 316 (0.267 μm/yr) is justified because it is based on a statistical analysis of all known relevant experimental rate data.

   Use of a constant corrosion rate sampled from a lognormal distribution ranging from 0.01 μm/yr to 0.51 μm/yr is justified because existing relevant experimental rate data do not conclusively demonstrate a time-dependence in the corrosion rate for Stainless Steel

Type 316. A constant rate is consistent with the model of Alloy 22 corrosion at late times.

In the igneous intrusion modeling case, where advective releases dominate, early doses are dominated by rapidly transporting fission products, such as ^{99}Tc. At later times when ^{239}Pu dominates the dose, TSPA sensitivity analyses indicate that the EBS release rate of ^{239}Pu is insensitive to the stainless steel corrosion rate. This is because the mean occupied sorption site capacity for radionuclide sorption onto corrosion products is 20% for the igneous intrusion modeling case, indicating that potentially overestimating the mass of corrosion products does not lead directly to overestimating sorption and underestimating releases of radionuclides.

3. Sorption of radionuclides onto other products of stainless steel corrosion besides the iron oxides, which would reduce release estimates, is conservatively neglected.

   The conceptual corrosion model provides for stainless steel waste package components degrading and failing quickly, thereby allowing water to access the waste form immediately after the waste package outer barrier is breached, which conservatively overestimates degradation rates and releases of radionuclides.

2. COMMITMENTS TO NRC

None.

3. DESCRIPTION OF PROPOSED LA CHANGE

None.

4. REFERENCES

BSC (Bechtel SAIC Company) 2004. *Aqueous Corrosion Rates for Waste Package Materials.* ANL-DSD-MD-000001 REV 01. Las Vegas, Nevada: Bechtel SAIC Company. ACC: DOC.20041012.0003.

SNL (Sandia National Laboratories) 2007a. *EBS Radionuclide Transport Abstraction.* ANL-WIS-PA-000001 REV 03. Las Vegas, Nevada: Sandia National Laboratories. ACC: DOC.20071004.0001; LLR.20080414.0023; DOC.20090623.0001.

SNL 2007b. *General Corrosion and Localized Corrosion of Waste Package Outer Barrier.* ANL-EBS-MD-000003 REV 03. Las Vegas, Nevada: Sandia National Laboratories. ACC: DOC.20070730.0003; DOC.20070807.0007; LLR.20080414.0018.

SNL 2008. *Total System Performance Assessment Model /Analysis for the License Application.* MDL-WIS-PA-000005 REV 00 AD 01. Las Vegas, Nevada: Sandia National Laboratories. ACC: DOC.20080312.0001.

RAI Volume 3, Chapter 2.2.1.3.4, Fourth Set, Number 3:

> Clarify the technical basis for imposing the pH buffering capacity of corrosion products as soon as a waste package is breached.
>
> Basis: The pH in the corrosion product domain is modeled on the basis of control by surface complexation reactions on steel corrosion products. Because stainless steel corrosion rates are relatively slow, it is possible that there could be a substantial period of time after waste package breach before corrosion products have accumulated sufficiently to control pH. Staff needs to understand whether DOE could be overestimating the pH buffering capacity of corrosion products during the stainless steel corrosion period.

1. RESPONSE

Imposing the pH buffering capacity of corrosion products as soon as a waste package is breached is supported by the expectation that considerable corrosion of the outer barrier and waste package internals will occur before the waste form is available for degradation. This expectation is otherwise excluded in the total system performance assessment (TSPA) model, which for conservative reasons assumes that the waste form is exposed to moisture immediately upon waste package breach. In the case of an early igneous intrusion, in which there may be little time for corrosion product accumulation, the highly conservative treatment of water and magma flow is expected to increase radionuclide releases far more than any potential decreases in releases due to possible initial overestimation of pH buffering capacity in the corrosion products domain.

The focus of this response is on the commercial spent nuclear fuel (SNF) packages because the slow corrosion rate of stainless steel is the basis of the RAI. Stainless steel is the only type of steel in the commercial SNF packages.

1.1 WASTE PACKAGE BREACH: EXPOSURE OF THE COMMERCIAL SNF TO FLUIDS

1.1.1 Treatment of Waste Package Component Corrosion/Failure

The TSPA model makes the conservative assumption that when the waste package outer barrier breaches (no matter what the mechanism), the fuel is immediately exposed to moisture (SNL 2008, Sections 6.3.7.4.1.3, 6.4.2.2, 6.5.1.4.2, and 6.6). However, exposure of the fuel to moisture prior to significant accumulation of corrosion products is unlikely. The two most likely causes of outer barrier breach are general corrosion and stress corrosion cracking induced by seismic damage (SAR Section 2.1.2.2.6 and SAR Figure 2.1-12). After these types of breaches, it is reasonable to expect that the waste package internals will begin corroding before the waste form is exposed. The internals include the inner vessel; transportation, aging, and disposal (TAD) canister; guide assembly; borated A, B, and C plates (basket structure); and fuel tubes. First, the inner vessel will need to breach to expose the TAD canister to water. During this time, corrosion products from the inner vessel will add to the corrosion products from the outer barrier. Next, the TAD canister will need to breach to expose the guide assembly, fuel basket, and fuel

tubes to water. The time needed for this to happen will permit further buildup of corrosion products, not only from the inner vessel and outer barrier, but also from the TAD canister. Although the TSPA model results are conservatively based on the assumption that the cladding is unavailable for radionuclide retardation (SNL 2008, Section 6.3.7.3.1), the more reasonable expectation is that even longer times are available for corrosion product accumulation when considering the time necessary for significant cladding degradation based on the industry cladding failure experience. Thus, by the time of radionuclide release, ample steel corrosion products are expected to generate significant pH buffering capacity in the corrosion products domain.

Commercial SNF consists of assemblies of Zircaloy tubing filled with UO_2 fuel pellets (SNL 2007a, Section 6.1[a]). The cladding is completely sealed and only fuel with failed cladding can interact with water or moist air. The distribution of failed cladding as-received has an expected value of 0.1% (SNL 2007a, Section 4.0[a]). After repository closure, additional cladding failure may occur due to mechanical damage from events associated with seismic activities such as rockfall or the accumulation of rubble in the drift. In the TSPA compliance model, the fuel corrodes as if bare fuel were exposed (SNL 2007a, Section 6.1.4). However, fuel degradation would only occur where the cladding was cracked, from the causes described above, and not over the entire surface area of the fuel. Therefore, the protection provided by the cladding is also expected to allow for steel corrosion product buildup prior to fuel degradation and radionuclide release.

1.1.2 Conservative Treatment of Flow (water and magmatic) in the Igneous Intrusion Modeling Case

In the igneous intrusion modeling case, there may be little time for accumulation of corrosion products if the intrusion occurs early in the modeling period and immediately exposes the waste form. The conservative assumption is made in the TSPA that the intruding magma fills every drift within the repository. Contact with magma damages all waste packages, drip shields, and fuel cladding such that these components no longer have waste isolation capability (SNL 2008, Section 6.5.1.1). The components remain in place but are simply assumed to allow advective flow through the waste package. Regarding uncertainties in the igneous intrusion modeling case related to waste dissolution, the TSPA has adopted a significant conservative position to account for this uncertainty by assuming that every waste package is contacted by the maximum amount of advecting water, an amount equal to the cross-sectional area of the drift (not the waste package) times the percolation flux (SNL 2008, Section 6.5.1.1). No credit is taken for entombment of the waste by the solidified magma, and the intruded basalt in the drift is assumed to provide no resistance to water flow. Furthermore, it is assumed that commercial SNF is instantly degraded (SNL 2008, Section 6.5.1.4.1) and that the entire mass of degraded fuel is contacted by the conservatively large flow of water (SNL 2008, Section 6.5.1.4.2). Because all of the waste packages and drip shields are failed, the entire seepage flux enters the waste package and is available for advective transport of radionuclides from the Engineered Barrier System (SNL 2007b, Section 6.7.1.1). Therefore, in the TSPA model, the magnitude of radionuclide transport to the unsaturated zone is controlled by the amount of seepage and the radionuclide solubilities (SNL 2008, Section 6.5.1.4.2). These significant conservatisms have an immediate conservative impact and apply for the remainder of the modeling period. Therefore,

in the case of an early igneous intrusion event, these conservatisms are expected to more than account for the uncertainties associated with the initial pH buffering capacity modeled for the corrosion products domain.

1.2 DISCUSSION OF THE LOWER PH RANGE IN THE WASTE FORM DOMAIN

The pH range in the corrosion products domain after waste package breach is approximately 7.0 to 8.4, whereas the pH range in the waste form domain is approximately 5.5 to 8.4 (see Table 1 of the response to RAI 3.2.2.1.3.4-3-002). The smaller range in the corrosion products domain is due to additional acid neutralizing capacity (ANC). The main reason for the additional ANC is that surface complexation reactions are considered in the corrosion products domain but are not considered in the waste form domain (as discussed in the response to RAI 3.2.2.1.3.4-3-002).

Steel corrosion occurs in both domains, producing significant ANC in the form of corrosion products. However, in the waste form domain, only the dissolution of corrosion products is considered when determining the ANC and the lower pH boundary (SNL 2007d, Section 6.10.1[a]). The exclusion of surface complexation modeling in the waste form domain is a simplification that causes lower pH values to be realized in the waste form domain. Allowing for the lower pH values is expected to be conservative because pH values below 7 cause increased release of radionuclides such as Pu, Np, U, Am, Th, and Pa from the waste form domain due to higher radionuclide solubilities (SNL 2007c). The stability of waste-form and iron-oxide colloids is also enhanced at pH values below 7 (see Figure 6 of the response to RAI 3.2.2.1.3.4-2-003).

Steel corrosion releases protons through the oxidation of reduced elements in the steel and the precipitation of iron-nickel oxides. The released protons act to reduce the pH of the water. However, corrosion of other materials in the waste form domain (aluminum alloys and waste forms) consumes protons and acts to raise the pH of the water (SNL 2007d, Section 6.10.1.1[a]). Furthermore, while steel corrosion releases protons to solution, it also produces the iron corrosion products that provide ANC to the system via both surface complexation and dissolution reactions. In this way, steel corrosion is a largely self-buffering reaction that, when surface complexation is included, prevents the pH from falling below 7 in the corrosion products domain. (For additional discussion of the pH buffering effects of corrosion products in the waste form and corrosion products domains, see the response to RAI 3.2.2.1.3.4-3-002.)

1.3 SUMMARY

The pH in the corrosion products domain is modeled on the basis of control by surface complexation reactions on steel corrosion products. Imposing the pH buffering capacity of corrosion products as soon as a waste package is breached is reasonable given the conservative treatment of waste package breach and materials corrosion. Several conservative simplifications used within the TSPA expose spent fuel to degradation immediately after outer barrier breach. Realistically, after outer barrier breach, several steel waste package internals will begin degrading before the waste form is available for degradation. Having corrosion products in the corrosion products domain as soon as the waste package is breached is reasonable, given the large amount of corrosion products that would likely be generated prior to fuel degradation.

Furthermore, significant conservative assumptions concerning flow within the igneous intrusion modeling case more than account for the uncertainties associated in the consideration of the amount of corrosion product buildup for pH moderation in the igneous intrusion scenario. Additionally, because surface complexation reactions are not included in the waste form domain calculations, which allows higher amounts of radionuclide release from the waste form domain, the lower range of pH entering the corrosion products domain from the waste form domain is expected to be conservatively low. Therefore, imposing the pH buffering capacity of corrosion products as soon as a waste package is breached is not expected to overestimate the pH buffering capacity of corrosion products during the stainless steel corrosion period.

2. COMMITMENTS TO NRC

None.

3. DESCRIPTION OF PROPOSED LA CHANGE

None.

4. REFERENCES

SNL (Sandia National Laboratories) 2007a. *Cladding Degradation Summary for LA.* ANL-WIS-MD-000021 REV 03 ADD 01. Las Vegas, Nevada: Sandia National Laboratories. ACC: DOC.20050815.0002; DOC.20070614.0002; DOC.20070703.0006.

SNL 2007b. *Abstraction of Drift Seepage.* MDL-NBS-HS-000019 REV 01 AD 01. Las Vegas, Nevada: Sandia National Laboratories. ACC: DOC.20070807.0001.

SNL 2007c. *Dissolved Concentration Limits of Elements with Radioactive Isotopes.* ANL-WIS-MD-000010 REV 06. Las Vegas, Nevada: Sandia National Laboratory. ACC: DOC.20070918.0010.

SNL 2007d. *In-Package Chemistry Abstraction.* ANL-EBS-MD-000037 REV 04 ADD 01. Las Vegas, Nevada: Sandia National Laboratories. ACC: DOC.20070816.0004; DOC.20051130.0007.

SNL 2008. *Total System Performance Assessment Model/Analysis for the License Application.* MDL-WIS-PA-000005 REV 00 AD 01. Las Vegas, Nevada: Sandia National Laboratories. ACC: DOC.20080312.0001.

MOL.20030422.0337

QA:QA

Characterization of Colloids Generated from Commercial Spent Nuclear Fuel Corrosion

Activity Title: Testing/Colloid Report

Activity Number: PAWTP30A

November 18, 2002

Revised March 28, 2003

C. J. Mertz, Robert J. Finch, Jeff A. Fortner, James L. Jerden, Jr., Yifen Tsai, James C. Cunnane, Patricia A. Finn

Chemical Engineering Division
Argonne National Laboratory
9700 South Cass Avenue
Argonne, IL 60439

TABLE OF CONTENTS

Page

List of Tables 3
List of Figures 5
Acronyms 7
Glossary of Terms 8

I. BACKGROUND AND SCOPE 10
A. Objectives 10
B. Background 10
C. Previous Data Reports 11
D. Test Planning and Related Documentation 12
E. Scope of Data Package 12
II. DATA ACQUISTION AND ANALYSIS 13
A. Experimental and Analytical Details 13
1. Experimental design 13
2. Analytical methods 14
Filtration 15
Inductively coupled plasma mass spectrometry (ICPMS) 15
High resolution alpha spectrometry 15
Dynamic Light Scattering (DLS) 16
Zeta Potential Measurements 18
Transmission Electron Microscopy 18
B. Test Matrix 19
C. Data Analysis 20
III. DESCRIPTION OF THE DATA 20
A. Data Dictionary 20
Leachate Concentrations 21
B. Data Organization 22
C. One-of-a-kind records 24
D. Accuracy and Precision 24
E. Uncertainties 26
F. Data Verification 27
IV. DISCUSSION 27
A. CSNF Colloids Generated in Unsaturated Tests 27
ATM-103 Fuel Colloids 30
ATM-106 Fuel Colloids 34
B. Uranium Mineral Phase Colloids under Saturated Conditions 38
Appendix 1 45
Appendix 2 49
Appendix 3 53

LIST OF TABLES

		Page
Table 1	Characteristics of CSNF Fuels Used in Unsaturated Drip Tests	14
Table 2	Correlation between Nanosphere Size Standards and DLS Count Rate	17
Table 3	Test Matrix for Uranium Substrate Colloidal Suspensions in Uranyl Nitrate or J-13 Groundwater	20
Table 4	Summary of Measured Quantities, Derived Quantities and Associated Uncertainty Estimates	21
Table 5	Summary of References to U-238 and Pu-239 Concentration Data	23
Table 6	Uranium and plutonium concentrations associated with various size fractions (particles, colloids, and dissolved) in leachates from ATM-103 HDR corrosion tests as a function of test duration.	33
Table 7	Colloid fraction determined from ratio of nuclide concentration in ATM-103 HDR leachates after filtration through large and small filters as a function of test duration.	34
Table 8	Uranium and plutonium concentrations associated with various size fractions (particles, colloids, and dissolved) in leachates from ATM-106 HDR corrosion tests as a function of test duration.	37
Table 9	Colloid fraction determined from ratio of nuclide concentration in ATM-106 HDR leachates after filtration through large and small filters as a function of test duration.	38
Table A1-1	Summary of DLS Analyses on Leachates from ATM-103 Spent Fuel Corrosion	43
Table A1-2	Summary of DLS Analyses on Leachates from Control Tests for ATM-103 and ATM-106	43
Table A1-3	Summary of DLS Analyses on Leachates from ATM-106 Spent Fuel Corrosion	44
Table A1-4	Summary of DLS Analyses on Leachates from ATM-109A, B and C Spent Fuel Corrosion	45
Table A2-1	Pu-239 Concentrations in ATM-103 HDR Tests	49

LIST OF TABLES – contd.

		Page
Table A2-2	Pu-239 Concentrations in ATM-103 LDR Tests	49
Table A2-3	Pu-239 Concentrations in ATM-103 HA Tests	49
Table A2-4	Pu-239 Concentrations in ATM-106 HDR Tests	50
Table A2-5	Pu-239 Concentrations in ATM-106 LDR Tests	50
Table A2-6	Pu-239 Concentrations in ATM-106 HA Tests	50
Table A2-7	Pu-239 Concentrations in ATM-109A HDR Tests	51
Table A2-8	Pu-239 Concentrations in ATM-109A HA Tests	51
Table A2-9	Pu-239 Concentrations in ATM-109B HA Tests	51
Table A2-10	Pu-239 Concentrations in ATM-109C HDR Tests	51
Table A2-11	Pu-239 Concentrations in ATM-109C HA Tests	51
Table A2-12	U-238 Concentrations in ATM-103 HDR Tests	52
Table A2-13	U-238 Concentrations in ATM-106 HDR Tests	52
Table A3-1	Summary of Dynamic Light Scattering Analyses on Colloidal Suspension of Meta-Schoepite and Uranium Dioxide in 10 mM Uranyl Nitrate	53

LIST OF FIGURES

		Page
Figure 1	Relationship between Count Rate and Number Concentration for Polystyrene Nanosphere Size Standards of Nominal Sizes	17
Figure 2	Comparison of Pu-239 concentrations analyzed by ICPMS and alpha spectrometry for leachate and strip solutions from CSNF corrosion tests	20
Figure 3	Relative Amount of Colloids Present in Leachates from Commercial Spent Nuclear Fuel Tests Sampled as a Function of Corrosion with EJ-13	29
Figure 4	Plutonium Concentration as a Function of pH in Unfiltered Leachates from Corrosion Tests with CSNF	31
Figure 5	Concentration of U-238 and Pu-239, and pH of the test leachates as a function of test duration for the ATM-103 HDR test for sampling periods between 5.2 to 8.7 years	32
Figure 6	Uranium concentrations associated with particles, colloids, and dissolved species in leachates from ATM-103 HDR corrosion tests as a function of test duration	33
Figure 7	Concentration of U-238 and Pu-239, and pH of the test leachates as a function of test duration for the ATM-106 HDR test for sampling periods between 5.2 to 8.7 years	36
Figure 8	Uranium concentrations associated with particles, colloids, and dissolved species in leachates from ATM-106 HDR corrosion tests as a function of test duration	37
Figure 9	TEM micrographs of metaschoepite and UO_{2+x} colloids from 10 mM uranyl nitrate, and metaschoepite and UO_{2+x} colloids from J-13 groundwater	41
Figure 10	Colloid size and number concentration for meta-schoepite and UO_{2+x} suspension in 10 mM uranyl nitrate as a function of elapsed time from colloidal suspension preparation	42

LIST OF FIGURES – contd.

Page

Figure 11 Zeta potential as a function of pH for meta-schoepite and UO_{2+x} colloids in 10 mM uranyl nitrate compared with UO_{2+x} colloids in 1 mM $NaClO_4$ 42

Figure 12 Concentration of uranium associated with various size fractions from a suspension of meta-schoepite and UO_{2+x} in J-13 groundwater 43

ACRONYMS

ANL	Argonne National Laboratory
ATM	Approved testing material
BWR	Boiling water reactor
Conc	Concentration
CSNF	Commercial spent nuclear fuel
DHLW	Defense high level waste
DLS	Dynamic light scattering
EDS	Energy dispersive X-ray fluorescence spectroscopy
EELS	Electron energy loss spectroscopy
EJ-13	Groundwater from the U.S. Geological Survey well "J-13" near Yucca Mountain, Nevada, that has been modified by reacting it with crushed Topopah Springs tuff at 90°C for 80 days (composition given in Table 2)
ELS	Electrophoretic light scattering
HA	Humid air test (commonly referred to "vapor test" in previous reports)
HDR	High drip-rate test: nominal injection rate of 0.75 mL each 3 to 4 days (1.5 mL/week)
ID	Sample identification
ICPMS	Inductively coupled plasma mass spectrometry
J-13	Groundwater from the U.S. Geological Survey well "J-13" near Yucca Mountain, Nevada
LDR	Low drip-rate test: nominal injection rate of 0.075 mL each 3 to 4 days (0.15 mL/week)
PS	Polystyrene
PWR	Pressurized water reactor
SN	Scientific notebook
TEM	Transmission Electron Microscopy
UFL	(also, UF) Unfiltered leachate
YMP	Yucca Mountain Site Characterization Project
ZP	Zeta Potential

GLOSSARY OF TERMS

Acid-strip: A process during which the internal surface of a stainless-steel reaction vessel is soaked in an aqueous solution of nitric and hydrofluoric acids, in an effort to dissolve radionuclides that have adhered to the vessel's interior surface.

Colloid: (also, Colloidal Particles) Submicrometer-sized particles with at least one dimension between 1 and 1000 nm whose properties are governed by Brownian motion. Practical definition for colloids in this report is material collected from leachate that is passed through filters with pore sizes based upon available filter sizes (between 1 or 5 nm and 450 or 1000 nm).

Corrosion Products: Solid compounds that form on the fuel during corrosion.

Dissolved Species: (also, Dissolved Fraction) Subnanometer species (i.e., ions, etc) typically < 1 nm in size. Practical definition is limited to the smallest filter size available in these experiments (i.e., 2 or 5 nm).

EJ-13 water: Groundwater pumped from the U.S. Geological Survey well "J-13" in Nevada that has been reacted with crushed tuff at 90°C for 80 days.

Fuel: Multi-grain fragments of the approved LWR test materials, ATM-103, ATM-106, ATM-109A, ATM-109B, and ATM-109C.

Fuel matrix: The solid UO_2 and substituents that are contained in the structure of the UO_2 as a solid solution, and which comprises the majority of spent fuel. The fuel matrix is distinguished from material that has phase-separated from the original UO2 during or subsequent to burn up in the nuclear reactor.

Gold Retainer: A thin gold mesh perforated with ~200-μm holes that was placed at the base of the Zircaloy-4 holder in the ATM-103 and ATM-106 high-drip tests after the 7.3 yr test interval.

J-13 water: Groundwater pumped from the U.S. Geological Survey well "J-13" in Nevada.

Leachate: Water that has accumulated in the bottom of a test vessel at the end of a test interval.

Particulate: Material in leachate that is greater than 450 or 1000 nm (limited by largest filter employed for tests).

pH: The negative of the base-ten log of the hydrogen-ion concentration measured in the leachate, measured at ambient hot-cell temperature (~25 – 30°C).

Sequential Filtration: A process whereby an aliquot of leachate is passed, through a series of filters with incrementally decreasing pore sizes. The series of filters consist of, first, a filter with 1000-nm pores, followed by a filter with 100-nm pores, and, finally, a filter with 50-nm pores.

Speciation: Classification of species or components based upon size (i.e., dissolved, colloidal, and particulate).

Unsaturated Tests: Tests under oxidizing conditions in which the relative humidity is 100%. There are three test types. They include a vapor test in which water vapor is present, a low-drip test in which a small amount of a simulated groundwater, EJ-13, is injected, and a high-drip test

in which ten times the amount of a simulated groundwater, EJ-13, is injected as in the low-drip test.

Zircaloy Holder: A cylindrical metal cup, 1 cm diameter x 1.5 cm tall, fabricated from Zircaloy-4 and used to hold the fuel fragments. The base of the cup contains 10-μm holes to allow solution drainage.

I. BACKGROUND AND SCOPE

A. Objectives

The purpose of this document is to summarize results on colloids generated from corrosion tests on commercial spent nuclear fuel (CSNF). Analyses presented here update results from on-going corrosion tests under Yucca Mountain repository relevant conditions (unsaturated testing at high drip rate, low drip rate and humid air conditions). In addition, the results from analyses on colloidal suspensions of uranium minerals phases in groundwater from Yucca Mountain or uranium saturated solutions are summarized.

B. Background

Colloids generated during waste form corrosion are potentially important in the performance assessment of the waste form in the repository. Colloids may transport radionuclides from a waste storage or disposal site in excess of amounts predicted solely on radionuclide elemental solubility limits. Recent studies at the Nevada Test Site (an unsaturated environment similar to Yucca Mountain) have shown the mobility of plutonium to be associated with colloids composed of clays, zeolites, and cristobalite [Kersting]. Numerous studies on nuclear waste glass corrosion have shown that clay colloids form and are prevalent in solution [Ebert; Buck; Geckeis]. However, few colloids have been detected in corrosion tests with commercial spent nuclear fuel [Finn 1994]. Likewise, colloidal transport has not been found to be a major mechanism for the transport of uranium at many natural analogue sites [Short; Miekeley]. However, experimental work on the formation of uranium oxide sols at pH and temperatures likely for a repository suggest that uranium substrate colloids must be considered [Ho].

The stability of dispersed colloids is dependent on numerous variables including pH, temperature, solution composition, etc. Colloidal interactions represent a balance between their dispersive properties (chargee repulsion) and their tendency to aggregate or sorb (intermolecular attraction). The ability to determine characteristic features of dispersed particles, such as size, shape, and surface potential, is important in determining their stability and behavior (i.e., dispersion, aggregation, or sorption) under a range of relevant environmental conditions. As such, this report presents results on the characterization of the physical and chemical nature of the solution-borne colloids that form during degradation of the waste forms, specifically as related to actinide releases.

This report summarizes the results of analyses on colloids from unsaturated corrosion tests on commercial spent nuclear fuel (CSNF) completed to date (8.7 years of testing for the CSNF) and not included in previous data reports. On-going unsaturated corrosion tests on CSNF were sampled periodically during the corrosion testing and the test solutions were analyzed for colloids to determine the nature of the colloids. The CSNF corrosion tests consist of two pressurized water reactor (PWR) fuels (ATM-103 and ATM-106) and three boiling water reactor (BWR) fuels (ATM109A, ATM109B, and ATM109C) being tested under unsaturated conditions at 90°C. These tests combine periodic injection of tuff-equilibrated J-13 groundwater into a sealed, stainless steel vessel containing fuel fragments in a zircaloy-4 sample holder at 90 °C. In

addition, colloidal suspensions of meta-schoepite and UO_{2+x} under saturated test conditions (in 10 mM uranyl nitrate or J-13 groundwater) at room temperature were characterized and are summarized in this report.

C. Previous Data Reports

The unsaturated tests with the ATM-103 and ATM-106 fuels were begun in September 1992 and, except for a six-month interruption during the first half of 1998, have been operating continuously during the 10 years since test initiation. Data obtained from these tests prior to 5.2 years have been reported previously (CRWMS M&O 2000) and will not be reported here. Data reported here correspond to samples taken during test intervals 5.2 through 8.7 years of reaction. Unsaturated tests with the ATM-109 fuels were begun in 1998 and have been operating continuously for over three years. Data reported for the ATM-109 fuel tests correspond to test intervals from test initiation through 3 years of reaction.

The unsaturated tests were run at 90°C and cooled to ambient temperature at test sampling. During the test interval, the leachate dripped from the fuel in the holder into water at the base of the vessel solutions (a Type 304L stainless-steel vessel). At the test sampling, the vessel was cooled to ambient laboratory temperature over a relatively brief period (typically less than 30 minutes). The concentrations reported in this report are those measured in aqueous solutions recovered from test vessels and measured at ambient temperature. Radionuclide "concentrations" reported in the previous data report for these tests (CRWMS M&O 2000) were not measured, but were calculated by determining the total mass of a given radionuclide recovered from each test vessel, including the mass in leachates plus the mass recovered during acid-stripping of reaction vessels, and dividing that total mass by the volume of solution recovered from each vessel during each sampling interval. Reporting such calculated concentrations was rationalized by the presumption that the total mass of every radionuclide recovered from each reaction vessel had been in solution at 90°C (as dissolved ions, colloids and/or particulates) when leachate dripped from the holder into water at the base of a vessel prior to sampling the leachate at ambient laboratory temperature. It would be difficult to determine the accuracy of this assumption due to the test configuration. Primarily for this reason, concentrations reported in this data report are those directly measured in the leachate at ambient temperatures and are, therefore, free of assumptions about what the concentrations of any radionuclide might have been at any temperature besides ambient (~25°C). The masses of nuclides removed from the vessel walls by acid stripping are also reported elsewhere (Finch et al. 2002).

In the previous report (CRWMS M&O 2000), Pu concentrations associated with colloids were determined from alpha spectrometry measurements of filters (50, 100, 1000 nm pore sizes) or the filtrate from a 5 nm pore size filter. The alpha spectra for the filters and filtrates (alpha planchets prepared by evaporation for the filtrates) typically have poor peak shape due to inelastic scattering from evaporites or alpha particles embedded in the membrane filter. Ideally, the alpha source should be a monolayer of alpha emitters which is achieved by electrodeposition (Schultz). This report uses alpha spectrometry measurements for Pu from filtrates that were electroplated or ICPMS results from filtrates for U or Pu isotopes. Dissolution of the filters followed by electrodeposition of the alpha emitters was not pursued.

D. Test Planning and Related Documentation

The principal investigator for this task is Carol Mertz. The test plan covering colloid work is "Waste Form Colloids Characterization and Concentration Studies" (SITP-02-WF-003, Rev. 00). The experimental work was performed in accordance with the Bechtel SAIC Company (BSC) prepared "ANL Statement of Quality Assurance Requirements," as implemented through the "Quality Assurance Plan for Technical Activities in Support of the Yucca Mountain Program" (YMP-02-001) and the associated Implementing, Administrative and Operating Procedures.

The work in the test plan is done in support of the License Application for the Yucca Mountain Project (YMP) as administered by Bechtel SAIC Company, LLC. This test plan was developed under the "Technical Work Plan for Waste Form Degradation Testing and Analyses in Support of SR and LA," TWP-WIS-MD-000008, Rev. 02.

This work supports the Total System Performance Assessment for the License Application (TSPA-LA) for a repository at Yucca Mountain, Nevada. More specifically, data obtained from this Task are to be used in the LA updates of the product document: MDL-EBS-PA-000004, Rev. 00. The documents supported by this test plan are covered by the technical work plan (TWP-WIS-MD-000008, Rev. 02).

E. Scope of Data Package

Data contained in this data package include concentrations measured in leachates and filtrates recovered from eleven corrosion tests conducted on three types of commercial spent UO_2 fuels (ATM-103, ATM-106, ATM-109). Three ATM-109 fuels were tested: ATM-109A, ATM-109B, and ATM-109C (a Gd-doped fuel). Test conditions include exposure of the fuels to modified groundwater ("EJ-13") at two rates of injection, as well as exposure to air saturated with water vapor (100% relative humidity). Descriptions of the test configurations and test matrices are given briefly in the following sections (additional information can be obtained in Finch et al. 2002).

The period covered by this report is for testing and sampling intervals following 5.2 years of reaction. The unsaturated fuel-corrosion tests at ANL were started in mid 1992 and the sampling intervals up to and including 4.8 years of reaction (i.e., data collected through mid 1997) were reported in a previous data package (CRWMS M&O 2000). The data reported here correspond to those collected from late 1997 through the end of 2001.

II. DATA ACQUISTION AND ANALYSIS

A. Experimental and Analytical Details

1. Experimental design

Two pressurized water reactor (PWR) fuels and three boiling water reactor (BWR) fuel types were used in the ANL corrosion tests. Testing on the corrosion of PWR and BWR fuels has been conducted for over eight and three years, respectively. The PWR fuels are designated ATM-103 and ATM-106. The ATM-103 fuel has a nominal burnup of 30 (MWd)/kg-U and a fission-gas-release of 0.25% (Guenther et al. 1988a). The ATM-106 fuel has a nominal burnup of 43 (MWd)/kg-U and a fission-gas-release of 11% (Guenther et al. 1988b). The BWR fuels are designated ATM-109A, ATM-109B, and ATM-109C. The three ATM-109 fuels came from three different fuel rods and have a range of burn-ups 64 to 72 (MWd)/kg-U. The ATM-109C fuel is doped with 2% Gd (Wolf et al., 2000).

For the ATM-103 and ATM-106 fuel tests up to the 6.8 year sampling, the fuel fragments were contained in a Zircaloy-4 holder that had a Zircaloy-4 retainer with 10-μm-diameter holes at its base. The small hole size at the base of the holder precluded fuel grains larger than 10 μm-diameter from being entrained with the leachate. The Zircaloy-4 retainers in the high-drip tests on ATM-103 and ATM-106 were replaced with new Zircaloy-4 retainers (with 10-μm-diameter holes) at the end of the 6.8-yr sampling interval; and these were subsequently replaced by gold retainers with 200-μm-diameter mesh size at the end of the 7.3-yr sampling interval. The Zircaloy-4 holders are housed in Type 304L stainless steel vessels. At the start of each test interval, the test vessel base contains approximately 5 mL of EJ-13 for drip tests and approximately 10 mL for vapor tests to ensure 100% relative humidity. The Zircaloy-4 holder is set on a ledge inside the test vessel. The vessel is sealed with a copper gasket and placed in a 90°C oven. For the drip tests, the top of the vessel is connected to a water injection system. Every 3 to 4 days, EJ-13 is injected onto the fuel in the high-drip and low-drip tests and air is flushed into the vessel to replenish the air. The injected water is determined by the increase in mass at the end of a test interval. In addition, the mass of water delivered with ten injections is measured at each test interval to determine the change in the injection system due to wear and radiation damage. The oven temperature is monitored and recorded with a data-logger, which records the temperature twice per 24-hr period and alarms for deviations greater than ±2°C. Further details on the test descriptions is provided in (CRWMS M&0 2000), (Finn et al. 1994), and (Finch et al. 2002).

Characteristics of the fuels used in these tests are summarized in Table 1.

Table 1. Characteristics of CSNF Fuels used in Unsaturated Drip Tests

Fuel	ATM-103	ATM-106 (NBD107)	ATM-109A (QCF1)	ATM-109B (QC B1A)	ATM-109C (QC D4A)
Reactor type	PWR	PWR	BWR	BWR	BWR
Nominal Burn-up (MWd/kg-U)	30[a]	43[b]	71[c]	72[c]	64[c]
Fission Gas Release (%)	< 0.25[a]	11[b]	4.4[c]	2.95[c]	3.5[c]
Years out of reactor at test initiation	12[a]	12[b]	7[c]	7[c]	7[c]
Test Type [d]	HDR LDR HA	HDR LDR HA	HDR HA	HA	HDR HA
Test Initiation	1992	1992	1998	1998	1998
Total Reaction Time	>10 yr	>10 yr	4 yr	4 yr	4 yr

[a] Guenther et al. (1988a) PNL-5109-103.
[b] Guenther et al. (1988b) PNL-5109-106.
[c] Wolf et al. (1999) YMP Data Report (YMP/SF-3A-319).
[d] HA = humid-air tests (also known as vapor tests), LDR = low drip-rate tests, and HDR = high drip-rate tests

2. Analytical methods

The characterization and quantification of colloids generated in the corrosion of CSNF under Yucca Mountain repository-relevant test conditions is essential to determine important waste form colloidal parameters that are necessary for predicting the radionuclide-associated colloid concentrations. The sampling of the tests and the various characterization techniques employed to characterize and quantify the colloids will be discussed in the following section.

CSNF Test Sampling Procedure

Each test was sampled periodically. During each sampling interval, the tests were interrupted to remove leachate and solid samples. Each test vessel was removed from the 90°C oven and cooled by placing the base of the vessel in contact with dry ice. Once cooled, the vessel was opened and the Zircaloy-4 holder with the reacted fuel fragments was removed and examined under an optical microscope.

Leachate was removed from the used test vessel and divided into aliquots (if a sufficient volume of leachate is available) for analysis by inductively coupled plasma mass spectroscopy (ICPMS), high-resolution alpha spectrometry, gamma spectroscopy, and dynamic light scattering. Alpha spectroscopy was discontinued after 2000; after the 7.7 and 1.5 year samplings

for the ATM-103 or ATM-106 and for the ATM-109 fuels, respectively. Selected aliquots were filtered as described below and the filtrates were also analyzed by ICP-MS, gamma spectrometry and alpha spectrometry, depending on the volume of liquid available. The pH of the leachate was measured at room temperature. After removing leachate from the test vessel, the interior of the test vessel was filled with an acid solution overnight at 90°C in order to dissolve any material remaining in the vessel.

Filtration

Filtration was used to separate various sized species (i.e., dissolved, colloidal, micron-sized particulate). The elemental composition and activity of radionuclides associated with each size fraction were determined using inductively coupled plasma-mass spectrometry and/or by nuclear spectroscopy (alpha and gamma spectrometry), respectively. Alpha spectrometry data are not available for sampling periods after January 2001. Several types of filters were employed for filtering the test solutions (cone, membrane, and microcentrifuge filters). Typically, an aliquot of all test solutions was passed through a 5 nm cone filter (the smallest pore size employed to determine the dissolved concentration; practical definition for dissolved species based upon available filters) and then centrifuged to recover the filtrate. In addition, sequential filtration of the test solution through a series of membrane filters with decreasing pore sizes was performed, if sufficient solution was available. The membrane filters were assembled in filter housings and the solution was passed through the membrane filter unit using a syringe. Additional filters were employed in 2000 for filtration of the test solutions. These filters were microcentrifuge filters of the following sizes: 200 and 450 nm. An ultracentrifuge was used to recover the filtrates for analysis.

Inductively coupled plasma mass spectrometry (ICPMS)

ICPMS is used to quantitatively analyze for most radionuclides; of interest here are mass numbers of uranium and the transuranium actinides, Np, Pu, Am, and Cm. Actinides analyzed by ICPMS include four isotopes of uranium: U-234, U-235, U-236, U-238; one neptunium isotope: Np-237; three plutonium isotopes: Pu-239, Pu-240, Pu-242; two americium isotopes: Am-241, Am-243; and Cm-244. Several of these isotopes can also be measured by other methods (see below). Results presented in this report include isotopes of uranium and Pu-239.

Potential isobaric interferences that can affect the accuracy and precision of ICPMS analyses of concern here include several natural isotopes present in EJ-13 water, notably the three most abundant isotopes of uranium (234, 235, and 238), as well as radiogenic isotopes from the fuel. This interference is expected to be relatively small for U-238 and Pu-239.

High resolution alpha spectrometry

High-resolution alpha spectrometry provides quantities of the following alpha-emitting isotopes: Pu-239 + Pu-240, Cm-244, Am-241 + Pu-238, Np-237, and Am-243. Alpha spectrometry cannot distinguish between the two Pu isotopes, Pu-239 and Pu-240; nor can Am-241 be distinguished from Pu-238. Calculating individual contributions from these two pairs of isotopes to alpha spectra requires knowledge of the relative contributions of each. It is reasonable to assume that Pu isotopes do not fractionate in these tests, and we can, therefore, use the ratio of Pu-239 to Pu-240 in the fuel being tested; these ratios are available from ORIGEN2 calculations tabulated by Guenther et al.(a and b) for ATM-103 and ATM-106. The

corresponding ratios for the ATM109 fuels are those determined by direct analysis of the fuel and reported by Wolf et al. (2000).

Americium and Pu might be expected to behave in chemically distinct ways, so that deconvoluting contributions to alpha spectra by Pu-238 and Am-241 is less straightforward. Because Pu-238 is expected to behave chemically the same as Pu-239 and Pu-240, the concentration of Pu-238 relative to the other Pu isotopes in a particular sample should be proportional to its relative concentration in the fuel. The corresponding concentration of Pu-238 might then be extracted from the combined contribution from both Am-241 and Pu-238 in the alpha spectrum using the concentration of Pu-239 and Pu-240 determined by alpha spectroscopy and subtracting the appropriate amount of Pu-238 from the combined Am-241+Pu-238 concentration measured by alpha spectrometry. In this way, confidence in the concentration of Pu-238 and, therefore, Am-241 determined by alpha depends on the analysis of Pu-239 and Pu-240 from the same sample. However, Am-241 is also analyzed by ICPMS and by gamma spectrometry, and Am-241 concentrations for a particular sampling interval can be compared among the three independent methods used, when available.

While both the ICP-MS and alpha techniques detect plutonium, the plutonium quantities are best quantified by alpha spectrometry where concentrations as low as 0.001 ppb are easily measured (at least an order of magnitude lower than detection limits obtained using ICP-MS). The americium is, in general, most accurately determined by the gamma spectroscopy, owing to its very low concentration in solution (americium is generally below detection limits for alpha spectrometry).

The alpha spectrometry samples were prepared by electroplating the solution and, at earlier sampling periods, were also prepared by evaporation. Electroplating the solution affords higher energy resolution than evaporation by reducing the inelastic scattering that plagues thick samples (electroplating minimizes salt evaporates). When combinations of evaporated and electroplated alpha spectra are available, data from electroplated samples were used in this report.

Gamma Spectroscopy

Gamma spectroscopy is used to quantify several radioisotopes, including Am-241, Cs-134, and Cs-137. Limited filtration data is available from gamma spectroscopy for Am associated with colloids, as such this data is not presented.

Dynamic Light Scattering (DLS)

Dynamic light scattering is used to determine the size of particles in the colloidal size range. Particle size calibration is performed using polystyrene (PS) size standards (nominal sizes of 30, 70, 100 and 300 nm). Conversion of the count rate to a number concentration for the uranium substrate colloidal suspensions in this study is based upon a calibration curve for polystyrene (PS) size standard solutions (Figure 1). Polystyrene solutions were diluted using ultrapure water (deionized, resistivity of 18 megaohm·cm) and the count rate was measured at a scattering angle of 90°. Colloid number concentrations for the uranium substrate suspensions were estimated assuming that the uranium substrate colloids are spherical and scatter light as efficiently

as the PS standards (the scattering intensity is proportional to the refractive index). Both of these assumptions are limited in their application for obtaining the absolute concentrations for the uranium substrate colloids, but are useful in examining trends. The refractive index of PS is 1.6 [Schurtenburger] compared with 2.4 for UO_2 [Ho]. Multiple DLS measurements were performed on each sample by varying experimental parameters. For stable colloidal suspensions, the size distributions were reproducible. Intensity weighted distributions are presented in this report.

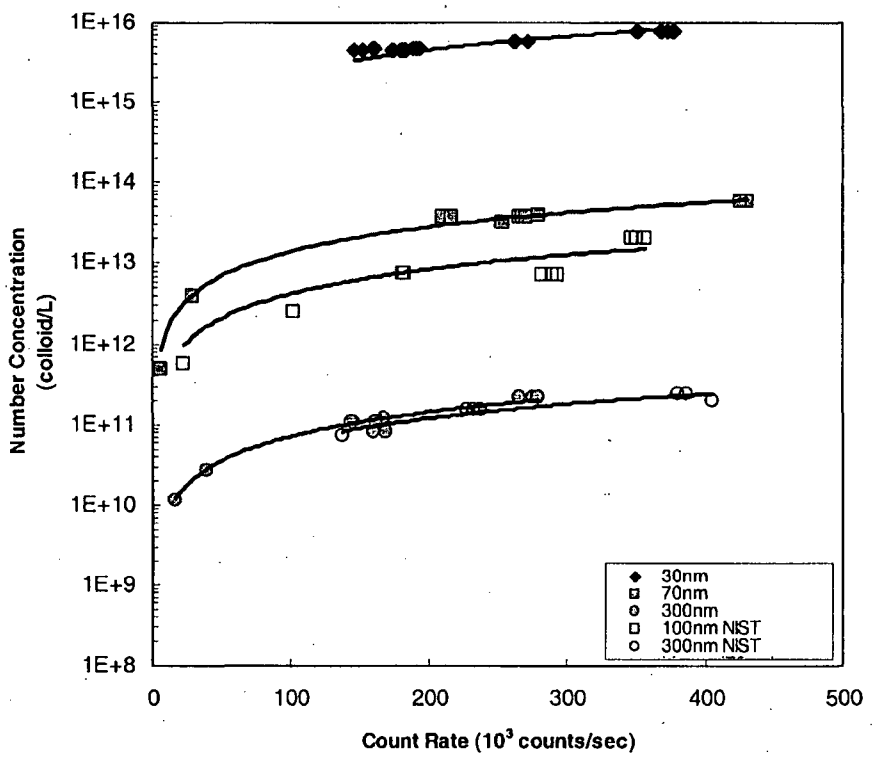

Figure 1. Relationship between measured count rate and calculated number concentration for polystyrene nanosphere size standards of nominal sizes.
Note: solid diamonds, 30 nm Duke Scientific Corp.; solid squares, 70 nm Duke Sci. Corp.; solid circles, 300 nm Duke Sci. Corp.; open squares, 100 nm NIST; open circles, 300 nm NIST). Solid lines represent linear least squares fit of data (equations for fits given in Table 2).

Table 2. Correlation between nanosphere size standards and DLS count rate.

Size/Manufacturer	Equation from Least Squares Fit of Data
30 nm Duke	Number Concentration (colloid/L) = 2e13 x Count Rate (kc/s)
70 nm Duke	Number Concentration (colloid/L) = 1e11 x Count Rate (kc/s)
100 nm NIST	Number Concentration (colloid/L) = 4e10 x Count Rate (kc/s)
300 nm Duke	Number Concentration (colloid/L) = 7e8 x Count Rate (kc/s)
300 nm NIST	Number Concentration (colloid/L) = 6e8 x Count Rate (kc/s)

Note: Equations used to convert count rate to number concentration for colloids of nominal size based upon least squares fit of data from nanosphere polystyrene size standards in Figure 1.

Zeta Potential Measurements

Zeta potential measurements were performed on a Zeta Plus unit from Brookhaven Instruments Corp. The performance of the instrument was checked with a mobility standard from NIST (geothite, SRM 1980). The measured mobility of the reference material was in excellent agreement with the certified mobility. The pH of the colloidal suspensions was adjusted to selected pH values with 0.1 M nitric acid or 0.1 M sodium hydroxide, and the solution was shaken to disperse the colloids prior to loading the sample in the electrophoresis cell. Multiple zeta potential measurements were performed at ambient laboratory temperature for each pH value.

Transmission Electron Microscopy

Transmission electron microscopy (TEM) is an excellent method for determining morphology, structure, and elemental and phase composition of colloid substrate materials [by energy dispersive x-ray spectroscopy (EDS), electron diffraction (ED), and electron energy loss spectroscopy (EELS)]. These techniques have been used to characterize colloid substrate phases formed in the corrosion of CSNF and DHLW and to obtain evidence that these colloid substrates are formed as a result of spallation of alteration layers and precipitated phases.

A small (~0.005 mL), unfiltered aliquot was collected from the test solution and wicked through a "holey" or lacey carbon film supported on a copper TEM support grid. The grid was examined for particulate material using TEM. Analyses were performed using a JEOL 2000FXII TEM operated at 200 kV and equipped with two Noran energy dispersive X-ray spectrometers, including a light element detector and also a Gatan 666 parallel electron energy loss spectrometer (EELS). Analysis of phases involved the use of the energy dispersive X-ray spectroscopy (EDS) and selected area electron diffraction (SAED). Images are taken using a 30-um objective aperture. The microscope camera lengths were calibrated using a polycrystalline aluminum standard.

Comparison of Isotopic Analyses

The two techniques used to analyze Pu-239 for this task (ICPMS, and alpha spectroscopy) have different sensitivities, detection limits, potential interferences, etc., so that masses and concentrations determined for Pu-239 by these analytical techniques may differ. Unless noted otherwise, there is no *a priori* reason to assign more or less confidence to any particular concentration value that has been analyzed by either of these analytical techniques. In fact, comparisons of concentrations for Pu-239 determined by these analytical techniques can provide useful information about analytical uncertainties. We have found that agreement within about 50% is common and reasonable with measured concentrations above approximately 0.1 ppb (Refer to Figure 2 for Pu-239 data analyzed by ICPMS and alpha spectrometry). As a rule, ICPMS is probably the least sensitive technique among those used here, and alpha spectroscopy the most sensitive (i.e., highest and lowest limits of detection, respectively). Isotope masses and concentrations that were analyzed but were below the lower limit of detection are indicated in the tables as "bd" (below detection). Entries in the tables that have a dash in place of an entry indicate isotope analyses that were not performed or are otherwise unavailable for any of several possible reasons, including a dry test vessel, insufficient solution volume, analytical problems, etc.

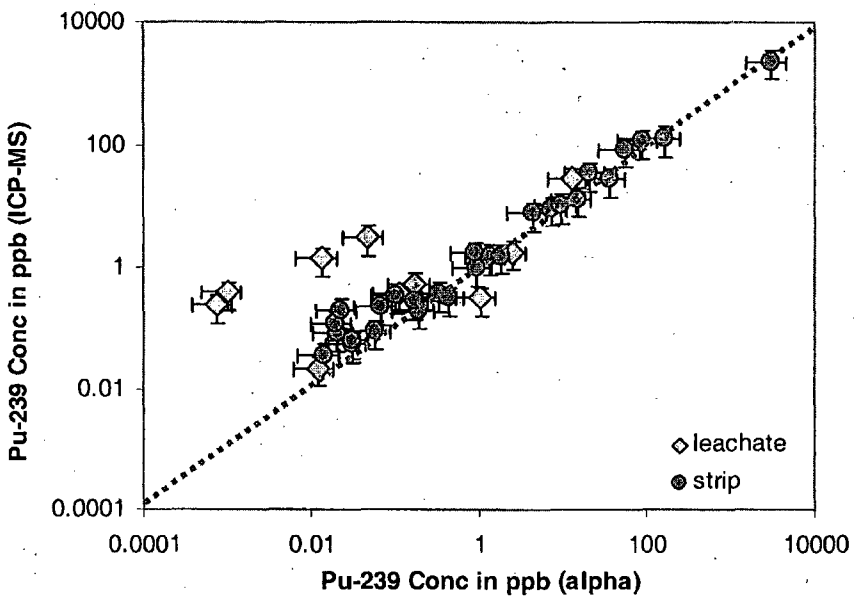

Figure 2. Comparison of Pu-239 concentrations analyzed by ICPMS and alpha spectrometry for leachate and strip solutions from CSNF corrosion tests.

Detection Limits

Mass releases and concentrations from intervals for which sample analyses were at or below the lower limit of detection for a given analytical method are not reported in the data tables. Isotopes present at concentrations at or below the lower limit of detection are reported as "less than" values to the task PI by the analyst. These detection limits vary among techniques and individual samples for a variety of reasons, some of which are generally applicable and others are unique to a particular sample or sampling interval; they are not reported here. Instead, all "less-than" values are reported here as "below detection" (designated as "bd" in the data tables).

B. Test Matrix

The test matrix for the CSNF tests is described in detail elsewhere (Finch et al. 2002). The unsaturated testing employs five fuels: ATM-103, ATM-106 and ATM-109A, ATM109B, and ATM-109C (refer to Table 1). The matrix includes six "drip" tests in which a modified groundwater, EJ-13, is injected periodically at two rates and five humid-air tests in which each test vessel is sealed with a small volume of water (~10 mL) but no water is injected between samplings. There are two (nominal) injection rates: 1.5 mL per week ("high") and 0.15 mL per week ("low"), with one-half the weekly injection volume being injected every three or four days. The tests are conducted at 90°C, which is in the range of expected repository temperatures approximately 1000 years after closure. One control test (injection vessel without fuel) is also being conducted, and samplings are performed for the control test in the same manner as for the other tests.

In addition, some test data are presented from hydrologically saturated tests with uranium dioxide and meta-schoepite colloids in uranyl nitrate or J-13 groundwater. The test matrix for these tests is shown in Table 3. The suspensions were prepared and the colloidal properties were characterized by the techniques described in Section 2 (Analytical Methods).

Table 3. Test matrix for uranium substrate colloidal suspensions in uranyl nitrate or J-13 groundwater.

Solution ID	Uranium substrate	Diluent	Conc of Uranium substrate in diluent (g/mL)	pH	Reference: SN/page
--	--	10mM uranyl nitrate	--	4.80	1831/10-11
CM1831/16-2	meta-schoepite and UO_{2+x}	10mM uranyl nitrate	0.0010	5.06	1831/16, 1830/35
CM1831/16-3	meta-schoepite and UO_{2+x}	J-13 groundwater	0.00019	7.66	1831/16, 1830/35

C. Data Analysis

All of the measured and derived variables presented in this report are summarized in Table 4. In the case of derived variables, the method of calculation is identified and the uncertainty estimates are given. The accuracy and precision, as well as experimental uncertainties, are discussed below.

III. DESCRIPTION OF THE DATA

A. Data Dictionary

Table 4 provides a data dictionary of the experimental and derived values for which data are included. Where appropriate, equations are presented to define derived variables. Values include the measured parameters (colloid size, zeta potential, actinide concentrations and activities) and the derived parameters (colloid concentrations).

Table 4. Summary of measured quantities, derived quantities and associated uncertainty estimates.

Value	Type[a]	Definition and Equation	Uncertainty
Solution mass	M	Mass (g) of solution sample aliquot (leachate or acid strip) determined gravimetrically (ICPMS, and alpha required different size aliquots)	0.005% ICPMS; 10% Alpha
ICPMS Nuclide Concentration (Conc.)	M	Concentration measured in leachate or acid strip sample by ICPMS.	±50%
Activity	M	Activity (Bq) measured in leachate or acid strip by alpha spectroscopy.	±50% Alpha
Alpha Nuclide Concentration (Conc.)	D	Concentration in leachate or filtrates; calculated from activity in aliquot. Conc (ng/g) = Activity (Bq) / Spec.Act.[b] (Bq/g) / Sol. Mass (g) * 10^9 ng/g	±50%
Mass Release derived from Alpha data	D	Mass (g) of nuclide released from sample to base of vessel (also used for acid strip mass release). Mass (g) in aliquot = Activity (Ci) / Spec.Act.[b] (Ci/g) Mass (g) in test = Mass (g) in aliquot / (test Vol. / aliquot Vol.)	±51%
Colloid Size	M	Colloid size (nm) measured in leachate by DLS.	±10%
Colloid Concentration	D	Colloid concentration determined from calibration curve with nanosphere standard solutions. Count rate (±30% based upon multiple DLS measurements) versus Mass (g) of nanosphere standard solution / standard Vol. (g)	±50%
Colloid Zeta Potential	M	Zeta potential of colloid measured in leachate by zeta potential measurements.	±15%

[a]Variable Types: D = derived; M = measured.
[b]Spec. Act. = specific activity in Ci/g or Bq/g.

Leachate Concentrations

Concentrations reported here were measured at ambient laboratory temperature (~25°C). Corrections of raw analytical data include a correction factor for dilutions of sample aliquots (where applicable), including addition of acid prior to analysis.

Seven categories of solution concentrations are reported: those corresponding to unfiltered leachates (UFL), and to solutions that were passed through filters of six nominal pore sizes, ranging from 1000 nm to 5 nm. Leachate concentrations from solutions that were filtered through 1000 nm, 100 nm and 50 nm filters were obtained by passing a single solution aliquot sequentially through filters with progressively smaller pore sizes, three filtration steps for each aliquot. Leachate concentrations from solutions filtered through 450 nm, 200 nm and 5 nm filters correspond to separate aliquots of unfiltered leachate, each aliquot being passed once through one filter in a single filtration step.

UFL (Unfiltered Leachate) as used in Appendix 2 is the mass in grams of a given analyte in the unfiltered leachate solution as measured at ambient laboratory temperature.

Leachate is the liquid water recovered from the base of each test vessel during a sampling interval. Selected aliquots of leachate are filtered by various means, as prescribed in the test-sampling procedure, and as volume allows. The volume of leachate for each sampling interval is determined calculated as the difference between the total mass of each test vessel at the start of the test interval and that at the end of the test interval. Leachate mass is converted to volume assuming the density of the leachate is 1 g/mL.

Filtrate is a leachate aliquot that was passed through a filter. Filtration data reported in the data tables correspond to leachate concentrations measured after passing aliquots of leachate through filters with pore sizes designated in the data tables; these concentrations were also measured at ambient room temperature.

The pH of all leachates was measured at ambient laboratory temperature.

B. Data Organization

Data are presented in Appendices 1 through 3 arranged primarily by fuel type (ATM-103, ATM-106, ATM-109) and test type (HDR, LDR, HA). Colloidal sizing data determined by DLS analyses are provided in Appendix 1 for all of the tests. Data tables showing leachate concentrations in parts per billion (milligram of each radionuclide per kilogram of solution) or *ppb* are already reported in (Finch et al. 2002). The concentration in ppb was converted to mol/L (refer to Table 5 for reference to the data tables in Finch et al. 2002). Concentrations of Pu-239 and U-238 (in molarity) determined by ICPMS and/ or alpha spectrometry analyses are provided in Appendix 2 for the high drip-rate tests (ATM-103 HDR, ATM-106 HDR, ATM-109A HDR, and ATM-109C HDR), the low drip-rate tests (ATM-103 LDR and ATM-106 LDR), and the humid-air tests (ATM-103 HA, ATM-106 HA, ATM-109A HA, ATM-109B HA, and ATM-109C HA).

Table 5. Summary of references to U-238 and Pu-239 concentration data.

Test ID	*Fuel*	*Test Type**	*Isotope*	*Data Table Reference Number* [a]	*Analysis Method* [b]
S31J	ATM-103	LDR	U-238	DTC-75	ICP
			Pu-239	DTC-80	ICP
			Pu-239	DTC-91	alpha
S61J	ATM-106	LDR	U-238	DTC-93	ICP
			Pu-239	DTC-98	ICP
			Pu-239	DTC-109	alpha
S32J	ATM-103	HDR	U-238	DTC-1	ICP
			Pu-239	DTC-6	ICP
			Pu-239	DTC-19	alpha
S62J	ATM-106	HDR	U-238	DTC-20	ICP
			Pu-239	DTC-25	ICP
			Pu-239	DTC-37	alpha
S3V	ATM-103	HA	U-238	DTC-109	ICP
			Pu-239	DTC-116	ICP
			Pu-239	DTC-127	alpha
S6V	ATM-106	HA	U-238	DTC-129	ICP
			Pu-239	DTC-134	ICP
			Pu-239	DTC-145	alpha
S9AJ	ATM-109A	HDR	U-238	DTC-39	ICP
			Pu-239	DTC-44	ICP
			Pu-239	DTC-55	alpha
S9CJ	ATM-109C	HDR	U-238	DTC-57	ICP
			Pu-239	DTC-62	ICP
			Pu-239	DTC-73	alpha
S9AV	ATM-109A	HA	U-238	DTC-147	ICP
			Pu-239	DTC-152	ICP
			Pu-239	DTC-163	alpha
S9BV	ATM-109B	HA	U-238	DTC-165	ICP
			Pu-239	DTC-170	ICP
			Pu-239	DTC-181	alpha
S9CV	ATM-109C	HA	U-238	DTC-183	ICP
			Pu-239	DTC-188	ICP
			Pu-239	DTC-199	alpha

* LDR = low drip rate; HDR = high drip rate; HA = saturated water vapor (humid air).
[a] Concentration data table number (Reference to tables in Appendix 2 of Finch et al. 2002).
[b] ICP = ICP-MS; alpha = alpha spectrometry
Note: The groundwater used in these tests is EJ-13 (refer to Finch et al. 2002 for details).

C. One-of-a-kind records

Supporting data are recorded in the scientific notebooks or are on file in the QA records at ANL.

D. Accuracy and Precision

Accuracy and precision of analytical measurements are estimated and discussed in this section. However, these measurement uncertainties do not include all components of experimental uncertainty. Factors such as differences in fuel segment inventories, pellet cracking patterns, or loss of fragments during test preparation or performance are not included in measurement uncertainties but are discussed below in the Uncertainties section.

Maximum estimates of measurement uncertainty were made for both ICPMS and gamma spectroscopy measurements based on replicate analyses of NIST-traceable standards analyzed according to approved standard operating procedures. For ICPMS, the maximum uncertainty is ±10% for elemental analyses and ±50% for nuclide analyses. Thus, the maximum measurement uncertainty is ±10% for reported elements such as potassium, calcium, and uranium, and ±50% for nuclides such as ^{90}Sr, ^{99}Tc, ^{129}I, ^{237}Np, and ^{239}Pu.

Solution volumes were determined by measuring the mass of an aliquot and dividing it by the density of the solution. All solution mass/volume determinations were made at ambient laboratory temperatures assuming that the density of the solutions was 1.0. The error associated with this assumption is around 0.2%. The weighed mass for aliquots for gamma and ICPMS analyses is typically 4 grams of solution with the balance accuracy being 0.0002 g. The relative magnitude of the error from this source is thus approximately 0.005% for each aliquot. The weighed mass for aliquots for alpha counting of the leachate, the 5-nm filtrate from the leachate, and the acid-strip is 0.20 g with the balance accuracy being 0.02 g. The magnitude of relative error from this source is thus approximately 10%.

The accumulation of indeterminate errors where the values with which the errors are associated are combined as sums or differences can be estimated by taking the square root of the sum of the squares of the individual absolute variances [Cunnane, 2001]. For example,

$$(S_y)^2 = (S_a)^2 + (S_b)^2 + (S_c)^2 + \ldots (S_n)^2 \qquad (1)$$

Where (S_y) is the standard deviation of the sum and (S_a), (S_b) and (S_c) are standard deviations of the values in the sum. The propagation of errors in the case of multiplication and division can be estimated in a similar way. For example,

$$(S_y)_r^2 = (S_a)_r^2 + (S_b)_r^2 + (S_c)_r^2 + \ldots (S_n)_r^2 \qquad (2)$$

Where in this case $(S_y)_r$ is the relative variance of the result of the multiplication or division calculation and $(S_a)_r$, $(S_b)_r$ and $(S_c)_r$ are the relative errors associated with the individual values in the calculation.

We can use this type of treatment to determine the dominant source of error in the data presented in this report. The values used in this estimate include errors associated with the density of water, the leachate mass determination, the aliquot mass determination and error associated with the analytical method.

Propagated Error for ICP-MS = $[(0.2)^2 + (0.005)^2 + (0.005)^2 + (50.0)^2]^{-0.5} = 50\%$

Propagated Error for Alpha data = $[(0.2)^2 + (0.005)^2 + (10.0)^2 + (50.0)^2]^{-0.5} = 51\%$

These error propagation estimates indicate that statistical errors in the analytical measurements dominate the uncertainties of these data. Similarly, it can be shown based on this methodology that the errors associated with derived quantities (e.g. see Table 4) that involve multiplications and divisions, such as nuclide fractional release values, will also be dominated by the errors associated with the analytical measurements (approximately ±50% for ICP-MS and alpha counting). Based on extensive characterization of ATM-103 and ATM-106 [Guenther, 1986 a,b], the uncertainty in the inventories is relatively small. ATM-109 has had significantly less characterization, but burnup analysis, gamma scan characterization, and inventory determination of selected nuclides was performed [Wolf et al., 2000]. A conservative value of ±10% is assigned to the estimate of uncertainty in fuel inventories. Thus, this source of uncertainty does not significantly increase overall uncertainties, as shown above, due to the relatively high errors associated with the analytical methods.

Uncertainties associated with these data and experiments include measurement uncertainties and uncontrolled experimental factors. Measurement uncertainties arise from determination of mass, calculation of volume, determination of particle sizes by filtration, and measurement of concentrations by ICPMS. Experimental uncertainties include localized inhomogeneity of nuclides in irradiated metallic uranium fuel, loss of sludge particles from the sample holder during sampling operations, and most significantly the extrapolation of results from only two samples of irradiated fuel.

Separation of nano-scale charged particles by means of filtration is subject to errors associated with charge interactions between particles and filter substrate and uncertainties associated with filtration of particles with irregular morphology. However, because excellent particle size agreement was observed for waste form colloids using three technically unrelated methods of colloid analysis (TEM, DLS, and filtration/ICP-MS), the uncertainty associated with colloid filtration is considered small. Together, these measurement errors are considered negligible relative to the maximum error associated with ICP-MS measurements which is ±50% for nuclides. Thus the measurement uncertainty for the values reported is estimated at ±50%.

E. Uncertainties

The primary sources of uncertainty, other than analytical accuracy and precision, associated with the unsaturated tests are: (1) those introduced by the original test design, (2) those introduced by reconfiguration of the experimental set-up, (3) those introduced from inevitable experimental problems, such as vessels going dry and small pieces of fuel falling into the leachate, and (4) those introduced by the uncontrolled experimental factors that may influence the dissolution behavior (nuclide release) of the spent fuel samples.

Some uncertainty about the nature of the colloids generated in the unsaturated tests is derived from the original experimental set-up due to a number of factors: the influence of pH and temperature, the flow of the groundwater over the fuel, the influence of the fuel holder's hole size at the base, and the sorption behavior in the leachate reservoir (or test vessel). These tests were designed to simulate CSNF degradation under a likely water contact scenario at YM, however, in terms of individual processes that occur, the data they yield is often difficult to interpret. One must attempt to deconvolute the various processes (sorption, diffusion, sedimentation, etc) effecting various experimental parameters of interest (i.e., the concentration of colloids generated during corrosion of CSNF).

First, the stability of colloids is known to be influenced by pH (which is dependent upon colloid phase composition and surface charge characteristics), thus the transport of any colloids from the local conditions at the fuel and holder to the solution in the vessel would most likely result in a large pH and solution chemistry difference. The solution in the bottom of the collection vessel most likely evolves during the test duration, but it will probably never represent the local pH at the surface of the fuel and alteration products. As such, large differences in the solution chemistries may promote lower concentrations of colloids through destabilization, deposition or sorption mechanisms.

The transport of colloids in an unsaturated environment is influenced by the film thickness of the groundwater [Wan and Wilson]. Wan and other researchers [Wan and Wilson, Wan and Tokunaga, Veerapaneni et al. 2000, Lenhart and Saiers] have shown that a critical thin film thickness for a given particle size exists which inhibits colloid transport. The film thickness in the CSNF drip tests is unknown and due to the large surface area introduced by the alteration products is probably very small compared with any colloids that would form. The even distribution of alteration products over the fuel surfaces in the ANL tests suggest that the groundwater dripped on fuel has contacted all the surfaces; there is no evidence of channeling on the fuel fragments.

Uncertainties caused by reconfiguration (e.g., changing sample retainers) and experimental problems (evaporation of leachate, spent fuel particles falling into leachate) have been clearly identified and discussed throughout the report and are clearly marked on data plots and data tables. For example, the data plots in Figures 2, 6, and 10 identify when the new gold mesh sample retainer was put in, when vessels went dry and when fuel fragments fell into the leachate. The amount of evaporation of leachate from the tests is reported in [Finch et al. 2002, Tables 8 to 18]. These tables show leachate volumes recovered during each sampling interval (Interval End Vol.), pH measured in the leachate and the total volume of leachate that would have been recovered ("expected") if all water injected during each test interval had been (based

on the nominal injection volume of 1.5 mL per week). The difference between volumes of leachate recovered and the expected volumes provide an indication of injection efficiency and vessel leakage during each test interval. The uncertainties from experimental reconfiguration and experimental problems should be treated on a sample by sample basis when using the data.

Another source of uncertainty related to the test configurations is caused by the fact that the tests are cooled from the 90°C test temperature to ambient laboratory temperature (around 25°C) for sampling. This procedure does not affect the total nuclide release or fractional release data, because any sorption or plating out of nuclides onto the steel vessel walls is captured in the acid strip procedure. However, this cooling may influence the leachate chemistry and the stability of colloids in solution. Thus, the measured nuclide concentrations may not accurately represent what the concentrations were at 90°C, as colloids may precipitate and aggregate upon cooling or the sorption to behavior on the stainless steel vessel may be enhanced. Thus, the data reported in Appendix 2 are free of assumptions about what the concentrations of any radionuclide might have been at any temperature besides ambient. Concentrations reported here are simply concentrations of radionuclides in an aqueous solution that has been in contact with a stainless steel vessel that had been cooled from 90°C to ambient over a relatively brief period (typically less than 30 minutes).

Some uncertainty in the reported data is also introduced by the fact that we do not directly measure some key experimental factors during the tests. The most important of these factors include pH and dissolved oxygen, which have been shown by Shoesmith (2000) to play important roles in the dissolution behavior of UO_2 and perhaps UO_2 spent fuels. These factors are known at the beginning of each test interval but their precise values or activities are uncertain during testing at 90°C. Additional discussion of these factors is found in the unsaturated UO_2 testing data report (Finch et al. 2002).

F. Data Verification

Data spreadsheets were verified according to ANL QA procedure, YMP-AP-005, "Administrative Procedure for Performance of Data Verifications."

IV. DISCUSSION

The following section discusses results on colloids from (A) unsaturated corrosion tests of commercial spent nuclear fuel and (B) saturated tests of uranium mineral phases. Background on the experiments and analytical techniques employed were presented in previous sections of this report.

A. CSNF Colloids Generated in Unsaturated Tests

Few colloids have been detected in the test solutions from unsaturated corrosion tests of commercial spent nuclear fuel under likely water contact scenarios at Yucca Mountain. Both dynamic light scattering (DLS) and filtration techniques used to characterize the colloids generated from the spent fuel tests gave consistent results. The results obtained from DLS will be discussed first.

The DLS results shown in Figure 3 represent the amount of colloids in the leachate from the commercial spent fuel tests on-going at Argonne National Laboratory (represented in Figure 3 according to fuel type: ATM-103, ATM-106, and ATM-109). No distinction was made in Figure 3 between the various corrosion tests (high drip, low drip, or humid air); nor between the ATM-109 fuel types (A, B, or C). The DLS measurements were made on an aliquot taken at a sampling period (represented as the total test duration for the fuel corrosion). While no distinction except for fuel type was made in Figure 3, all the individual DLS test results are listed in Appendix 1.

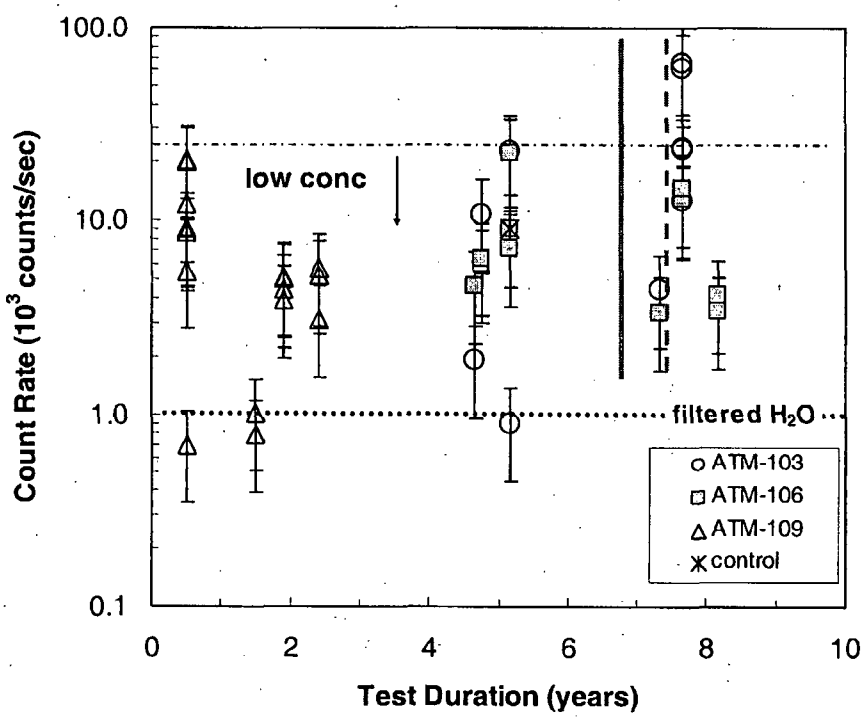

Figure 3. Relative amount of colloids present in leachates from commercial spent nuclear fuel tests sampled as a function of corrosion with EJ-13.
Note: The DLS results for the unsaturated drip tests are displayed for the ATM-103 (circle symbol), ATM-106 (square symbol), and ATM-109 (triangle symbols) fuels. The control tests for the ATM-103 and ATM-106 drip tests are displayed as the asterisk symbol. The solid (~6.8 yr) and dashed vertical lines (~7.3 yr) correspond to installation of a new zircaloy-4 retainer with 10 micron holes and a new gold screen with 200 micrometer holes, respectively.

As shown in Figure 3, the count rate is low (<30 kc/s) for the all of the unsaturated corrosion test leachates, except for one leachate at 7.7 years (ATM-103 HDR test). A low count rate indicates that particulates and/ or colloids are present in the leachate above the background of filtered water (< 1 kc/s). The count rate for the leachates from the 5.2 year ATM-103 high drip rate test and some of the ATM-109 tests were below the background for filtered water and thus colloids are not detected. Even the control test (test run with EJ-13 groundwater and no fuel) for the spent fuel unsaturated tests indicate a low count rate and the presence of particulate above the

background for filtered water. For the majority of the leachates analyzed for colloids using DLS, the size distribution was not resolved. Thus, even though a count rate above the background of filtered water indicates particulates are in the solution, the size distribution was not resolved with DLS due to the high polydispersity of the system and/or an unstable particulate suspension. While it is desirable to report a particle concentration for the spent fuel colloids, the conversion to a particle concentration from the DLS count rate is based upon the particle size and this was not possible for the majority of the leachates where the particle size was not resolved using DLS. Thus, the count rate for the CSNF leachates showed that only a small amount of particulate is present in the solutions above the background of filtered water.

The test configuration changes that occurred at 6.8 and 7.3 years (refer to Experimental Section for details) for the high drip rate ATM-103 and ATM-106 fuel tests were quite disruptive (fuel fragments and alteration products were transferred to new holder) and should have allowed a significant amount of colloidal material to be transported to the leachate. While the change to a new retainer with 10 micrometer holes and then later to a mesh with larger holes (200 micrometer holes) seemed to affect the amount of colloids and/ or particulate suspended in the leachate, the concentration remained low. The count rate for the samplings periods after the test configuration change was low and was similar to other sampling periods where the test configuration did not change. However, in one case, the count rate for the ATM-103 fuel high drip rate leachate at 7.7 years (after the 200 micron mesh test configuration change) indicated that some colloids were present and the size distribution was resolved (~150 nm) (See data in Appendix 1, Table A1-1). Since DLS is used to determine the size distribution of colloids and can not determine the composition of the colloids, ICP-MS and TEM are employed to get additional information about the colloids. Filtration results (from ICP-MS analyses) indicate that the uranium was associated with the particulate fraction (refer to the following section on ATM-103 colloids). As a low population of colloids was present, the composition of these colloids was not identified using TEM. These colloids appeared to be unstable and subsequently dropped to the very low concentration range when analyzed by DLS three months later.

Similar to the DLS results, very low concentrations of colloids were indicated from filtration results of plutonium and uranium concentrations in the leachates from the fuels tested under unsaturated conditions. The filtration results presented in this report focus on the U and Pu data since U is the primary constituent of the fuel and Pu is important for assessing the long-term performance of the fuel. The U and Pu concentrations associated with the colloidal fraction were bounded by the concentration in the unfiltered aliquot (supporting data is provided in the following section's discussion for the respective fuels).

Figure 4 shows the concentration of plutonium in the unfiltered leachate as a function of pH from all the fuels tested. No distinction was made in Figure 4 between the various corrosion tests (high drip, low drip, or humid air); nor between the ATM-109 fuel types (A, B, or C). The CSNF tests were run at 90°C and cooled to ambient laboratory temperature for sampling, thus literature data for Pu solubility in J-13 groundwater at 25 and 90°C is provided [Efurd]. For the majority of the CSNF fuel leachates, the plutonium concentration in the filtrates was bounded (set as an upper limit) by the Pu solubility limit in J-13 at 25° or 90°C or the concentration was below the detection limit for the alpha spectrometry or ICP-MS techniques. However, some Pu leachate concentrations were approximately an order of magnitude higher than the concentrations found in the majority of the tests and are at the solubility limit or supersaturated

for Pu in J-13. In these cases, the high Pu concentrations are explained by fragments of fuel that had been found in the leachate (fallen from the fuel retainer to the test solution at the base of the vessel). The filtration results from the high drip rate tests with the ATM-103 and ATM-106 fuels will be discussed in the following text. Only sporadic filtration data is available from the low drip rate and humid air CSNF tests; these will not be discussed here.

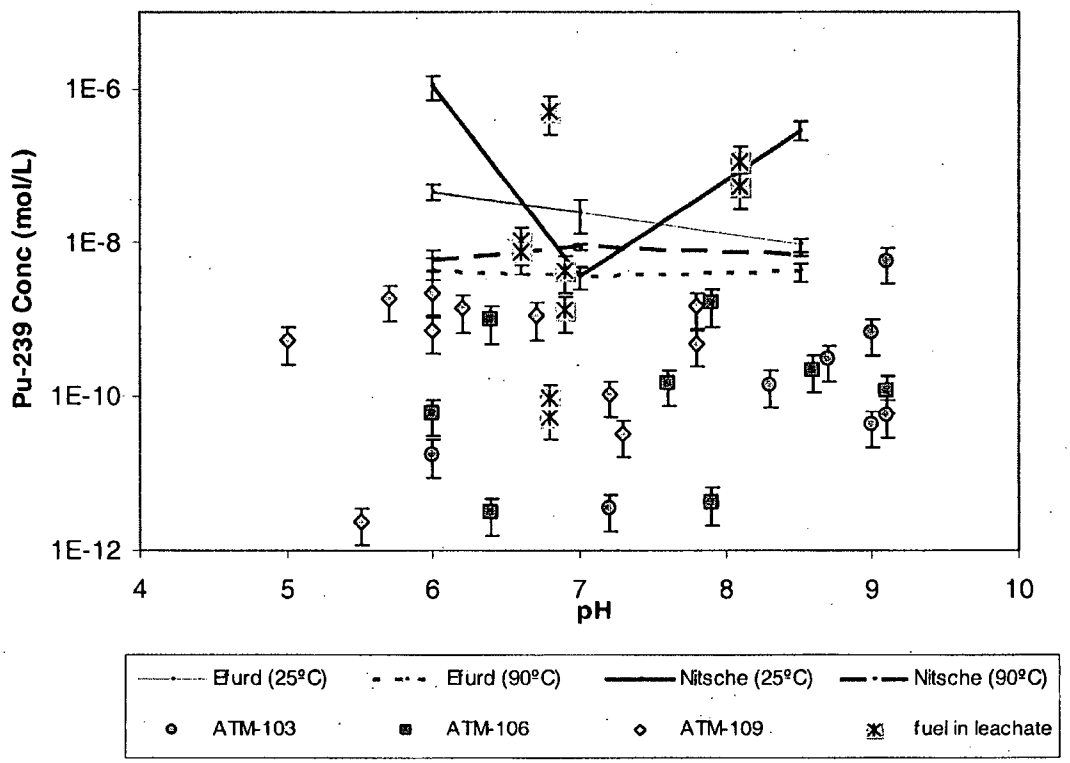

Figure 4. Plutonium concentration as a function of pH in unfiltered leachates from corrosion tests with CSNF.
Note: fuel in leachate = fuel fragments found in test solution.
Literature data for Pu in J-13 at 25 and 90°C [Efurd] is represented by the lines.

ATM-103 Fuel Colloids

The following section discusses results from high drip rate corrosion tests on the ATM-103 fuel. The high drip rate tests consistently had sufficient leachate available for colloidal analyses. The concentrations of U-238 and Pu-239 in the unfiltered leachates and filtrates from ATM-103 high drip rate corrosion tests are shown in Figure 5. (Data tables are given in Appendix 2.) The concentrations in the unfiltered leachates are an upper bound for the concentrations in the filtrates; the unfiltered leachates will be discussed first. The uranium concentration of the unfiltered leachate is on the order of 10^{-9} M at the 5.2 and 6.3 year samplings of the CSNF unsaturated tests (Figure 5a), while the samplings of the tests at 5.7, 7.3, 7.7, 8.2, and 8.7 are two to three orders of magnitude higher (uranium concentrations in the unfiltered leachate of 10^{-7} to 10^{-6} M; Figure 5a). It is important to note that test configuration changes to the spent fuel holder occurred at 6.8 and 7.3 years. Thus, the samplings at 7.3 and 7.7

years correspond to the leachates directly following the change to a new Zircaloy-4 retainer with 10 micrometer holes and then later to a gold-mesh with larger holes (200 micrometer holes), respectively. The highest concentration of U-238 corresponds to the holder change with the large diameter holes (new gold mesh retainer). While the test configuration changes can be used to explain the large releases, the relatively high concentration observed at 5.7 years (prior to the test holder change) is unexplained. The trends discussed above for U-238 were also observed for Pu-239 in the unfiltered leachates (Figure 5b). Next, the filtration data for uranium and plutonium will be discussed.

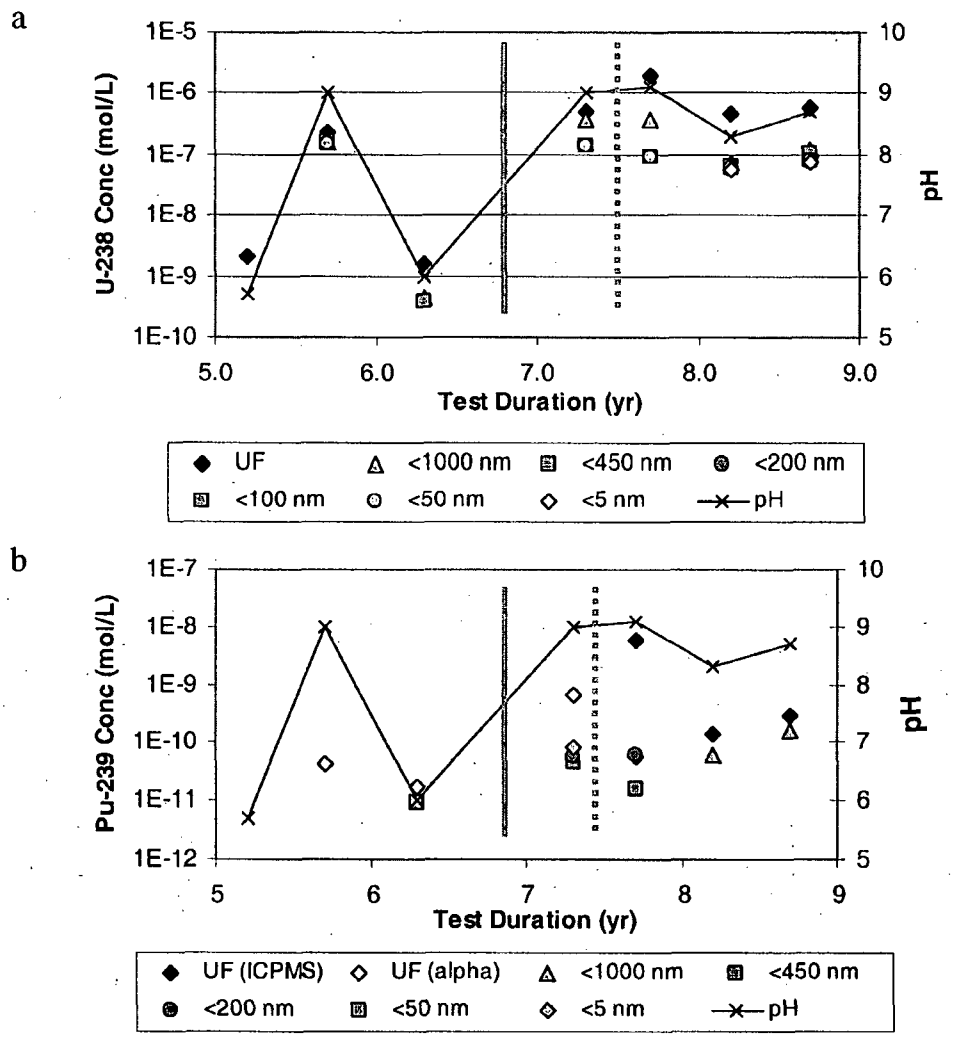

Figure 5. Concentration of (a) U-238 and (b) Pu-239, and pH of the test leachates as a function of test duration for the ATM-103 HDR test for sampling periods between 5.2 to 8.7 years. Note: Solid and open symbols are the unfiltered (UF) leachate and filtrate concentrations (see legend). The pH is represented by the x symbols and the line. The solid (~6.8 yr) and dashed vertical lines (~7.3 yr) correspond to installation of a new zircaloy-4 retainer with 10 micron holes and a new gold screen with 200 micrometer holes, respectively.

The concentration of U-238 and Pu-239 associated with various size fractions for the ATM-103 high drip rate corrosion test (HDR) sampled from 5.7 to 8.7 years is shown in Figure 6 and Table 6. The concentrations plotted in Figure 6 and the values in Table 6 were calculated from unfiltered leachates (UFL) and filtrate concentrations given in Finch 2002 (Appendix 2). As limited filtration data is available for Pu-239 (refer to Table 6), the U-238 data will be used predominantly to discuss the colloid releases. Filtration was not performed on the leachate from the 5.2 year sampling (one-third of the expected volume was recovered) and the vessel was dry at 6.8 years; thus no data is available for these sampling periods. While data for other uranium isotopes (U-234, U-235, and U-236) is available (Finch 2002), it is not presented here. The data presented for the U-238 size fractions in this section were consistent with the speciation (particulate, colloidal, and dissolved species) of the other uranium isotopes. No isotopic differences were expected for these leachates or filtrates and the concentrations of the uranium isotopes in the leachates are proportional to the amount in the fuel. The data on the filtrates will be discussed next.

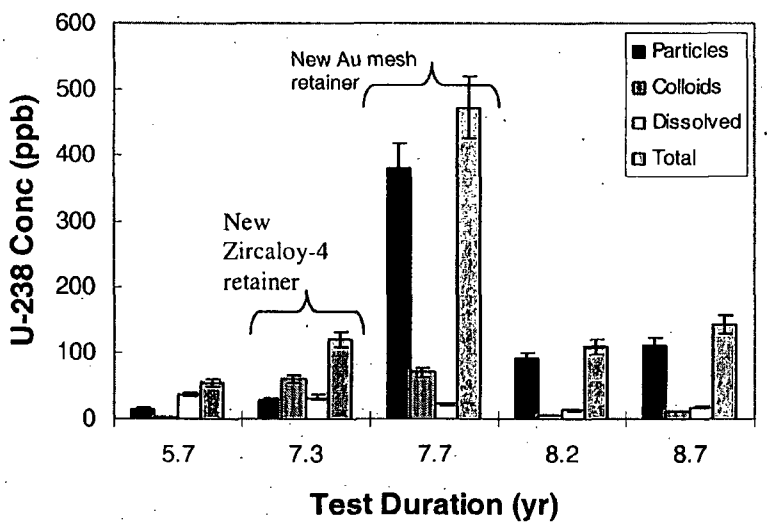

Figure 6. Uranium concentrations associated with particles, colloids, and dissolved species in leachates from ATM-103 HDR corrosion tests as a function of test duration.
Note: Concentration of the species were calculated from size fractions: $Conc_{particles}$ (>1000 nm), $Conc_{colloids}$ (50-1000 or 5-1000 nm), $Conc_{dissolved}$ (<50 nm or <5 nm) and $Conc_{Total}$ (unfiltered aliquot).

Table 6. Uranium and plutonium concentrations associated with various size fractions (particles, colloids, and dissolved) in leachates from ATM-103 HDR corrosion tests as a function of test duration.

Test Duration (yr)	$Conc_{particles}$ (ppb)	$Conc_{colloids}$ (ppb)	$Conc_{dissolved}$ (ppb)	$Conc_{particles}$ (ppb)	$Conc_{colloids}$ (ppb)	$Conc_{dissolved}$ (ppb)
Isotope	U-238	U-238	U-238	Pu-239	Pu-239	Pu-239
5.7	14	2.8	37	--	--	--
6.3	--	--	--	0.0019*	--	0.0023
7.3	28	60	33	0.15	0	0.019
7.7	380	71	22	--	--	--
8.2	91	4.9	13	--	--	--
8.7	110	12	18	--	--	--

Note: Concentration of the species were calculated from size fractions: $Conc_{particles}$ (>1000 or 450 nm), $Conc_{colloids}$ (50-1000 or 5-1000 nm), $Conc_{dissolved}$ (<50 nm or <5 nm). See Table 7 for filters sizes employed for filtration.

* This value is the concentration associated with particles + colloids, as UFL was used to calculate the concentration.

The uranium concentrations in filtrates from the 5.7 year sampling indicated that the main fraction was dissolved (70%) and a minor fraction was colloidal (~5%). At the 7.3 year sampling (first sampling subsequent to the placement of the new zircaloy-4 holder), approximately 50% of the uranium was in the colloidal fraction. The uranium concentration in the leachates after the test configuration change to the gold mesh retainer was dominated by the particulate fraction (represented by the difference between the concentration for the UFL and 1000 nm filter), where for these test sampling periods approximately 80% of the filtered uranium was the particulate fraction. The remaining 20% of the uranium was distributed almost evenly between the dissolved (represented by the concentration from the smallest filter) and colloidal fractions (represented by difference between the concentration for the largest and the smallest filters; refer to Table 6).

The importance of the colloids in the leachate was indicated by the ratio of the uranium concentration in solution after filtration through the largest filter ($Conc_{Coll+Diss}$) and the concentration from filtration through the smallest filter ($Conc_{Diss}$). Table 7 summarizes the colloid fraction for U-238 and Pu-239 being retained by the smallest filter. If no colloids are detected, this ratio is one. The filter sizes for the colloid and dissolved species varied for the test samplings. Filter sizes employed for the samplings are listed in Table 7. The dissolved fraction was <50 nm or <5 nm and the colloid fraction was one of the following ranges: 5-1000, 5-450, 50-1000, or 50-UFL. These definitions were based upon experimental constraints of available filters. Values for $Conc_{Coll+Diss}$ / $Conc_{Diss}$ were approximately one for most of the ATM-103 HDR corrosion tests. In the one case (at 7.3 years) where the U-238 and Pu-239 ratios can be compared, the ratio for the colloid fraction for U-238 and Pu-239 differ by a factor of three, indicating that sorption or self-coagulation of Pu-239 with particles >450 nm on the 450 nm filter membrane may have occurred. The 7.7 year sampling period had a factor of four increase in the uranium concentration associated with colloids and the increase corresponded to the test configuration change (placement of the new gold mesh retainer).

Table 7. Colloid fraction determined from ratio of nuclide concentration in ATM-103 HDR leachates after filtration through large and small filters as a function of test duration.

Test Duration (yr)	$Conc_{Coll+Diss}$ / $Conc_{Diss}$	Large/Small Filter Sizes (nm)	$Conc_{Coll+Diss}$ / $Conc_{Diss}$	Large/Small Filter Sizes (nm)
Isotope	U-238	U-238	Pu-239	Pu-239
5.7	1.1	1000/50	--	--
6.3	--	--	<1*	UFL/50
7.3	2.8	1000/50	<1	450/5
7.7	4.3	1000/50	--	--
8.2	1.4	1000/5	--	--
8.7	1.6	1000/5	--	--

Note: Concentration of the species were calculated from size fractions in Table 6.
$Conc_{Coll+diss}$ = concentration in filtrate from largest filter used.
$Conc_{Diss}$ = concentration in filtrate from smallest filter used.
* This ratio includes a contribution from particulate as the UFL was used to calculate the ratio.

ATM-106 Fuel Colloids

The following section discusses results from high drip rate corrosion tests on the ATM-106 fuel, as the high drip rate tests consistently had sufficient leachate available for colloidal analyses. The concentrations of U-238 and Pu-239 in the unfiltered leachates and filtrates from ATM-106 high drip rate corrosion tests are shown in Figure 7. (Data tables are given in Appendix 2.) The concentrations in the unfiltered leachates are an upper bound for the concentrations in the filtrates; the unfiltered leachates will be discussed first. The uranium concentration of the unfiltered leachate is on the order of 10^{-8} M at the 6.3 and 6.8 year samplings of the CSNF unsaturated tests (Figure 7a), while the samplings of the tests at 5.7, 7.3, 8.2, and 8.7 are an order of magnitude higher (uranium concentrations in the unfiltered leachate of 10^{-7}; Figure 7a). It is important to note that test configuration changes to the spent fuel holder occurred at 6.8 and 7.3 years. Thus, the samplings at 7.3 and 7.7 years correspond to the leachates directly following the change to a new Zircaloy-4 retainer with 10 micrometer holes and then later to a gold-mesh with larger holes (200 micrometer holes), respectively. The highest concentration of U-238 (1×10^{-6} M, Figure 7a) corresponds to the sampling at 5.2 years (prior to the test configuration changes) and the high uranium concentration is unexplained at this time. The next highest concentration of U-238 in the unfiltered leachate (7×10^{-7} M, Figure 7a) corresponds to the placement of the new gold-mesh retainer with the large diameter holes. The trends discussed above for U-238 were also observed for Pu-239 in the unfiltered leachates (Figure 7b). Next, the data for uranium and plutonium concentrations in filtrates will be discussed.

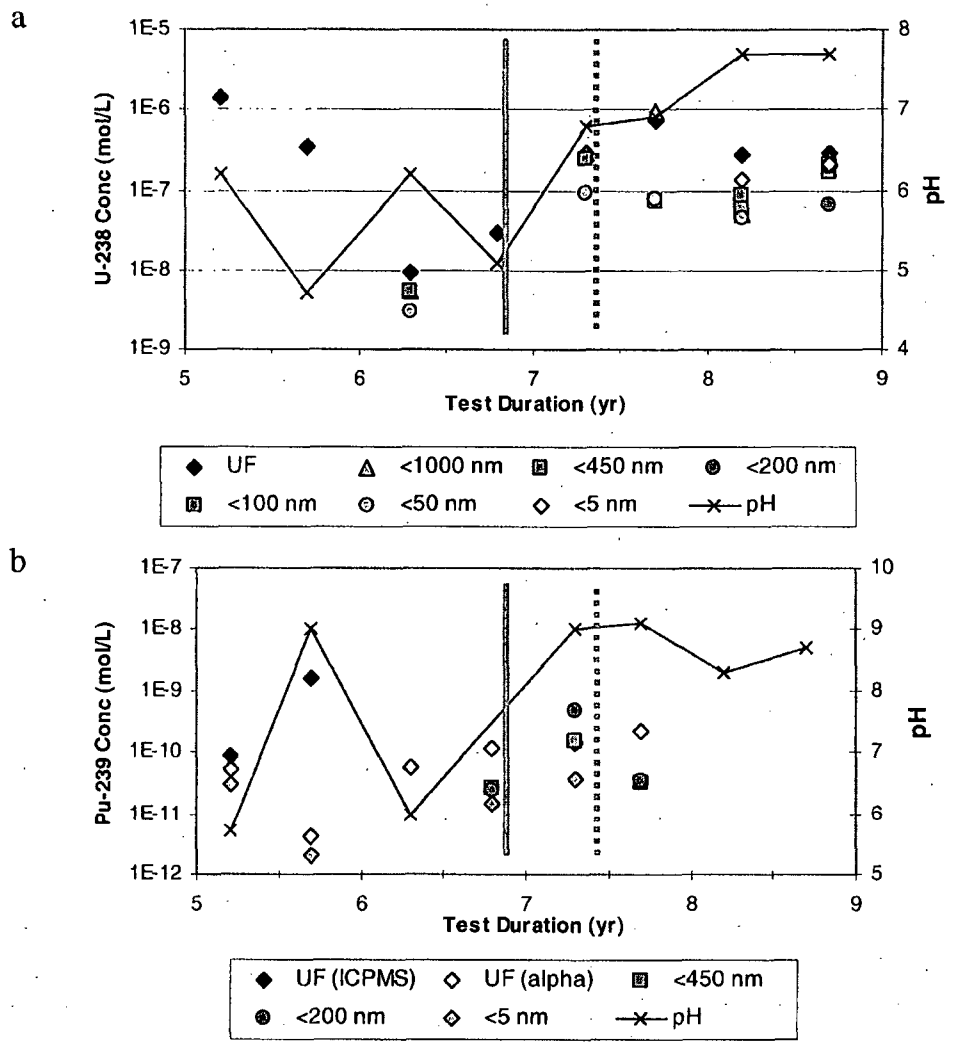

Figure 7. Concentration of (a) U-238 and (b) Pu-239, and pH of the test leachates as a function of test duration for the ATM-106 HDR test for sampling periods between 5.2 to 8.7 years. Note: Solid and open symbols are the unfiltered (UF) leachate and filtrate concentrations. The pH is represented by the x symbols and the line. The solid (~6.8 yr) and dashed vertical lines (~7.3 yr) correspond to installation of a new zircaloy-4 retainer with 10 micron holes and a new gold screen with 200 micrometer holes, respectively.

The concentration of U-238 and Pu-239 associated with various size fractions for the ATM-106 high drip rate corrosion test (HDR) sampled from 6.3 to 8.7 years is shown in Figure 8 and Table 8. The concentrations plotted in Figure 8 and the values in Table 8 were calculated from unfiltered leachate (UFL) and filtrate concentrations given in elsewhere (Appendix 2 in Finch 2002). As limited filtration data is available for Pu-239 (refer to Table 8), the U-238 data will be used predominantly to discuss the colloid releases. Filtrates were not submitted for ICP-MS analyses for the 5.2 and 6.8 year samplings where significant volumes losses occurred in the tests (only one-third and one-tenth of the expected volumes were recovered at 5.2 and 6.8 year samplings, respectively); thus no U-238 data is available for these sampling periods. In addition, filtrates were not submitted for ICP-MS analyses for the 5.7 year sampling, and no U-238 data is

available for this sampling period. While data for other uranium isotopes (U-234, U-235, and U-236) is available (Finch 2002), it is not presented here. The data presented for the U-238 size fractions in this section were consistent with the speciation (particulate, colloidal, and dissolved species) of the other uranium isotopes. No isotopic differences were expected for these leachates or filtrates and the concentrations of the uranium isotopes in the leachates are proportional to the amount in the fuel. The data on the filtrates will be discussed next.

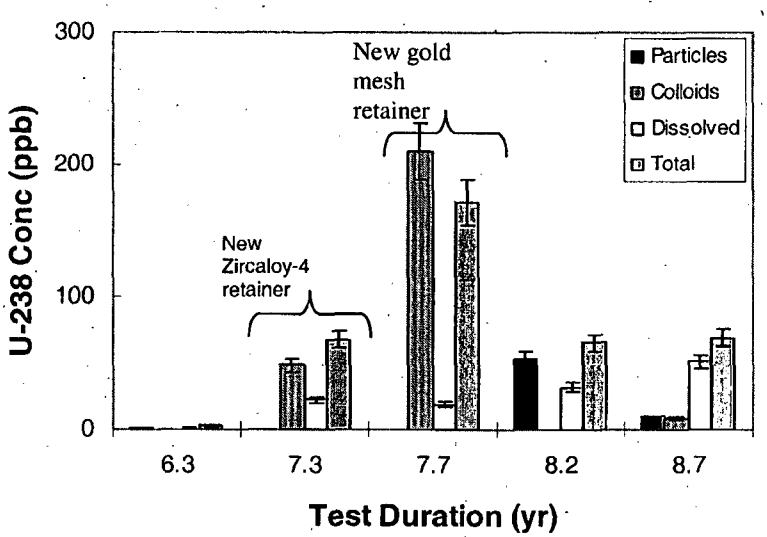

Figure 8. Uranium concentrations associated with particles, colloids, and dissolved species in leachates from ATM-106 HDR corrosion tests as a function of test duration.
Note: Concentration of the species were calculated from size fractions: $Conc_{particles}$ (>1000 nm), $Conc_{colloids}$ (50-1000 or 5-1000 nm), $Conc_{dissolved}$ (<50 nm or <5 nm) and $Conc_{Total}$ (unfiltered aliquot).

The speciation of uranium from the various sized filters varied greatly between sampling periods for the ATM-106 HDR corrosion tests (refer to Table 8). At 6.3 years, the uranium concentration was low and was almost evenly distributed between the particulate, colloidal and dissolved fractions (25-45%). The samplings at 7.3 and 7.7 years correspond to the leachates directly following the change to a new retainer with 10 micrometer holes and then later to a mesh with larger holes (200 micrometer holes) (refer to Section II.A.1 for details). At the 7.3 year sampling (first sampling subsequent to the placement of the new zircaloy-4 holder), approximately 70% of the uranium was in the colloidal fraction and 30% was in the dissolved fraction. The uranium concentration in the leachates after the test configuration change to the gold mesh retainer (7.7 year sampling) was also dominated by the colloidal fraction (~90%) with the remaining 10% of the uranium present as dissolved species less than 50 nm (refer to Figure 8 and Table 8. While the concentration of uranium in the unfiltered leachate increased subsequent to the test configuration changes (refer to Figure 7a at 7.3 and 7.7 year samplings), the concentration of uranium is less than or equal to the uranium concentration at samplings prior to the test configuration changes(5.2 and 5.7 year samplings). No speciation data was available for U-238 for the 5.2 and 5.7 year samplings, but Pu-239 data is available from alpha spectrometry analyses. Based upon the Pu-239 associated with various species (particulate, colloidal, and dissolved), the Pu-239 is evenly distributed between the particulate and/ or colloids (>5 nm

fraction) and dissolved species for the 5.2 and 5.7 year samplings. While the test configuration change appears to have caused the increase in the release of colloids, the other samplings periods (refer to 5.2 and 5.7 year samplings in Figure 7a) with similar or higher uranium concentrations in the unfiltered leachate are not be explained at this time. Sampling periods following the test configuration changes resulted in significantly less colloidal material being released. At 8.2 years, approximately 60% of the uranium in solution was found as particulate (>1000 nm), none in the colloidal fraction, and 40% as the dissolved fraction. At 8.7 years, ~70% of the uranium in the leachate was in the dissolved fraction.

Table 8. Uranium and plutonium concentrations associated with various size fractions (particles, colloids, and dissolved) in leachates from ATM-106 HDR corrosion tests as a function of test duration.

Test Duration (yr)	$Conc_{particles}$ (ppb)	$Conc_{colloids}$ (ppb)	$Conc_{dissolved}$ (ppb)	$Conc_{particles}$ (ppb)	$Conc_{colloids}$ (ppb)	$Conc_{dissolved}$ (ppb)
Isotope	U-238	U-238	U-238	Pu-239	Pu-239	Pu-239
5.2	--	--	--	0.0052 (a)*; 0.014 (i)*	--	0.0073
5.7	--	--	--	0.00054 (a)*; 0.38 (i)*	--	0.00047
6.3	0.95	0.56	0.70	--	--	--
6.8	--	--	--	0.022	0.0026	0.0035
7.3	0	48	22	--	--	--
7.3	--	--	--	0	0.029	0.0088
7.7	0	210	19	--	--	--
8.2	53	0	32	--	--	--
8.7	9.6	8.6	51	--	--	--

Note: Concentration of the species were calculated from size fractions: $Conc_{particles}$ (>1000 or 450 nm), $Conc_{colloids}$ (50-1000 or 5-1000 nm), $Conc_{dissolved}$ (<50 nm or <5 nm). See Table 7 for filters sizes employed in filtration. Shaded cells indicate that fuel was found in leachate at test sampling.
* This value is the concentration associated with particles + colloids
(a) alpha spectrometry data
(i) ICP-MS data

As previously discussed for the ATM-103 HDR tests, the importance of the colloids in the leachate was indicated by the ratio of the uranium concentration in solution after filtration through the largest filter ($Conc_{Coll+Diss}$) and the smallest filter ($Conc_{Diss}$). Table 9 summarizes the colloid fraction from ATM-106 HDR tests for U-238 and Pu-239 being retained by the smallest filter. If no colloids are detected, this ratio is one. The filter sizes for the colloid and dissolved species varied for the test samplings. Filter sizes employed for the samplings are listed in Table 9. The dissolved fraction was <50 nm or <5 nm, and the colloid fraction was one of the following ranges: 5-1000, 5-450, 50-1000, or 50-UFL. These definitions were based upon experimental constraints of available filters. Values for $Conc_{Coll+Diss}$ / $Conc_{Diss}$ were approximately 1-3 for most of the ATM-103 HDR corrosion tests. In the one case (at 7.3 years) where the U-238 and Pu-239 ratios can be compared, the ratio for the colloid fraction for U-238 and Pu-239 are in good agreement (3.2 versus 2.1, respectively), indicating that the U and Pu are associated with the same species in the leachate. The 7.7 year sampling period had a factor of 12

increase in the uranium concentration associated with colloids and the increase corresponded to the test configuration change (placement of the new gold mesh retainer). These colloids were low in concentration based upon DLS results (count rate of 13-15 kc/s from Appendix 1, Table A1-3). At the 5.2 year sampling, the ratios for Pu-239 from two different analysis techniques (alpha spectrometry and ICP-MS) are in good agreement. However, the ratio for the colloid fraction at the 5.7 year sampling determined from ICP-MS analysis is higher than the ratio from alpha spectrometry by 400 times. The value from the ICP-MS analysis appears to be highly questionable, since the ratio for the colloid fraction determined from alpha spectrometry analyses is consistent with ratios from other sampling periods.

Table 9. Colloid fraction determined from ratio of nuclide concentration in ATM-106 HDR leachates after filtration through large and small filters as a function of test duration.

Test Duration (yr)	$Conc_{Coll+Diss}$ / $Conc_{Diss}$	Large/Small Filter Sizes (nm)	$Conc_{Coll+Diss}$ / $Conc_{Diss}$	Large/Small Filter Sizes (nm)
Isotope	U-238	U-238	Pu-239	Pu-239
5.2	--	--	1.7 (a)*; 2.9 (i)*	UFL/5
5.7	--	--	2.1 (a)*; 810 (i)*	UFL/5
6.3	1.8	1000/50	--	--
6.8	--	--	1.7	450/5
7.3	3.2	1000/50	--	--
7.3	--	--	2.1	450/5
7.7	12	1000/50	--	--
8.2	<1	1000/5	--	--
8.7	1.2	1000/5	--	--

Note: Concentrations of the species were calculated from size fractions in Table 8.
$Conc_{Coll+diss}$ = concentration in filtrate from largest filter used.
$Conc_{Diss}$ = concentration in filtrate from smallest filter used.
(a) alpha spectrometry data
(i) ICP-MS data
* This ratio includes a contribution from particulate as the UFL was used to calculate the ratio.

In summary, the release of particulate or colloids from the ATM-103 and ATM-106 HDR tests seems to correlate well with a disruptive event such as the test configuration change (placement of fuel in holders with new retainers of larger pore sizes). However, those colloids or particulate in the leachates subsequent to the test configuration changes are low in concentration. The stability of these phases is unknown at this time.

B. Uranium Mineral Phase Colloids under Saturated Conditions

As uranium-based spent nuclear fuels will be prevalent at the high-level waste repository at Yucca Mountain (oxidizing conditions), we have examined the colloidal properties of a mixture of two uranium minerals under saturated conditions that promote stable colloids. This section presents results of analyses on colloidal suspensions of meta-schoepite, $((UO_2)_4)(OH)_6 \cdot 5H_2O$, and UO_{2+x}, in 10 mM uranyl nitrate or J-13 groundwater (a 1 mg/mL suspension of the uranium minerals in 10 mM uranyl nitrate (pH 5.1) or a 0.2 mg/mL suspension in J-13 groundwater (pH 7.7). The uranyl nitrate solution (10 mM and pH 4.8) was chosen since it is within a stable region for the meta-schoepite mineral. A suite of techniques was used to

characterize the colloids including dynamic light scattering, transmission electron microscopy, and zeta potential measurements (additional details can be found in Mertz et al., 2002).

TEM micrographs of typical uranium-based colloids (either meta-schoepite or uranium dioxide) observed in solution from tests with the 10 mM uranyl nitrate and J-13 groundwater solutions appear in Figure 9. The crystalline phase of the colloids was identified using electron diffraction. These colloid phases were found to span a large range of sizes from nanometers to particles exceeding several micrometers in at least one dimension. Large 200 nm colloids of meta-schoepite and UO_{2+x} were dominant in the 10 mM uranyl nitrate suspension (Figure 9 a and b). The colloids detected in the tests with J-13 groundwater (Figure 9 c and d) exhibited two colloid types: large 100- to 200-nm UO_{2+x} colloids and needle-like colloids of meta-schoepite (with extremely fine microstructure exhibited for the meta-schoepite colloids). Some evidence of uranyl silicates was noted, although these phases were rare.

The meta-schoepite and uranium dioxide colloids in 10 mM uranyl nitrate were monitored in situ using DLS from the initial solution preparation until 100 days later for changes in the size and concentration of the colloids. Replicate measurements for the sizing and concentration measurements are shown in Figure 10. The size of the colloids remains constant over the time period (average size of 216 $\pm$ 23 nm and 206 $\pm$ 7 nm, at 1 and 101 days after sampling, respectively). In addition, the size distribution remained the same (polydispersity of 0.20 $\pm$ 0.04 and 0.20 $\pm$ 0.05, at 1 and 101 days, respectively). The concentration of uranium substrate colloids was estimated using the 100 nm PS NIST standard curve fit equation (based upon the curve in Figure 1) which will overestimate the concentration for the 200 nm uranium substrate colloids. However, the concentration of the colloids decreased steadily over the hundred days implying sedimentation or sorption of the colloids occurred, since the size distribution remained constant.

Zeta potential measurements were performed on the meta-schoepite and uranium dioxide suspension (mixture) in 10 mM uranyl nitrate and on UO_{2+x} colloids in 1 mM $NaClO_4$ (Figure 11) to determine the zeta potential as a function of pH. The zeta potential curve for the meta-schoepite + UO_{2+x} colloidal suspension is unstable with respect to the zeta potential (<20 mV) at pH values $\leq$ 5. The UO_{2+x} colloids maintain a large negative zeta potential over the pH range of 2 to 11.5 (solid squares in Figure 11), indicating a stable colloidal suspension with zeta potentials > 20 mV. The point of zero charge (PZC) for $UO_{2.3}$ in the literature (3 and 4.5) [Parks] is in good agreement with the pzc of 2 determined for UO_{2+x} in 1 mM $NaClO_4$. Zeta potential measurements for the meta-schoepite and UO_{2+x} suspension in 10 mM uranyl nitrate indicated that the colloids are not stable at pH values less than or equal to five. In this pH region ($\leq$5), the zeta potential of the colloids is zero or slightly negative suggesting selective coagulation for a mixed colloidal suspension [Pugh]. A positive zeta potential for the meta-schoepite colloids could explain this behavoir and can be confirmed by zeta potential measurements on a suspension of meta-schoepite colloids. At pH values of 5.5 and higher, the meta-schoepite and UO_{2+x} colloids are stable and have zeta potential values of –30 to –60 mV. As a check of the stability and reproducibility of the ELS measurements, the zeta potential measurements were repeated at pH values of 5.5 and 7. The zeta potentials were in excellent agreement with measurements made one or two days earlier, thus indicating that the zeta potentials were reproducible and that the sample appeared to be stable.

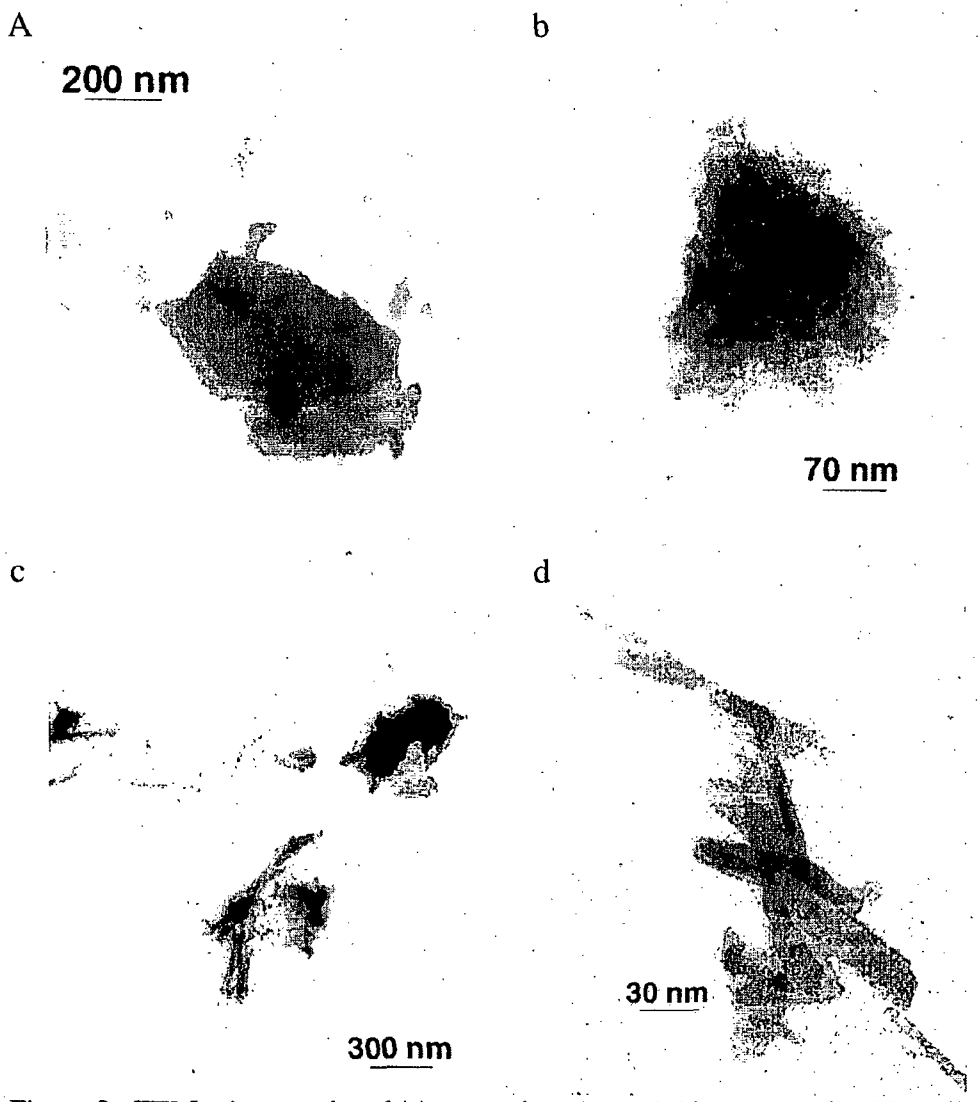

Figure 9. TEM micrographs of (a) metaschoepite and (b) uranium dioxide colloids from 10 mM uranyl nitrate, (c) metaschoepite (needle-like) and uranium dioxide (globular) colloids from J-13 groundwater, and (d) metaschoepite colloids from J-13 groundwater.

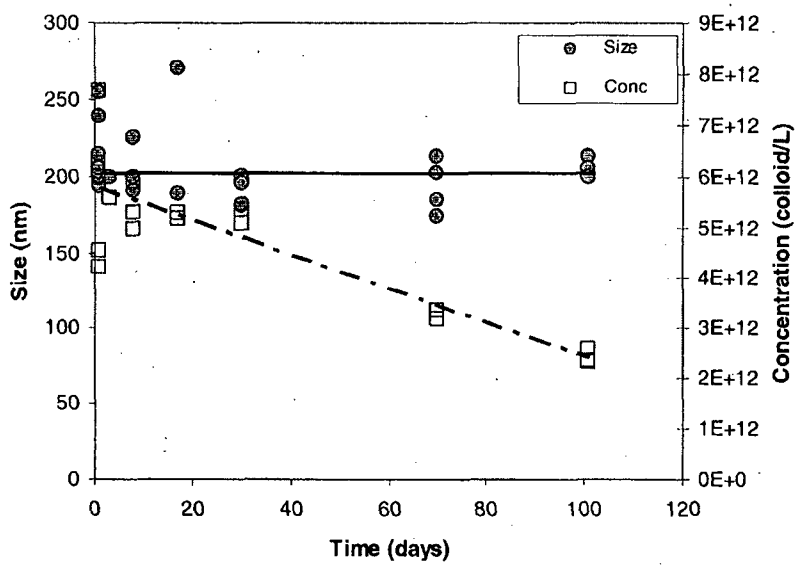

Figure 10. Colloid size (solid circles, solid line) and number concentration (open squares, dashed line) for meta-schoepite and UO_{2+x} suspension in 10 mM uranyl nitrate as a function of elapsed time from colloidal suspension preparation. Lines are drawn to show trends.

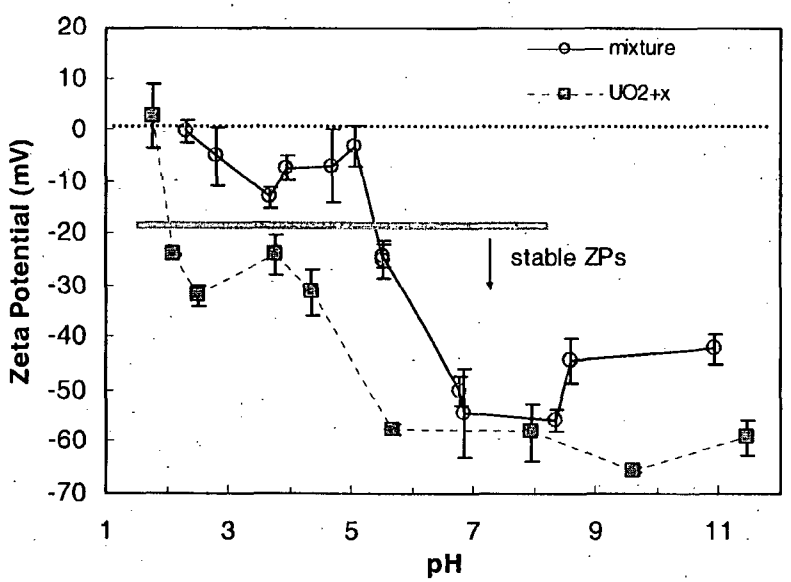

Figure 11. Zeta potential as a function of pH for a mixture of meta-schoepite and UO_{2+x} colloids in 10 mM uranyl nitrate (open circles, solid line) compared with UO_{2+x} colloids in 1 mM $NaClO_4$ (solid squares, dashed line). Error bars show standard deviation from multiple measurements.

As the colloids observed by TEM in this study were uranium substrate colloids, filtrates of the meta-schoepite and uranium dioxide in J-13 groundwater suspension were analyzed using ICP-MS to determine the uranium concentration associated with the various size fractions (Figure 12). The uranium that passed through the 5,000 nominal molecular weight filter is considered the dissolved fraction and corresponds to less than 2 nm. The colloidal fraction for these tests is defined as the uranium fraction between 2 and 450 nm. While uranium associated with a particulate fraction is greater than 450 nm in size (as with the CSNF tests, this is an operational definition and is limited by the largest filter). Of the total uranium present in solution, the largest fraction is the dissolved species (84%). Much smaller percentages of uranium are associated with the colloidal (12%) and the particulate (4%) fractions. The concentration of uranium in the colloidal fraction at 670 ppb appears to allow easy detection of colloids by TEM. The stability of these of these colloids with respect to dissolution or agglomeration can be confirmed with additional experiments.

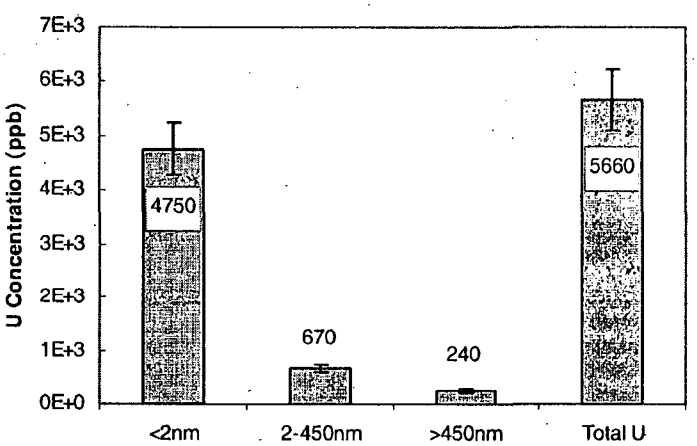

Figure 12. Concentration of uranium associated with various size fractions from a suspension of meta-schoepite and UO_{2+x} in J-13 groundwater. Results from filtration and ICPMS analyses of the suspension. Error bars show estimated accuracy of 10% for the ICPMS technique.

The results in this section show that colloidal suspensions of uranium substrate colloids are possible under repository relevant conditions, but the uranium speciation is dominated by the dissolved fraction. The meta-schoepite and uranium dioxide colloids presented in this paper are stable under short duration tests with respect to dissolution and interparticle interactions at near neutral and higher pH values. The size and concentration of the colloids can be used in transport models to suggest potential transport of these species in the subsurface. Additional characterization of these colloids and their long-term stability under various repository relevant scenarios are warranted.

REFERENCES

E.C. Buck and J.K. Bates (1999) "Microanalysis of Colloids and Suspended Particles from Nuclear Waste Glass Alteration," *Applied Geochemistry*, 14, 635-653.

J.C. Cunnane (2001) "YMP Guidelines Concerning Measurement Uncertainties." ANL QA # YMP-12-469.

CRWMS M&O (2000) Commercial Spent Nuclear Fuel Degradation in Unsaturated Drip Tests. Input Transmittal WP-WP-99432.T. Las Vegas, Nevada: CRWMS M&O ACC: MOL.20000107.0209.

W. L. Ebert and J. K. Bates (1993) "A Comparison of Glass Reaction at High and Low Glass Surface/Solution Volume," *Nuclear Technology,* 104, 372-384.

D.W. Efurd, W. Runde, J.C. Banar, D.R. Janecky, J.P. Kaszuba, P.D. Palmer, F.R. Roensch, and C.D. Tait (1998) *Environ. Sci. Technol.,* 32, 3893.

R.J. Finch, J.L. Jerden, Jr., C.J. Mertz, Y. Tsai, J.C. Cunnane, and P.A. Finn (2002) "Unsaturated Testing of Bare UO2 Fuel Fragments: Data Report," YMP Activity PAWC1M5.

P. A. Finn, E. C. Buck, M. Gong, J. C. Hoh, J. W. Emery, L. D. Hafenrichter, and J. K. Bates, (1994) "Colloidal Products and Actinide Species in Leachate from Spent Nuclear Fuel," *Radiochem, Acta,* 66/67, 189-195.

Geckeis, H., Grambow, B., Loida, A., Luckscheiter, B., Smailos, E., and Quinones, J. (1998) "Formation and Stability of Colloids under Simulated Near Field Conditions," *Radiochem. A*cta, 82, 123-128.

R. J. Guenther, D.E. Blahnik, T.K. Campbell, U.P. Jenquin, J.E. Mendel, L.E. Thomas, and C.K. Thornhill (1988a) "Characterization of Spent Fuel: Approved Testing Material – ATM-103," PNL-5109-103, April 1988, Richland, WA.

R. J. Guenther, D.E. Blahnik, T.K. Campbell, U.P. Jenquin, J.E. Mendel, and C.K. Thornhill (1988b) "Characterization of Spent Fuel: Approved Testing Material – ATM-106," PNL-5109-106, October 1988, Richland, WA.

C. H. Ho and N. H. Miller (1986) "Formation of Uranium Oxide Sols in Bicarbonate Solutions,"*J. Colloid Interface Sci.*, 113, 232-240.

A.B. Kersting, D.W. Efurd, D.L. Finnegan, D.J. Rokop, D.K. Smith, and J.L. Thompson, (1999) "Migration of Plutonium in Ground Water at the Nevada Test Site," *Nature*, 397, 56-59.

J.J. Lenhart and J.E. Saiers (2002) "Transport of Silica Colloids through Unsaturated Porous Media: Experimental Results and Model Comparisons," *Environ. Sci. Technol.* 36, 769-777.

C.J. Mertz, J.A. Fortner, and Y. Tsai (2002) "Understanding the Behavior and Stability of Some Uranium Mineral Colloids," Mater. Res. Soc. Proc., Fall 2002, Boston, MA, Submitted for publication.

N. Miekeley, H. Coutinho de Jesus, C. L. Porto da Silveira, and C. Degueldre (1992) *J. Geochem. Explor.*, 45, 409.

G.A. Parks (1964) "The Isoelectric Points of Solid Oxides, Solid Hydroxides, and Aqueous Hydroxo Complex Systems," 177-198.

R.J. Pugh (1992) "Selective Coagulation of Colloidal Mineral Particles," Colloid Chemistry in Mineral Processing, Vol. 12, Eds. J.S. Laskowski and J. Ralston, New York, NY: Elsevier, 268-271.

M. K. Schultz, "Sample Preparation for Low-Level Alpha-Spectrometry- Air Filters, Water, and Soils," ORTEC Technical Specifications and Recommendations.

P. Schurtenberger and M.E. Newman (1993) "Characterization of Biological and Environmental Particles Using Static and Dynamic Light Scattering," Environmental Particles, Vol. 2, J. Buffle and H.P. vanLeeuwen, Eds., Lewis Pub., Boca Raton, FL 37-115.

S.A. Short, R.T. Lowson, and J. Ellis (1988) *Geochimica et Cosmochimica Acta*, **52**, 2555.

S. Veerapaneni, J. Wan, and T.K. Tokunaga (2000) "Motion of Particles in Film Flow," *Environ. Sci. Technol.* 34, 2465-2471.

J. Wan and T.K. Tokunaga (1997) "Film Straining of Colloids in Unsaturated Porous Media: Conceptual Model and Experimental Testing," *Environ. Sci. Technol.* 31, 2413-2420.

J. Wan and J.L. Wilson (1994) "Colloid Transport in unsaturated porous media," *Water Resources Res.* 30, 857-864.

S.F. Wolf, D.L. Bowers, and J.C. Cunnane (2000) "Analysis of Spent Nuclear Fuel Samples from Three Mile Island and Quad Cities Reactors: Final Report" Chemical Technology Division, Argonne National Laboratory. YMP Data Report, ANL QA # YMP/SF-3A-319.

Appendix 1

Table A1-1. Summary of DLS Analyses on Leachates from ATM-103 Spent Fuel Corrosion Tests

Waste Form	Test Duration (months)	Test Type	Test Duration (yr)	Sample ID	Summary of DLS Analyses: Size[a] (nm)	Count Rate[b] (kc/s)	Conc[c] (particles/L)	Size Std Equation[d]	Data Reference: DLS Reference	SN / page	Comments
ATM-103	prior to 56	all	prior to 4.7	–	–	–	–	–	–	–	aliquots not available for DLS prior to 4.7 yr
ATM-103	56	low drip	4.7	S31J-56	NR	–	–	–	S31J56.dat	1381/90	
ATM-103	56	vapor	4.7	S3V - 56	NR	1.9	–	–	S3V56.dat	1381/83-85	
ATM-103	57	high drip	4.8	S32J - 57	NR	10.8	–	–	S32J57.dat	1381/89	
ATM-103	62	high drip	5.2	S32J - 62	NR	0.9	–	–	S32J62.dat	1381/172	
ATM-103	62	vapor	5.2	S3V - 62	NR	23.1	–	–	S3V62.dat	1381/172,173	
ATM-103	69	low drip	5.8	S31J - 69	–	–	–	–	–	–	
ATM-103	69	high drip	5.8	S32J -69	–	–	–	–	–	–	
ATM-103	75	high drip	6.3	S32J - 75	–	–	–	–	–	–	
ATM-103	88	high drip	7.3	S32J - 88	NR	4.399	–	–	Finn0600.sz2	1644/68	
ATM-103	92	high drip	7.7	S32J -92	NR	12.728	–	–	Finn1000.sz2	1644/115-116	monitored aliquot @ 8 days after sampling
ATM-103	92	high drip	7.7	S32J -92	161.4	61.3	2.452E+12	100 nm NIST	Finn1000.sz2	1644/115-116	monitored aliquot @ 8 days after sampling
ATM-103	92	high drip	7.7	S32J -92	150.0	66.3	2.652E+12	100 nm NIST	Finn1000.sz2	1644/115-116	monitored aliquot @ 8 days after sampling
ATM-103	92	high drip	7.7	S32J -92	–	23.6	9.44E+11	100 nm NIST	Finn1000.sz2	1644/115-116	monitored aliquot @ 9 days after sampling
ATM-103	92	high drip	7.7	S32J -92	139.5	–	–	–	Finn1000.sz2	1644/115-116	monitored aliquot @ 9 days after sampling
ATM-103	92	high drip	7.7	S32J -92	168.3	–	–	–	Finn1000.sz2	1644/115-116	monitored aliquot @ 9 days after sampling
ATM-103	92	high drip	7.7	S32J -92	–	23.8	9.52E+11	100 nm NIST	PF061401.sz2	1644/115-116	monitored aliquot @ 91 days after sampling
ATM-103	92	high drip	7.7	S32J -92	173.5	–	–	–	PF061401.sz2	1644/115-116	monitored aliquot @ 91 days after sampling
ATM-103	92	high drip	7.7	S32J -92	158.2	–	–	–	PF061401.sz2	1644/115-116	monitored aliquot @ 91 days after sampling
ATM-103	98	high drip	8.2	S32J -98	NR	4.23	–	–	PF041801.sz2	1644/164	
ATM-103	98	high drip	8.2	S32J -98	NR	3.884	–	–	PF041801.sz2	1644/164	

NR size distribution not resolvable using DLS
– not available or not analyzed
a Average colloid size determined by DLS
b Count rate determined using laser power of 3 mW (514.5 nm argon ion laser)
c Concentration calculated from count rate (at 3 mW) using equation for PS size standard indicated in Size Std Equation column.
d Equation for size standard that is closest in size to the spent fuel colloids (thus only for colloid sizes resolved by DLS).

Appendix 1

Table A1-2. Summary of DLS Analyses on Leachates from Control Tests for ATM-103 and ATM-106

Waste Form	Test Duration (months)	Test Type	Test Duration (yr)	Sample ID	Summary of DLS Analyses: Size [a] (nm)	Count Rate [b] (kcls)	Conc [c] (particles/L)	Size Std Equation [d]	Data Reference: DLS Reference	SN / page	Comments
control		all	prior to 4.7	--	--	--	--	--	--	--	aliquots not available for DLS prior to 4.7 yr
control	56	control	4.7	CC1J-56	NR	--	--	--	CC1J56.dat	1381/84-85	
control	62	control	5.2	CC1J-62	NR	9.0	--	--	CC1J62.dat	1381/172,173	
control	69	control	5.8	CC1J-69	--	--	--	--	--	--	

NR size distribution is not resolvable
-- not available or not analyzed
a Average colloid size determined by DLS
b Count rate determined using laser power of 3 mW (514.5 nm argon ion laser)
c Concentration calculated from count rate (at 3 mW) using equation for PS size standard indicated in Size Std Equation column.
d Equation for size standard that is closest in size to the spent fuel colloids (thus only for colloid sizes resolved by DLS).

Appendix 1

Table A1-3. Summary of DLS Analyses on Leachates from ATM-106 Spent Fuel Corrosion Tests

Waste Form	Test Duration (months)	Test Type	Test Duration (yr)	Sample ID	Summary of DLS Analyses: Size[a] (nm)	Count Rate[b] (kc/s)	Conc[c] (particles/L)	Size Std Equation[d]	Data Reference: DLS Reference	SN / page	Comments
ATM-106		all	prior to 4.7	--	-	-	-	--	--		aliquots not available for DLS prior to 4.7 yr .
ATM-106	56	vapor	4.7	S6V - 56	330	4.6	2.76E+09	300 nm NIST	S6V56.dat	1381/83-85, 133-134,187-188	
ATM-106	56	low drip	4.7	S61J-56	NR	-	-	--	S61J56.dat	1381/84-85	
ATM-106	57	high drip	4.8	S62J - 57	NR	5.9	-	--	S62J57.dat	1381/89-90	
ATM-106	57	high drip	4.8	S62J - 57	NR	6.4	-	--	S62J57.dat	1381/89-90	
ATM-106	62	high drip	5.2	S62J - 62	NR	22.5	-	--	S62J62.dat	1381/172	
ATM-106	62	vapor	5.2	S6V - 62	NR	7.2	-	--	S6V62.dat	1381/172,173	
ATM-106	62	vapor	5.2	S6V - 62	NR	9	-	--	S6V62.dat	1381/172,173	
ATM-106	69	high drip	5.8	S62J - 69	-	-	-	--	--	--	
ATM-106	69	vapor	5.8	S6V - 69	-	-	-	--	--	--	
ATM-106	75	high drip	6.3	S62J -75	-	-	-	--	--	--	
ATM-106	88	high drip	7.3	S62J - 88	NR	3.395	-	--	Finn0600.sz2	1644/68	
ATM-106	92	high drip	7.7	S62J -92	NR	13	-	--	Finn1000.sz2	1644/115-116	
ATM-106	92	high drip	7.7	S62J -92	NR	14.72	-	--	Finn1000.sz2	1644/115-116	
ATM-106	98	high drip	8.2	S62J -98	NR	4.135	-	--	PF041801.sz2	1644/164	
ATM-106	98	high drip	8.2	S62J -98	NR	3.416	-	--	PF041801.sz2	1644/164	

NR size distribution is not resolvable
\- not available or not analyzed
a Average colloid size determined by DLS
b Count rate determined using laser power of 3 mW (514.5 nm argon ion laser)
c Concentration calculated from count rate (at 3 mW) using equation for PS size standard indicated in Size Std Equation column.
d Equation for size standard that is closest in size to the spent fuel colloids (thus only for colloid sizes resolved by DLS).

Appendix 1

Table A1-4. Summary of DLS Analyses on Leachates from ATM-109A, B and C Spent Fuel Corrosion Tests

Waste Form	Gadolinium (%)	Test Duration (months)	Test Type	Test Duration (yr)	Sample ID	Summary of DLS Analyses: Size[a] (nm)	Count Rate[b] (kcls)	Conc[c] (particles/L)	Data Reference: DLS Reference	SN / page	Comments
ATM-109A	no	6	high drip	0.5	S9AJ -6	NR	12.1	--	1644/186	PF071701.sz2	
ATM-109A	no	6	high drip	0.5	S9AJ -6	NR	9.159	--	1644/186	PF071701.sz2	
ATM-109C	2%	6	high drip	0.5	S9CJ - 6	NR	20	--	1644/186	PF071701.sz2	
ATM-109C	2%	6	high drip	0.5	S9CJ - 6	NR	20.4	--	1644/186	PF071701.sz2	
ATM-109A	no	6	vapor	0.5	S9AV -6	NR	0.688	--	1644/186	PF071701.sz2	
ATM-109A	no	6	vapor	0.5	S9AV -6	NR	5.524	--	1644/186	PF071701.sz2	
ATM-109B	no	6	vapor	0.5	S9BV -6	NR	9.114	--	1644/186	PF071701.sz2	
ATM-109B	no	6	vapor	0.5	S9BV -6	NR	8.62	--	1644/186	PF071701.sz2	
ATM-109A	no	12	high drip	1.0	S9AJ-12	--	--	--	--	--	
ATM-109C	2%	12	high drip	1.0	S9CJ-12	--	--	--	--	--	
ATM-109A	no	12	vapor	1.0	S9AV-12	--	--	--	--	--	
ATM-109B	no	12	vapor	1.0	S9BV-12	--	--	--	--	--	
ATM-109A	no	18	high drip	1.5	S9AJ-18	NR	0.782	--	1644/63-64	Finn0600.sz2	
ATM-109C	2%	18	high drip	1.5	S9CJ-18	NR	1.014	--	1644/63-64	Finn0600.sz2	
ATM-109A	no	23	high drip	1.9	S9AJ-23	NR	3.88	--	1644/115-116	Finn1000.sz2	
ATM-109A	no	23	high drip	1.9	S9AJ-23	NR	4.41	--	1644/115-116	Finn1000.sz2	
ATM-109C	2%	23	high drip	1.9	S9CJ-23	NR	4.89	--	1644/115-116	Finn1000.sz2	
ATM-109C	2%	23	high drip	1.9	S9CJ-23	NR	5.09	--	1644/115-116	Finn1000.sz2	
ATM-109A	no	29	high drip	2.4	S9AJ - 29	NR	5.682	--	1644/164	PF041801.sz2	
ATM-109A	no	29	high drip	2.4	S9AJ - 29	NR	5.252	--	1644/164	PF041801.sz2	
ATM-109C	2%	29	high drip	2.4	S9CJ - 29	NR	3.089	--	1644/164	PF041801.sz2	
ATM-109C	2%	29	high drip	2.4	S9CJ - 29	NR	3.123	--	1644/164	PF041801.sz2	

NR size distribution is not resolvable
-- not available or not analyzed
a Average colloid size determined by DLS
b Count rate determined using laser power of 3 mW (514.5 nm argon ion laser)
c Concentration calculated from count rate (at 3 mW) using equation for PS size standard indicated in Size Std Equation column.
d Equation for size standard that is closest in size to the spent fuel colloids (thus only for colloid sizes resolved by DLS).

Appendix 2

Data tables for the concentration of Pu-239 and U-238 in leachates and filtrates of CSNF unsaturated tests (reported in units of moles/liter) for test intervals of 5.2 to 8.7 years (ATM-103 and -106 fuels) and 0.5 to 3 years (ATM-109 fuels). Concentrations in unfiltered leachates (UFL) and filtrates from various filters (1000, 450, 200, 50, and 5 nm) were analyzed by alpha spectrometry and ICP-MS and are reported in the following tables.

Table A2-1. Pu-239 Concentrations in ATM-103 HDR Tests

Fuel	Duration	Test Vol	Test	Pu-239 Concentration (in mol/L)						
(Test ID)	(years)	(mL)	pH	UFL (a)	UFL (i)	1000 (i)	450 (a)	200 (a)	50 (a)	5 (a)
ATM-103	5.2	13.55	5.7	bd	bd	--	--	--	--	bd
HDR	5.7	38.75	9.0	4.18E-11	bd	bd	--	--	--	bd
(S32J)	6.3	22.00	6.0	1.74E-11	bd	bd	--	--	9.50E-12	bd
	6.8	0	dry	--	--	--	--	--	--	--
	7.3	29.86	9.0	6.80E-10	bd	bd	4.60E-11	5.53E-11	--	8.07E-11
	7.7	23.96	9.1	5.67E-11	5.83E-09	bd	1.65E-11	6.32E-11	--	--
	8.2	36.7	8.3	--	1.41E-10	5.95E-11	--	--	--	--
	8.7	37.38	8.7	--	3.04E-10	1.57E-10	--	--	--	--

(a) alpha spectrometry data; (i) ICP-MS data

Table A2-2. Pu-239 Concentrations in ATM-103 LDR Tests

Fuel	Duration	Test	Test Vol	Pu-239 Concentration (in mol/L)		
(Test ID)	(years)	pH	(mL)	UFL (a)	UFL (i)	5 (a)
ATM-103	5.2	6.9	5.56	4.43E-09	1.31E-09	2.19E-10
LDR	5.7	7.2	6.88	3.48E-12	bd	--
(S31J)	7.3	dry	0.00	--	--	--

(a) alpha spectrometry data; (i) ICP-MS data

* shaded cells indicate that fuel was found in leachate

Table A2-3. Pu-239 Concentrations in ATM-103 HA Tests

Fuel	Duration	Test	Test Vol	Pu-239 Concentration (in mol/L)		
(Test ID)	(years)	pH	(mL)	UFL (a)	UFL(i)	5 (a)
ATM-103	5.2	6.6	9.14	1.04E-08	7.59E-09	1.95E-09
HA	5.7	nd*	2.02	--	5.31E-06	--
(S3V)	7.3	dry	0.00	--	--	--

(a) alpha spectrometry data; (i) ICP-MS data

* shaded cells indicate that fuel was found in leachate

Appendix 2

Table A2-4. Pu-239 Concentrations in ATM-106 HDR Tests

Fuel (Test ID)	Duration (years)	Test pH	Test Vol (mL)	Pu-239 Concentration (in mol/L) UFL (a)	UFL(i)	450 (a)	200 (a)	5 (a)
ATM-106	5.2	6.8	11.85	5.23E-11	9.00E-11	--	--	3.06E-11
HDR	5.7	7.9	38.00	4.21E-12	1.60E-09	--	--	1.97E-12
(S62J)	6.3	6	29.09	5.88E-11	bd	--	--	--
	6.8	9.1	4.47	1.18E-10	bd	2.57E-11	2.37E-11	1.48E-11
	7.3	7.6	21.61	1.44E-10	bd	1.59E-10	4.70E-10	3.67E-11
	7.7	8.6	28.33	2.20E-10	bd	3.17E-11	3.38E-11	--

(a) alpha spectrometry data; (i) ICP-MS data

* shaded cells indicate that fuel was found in leachate

Table A2-5. Pu-239 Concentrations in ATM-106 LDR Tests

Fuel (Test ID)	Duration (years)	Test pH	Test Vol (mL)	Pu-239 Concentration (in mol/L) UFL (a)	UFL(i)	5 (a)
ATM-106	5.2	dry	0	--	--	--
LDR	5.7	6.8	2.24	--	5.13E-07	5.12E-11
(S61J)	7.3	nd	0.27	2.02E-10	1.30E-08	--

(a) alpha spectrometry data; (i) ICP-MS data

* shaded cells indicate that fuel was found in leachate

Table A2-6. Pu-239 Concentrations in ATM-106 HA Tests

Fuel (Test ID)	Duration (years)	Test pH	Test Vol (mL)	Pu-239 Concentration (in mol/L) UFL (a)	UFL(i)	5 (a)
ATM-106	5.2	8.1	10.1	5.59E-08	1.17E-07	8.25E-10
HA	5.7	6.4	8.39	3.16E-12	9.77E-10	--
(S6V)	7.3	dry	0	--	--	--

(a) alpha spectrometry data; (i) ICP-MS data

* shaded cells indicate that fuel was found in leachate

Appendix 2

Table A2-7. Pu-239 Concentrations in ATM-109A HDR Tests

Fuel (Test ID)	Duration (years)	Test pH	Test Vol (mL)	Pu-239 Concentration (in mol/L) UFL (a)	UFL(i)	450 (a)	200 (a)	5 (a)
ATM-109A	0.4	5.7	38.41	1.87E-09	bd	–	--	--
HDR	1	5.5	19.02	2.38E-12	bd	–	--	5.13E-12
(S9AJ)	1.5	7.2	34.87	1.04E-10	bd	3.26E-11	2.93E-11	1.63E-11
	2	8.7	24.19	bd	bd	5.06E-12	bd	bd

(a) alpha spectrometry data; (i) ICP-MS data

Table A2-8. Pu-239 Concentrations in ATM-109A HA Tests

Fuel (Test ID)	Duration (years)	Test pH	Test Vol (mL)	Pu-239 Concentration (in mol/L) UFL (a)	UFL(i)
ATM-109A	0.4	6	9.52	7.16E-10	2.23E-09
HA	1	6.1	9.27	bd	bd
(S9AV)	1.5	dry	0.02	--	--

(a) alpha spectrometry data; (i) ICP-MS data

Table A2-9. Pu-239 Concentrations in ATM-109B HA Tests

Fuel (Test ID)	Duration (years)	Test pH	Test Vol (mL)	Pu-239 Concentration (in mol/L) UFL (a)	UFL(i)
ATM-109B	0.4	5	9.23	5.24E-10	bd
HA	1	7.3	9.85	3.15E-11	bd
(S9BV)	1.5	–	0.05	--	--
	3	dry	–	--	--

(a) alpha spectrometry data; (i) ICP-MS data

Table A2-10. Pu-239 Concentrations in ATM-109C HDR Tests

Fuel (Test ID)	Duration (years)	Test pH	Test Vol (mL)	Pu-239 Concentration (in mol/L) UFL (a)	UFL(i)	450 (a)	200 (a)	5 (a)
ATM-109C	0.4	6.2	36.70	1.36E-09	bd	–	--	--
HDR	1	7.9	29.93	bd	bd	–	--	--
(S9CJ)	1.5	7.8	14.20	4.72E-10	1.49E-09	4.64E-12	7.09E-12	1.12E-11
	2	8.8	19.18	--	bd	–	--	--

(a) alpha spectrometry data; (i) ICP-MS data

Table A2-11. Pu-239 Concentrations in ATM-109C HA Tests

Fuel (Test ID)	Duration (years)	Test pH	Test Vol (mL)	Pu-239 Concentration (in mol/L) UFL (a)	UFL(i)
ATM-109C	0.4	6.7	9.80	1.09E-09	bd
HA	1	6.4	0.72	--	bd
(S9CV)	1.5	–	0.03	--	--

(a) alpha spectrometry data; (i) ICP-MS data

Appendix 2

Table A2-12. U-238 Concentrations in ATM-103 HDR Tests

Fuel (Test ID)	Duration (yr)	U-238 Concentrations (in mol/L)							
		UFL	Strip	1000 nm	100 nm	50 nm	450 nm	200 nm	5 nm
ATM-103	5.2	2.18E-09	3.38E-07	--	--	--	--	--	--
HDR	5.7	2.27E-07	5.38E-07	1.66E-07	1.58E-07	1.54E-07	--	--	--
(S32J)	6.3	1.59E-09	1.89E-06	4.45E-10	3.74E-10	bd	--	--	--
	6.8	--	1.59E-06	--	--	--	--	--	--
	7.3	5.09E-07	2.93E-06	3.90E-07	1.42E-07	1.38E-07	--	--	--
	7.7	1.98E-06	3.63E-05	3.89E-07	9.20E-08	9.05E-08	--	--	--
	8.2	4.57E-07	1.67E-05	7.51E-08	6.47E-08	6.01E-08	6.14E-08	5.79E-08	5.43E-08
	8.7	5.98E-07	1.82E-05	1.24E-07	8.08E-08	8.08E-08	1.05E-07	7.69E-08	7.52E-08

Note: ICP-MS analyses for U-238 data.

Table A2-13. U-238 Concentrations in ATM-106 HDR Tests

Fuel (Test ID)	Duration (yr)	U-238 Concentrations (in mol/L)							
		UFL	Strip	1000 nm	100 nm	50 nm	450 nm	200 nm	5 nm
ATM-106	5.2	1.39E-06	3.24E-06	--	--	--	--	--	--
HDR	5.7	3.36E-07	4.64E-08	--	--	--	--	--	--
(S62J)	6.3	9.24E-09	7.68E-07	5.27E-09	5.36E-09	2.91E-09	--	--	--
	6.8	2.88E-08	6.08E-06	--	--	--	--	--	--
	7.3	2.83E-07	1.16E-05	2.94E-07	2.48E-07	9.28E-08	--	--	--
	7.7	7.18E-07	1.02E-04	9.59E-07	7.46E-08	7.94E-08	--	--	--
	8.2	2.73E-07	4.20E-05	4.99E-08	5.95E-08	4.50E-08	8.96E-08	5.40E-08	1.33E-07
	8.7	2.89E-07	1.62E-05	2.49E-07	2.11E-07	1.94E-07	1.68E-07	6.66E-08	2.14E-07

Note: ICP-MS analyses for U-238 data.

Appendix 3

Table A3-1. Summary of dynamic light scattering analyses on colloidal suspension of meta-schoepite and uranium dioxide in 10 mM uranyl nitrate (pH = 5.06).

Sample ID	time elapsed from prep (d)	d1 Size[a] (nm)	d2 Size[a] (nm)	Avg d1 size (nm)	d1 Std Dev (nm)	Count Rate[b] (kc/s)	Conc[c] (coll/L)	Avg Conc (coll/L)	Std Dev Conc (coll/L)	Poly-dispersity	Avg Poly	Std Dev Poly	Conc[c] (ug/mL)	Avg Conc (ug/mL)	Std Dev Conc (ug/mL)
CM1831/10-1	Initial sample prep date = 4/29/2002			--	--	--	--	--	--	--	--	--	--	--	--
CM1831/10-1	1	193.5	>1000	216	23	152	6.08E+12	5.79E+12	1.25E+12	0.241	0.204	0.035	3.62	3.44E+00	7.44E-01
CM1831/10-1	1	239	>1000			149	5.96E+12			0.186			3.55		
CM1831/10-1	1	214.6	>1000			113.6	4.54E+12			0.161			2.70		
CM1831/10-1	1	199.5	>1000							0.195					
CM1831/10-1	1	202.2	>1000			191.6	7.66E+12			0.240			4.56		
CM1831/10-1	1	254.7	>1000			156.1	6.24E+12			0.236			3.72		
CM1831/10-1	1	205.1				105.8	4.23E+12			0.167			2.52		
CM1831/10-1	3	199.6	>1000	200		139.5	5.58E+12	5.58E+12		0.314	0.314		3.32	3.32E+00	
CM1831/10-1	8	225.3	>1000	205	18	147.1	5.88E+12			0.856			3.50		
CM1831/10-1	8	199.7	>1000			132.3	5.29E+12			0.139			3.15		
CM1831/10-1	8	191.1	>1000			124.1	4.96E+12			0.197			2.95		
CM1831/10-1	17	270.3	>1000	230	58	128.8	5.15E+12	5.22E+12	9.33E+10	0.139	0.188	0.069	3.07	3.10E+00	5.55E-02
CM1831/10-1	17	188.7	>1000			132.1	5.28E+12			0.237			3.14		
CM1831/10-1	30			191	9	133.6	5.34E+12	5.20E+12	1.98E+11		0.354	0.237	3.18	3.10E+00	1.18E-01
CM1831/10-1	30	180.5	>1000			126.6	5.06E+12			0.776			3.01		
CM1831/10-1	30	182.4	>1000							0.292					
CM1831/10-1	30	198.1	>1000							0.221					
CM1831/10-1	30	200.2	>1000							0.245					
CM1831/10-1	30	195.8	>1000							0.237					
CM1831/10-1	70			194	18	84	3.36E+12	3.27E+12	1.22E+11		0.227	0.085	2.00	1.95E+00	7.24E-02
CM1831/10-1	70					79.7	3.19E+12						1.90		
CM1831/10-1	70	174.2	>1000							0.352					
CM1831/10-1	70	213.9	>1000							0.176					
CM1831/10-1	70	202.2	>1000							0.171					
CM1831/10-1	70	184.6	>1000							0.207					
CM1831/10-1	101	213.5	>1000	206	7	58.2	2.33E+12	2.42E+12	1.44E+11	0.243	0.204	0.048	1.39	1.44E+00	8.55E-02
CM1831/10-1	101	205.8	>1000			58.8	2.35E+12			0.151			1.40		
CM1831/10-1	101	199.7	>1000			64.7	2.59E+12			0.218			1.54		

a Colloid size determined by DLS; bimodal distribution (d1 = diameter of one population, d2 = diameter of second population, not resolved using DLS since beyond the range)

b Count rate determined using laser power of 3 mW (514.5 nm argon ion laser)

c Concentration calculated from count rate (at 3 mW) using equation for 100 nm NIST PS size standard.

YMP	**Model** **Error Resolution Document** *Complete only applicable items.*	QA: QA Page 1 of 50

1. Document Number: ANL-WIS-PA-000001	**2. Revision/Addendum:** REV 03	**3. ERD:** 02
4. Title: EBS Radionuclide Transport Abstraction	**5. No. of Pages Attached:** 49	

6. Description of and Justification for Change (Identify affected pages, applicable CRs and TBVs):

This Error Resolution Document (ERD) addresses issues identified in eight condition reports (CRs) associated with analysis/model report *EBS Radionuclide Transport Abstraction*, ANL-WIS-PA-000001 REV 03 [DIRS 177407], None of the changes documented in this ERD has any impact upon the conclusions of ANL-WIS-PA-000001 REV 03, nor on any downstream citation of ANL-WIS-PA-000001 REV 03, including the License Application (LA), the Final Environmental Impact Statement (FEIS), or the Supplemental Environmental Impact Statement (SEIS).

1) CR 12867 identifies a number of typographical errors, omissions, and needed clarifications in ANL-WIS-PA-000001 REV 03. Resolution of CR 12867 is addressed in Section I.

2) CR 12998 concerns the model for radionuclide sorption onto corrosion products that is developed in ANL-WIS-PA-000001 REV 03. In certain cases, the model may overestimate sorption of radionuclides, thereby underestimating releases. Resolution of CR 12998 is addressed in Section II.

3) CR 13093 identifies repository design data in ANL-WIS-PA-000001 REV 03, Section 4 and Appendix I, that are incorrectly referenced to certain tables in the design TSPA Data Input Package (TDIP) documents. The data are not found in the cited tables, but rather in other tables and figures in the design TDIPs. Resolution of CR 13093 is addressed in Section III.

4) CR 10788 addresses a procedural non-compliance regarding qualification of external source data used as direct input. A review of ANL-WIS-PA-000001 REV 03 revealed that most of the information required for the qualification of external data was presented in the document, but some of the documentation requirements of SCI-PRO-001, *Qualification of Unqualified Data*, were omitted. Resolution of CR 10788 is addressed in Section IV.

5) CR 13657 identifies incorrect references in Figures 7.2-13 and 7.2-14. Resolution of CR 13657 is addressed in Section V.

6) CR 13740 identifies errors in describing the concentration of competing cations in the validation of the competitive surface complexation model in ANL-WIS-PA-000001 REV 03, Section 7.2.3. Concentrations characterized as "highest" should be "lowest." Resolution of CR 13740 is addressed in Section VI.

	Printed Name	Signature	Date
7. Checker	Carl Axness	Robert MacKinnon for	06/18/09
8. QCS/QA Reviewer	Peter Persoff	Peter Persoff	06/17/2009
9. Originator	James D. Schreiber	James D. Schreiber	6/18/2009
10. Responsible Manager	Robert J. MacKinnon	Robert MacKinnon	06/18/09

INTENTIONALLY LEFT BLANK

(Block 6, Continued)

7) CR 13678 identifies two figures, Figures 6.5-10 and 6.5-11, in ANL-WIS-PA-000001 REV 03, Section 6.5.2.4.6 that contain illegible figure and axis labels. These figures are a matrix of plots shown together, but are of a very poor resolution. Resolution of CR 13678 is addressed in Section VII.

8) CR 13643 indicates that Eq. 6.5.1.2-9, p. 6-149, which describes the rate of formation of "embedded" colloids, incorrectly uses the aqueous concentration and should instead use the total concentration that includes the mass in all phases, both aqueous and stationary. Resolution of CR 13643 is addressed in Section VIII.

I. CR 12867 Resolution

In CR 12867, file "EBS RTA REV03 Typos 2008[1].doc" identifies 39 typographical errors, omissions, or clarifications needed in ANL-WIS-PA-000001 REV 03. In this section, 33 of those issues are addressed. The remaining 6 issues have been addressed in response to other CRs. Specifically, Item 16 in the CR 12867 file mentions that addition of a description of how parameter Diff_Path_Length_Invert_Top_a is computed on p. 6-191, following Eq. 6.5.2.3-5, would improve transparency; this issue was resolved in ANL-WIS-PA-000001 REV 03 ERD 01, pp. 6 – 8, in response to CR 11816. Item 15 in the CR 12867 file concerns a typographical error in reporting the ranges of this parameter on p. 8-18, Table 8.2-4; this was also resolved in ANL-WIS-PA-000001 REV 03 ERD 01, pp. 6 – 8, in response to CR 11816. Four other typographical errors involving FHH parameters (Items 11 – 14 in the CR 12867 file) were corrected in ANL-WIS-PA-000001 REV 03 ERD 01, pp. 6 – 8, in response to CR 11755.

CR 12867 is resolved by the following 33 changes (in which underlining indicates the original text to be changed and the revised text) to ANL-WIS-PA-000001 REV 03. Seven additional changes (#34 – #40) clarify text or correct errors that were identified subsequent to CR 12867 being issued. None of these changes impacts the conclusions of the document, and no downstream usage—neither the LA nor other project documents—is impacted. Changes to the DIRS that are noted below are marked up on the point-in-time DIRS report, and the revised DIRS report is processed in accordance with SCI-PRO-004, *Managing Technical Product Inputs*; the marked-up pages from the DIRS report are appended to this ERD.

1. p. 4-47, Table 4.1-20: Add row under "TAD Canister and Waste Package Characteristics" for: "Inner vessel length, 216.50 in., SNL 2007 [DIRS 179394], Table 4-3." This parameter is used on p. 6-166, Section 6.5.2.1.1.2, to compute the diffusive area for the path excluding the outer barrier, parameter Diff_Area_CSNF_2, of 29.9 m^2. The DIRS entry for SNL 2007 [DIRS 179394] in the DIRS list for ANL-WIS-PA-000001 REV 03 is modified to include this particular direct input, as follows:

DIRS entry for SNL 2007 [DIRS 179394] for ANL-WIS-PA-000001 REV 03

Table 4-3	Section 6.3.3.2.3;Tables 4.1-20 and 6.5-5	Outer corrosion barrier outside diameter; inner vessel outside diameter; outer corrosion barrier length; outer barrier thickness; outer lid thickness; inner vessel thickness	Direct Input	N/A	N/A	TBV-8615 Resolved

Revised DIRS entry for SNL 2007 [DIRS 179394] for ANL-WIS-PA-000001 REV 03 ERD 02

Table 4-3	Section 6.3.3.2.3;Tables 4.1-20 and 6.5-5	Outer corrosion barrier outside diameter; inner vessel outside diameter; outer corrosion barrier length; outer barrier thickness; outer lid thickness; inner vessel thickness; inner vessel length	Direct Input	N/A	N/A	TBV-8615 Resolved

2. p. 4-47, Table 4.1-20, 4th row from bottom: For entry "TMI canister guide tube cross section width," change source "p. 25" to "p. 30." This parameter is used in the output DTN: SN0703PAEBSRTA.001, file *5-DHLW-SNF DOE Long + TMI SNF + 21-PWR TAD 9-19-2007 Final TDIP.xls*, worksheet "5-DHLW-DOE Long + TMI SNF" to estimate masses of steels and corrosion products reported in Table 6.3-9 on pp. 6-88 – 6-89, Section 6.3.4.3.4.1. The DIRS entry for DOE 2003 [DIRS 164970] in the DIRS list for ANL-WIS-PA-000001 REV 03 is modified to include this particular input, which had not been listed. In addition, the input usage is revised to be Direct Input, rather than Indirect Input, since the inputs in this DIRS entry are used to obtain parameter Mass_Steel_CDSP_1b used in the TSPA. The DIRS entry is revised as follows:

DIRS entry for DOE 2003 [DIRS 164970] for ANL-WIS-PA-000001 REV 03

p. 30	Table 4.1-20	DSNF Characteristics - TMI canister guide tube length	Indirect Input	N/A	N/A	N/A

Revised DIRS entry for DOE 2003 [DIRS 164970] for ANL-WIS-PA-000001 REV 03 ERD 02

p. 30	Table 4.1-20	DSNF Characteristics - TMI canister guide tube length; TMI canister guide tube cross section width	Direct Input	Data	Qualified	N/A

3. p. 4-49, Table 4.1-22: Clarify that there are two different spread rings in the waste package: Change (3rd row) "Spread Ring" to "TAD Canister Spread Ring" and change (12th row) "Spread Ring" to "Waste Package Spread Ring." (The DIRS entry for the cited reference is not impacted because it does not identify individual waste package components.)

4. p. 6-6, bullet number 4, last line: Change "6.3.3.3)." to "6.3.3.2.5)."

5. p.6-19, 1st paragraph, line 5: Delete "A model of advective flow of water through stress corrosion cracking (SCCs) is presented in Section 6.3.3.1." (A SCC advective flow model is presented in the cited FEP, but not in ANL-WIS-PA-000001 REV 03.)

6. p.6-19, 1st paragraph, line 5: Change "6.3.3.3" to "6.3.3.2.5."

7. p.6-19, 1st paragraph, line 6: Change "6.3.3.4" to "6.3.3.3."

8. p.6-19, 1st paragraph, last line: Change "6.3.3.5" to "6.3.3.4." (Note: there is no section 6.3.3.5.)

9. p. 6-19, last line; p. 6-20, 1st 2 lines: Change "The TAD canister design has not been finalized; for purposes of estimating the masses of internal components, the Site-Specific Canister design is used for the TAD canister design (see Table 4.1-21 for a complete list of drawings used in this report)." to "The TAD canister design was not finalized until after analyses discussed in this report were completed; for purposes of estimating the masses of internal components, the Site-Specific Canister design was used for the TAD canister design (see Tables 4.1-20, 4.1-21, and 4.1-22 for a complete list of EBS component design information, component dimensions, and component masses and numbers, respectively, that are used in this report; see Table 4.1-23 for comparisons of component masses used in this report with final design values)."

10. p.6-20, Section 6.3.3.2, 1st paragraph, line 4: Change "Sections" to "Section."

11. p.6-27, Section 6.3.3.2.5, 1st paragraph, line 2: Change "thorough" to "through."

12. p.6-28, 1st paragraph after Equation 6.3.3.2.5-1, last line: Change "6.3.3.2.4" to "6.3.3.2.5." (Note: flow through stress corrosion cracks is not discussed until 6.3.3.2.5.)

13. p. 6-87, line 1: Change "6.3.3.1.1" to "6.3.3.1." (Note: there is no section 6.3.3.1.1.)

14. p. 6-88, Table 6.3-8: Clarify that there are 2 different spread rings in the waste package—one between the TAD shield plug and outer seal plate, the other between the inner top lid and outer (Alloy 22) lid. Change footnote b from "...Inner Seal Plug, Spread Ring, Spread Ring Filler Segment, ..., Inner Top Lid, Inner Bottom Lid" to "...Inner Seal Plug, TAD Spread Ring, Spread Ring Filler Segment, ..., Inner Top Lid, Overpack Spread Ring, Inner Bottom Lid."

15. p. 6-90, end of 1st paragraph: Change "approximately 1196 m^2" to "approximately 1195 m^2" (to be consistent with value reported in Table 6.3-10).

16. p. 6-90, 2nd paragraph, lines 2-7: Change "The volume inside the 21-PWR TAD waste package overpack outer corrosion barrier is calculated from dimensional data given in SNL 2007 [DIRS 179394], Table 4-3: The outer corrosion barrier outside diameter is 1.8816 m and thickness is 0.0254 m. The inside length is estimated from the inner vessel length of 5.4991 m and total outer corrosion barrier-inner vessel end-to-end gaps of 0.1128 m, which give an inside volume of 14.77 m^3 for the overpack. Then the initial void volume is 7.99 m^3" to "The volume inside the 21-PWR TAD waste package overpack outer corrosion barrier is

calculated from the following dimensional data given in SNL 2007 [DIRS 179394], Table 4-3: The outer corrosion barrier outside diameter is 1.8816 m and the wall thickness is 0.0254 m, so the outer corrosion barrier inside diameter is 1.8308 m. The outer corrosion barrier inside length is estimated by summing the enclosed inner vessel length of 5.4991 m, the outer corrosion barrier-inner vessel end-to-end top gap of 0.0445 m, and the outer corrosion barrier-inner vessel end-to-end bottom gap of 0.0683 m, for a total inside length of 5.6119 m. With these dimensions, the cylindrical overpack outer corrosion barrier has an inside volume of 14.77 m^3. Then, subtracting the volume of solid components contained within the overpack (6.82 m^3, from Table 6.3-10), the initial void volume is 7.95 m^3." (Note that the initial average porosity of 0.54 reported at the end of this sentence is unchanged by this correction.)

17. p. 6-91, Table 6.3-10: Change fuel rod total surface area "636.93" to "636.94." (Note: the calculation following Table 6.3-10, footnote d, gives 636.9367, correctly rounded to 636.94.)

18. p. 6-91, Table 6.3-10: Entry for Total Volume of Fuel Basket C-Plate needs to be aligned with rest of column; entries in Total Mass column for Spread Ring, Outer Seal Plate, and Total need to be aligned with rest of column. (Total value is misaligned due to footnote superscript; the number should be right-aligned, with footnote superscript extending beyond alignment to the right.)

19. p. 6-91, Table 6.3-10: Since *all* of the Total Mass values are the preliminary values listed in Table 4.1-23, delete the footnote f on Component names in the Component column as well as footnote f itself. In footnote a referring to Total Mass values, change "SNL 2007 [DIRS 179394], Tables 4-3 and A-1, except for preliminary values listed in Table 4.1-23." to "Preliminary values listed in Table 4.1-23." The DIRS entries are revised as follows (new DIRS entries are not shown in the appended DIRS mark-up but are listed in Attachment I):

DIRS entries for SNL 2007 [DIRS 179394] for ANL-WIS-PA-000001 REV 03

Table 4-3	Section 6.3.4.3.4.2	The volume inside the 21 PWR TAD waste package overpack outer corrosion barrier	Indirect Input	N/A	N/A	TBV-8615 Resolved
Table 4-2	Tables 4.1-21 and 6.5-5; Section 6.3.4.3.4.2	Component Dimensions in a 21-PWR Site-Specific Canister	Direct Input	N/A	N/A	TBV-8615 Resolved

Revised/new DIRS entries for SNL 2007 [DIRS 179394] for ANL-WIS-PA-000001 REV 03 ERD 02

Table 4-3	Section 6.3.4.3.4.2	Dimensional data for a 21 PWR TAD waste package overpack outer corrosion barrier	Indirect Input	N/A	N/A	TBV-8615 Resolved

Table 4-2	Tables 4.1-21 and 6.5-5	Component Dimensions in a 21-PWR Site-Specific Canister	Direct Input	N/A	N/A	TBV-8615 Resolved
Tables A-1 and A-3	Section 6.3.4.3.4.2; Table 6.3-10	Typical measurements and surface areas for 21-PWR TAD waste package components	Indirect Input	N/A	N/A	N/A

20. p. 6-143, full line before Equation 6.5.1.1.3-1: Change "6.3.3.3" to "6.3.3.2.5."

21. p. 6-143, last full paragraph (starting with "As with the drip"), last sentence: Change "to 1.022 m –or a 5-_DHLW" to "to 1.022 m for a 5-DHLW." (Note: no space after "5-.")

22. p. 6-163: Change bold heading "**CSNF Waste Packages Properties**" to section heading "**6.5.2.1.1 CSNF Waste Packages Properties.**" (Since the Table of Contents lists sections only to three levels, e.g., 6.5.2, this change does not impact the Table of Contents.)

23. p. 6-166, 2nd full paragraph (starting with "The diffusive areas"), 3rd line: Change "(radius of 0.819 m, from Section 2.4.2.1)" to "(radius of 0.819 m, from outside diameter of 66.5 in. (SNL 2007 [DIRS 179394], Section 4.1.1.1); and 1.00 in. thickness, (SNL 2007 [DIRS 179394], Table 4-2))." (The DIRS entries for this reference in the DIRS list for ANL-WIS-PA-000001 REV 03 are not impacted because these same data are cited and used in the same way in the preceding paragraph in this section.)

24. p. 6-174, Table 6.5-5, 6th row from bottom: Change heading "Component and Source" to be centered instead of left-justified.

25. p. 6-176, Table 6.5-7, Comments for Specific surface area of NiO and Cr_2O_3: Change "Based on data in Table 6.3-10" to "Based on data in Table 6.3-7" (changes in 2 rows).

26. p. 6-180, Figure 6.5-4 caption: Delete "Constant RH." (Plot is water saturation as a function of RH.)

27. p. 6-181, Figure 6.5-5 caption: Delete "Constant RH." (Plot is water saturation as a function of RH.)

28. p. 6-189, Figure 6.5-8 caption: Change "Constant RH" to "Constant RH = 95%."

29. p. 6-231, last line before Section 6.5.2.7.2: Change "FEP Number 2.1.13.01A" to "FEP Number 2.1.13.01.0A." This same correction is needed in the DIRS entry for the cited reference (DTN: MO0706SPAFEPLA.001 [DIRS 181613]), used in Section 6.5.2.7.1, in the DIRS list for ANL-WIS-PA-000001 REV 03. See Item 32 below for the revised DIRS entry.

30. p. 6-255, 3rd line: Change "3.77×10^{-5} mol m^{-3}" (molar density of ideal gas) to "3.77×10^{-5} mol cm^{-3}."

31. p. 6-255, 2nd paragraph (starting with "The maximum diffusion"): Change "1196 m^2 (from Table 6.3-11)" to "1195 m^2 (from Table 6.3-10)." (Note: 2 errors corrected.)

32. p. 6-304, 1st full paragraph (starting with "The drip shield"), 4th line: Change "FEP Number 2.1.08.11.0A" to "FEP Number 2.1.08.14.0A." This same correction is needed in the DIRS entry for the cited reference (DTN: MO0706SPAFEPLA.001 [DIRS 181613]), used in Section 6.7, in the DIRS list for ANL-WIS-PA-000001 REV 03. The DIRS entries for DTN: MO0706SPAFEPLA.001 [DIRS 181613] are revised as follows:

DIRS entries for DTN: MO0706SPAFEPLA.001 [DIRS 181613] for ANL-WIS-PA-000001 REV 03

FEP Number 2.1.13.01A	Section 6.5.2.7.1	Radiolysis is screened out.	Indirect Input	N/A	N/A	N/A
FEP Number 2.1.08.14.0A	Sections 6.3.3.2.5 and 6.3.3.3	Dripping onto the waste package from condensation on the underside of the drip shield is screened out.	Indirect Input	N/A	N/A	N/A
FEP Number 2.1.08.11.0A	Section 6.7	Condensation on the underside of the drip shield screened out.	Indirect Input	N/A	N/A	N/A

Revised DIRS entries for DTN: MO0706SPAFEPLA.001 [DIRS 181613] for ANL-WIS-PA-000001 REV 03 ERD 02

FEP Number 2.1.13.01.0A	Section 6.5.2.7.1	Radiolysis is screened out.	Indirect Input	N/A	N/A	N/A
FEP Number 2.1.08.14.0A	Sections 6.3.3.2.5, 6.3.3.3, and 6.7	Dripping onto the waste package from condensation on the underside of the drip shield is screened out.	Indirect Input	N/A	N/A	N/A
~~FEP Number 2.1.08.11.0A~~	~~Section 6.7~~	~~Condensation on the underside of the drip shield screened out.~~	~~Indirect Input~~	~~N/A~~	~~N/A~~	~~N/A~~

33. p. 6-304, 2nd full paragraph (starting with "The waste package"), 10th line: Change "6.3.3.3" to "6.3.3.2.5."

34. p. 6-224, 3rd definition following Equation 6.5.2.5-22, for "effective diffusive conductance between UZ fracture and matrix cells": Change "$\hat{D}_{ilf}$" to "$\hat{D}_{imf}$." This error was not identified in CR 12867.

35. p. 5-3, 2nd paragraph of *Basis*, 10th line: Change "Since the lifetime of stainless steel components ranges from 49,800 yr to 5.08×10^6 yr (as estimated in Section 6.5.2.2.1)" to "Since the lifetime of stainless steel components ranges from 49,800 yr to 2.54×10^6 yr (depending on component thickness, as estimated for the inner vessel in Section 6.5.2.2.1)". This error was not identified in CR 12867.

36. p. 6-181, 11th line: Change "For stainless steel, the lifetime ranges from 49,800 yr to 5.08 × 10^6 yr" to "For stainless steel, the lifetime ranges from 49,800 yr to 2.54 × 10^6 yr." This error was not identified in CR 12867.

37. p. 6-181, 11th line: Change "For carbon steel, the lifetime ranges from 118 yr to 1,270 yr" to "For carbon steel, the lifetime ranges from 118 yr to 635 yr." This error was not identified in CR 12867.

38. p. 6-187, last line, and p. 6-188, 1st line: Change "In this example, stainless steel has a lifetime of 20,800 yr" to "In this example, stainless steel has a lifetime of 20,800 yr, based on the maximum component thickness of 9.525 mm in this domain (Table 6.5-5) and a corrosion rate of 0.229 μm yr^{-1}." This clarification is needed because an earlier statement (clarified in Item #35 above) could have been interpreted to mean that the *minimum* lifetime of stainless steel components is 49,800 yr. This clarification was not identified in CR 12867.

39. p. 6-218, paragraph preceding Eq. 6.5.2.5-1, 2nd line: Change "(Equation 6.5.1.2-48)" to "(Equation 6.5.1.2-47)." This error was not identified in CR 12867.

40. pp. 6-234 – 6-235; several equation number references need to be corrected. These errors were not identified in CR 12867.

    a. p. 6-234, paragraph following Eq. 6.5.2.7.2-8: Change "Equation 6.5.2.7-1" to "Equation 6.5.2.7.2-1" (2 occurrences).
    b. p. 6-234, sentence preceding Eq. 6.5.2.7.2-10: Change "Equation 6.5.2.7-1" to "Equation 6.5.2.7.2-1."
    c. p. 6-235, sentence following Eq. 6.5.2.7.2-14: Change "Equations 6.5.2.7-13 and 6.5.2.7-14" to "Equations 6.5.2.7.2-13 and 6.5.2.7.2-14."
    d. p. 6-235, sentence following Eq. 6.5.2.7.2-14: Change "Equations 6.5.2.7-6 and 6.5.2.7-7" to "Equations 6.5.2.7.2-6 and 6.5.2.7.2-7."

II. CR 12998 Resolution

CR 12998 points out that, in certain modeling cases in the License Application TSPA (TSPA-LA), sorption of radionuclides onto steel corrosion products is over-predicted, with the nonphysical result that the number of moles of radionuclide sorbed exceeds the number of sorption sites available. This occurs in approximately 5% of the simulations in the TSPA-LA (Figure 1), primarily in the Igneous Intrusion Modeling Case for 10,000 years. To resolve CR 12998, the potential impact of the overestimation of sorption on the predicted mean annual dose is evaluated in this ERD by developing a supplemental sorption model that is more accurate under the conditions where the current sorption model breaks down. This supplemental model was tested in a subset of the TSPA-LA analysis to show that an improved sorption model has an insignificant impact on repository performance, i.e., on predicted dose. Since the impact is insignificant, no further action is required to resolve CR 12998. No downstream usage—neither the LA nor other project documents—is impacted.

II.1. Input Data

The models run for this analysis use the same inputs to the TSPA-LA model and are documented in *Total System Performance Assessment Model /Analysis for the License Application* (SNL 2008 [DIRS 183478], Section 4[a]), except where indicated in the Section II.3 below. The source of the regression coefficients for the sorption model in the TSPA-LA is *EBS Radionuclide Transport Abstraction* (SNL 2007 [DIRS 177407], Table 6.5-14).

II.2. Software

The software codes used for this analysis were from the same set of software codes used to run the TSPA-LA Model v5.005 in the TSPA-LA model report (SNL 2008 [DIRS 183478], Section 3[a]). These software codes are qualified and controlled per Lead Laboratory procedure IM-PRO-003, *Software Management*. No software was modified for this analysis. In addition, GoldSim V. 9.60.300 (STN: 10344-9.60-03. [DIRS 184387]) was used to query TSPA baseline simulations and to perform sensitivity analyses with the TSPA model. MView V. 4.0 (STN: 10072-4.0-01 [DIRS 181049] was used for performing regression analyses based on TSPA results. EXDOC_LA V. 2.0 (STN: 11193-2.0-00 [DIRS 182102]) was used to calculate expected values for quantities of interest. PHREEQC V. 2.11.01 (STN: 10068-2.11-01 [DIRS 185868]) was used to perform geochemical modeling and to evaluate the effects of major ions that compete for sorption sites.

Commercial off-the-shelf software, including Microsoft Word and Microsoft Excel, was used in this work. This software is exempt from qualification per Section 2.0 of IM-PRO-003, *Software Management*. Microsoft Word and Microsoft Excel are standard software applications used widely throughout the Yucca Mountain Project (YMP). They provide standard word processing and spreadsheet functions. There are no limitations on the use of the commercial off-the-shelf software used in this document related to their specified functions. No macros or special software routines were used by, or developed for, this software. The work was conducted using Yucca Mountain Project-standard desktop computers.

II.3. Analysis

Overestimation of sorption is primarily restricted to the Igneous Intrusion Modeling Case, although it also occurs in rare instances in the Seismic Ground Motion Modeling Case for 10,000 years (Figure 2). In the Igneous Intrusion Modeling Case for 10,000 years, instantaneous degradation of the CSNF waste form following the igneous intrusive event, coupled with higher CO_2 partial pressures (P_{CO_2}) (sometimes exceeding 10^{-2} bar) early in the repository history, leads to high dissolved concentrations and large mass releases by advection and diffusion from Cell 1 (waste form) of the TSPA discretized EBS transport model, at a time when only a small fraction of the steel has corroded and the amount of corrosion products on which sorption can occur is still small. In realizations where the sorption capacity is exceeded, the dissolved concentration of ^{238}U in Cell 1 is typically greater than 10^{-4} mol/L, and the number of sorption sites per liter of water is typically less than 2 mol-sites/L (a value below the 10th percentile of the range, which varies from about 1 to 12 mol-sites/L). Under such conditions, the sorption abstraction calculates low K_d values for uranium (Figure 3). However, the predicted K_d values are not low enough, and sorption is slightly over-predicted. This results from the inherent uncertainty in the

multiple regression model used in the TSPA-LA calculations (referred to here as the "base-case K_d model"), which was developed based on the competitive sorption calculations performed using PHREEQC (SNL 2007 [DIRS 177407], Section 6.5.2.4). The coefficient of determination (R^2) is about 0.95 for the regression model that is used to predict uranium sorption (SNL 2007 [DIRS 177407], Table 6.5-14). However, this regression model is based on a large dataset, consisting of the results of PHREEQC simulations with independent parameters that range over several orders of magnitude. When only those data corresponding to high dissolved uranium concentrations (>10^{-4} mol/L) and low sorption sites per liter of water (< 4 mol-sites/L) are considered, the regression model does not provide a good fit (Figure 4a). By performing a multiple regression on the reduced data set, the predictive capability improves for these conditions (Figure 4b). The new regression calculation is contained in the output DTN: MO0812TSPAOSIA.000, in worksheet "U_regress_High_U" of spreadsheet, *Final_Surf_Complx_Regression.xls*. The new regression equation (referred to as the "adjusted K_d model") has the following form:

$$\log_{10}(U_{CP}) = 0.359 - 0.038\, pCO_2 + 0.006\, (pCO_2)^2 + 1.00 \log_{10}(spl) - 0.012 \log_{10}(U) - 0.007\, [\log_{10}(U)]^2, \qquad \text{(Eq. 1)}$$

where U_{CP} is the amount of uranium sorbed onto corrosion products in units of sorbed moles per liter of water, U is the dissolved uranium concentration in discretized EBS transport model Cell 2 (waste package corrosion products) in mol/L, spl is the concentration of sorption sites in units of mol-sites/L, and pCO_2 is the negative base-10 log of P_{CO_2}, with P_{CO_2} in units of bar.

Applying Equation 1 (the adjusted K_d model) under the applicable sets of conditions results in lower K_d values for uranium. When the adjusted K_d model is used to recalculate model results for those realizations where sorption capacity was originally exceeded appreciably (by a factor of 2 to 3), the fraction of the sorption capacity that is filled, following an initial pulse, rapidly returns to a value near 1.0 (Figure 5). The Igneous Intrusion Modeling Case for 10,000 years was rerun implementing the adjusted K_d model when the dissolved uranium concentration exceeded 10^{-4} mol/L and concentration of sorption sites was less than 4 mol-sites/L, and the mean annual dose was compared with TSPA-LA results to investigate the effect of using the adjusted K_d model. As shown in Figure 6, the mean annual dose remains largely unchanged. The maximum mean dose increase using the adjusted K_d model was about 0.2% over the TSPA-LA results, indicating that the small number of realizations where the sorption capacity is exceeded does not impact the mean dose. This demonstration that the overestimation of sorption in the TSPA-LA does not significantly impact repository performance resolves CR 12998, and no further action is required.

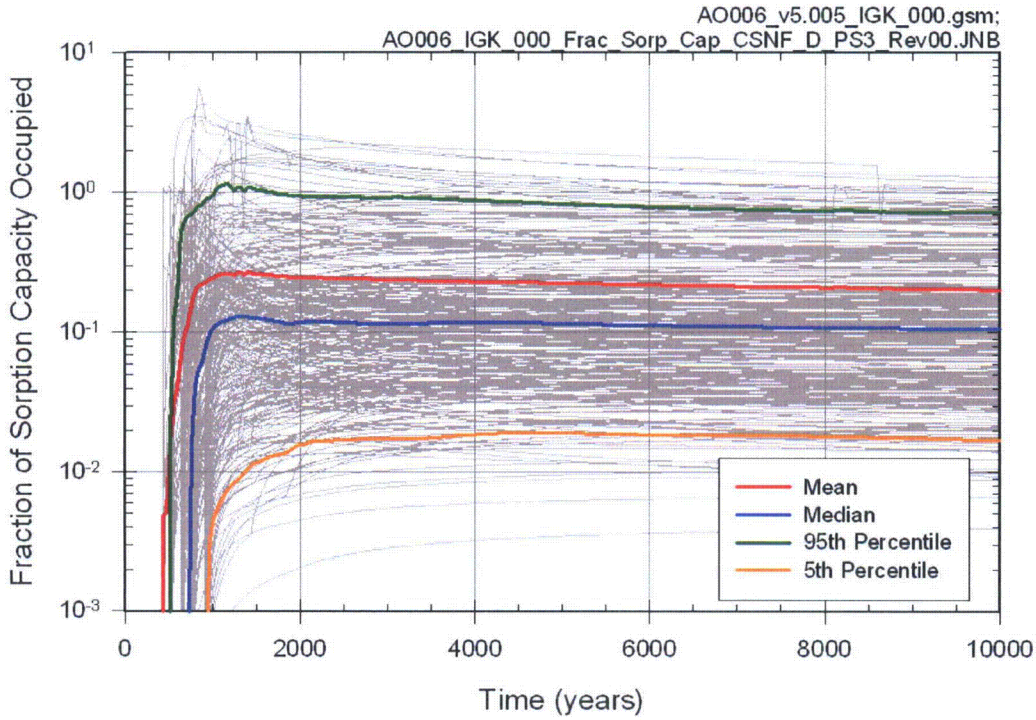

Output DTN: MO0812TSPAOSIA.000, file MO0812TSPAOSIA_000.zip

Figure 1. Fraction of Sorption Capacity Occupied for All 300 Realizations in CSNF Waste Packages in Percolation Subregion 3 Dripping Environments after an Igneous Intrusion at 100 Years

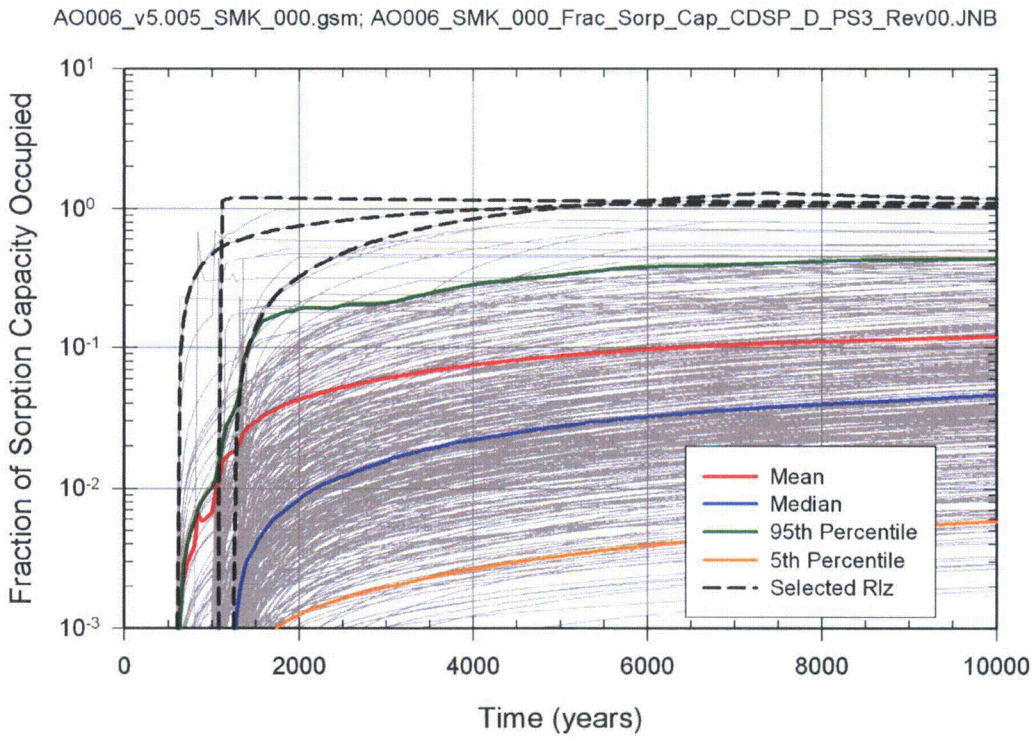

Note: Selected realizations (Rlz) indicate instances where sorption is overestimated.
Output DTN: MO0812TSPAOSIA.000, file MO0812TSPAOSIA_000.zip

Figure 2. Fraction of Sorption Capacity Occupied for 300 Realizations in Damaged CDSP Waste Packages under Percolation Subregion 3 Dripping Environments after a Seismic Ground Motion Event at 200 Years.

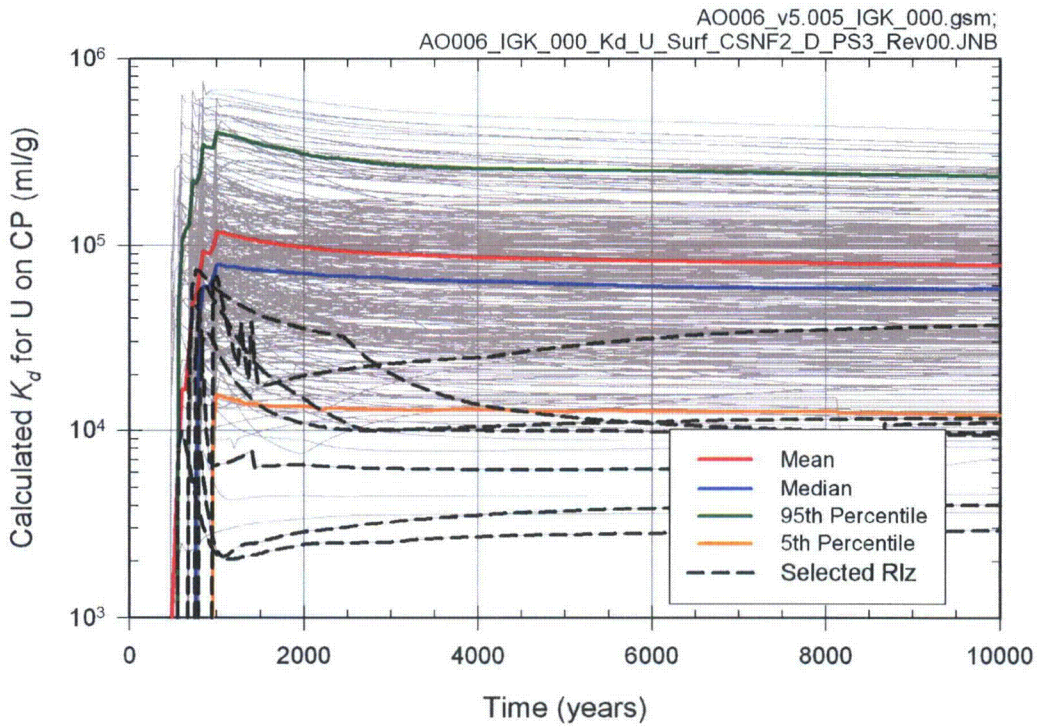

Note: Selected realizations (Rlz) are those instances where sorption is overestimated.

Output DTN: MO0812TSPAOSIA.000, file MO0812TSPAOSIA_000.zip

Figure 3. Calculated K_d for Uranium on the Stationary Corrosion Products in CSNF Waste Packages in Percolation Subregion 3 Dripping Environments after an Igneous Intrusion at 100 Years

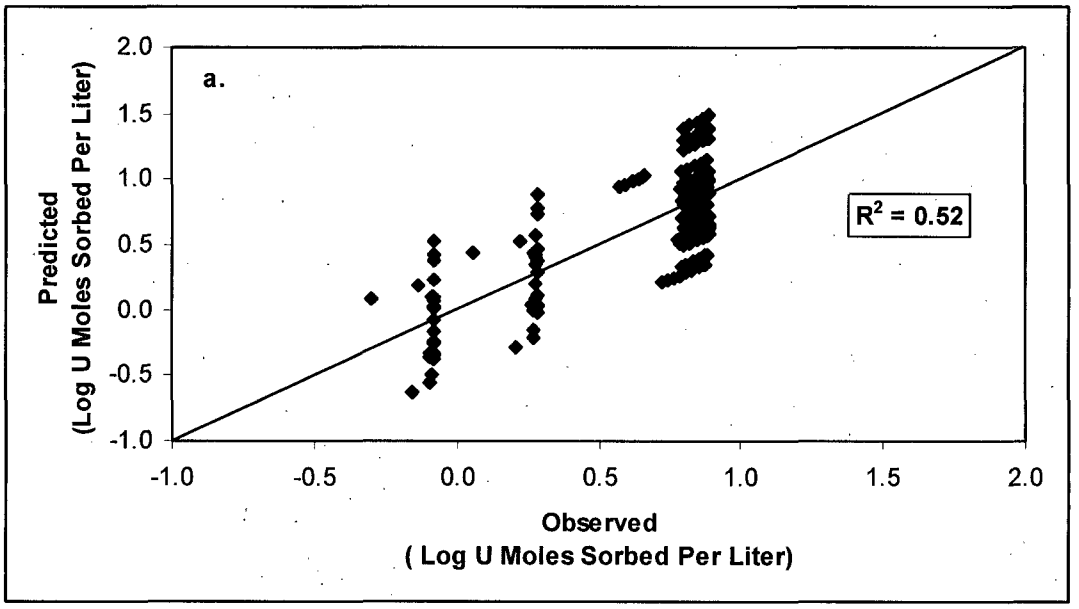

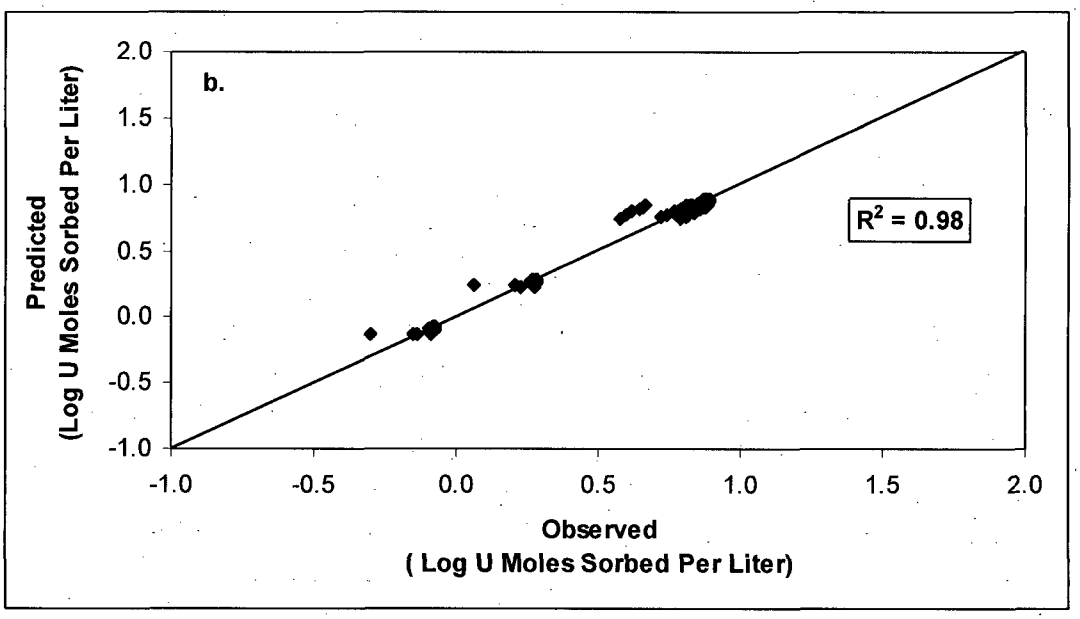

NOTE: The only data sets included are those where dissolved uranium concentration is greater than 10^{-4} mol/L and the sorption sites are less than 4 mol-sites/L.

Output DTN: MO0812TSPAOSIA.000, worksheets 'U_data_High_U' and 'U_regress_High_U' in spreadsheet *Final_Surf_Complx_Regression.xls*

Figure 4. Comparison of Predictive Capability of Uranium Sorption (log of moles sorbed per liter of water) Using (a) Base-Case K_d Model and (b) Adjusted K_d Model

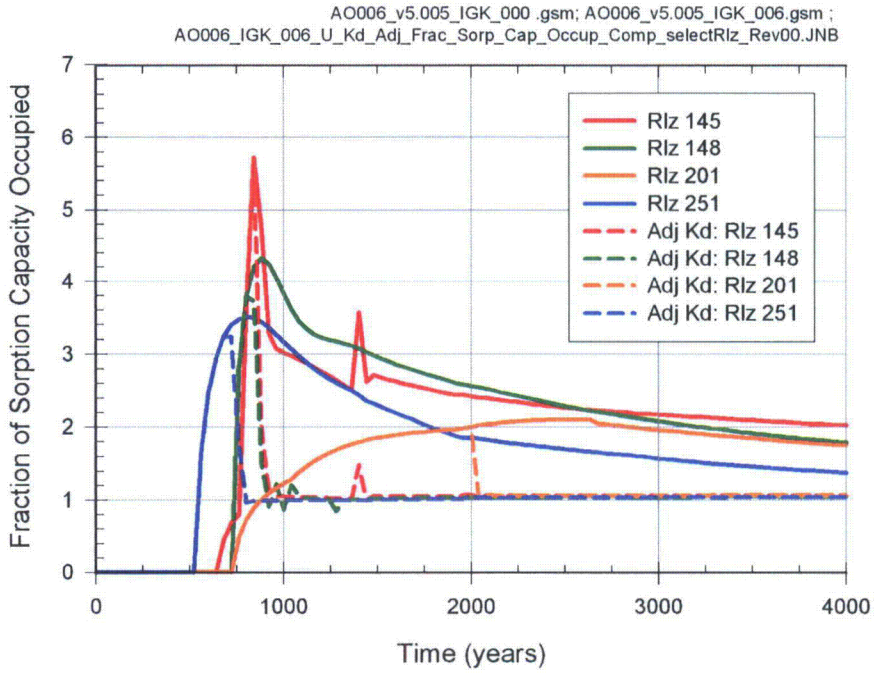

Output DTN: MO0812TSPAOSIA.000, file MO0812TSPAOSIA_000.zip

Figure 5. Comparison of Fraction of Sorption Capacity Occupied for Selected Realizations (Rlz) Using Base-Case K_d Model and Adjusted K_d Model for Igneous Intrusion Modeling Case for 10,000 Years for CSNF Waste Packages in Percolation Subregion 3 Seep Environment

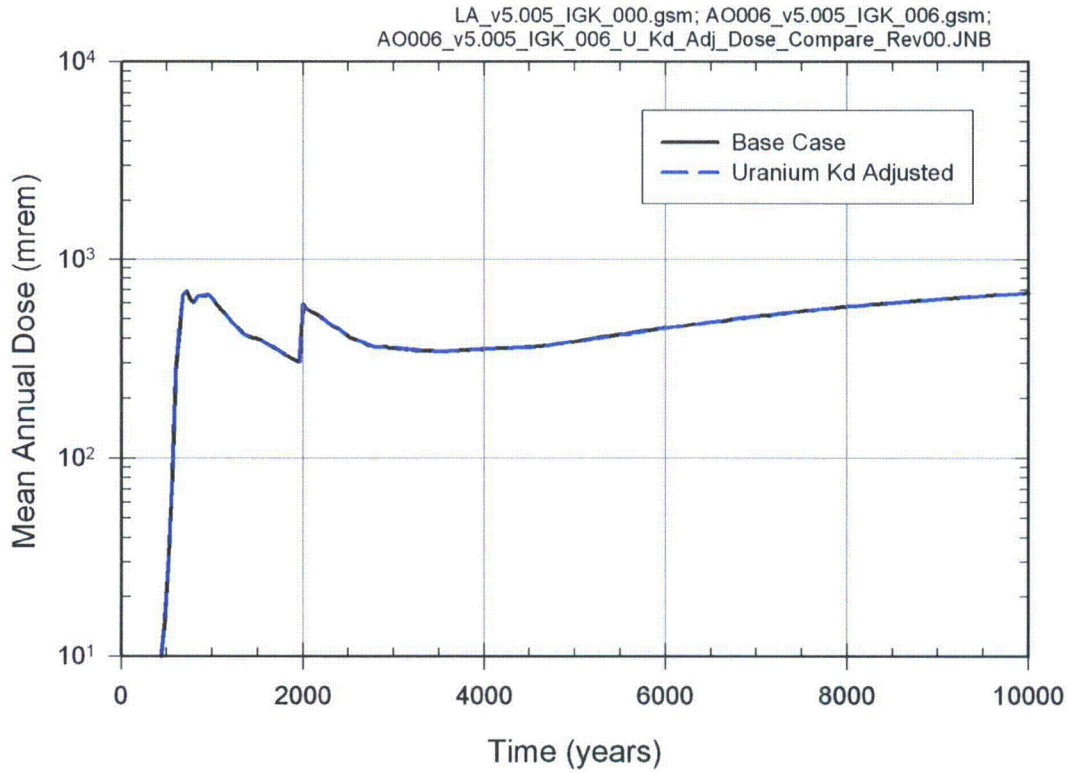

Output DTN: MO0812TSPAOSIA.000, file MO0812TSPAOSIA_000.zip

Figure 6. Comparison of Mean Annual Dose Using Base-Case K_d Model and Adjusted K_d Model for Sorption of Uranium on the Corrosion Products for Igneous Intrusion Modeling Case for 10,000 Years

III. CR 13093 Resolution

CR 13093 is resolved by correcting references to design TDIPs in Table 4.1-20, Section 6.5.2.3, and Appendix I of ANL-WIS-PA-000001 REV 03. The following changes are made (see DIRS changes at the end of this list):

1. Table 4.1-20, p. 4-46: For Model Input "Maximum depth of invert," change the Value from "4 ft. 4 in." to "52 in.," and change the Source from "SNL 2007 [DIRS 179354], Table 4-1, Parameter Number 01-10" to "SNL 2007 [DIRS 179354], Figure 4-1."

2. p. 6-190, Section 6.5.2.3, 1st paragraph, lines 3-4: Change "maximum invert thickness of $t_{I,max}$ = 4 ft 4 in. = 1.321 m (SNL 2007 [DIRS 179354], Table 4-1, Parameter Number 01-10)" to "maximum invert thickness of $t_{I,max}$ = 52 in. = 1.321 m (SNL 2007 [DIRS 179354], Figure 4-1)." This change was not specified in CR 13093, but is made to be consistent with the change described in the preceding item.

3. Appendix I, p. I-1, Section I.1, 1st paragraph, lines 7-9: Change "The domain width is 40.5 m, which is half the distance between centers of waste emplacement drifts (SNL 2007 [DIRS 179466], Table 4-1, Parameter No. 01-04)" to "The domain width is 40.5 m, which is half the distance between centers of waste emplacement drifts (SNL 2007 [DIRS 179466], Table 4-1, Parameter No. 01-13)." This error was not listed in CR 13093, but was identified when the DIRS was inspected in responding to this CR.

4. Appendix I, p. I-3, last paragraph, lines 6-7: Change "The drift diameter is 5.5 m (SNL 2007 [DIRS 179466], Table 4-1, Parameter No. 01-04)" to "The drift diameter is 5.5 m (SNL 2007 [DIRS 179466], Table 4-1, Parameter No. 01-10)."

5. Appendix I, p. I-3, last paragraph, lines 11-14: Change "The current invert design calls for a maximum depth of 1.32 m (4 ft 4 in.) ... (SNL 2007 [DIRS 179354], Table 4-1, Parameter No. 01-13A)" to "The current invert design calls for a maximum depth of 1.32 m (52 in.) ... (SNL 2007 [DIRS 179354], Figure 4-1)." In addition to this change in Appendix I text, this input data reference in Appendix I should be included in the DIRS for ANL-WIS-PA-000001 REV 03; this omission was not listed in CR 13093, but was identified when the DIRS was inspected in response to this CR.

The DIRS entries for ANL-WIS-PA-000001 REV 03 are revised as follows to resolve CR 13093. Changes to the DIRS noted below are marked up on the point-in-time DIRS report, and the revised DIRS report is processed in accordance with SCI-PRO-004, *Managing Technical Product Inputs*; the marked-up pages from the DIRS report are appended to this ERD (new DIRS entries are not shown in the appended DIRS mark-up but are listed in Attachment I).

DIRS entry for SNL 2007 [DIRS 179354] for ANL-WIS-PA-000001 REV 03

Table 4-1, Parameter Number 01-10	Table 4.1-20; Section 6.5.2.3	Maximum depth of invert	Indirect Input	N/A	N/A	TBV-8613 Resolved

Revised DIRS entry for SNL 2007 [DIRS 179354] for ANL-WIS-PA-000001 REV 03 ERD 02

Figure 4-1	Table 4.1-20; Section 6.5.2.3; Appendix I.1	Maximum depth of invert	Indirect Input	N/A	N/A	TBV-8613 Resolved

DIRS entry for SNL 2007 [DIRS 179466] for ANL-WIS-PA-000001 REV 03

Table 4-1; Parameter 01-04	Appendix I.1	Development of the grid of the two-dimensional symmetry model	Indirect Input	N/A	N/A	TBV-8614 Resolved

Revised and new DIRS entries for SNL 2007 [DIRS 179466] for ANL-WIS-PA-000001 REV 03 ERD 02

Table 4-1; Parameter 01-13	Appendix I.1	Distance between centers of waste emplacement drifts	Indirect Input	N/A	N/A	TBV-8614 Resolved
Table 4-1; Parameter 01-10	Appendix I.1	Drift diameter	Indirect Input	N/A	N/A	N/A

None of the changes in response to CR 13093 impacts the conclusions of ANL-WIS-PA-000001 REV 03, and no downstream usage—neither the LA nor other project documents—is impacted.

IV. CR 10788 Resolution

CR 10788 addresses a procedural non-compliance regarding qualification of external source data used as direct input. A review of ANL-WIS-PA-000001 REV 03 revealed that most of the information required for the qualification of external data was presented in the document, but some of the documentation requirements of SCI-PRO-001, *Qualification of Unqualified Data*, were omitted. The documentation deficiency is resolved by Table 1, which contains the external sources listed in Section 4 of ANL-WIS-PA-000001 REV 03 and used as direct input. The table contains the method used for qualification, the rationale for choosing that method, the qualification attributes, and the location within the document where the qualification information is presented.

For most of the inputs listed in Table 1, attribute 10, corroboration with other data, is listed as one of the attributes used for demonstrating qualification for intended use. For site density (goethite and HFO), specific surface area (goethite, HFO, and CSNF-related oxides), and water vapor adsorption isotherm (iron oxides and CSNF-related oxides), the input values coming from different sources were combined to provide ranges or probability distributions for use in the analysis. The last column of Table 1 indicates the location within the document where the data were compiled and distributions were developed. All of the values are considered qualified because they are corroborated by the other values in each data set. All inputs are judged to be qualified for intended use within ANL-WIS-PA-000001 REV 03, in accordance with SCI-PRO-006, *Models*, Section 6.2.1.L(3), based on the qualification attributes listed in Table 1.

For one of the direct inputs listed in Table 1, Ebert et al. (1991 [DIRS 111028]), the qualification documentation within Section 4 is revised so that the data is qualified in accordance with SCI-PRO-001, as required by SCI-PRO-006, Section 6.2.1.L(1), which applies to data developed by YMP participants. The first paragraph of p. 4–13 is revised as follows, with new text underlined:

> **Water vapor isotherm for HLW glass**—The Frenkel-Halsey-Hill (FHH) adsorption isotherm parameters *k* and *s* for HLW glass are provided by Ebert et al. (1991 [DIRS 111028], p. 134, Figure 1b). <u>The parameters were determined by curve-fitting data representing the number of water monolayers versus relative humidity for HLW glass. Ebert et al. (1991 [DIRS 111028], p. 134, Figure 1a) also present an isotherm for natural</u>

obsidian that shows lower values of adsorption than for the HLW glass. The natural obsidian isotherm is corroborated by a nearly identical isotherm for silica and quartz presented in Hagymassy et al. (1968 [DIRS 111034], p. 489). Corroboration of the natural obsidian isotherm by Hagymassy et al. (1968 [DIRS 111034]) gives confidence that the isotherm measured by Ebert for nuclear waste glass is also accurate. Ebert has studied HLW glass at Argonne National Laboratory for many years and has published many articles in peer-reviewed journals. These data were developed by Ebert while supporting the project and are reported in *Defense HLW Glass Degradation Model* (BSC 2004 [DIRS 169988], Section 6.5.3.1). The values of isotherm parameters *k* and *s* are qualified in accordance with SCI-PRO-001. The data qualification team consisted of James Schreiber (B.S. and M.S. Chemical Engineering, with twenty years experience in nuclear waste management) and Susan LeStrange (M.S. Chemical Engineering, Ph.D. Agricultural Engineering, with expertise in geochemistry and chemical transport). The data qualification team concluded that the data are corroborated by Hagymassy et al. (1968 [DIRS 111034]). Therefore, the data are qualified and appropriate for use in the RTA.

The following new reference is added to Section 9.1

111034 Hagymassy, J., Jr.; Brunauer, S.; and Mikhail, R.Sh. 1969. "Pore Structure Analysis by Water Vapour Absorption. Part 1. T-Curves for Water Vapour." *Journal of Colloid and Interface Science, 29,* (3), 485-491. New York, New York: Academic Press. TIC: 246076.

In Table 6.5–9, change the value of "FHH adsorption isotherm parameter *k* for HLW glass", from "13.2" to "3.2".

The DIRS entries for "Input usage" for some of the inputs in Section 4 were incorrectly classified as "Indirect Input" rather than "Direct Input". In addition, the DIRS entries for "Input Category" for some inputs were incorrectly labeled as "Data" rather than "Established Fact". The changes to the DIRS are provided in Table 2. Table 2 also lists various other changes to the DIRS, including further changes prompted by the Indirect/Direct reclassification described in this section as well as related miscellaneous clarifications and corrections that were made in response to CR 10788.

None of the changes in response to CR 10788 impacts the conclusions of ANL-WIS-PA-000001 REV 03. As a result, neither the LA nor other project documents is impacted.

Table 1. Data Qualification for External Source Data Qualified for Intended Use in Document ANL-WIS-PA-000001 REV 03

Input	Source	Description	Method[1] (Rationale)[2]	Attribute[3]	Locations within AMR Where Data Are Listed and Where Qualification Is Documented or Corroboration Is Demonstrated
McCafferty and Zettlemoyer 1970 [DIRS 154382]	p. 454	Water molecule cross-sectional area, A_w	5 (a,b)	1, 3, 7, 10	Table 4.1-11, p. 4-12
	Figure 3	Water Vapor Adsorption Isotherms for α-Fe_2O_3	5 (a)	3, 10	Table 4.1-19, p. 4-33, Section 6.3.4.3.2, p. 6-72, Figure 6.3-34, output DTN: SN0703PAEBSRTA.001 [DIRS 185343], file *Corrosion Products Composite Isotherm 7-19-2007.xls*
Towe and Bradley 1967 [DIRS 155334]	p. 386	Density of HFO	5 (b)	3, 7, 10	Table 4.1-11, pp. 4-15 and 4-16
Ebert, Hoburg, and Bates 1991 [DIRS 111028]	p. 134, Figure 1b	Parameters *k* and *s* in FHH water vapor adsorption isotherm for HLW glass	5 (c)	1, 3, 7, 10	Table 4.1-11, p. 4-13, Section IV of this ERD
Rodda et al. 1996 [DIRS 173710]	Table 1, Table 5	Goethite site density	5 (a)	7, 10	Table 4.1-12, pp. 4-13 through 4-15, Tables 6.3-4 and 6.3-5
	p. 365	Goethite specific surface area	5 (a)	7, 10	Table 4.1-12, pp. 4-13 through 4-15, Section 6.3.4.3.3, Appendix K, Figure K-5, output DTN: SN0703PAEBSRTA.001 [DIRS 185343], file *Goethite specific surface area 7-12-2007.xls*
Hiemstra and Van Riemsdijk 1996 [DIRS 173023]	p. 498	Goethite site density	5 (a)	7, 10	Table 4.1-12, pp. 4-13 through 4-15, Tables 6.3-4 and 6.3-5
Villalobos et al. 2003 [DIRS 173017]	Table 2	Goethite site density	5 (a)	7, 10	Table 4.1-12, pp. 4-13 through 4-15, Tables 6.3-4 and 6.3-5
	Table 2	Goethite specific surface area	5 (a)	7, 10	Table 4.1-12, pp. 4-13 through 4-15, Section 6.3.4.3.3, Appendix K, Figure K-5, output DTN: SN0703PAEBSRTA.001 [DIRS 185343], file *Goethite specific surface area 7-12-2007.xls*
Trivedi et al. 2001 [DIRS 173021]	Table 3	Goethite site density	5 (a)	7, 10	Table 4.1-12, pp. 4-13 through 4-15, Tables 6.3-4 and 6.3-5
	Table 3	Goethite specific surface area	5 (a)	7, 10	Table 4.1-12, pp. 4-13 through 4-15, Section 6.3.4.3.3, Appendix K, Figure K-5, output DTN: SN0703PAEBSRTA.001 [DIRS 185343], file *Goethite specific surface area 7-12-2007.xls*

Table 1. Data Qualification for External Source Data Qualified for Intended Use in Document ANL-WIS-PA-000001 REV 03 (Continued)

Input	Source	Description	Method[1] (Rationale)[2]	Attribute[3]	Locations within AMR Where Data Are Listed and Where Qualification Is Documented or Corroboration Is Demonstrated
Naveau et al. 2005 [DIRS 173018]	p. 6	Goethite site density	5 (a)	7, 10	Table 4.1-12, pp. 4-13 through 4-15, Tables 6.3-4 and 6.3-5
	p. 6	Goethite specific surface area	5 (a)	7, 10	Table 4.1-12, pp. 4-13 through 4-15, Section 6.3.4.3.3, Appendix K, Figure K-5, output DTN: SN0703PAEBSRTA.001 [DIRS 185343], file *Goethite specific surface area 7-12-2007.xls*
Coughlin and Stone 1995 [DIRS 173030]	Table 1	Goethite site density	5 (a)	7, 10	Table 4.1-12, pp. 4-13 through 4-15, Tables 6.3-4 and 6.3-5
	Table 1	Goethite specific surface area	5 (a)	7, 10	Table 4.1-12, pp. 4-13 through 4-15, Section 6.3.4.3.3, Appendix K, Figure K-5, output DTN: SN0703PAEBSRTA.001 [DIRS 185343], file *Goethite specific surface area 7-12-2007.xls*
Grossl et al. 1997 [DIRS 173032]	p. 322	Goethite site density	5 (a)	7, 10	Table 4.1-12, pp. 4-13 through 4-15, Tables 6.3-4 and 6.3-5
	p. 322	Goethite specific surface area	5 (a)	7, 10	Table 4.1-12, pp. 4-13 through 4-15, Section 6.3.4.3.3, Appendix K, Figure K-5, output DTN: SN0703PAEBSRTA.001 [DIRS 185343], file *Goethite specific surface area 7-12-2007.xls*
Fendorf et al. 1996 [DIRS 173034]	p. 100	Goethite site density	5 (a)	7, 10	Table 4.1-12, pp. 4-13 through 4-15, Tables 6.3-4 and 6.3-5
	p. 100	Goethite specific surface area	5 (a)	7, 10	Table 4.1-12, pp. 4-13 through 4-15, Section 6.3.4.3.3, Appendix K, Figure K-5, output DTN: SN0703PAEBSRTA.001 [DIRS 185343], file *Goethite specific surface area 7-12-2007.xls*
Duc et al. 2003 [DIRS 173019]	Table 2	Goethite site density	5 (a)	7, 10	Table 4.1-12, pp. 4-13 through 4-15, Tables 6.3-4 and 6.3-5
	Table 1	Goethite specific surface area	5 (a)	7, 10	Table 4.1-12, pp. 4-13 through 4-15, Section 6.3.4.3.3, Appendix K, Figure K-5, output DTN: SN0703PAEBSRTA.001 [DIRS 185343], file *Goethite specific surface area 7-12-2007.xls*
Pivovarov 1997 [DIRS 173714]	Table 1	Goethite site density	5 (a)	7, 10	Table 4.1-12, pp. 4-13 through 4-15, Tables 6.3-4 and 6.3-5

Table 1. Data Qualification for External Source Data Qualified for Intended Use in Document ANL-WIS-PA-000001 REV 03 (Continued)

Input	Source	Description	Method[1] (Rationale)[2]	Attribute[3]	Locations within AMR Where Data Are Listed and Where Qualification Is Documented or Corroboration Is Demonstrated
Gräfe et al. 2004 [DIRS 173751]	p. 6561	Goethite site density	5 (a)	7, 10	Table 4.1-12, pp. 4-13 through 4-15, Tables 6.3-4 and 6.3-5
	p. 6562	Goethite specific surface area	5 (a)	7, 10	Table 4.1-12, pp. 4-13 through 4-15, Section 6.3.4.3.3, Appendix K, Figure K-5, output DTN: SN0703PAEBSRTA.001 [DIRS 185343], file *Goethite specific surface area 7-12-2007.xls*
Missana et al. 2003 [DIRS 173759]	p. 296	Goethite site density	5 (a)	7, 10	Table 4.1-12, pp. 4-13 through 4-15, Tables 6.3-4 and 6.3-5
	Table 3	Goethite specific surface area	5 (a)	7, 10	Table 4.1-12, pp. 4-13 through 4-15, Section 6.3.4.3.3, Appendix K, Figure K-5, output DTN: SN0703PAEBSRTA.001 [DIRS 185343], file *Goethite specific surface area 7-12-2007.xls*
Lützenkirchen et al. 2002 [DIRS 173757]	p. 3394, Table 1	Goethite site density	5 (a)	7, 10	Table 4.1-12, pp. 4-13 through 4-15, Tables 6.3-4 and 6.3-5
Müller and Sigg 1992 [DIRS 173760]	p. 519	Goethite site density	5 (a)	7, 10	Table 4.1-12, pp. 4-13 through 4-15, Tables 6.3-4 and 6.3-5
	p. 519	Goethite specific surface area	5 (a)	7, 10	Table 4.1-12, pp. 4-13 through 4-15, Section 6.3.4.3.3, Appendix K, Figure K-5, output DTN: SN0703PAEBSRTA.001 [DIRS 185343], file *Goethite specific surface area 7-12-2007.xls*
Randall et al. 1999 [DIRS 173709]	Table 1	Goethite site density	5 (a)	7, 10	Table 4.1-12, pp. 4-13 through 4-15, Tables 6.3-4 and 6.3-5
	Table 1	Goethite specific surface area	5 (a)	7, 10	Table 4.1-12, pp. 4-13 through 4-15, Section 6.3.4.3.3, Appendix K, Figure K-5, output DTN: SN0703PAEBSRTA.001 [DIRS 185343], file *Goethite specific surface area 7-12-2007.xls*
Felmy and Rustad 1998 [DIRS 173708]	p. 26	Goethite site density	5 (a)	7, 10	Table 4.1-12, pp. 4-13 through 4-15, Tables 6.3-4 and 6.3-5
	p. 27	Goethite specific surface area	5 (a)	7, 10	Table 4.1-12, pp. 4-13 through 4-15, Section 6.3.4.3.3, Appendix K, Figure K-5, output DTN: SN0703PAEBSRTA.001 [DIRS 185343], file *Goethite specific surface area 7-12-2007.xls*

Table 1. Data Qualification for External Source Data Qualified for Intended Use in Document ANL-WIS-PA-000001 REV 03 (Continued)

Input	Source	Description	Method[1] (Rationale)[2]	Attribute[3]	Locations within AMR Where Data Are Listed and Where Qualification Is Documented or Corroboration Is Demonstrated
Hongshao and Stanforth 2001 [DIRS 173754]	p. 4754	Goethite site density	5 (a)	7, 10	Table 4.1-12, pp. 4-13 through 4-15, Tables 6.3-4 and 6.3-5
	p. 4754	Goethite specific surface area	5 (a)	7, 10	Table 4.1-12, pp. 4-13 through 4-15, Section 6.3.4.3.3, Appendix K, Figure K-5, output DTN: SN0703PAEBSRTA.001 [DIRS 185343], file *Goethite specific surface area 7-12-2007.xls*
Buerge-Weirich et al. 2002 [DIRS 173752]	p. 329	Goethite site density	5 (a)	7, 10	Table 4.1-12, pp. 4-13 through 4-15, Tables 6.3-4 and 6.3-5
	p. 329	Goethite specific surface area	5 (a)	7, 10	Table 4.1-12, pp. 4-13 through 4-15, Section 6.3.4.3.3, Appendix K, Figure K-5, output DTN: SN0703PAEBSRTA.001 [DIRS 185343], file *Goethite specific surface area 7-12-2007.xls*
Boily et al. 2001 [DIRS 173707]	Table 3	Goethite site density	5 (a)	7, 10	Table 4.1-12, pp. 4-13 through 4-15, Tables 6.3-4 and 6.3-5
	Table 3	Goethite specific surface area	5 (a)	7, 10	Table 4.1-12, pp. 4-13 through 4-15, Section 6.3.4.3.3, Appendix K, Figure K-5, output DTN: SN0703PAEBSRTA.001 [DIRS 185343], file *Goethite specific surface area 7-12-2007.xls*
Gao and Mucci 2001 [DIRS 173750]	p. 2364	Goethite site density	5 (a)	7, 10	Table 4.1-12, pp. 4-13 through 4-15, Tables 6.3-4 and 6.3-5
	p. 2362	Goethite specific surface area	5 (a)	7, 10	Table 4.1-12, pp. 4-13 through 4-15, Section 6.3.4.3.3, Appendix K, Figure K-5, output DTN: SN0703PAEBSRTA.001 [DIRS 185343], file *Goethite specific surface area 7-12-2007.xls*
Robertson and Leckie 1997 [DIRS 173763]	Table 4	Goethite site density	5 (a)	7, 10	Table 4.1-12, pp. 4-13 through 4-15, Tables 6.3-4 and 6.3-5
	Table 3	Goethite specific surface area	5 (a)	7, 10	Table 4.1-12, pp. 4-13 through 4-15, Section 6.3.4.3.3, Appendix K, Figure K-5, output DTN: SN0703PAEBSRTA.001 [DIRS 185343], file *Goethite specific surface area 7-12-2007.xls*

Table 1. Data Qualification for External Source Data Qualified for Intended Use in Document ANL-WIS-PA-000001 REV 03 (Continued)

Input	Source	Description	Method[1] (Rationale)[2]	Attribute[3]	Locations within AMR Where Data Are Listed and Where Qualification Is Documented or Corroboration Is Demonstrated
Lövgren et al. 1990 [DIRS 173771]	p. 1303	Goethite site density	5 (a)	7, 10	Table 4.1-12, pp. 4-13 through 4-15, Tables 6.3-4 and 6.3-5
	p. 1301	Goethite specific surface area	5 (a)	7, 10	Table 4.1-12, pp. 4-13 through 4-15, Section 6.3.4.3.3, Appendix K, Figure K-5, output DTN: SN0703PAEBSRTA.001 [DIRS 185343], file *Goethite specific surface area 7-12-2007.xls*
Machesky et al. 1991 [DIRS 173758]	p. 771	Goethite site density	5 (a)	7, 10	Table 4.1-12, pp. 4-13 through 4-15, Tables 6.3-4 and 6.3-5
	p. 770	Goethite specific surface area	5 (a)	7, 10	Table 4.1-12, pp. 4-13 through 4-15, Section 6.3.4.3.3, Appendix K, Figure K-5, output DTN: SN0703PAEBSRTA.001 [DIRS 185343], file *Goethite specific surface area 7-12-2007.xls*
Hayes and Leckie 1987 [DIRS 173817]	Table II	Goethite site density	5 (a)	7, 10	Table 4.1-12, pp. 4-13 through 4-15, Tables 6.3-4 and 6.3-5
	Table II	Goethite specific surface area	5 (a)	7, 10	Table 4.1-12, pp. 4-13 through 4-15, Section 6.3.4.3.3, Appendix K, Figure K-5, output DTN: SN0703PAEBSRTA.001 [DIRS 185343], file *Goethite specific surface area 7-12-2007.xls*
van Geen et al. 1994 [DIRS 144702]	Table 1	Goethite site density	5 (a)	7, 10	Table 4.1-12, pp. 4-13 through 4-15, Tables 6.3-4 and 6.3-5
	Table 1	Goethite specific surface area	5 (a)	7, 10	Table 4.1-12, pp. 4-13 through 4-15, Section 6.3.4.3.3, Appendix K, Figure K-5, output DTN: SN0703PAEBSRTA.001 [DIRS 185343], file *Goethite specific surface area 7-12-2007.xls*
Persson et al. 1998 [DIRS 173762]	p. 261, Table 1	Goethite site density	5 (a)	7, 10	Table 4.1-12, pp. 4-13 through 4-15, Tables 6.3-4 and 6.3-5
	p. 261, Table 1	Goethite specific surface area	5 (a)	7, 10	Table 4.1-12, pp. 4-13 through 4-15, Section 6.3.4.3.3, Appendix K, Figure K-5, output DTN: SN0703PAEBSRTA.001 [DIRS 185343], file *Goethite specific surface area 7-12-2007.xls*

Table 1. Data Qualification for External Source Data Qualified for Intended Use in Document ANL-WIS-PA-000001 REV 03 (Continued)

Input	Source	Description	Method[1] (Rationale)[2]	Attribute[3]	Locations within AMR Where Data Are Listed and Where Qualification Is Documented or Corroboration Is Demonstrated
Davis and Upadhyaya 1996 [DIRS 173743]	p. 1895	Goethite site density	5 (a)	7, 10	Table 4.1-12, pp. 4-13 through 4-15, Tables 6.3-4 and 6.3-5
	p. 1895	Goethite specific surface area	5 (a)	7, 10	Table 4.1-12, pp. 4-13 through 4-15, Section 6.3.4.3.3, Appendix K, Figure K-5, output DTN: SN0703PAEBSRTA.001 [DIRS 185343], file *Goethite specific surface area 7-12-2007.xls*
Xue and Traina 1996 [DIRS 173713]	p. 3163	Goethite site density	5 (a)	7, 10	Table 4.1-12, pp. 4-13 through 4-15, Tables 6.3-4 and 6.3-5
	p. 3161	Goethite specific surface area	5 (a)	7, 10	Table 4.1-12, pp. 4-13 through 4-15, Section 6.3.4.3.3, Appendix K, Figure K-5, output DTN: SN0703PAEBSRTA.001 [DIRS 185343], file *Goethite specific surface area 7-12-2007.xls*
Hansmann and Anderson 1985 [DIRS 173742]	p. 547	Goethite site density	5 (a)	7, 10	Table 4.1-12, pp. 4-13 through 4-15, Tables 6.3-4 and 6.3-5
	p. 546	Goethite specific surface area	5 (a)	7, 10	Table 4.1-12, pp. 4-13 through 4-15, Section 6.3.4.3.3, Appendix K, Figure K-5, output DTN: SN0703PAEBSRTA.001 [DIRS 185343], file *Goethite specific surface area 7-12-2007.xls*
Gabriel et al. 1998 [DIRS 130407]	pp. 124, 126	Goethite site density	5 (a)	7, 10	Table 4.1-12, pp. 4-13 through 4-15, Tables 6.3-4 and 6.3-5
	p. 123	Goethite specific surface area	5 (a)	7, 10	Table 4.1-12, pp. 4-13 through 4-15, Section 6.3.4.3.3, Appendix K, Figure K-5, output DTN: SN0703PAEBSRTA.001 [DIRS 185343], file *Goethite specific surface area 7-12-2007.xls*
Christophi and Axe 2000 [DIRS 173020]	Table 1	Goethite specific surface area	5 (a)	7, 10	Table 4.1-12, pp. 4-13 through 4-15, Section 6.3.4.3.3, Appendix K, Figure K-5, output DTN: SN0703PAEBSRTA.001 [DIRS 185343], file *Goethite specific surface area 7-12-2007.xls*
Cornejo et al. 1984 [DIRS 178660]	Table 1	HFO specific surface area	5 (a)	2, 10	Table 4.1-14, p. 4-16, Section 6.3.4.3.3, Appendix K, Figure K-4, output DTN: SN0703PAEBSRTA.001 [DIRS 185343], file *HFO_Sp_Surf_Area_Analysis 7-12-2007.xls*

Table 1. Data Qualification for External Source Data Qualified for Intended Use in Document ANL-WIS-PA-000001 REV 03 (Continued)

Input	Source	Description	Method[1] (Rationale)[2]	Attribute[3]	Locations within AMR Where Data Are Listed and Where Qualification Is Documented or Corroboration Is Demonstrated
Cornejo 1987 [DIRS 178659]	Table 1	HFO specific surface area	5 (a)	2, 10	Table 4.1-14, p. 4-16, Section 6.3.4.3.3, Appendix K, Figure K-4, output DTN: SN0703PAEBSRTA.001 [DIRS 185343], file *HFO_Sp_Surf_Area_Analysis 7-12-2007.xls*
Schwertmann et al. 2004 [DIRS 178734]	Table 1	HFO specific surface area	5 (a)	2, 10	Table 4.1-14, p. 4-16, Section 6.3.4.3.3, Appendix K, Figure K-4, output DTN: SN0703PAEBSRTA.001 [DIRS 185343], file *HFO_Sp_Surf_Area_Analysis 7-12-2007.xls*
Mitov et al. 2002 [DIRS 178686]	Table 5	HFO specific surface area	5 (a)	2, 10	Table 4.1-14, p. 4-16, Section 6.3.4.3.3, Appendix K, Figure K-4, output DTN: SN0703PAEBSRTA.001 [DIRS 185343], file *HFO_Sp_Surf_Area_Analysis 7-12-2007.xls*
Clausen and Fabricius 2000 [DIRS 178655]	Table 2	HFO specific surface area	5 (a)	2, 10	Table 4.1-14, p. 4-16, Section 6.3.4.3.3, Appendix K, Figure K-4, output DTN: SN0703PAEBSRTA.001 [DIRS 185343], file *HFO_Sp_Surf_Area_Analysis 7-12-2007.xls*
O'Reilly and Hochella 2003 [DIRS 178704]	Table 1	HFO specific surface area	5 (a)	2, 10	Table 4.1-14, p. 4-16, Section 6.3.4.3.3, Appendix K, Figure K-4, output DTN: SN0703PAEBSRTA.001 [DIRS 185343], file *HFO_Sp_Surf_Area_Analysis 7-12-2007.xls*
Sani et al. 2004 [DIRS 178727]	p. 2640	HFO specific surface area	5 (a)	2, 10	Table 4.1-14, p. 4-16, Section 6.3.4.3.3, Appendix K, Figure K-4, output DTN: SN0703PAEBSRTA.001 [DIRS 185343], file *HFO_Sp_Surf_Area_Analysis 7-12-2007.xls*
Hofmann et al. 2004 [DIRS 173783]	Table 1	HFO specific surface area	5 (a)	2, 10	Tables 4.1-14 and 4.1-19, p. 4-16, Section 6.3.4.3.3, Appendix K, Figure K-4, output DTN: SN0703PAEBSRTA.001 [DIRS 185343], file *HFO_Sp_Surf_Area_Analysis 7-12-2007.xls*
	Figure 8	Water Vapor Adsorption Isotherms for HFO	5 (a)	3, 10	Table 4.1-19, p. 4-33, Section 6.3.4.3.2, p. 6-72, Figure 6.3-34, output DTN: SN0703PAEBSRTA.001 [DIRS 185343], file *Corrosion Products Composite Isotherm 7-19-2007.xls*
Sauvé et al. 2000 [DIRS 178732]	Table 1	HFO specific surface area	5 (a)	2, 10	Table 4.1-14, p. 4-16, Section 6.3.4.3.3, Appendix K, Figure K-4, output DTN: SN0703PAEBSRTA.001 [DIRS 185343], file *HFO_Sp_Surf_Area_Analysis 7-12-2007.xls*
Weidler 1997 [DIRS 178741]	Table 1	HFO specific surface area	5 (a)	2, 10	Table 4.1-14, p. 4-16, Section 6.3.4.3.3, Appendix K, Figure K-4, output DTN: SN0703PAEBSRTA.001 [DIRS 185343], file *HFO_Sp_Surf_Area_Analysis 7-12-2007.xls*

Table 1. Data Qualification for External Source Data Qualified for Intended Use in Document ANL-WIS-PA-000001 REV 03 (Continued)

Input	Source	Description	Method[1] (Rationale)[2]	Attribute[3]	Locations within AMR Where Data Are Listed and Where Qualification Is Documented or Corroboration Is Demonstrated
Guzman et al. 1994 [DIRS 178669]	Table 1	HFO specific surface area	5 (a)	2, 10	Table 4.1-14, p. 4-16, Section 6.3.4.3.3, Appendix K, Figure K-4, output DTN: SN0703PAEBSRTA.001 [DIRS 185343], file *HFO_Sp_Surf_Area_Analysis 7-12-2007.xls*
Larsen and Postma 2001 [DIRS 178683]	Table 2	HFO specific surface area	5 (a)	2, 10	Table 4.1-14, p. 4-16, Section 6.3.4.3.3, Appendix K, Figure K-4, output DTN: SN0703PAEBSRTA.001 [DIRS 185343], file *HFO_Sp_Surf_Area_Analysis 7-12-2007.xls*
Leone et al. 2001 [DIRS 178684]	p. 1317	HFO specific surface area	5 (a)	2, 10	Table 4.1-14, p. 4-16, Section 6.3.4.3.3, Appendix K, Figure K-4, output DTN: SN0703PAEBSRTA.001 [DIRS 185343], file *HFO_Sp_Surf_Area_Analysis 7-12-2007.xls*
Davis and Leckie 1978 [DIRS 125591]	p. 95	HFO specific surface area	5 (a)	10	Table 4.1-14, p. 4-16, Section 6.3.4.3.3, Appendix K, Figure K-4, output DTN: SN0703PAEBSRTA.001 [DIRS 185343], file *HFO_Sp_Surf_Area_Analysis 7-12-2007.xls*
Liaw et al. 1989 [DIRS 178685]	Table 1	HFO specific surface area	5 (a)	2, 10	Table 4.1-14, p. 4-16, Section 6.3.4.3.3, Appendix K, Figure K-4, output DTN: SN0703PAEBSRTA.001 [DIRS 185343], file *HFO_Sp_Surf_Area_Analysis 7-12-2007.xls*
Crosby et al. 1983 [DIRS 178662]	Table II	HFO specific surface area	5 (a)	2, 10	Table 4.1-14, p. 4-16, Section 6.3.4.3.3, Appendix K, Figure K-4, output DTN: SN0703PAEBSRTA.001 [DIRS 185343], file *HFO_Sp_Surf_Area_Analysis 7-12-2007.xls*
Axe and Anderson 1995 [DIRS 178654]	p. 159	HFO specific surface area	5 (a)	2, 10	Table 4.1-14, p. 4-16, Section 6.3.4.3.3, Appendix K, Figure K-4, output DTN: SN0703PAEBSRTA.001 [DIRS 185343], file *HFO_Sp_Surf_Area_Analysis 7-12-2007.xls*
Van der Giessen 1966 [DIRS 178740]	Table 1	HFO specific surface area	5 (a)	2, 10	Table 4.1-14, p. 4-16, Section 6.3.4.3.3, Appendix K, Figure K-4, output DTN: SN0703PAEBSRTA.001, file *HFO_Sp_Surf_Area_Analysis 7-12-2007.xls*
Davies-Colley et al. 1984 [DIRS 178666]	p. 492	HFO specific surface area	5 (a)	2, 10	Table 4.1-14, p. 4-16, Section 6.3.4.3.3, Appendix K, Figure K-4, output DTN: SN0703PAEBSRTA.001 [DIRS 185343], file *HFO_Sp_Surf_Area_Analysis 7-12-2007.xls*
Tipping 1981 [DIRS 178737]	Table 1	HFO specific surface area	5 (a)	2, 10	Table 4.1-14, p. 4-16, Section 6.3.4.3.3, Appendix K, Figure K-4, output DTN: SN0703PAEBSRTA.001 [DIRS 185343], file *HFO_Sp_Surf_Area_Analysis 7-12-2007.xls*
Carlson and Schwertmann 1981 [DIRS 142788]	Table 1	HFO specific surface area	5 (a)	2, 10	Table 4.1-14, p. 4-16, Section 6.3.4.3.3, Appendix K, Figure K-4, output DTN: SN0703PAEBSRTA.001 [DIRS 185343], file *HFO_Sp_Surf_Area_Analysis 7-12-2007.xls*

Table 1. Data Qualification for External Source Data Qualified for Intended Use in Document ANL-WIS-PA-000001 REV 03 (Continued)

Input	Source	Description	Method[1] (Rationale)[2]	Attribute[3]	Locations within AMR Where Data Are Listed and Where Qualification Is Documented or Corroboration Is Demonstrated
Eggleton and Fitzpatrick 1988 [DIRS 173878]	Table 1	HFO specific surface area	5 (a)	2, 10	Table 4.1-14, p. 4-16, Section 6.3.4.3.3, Appendix K, Figure K-4, output DTN: SN0703PAEBSRTA.001 [DIRS 185343], file *HFO_Sp_Surf_Area_Analysis 7-12-2007.xls*
Conca and Wright 1992 [DIRS 100436]	Figure 2	Diffusion coefficients for granular materials	2 (e)	3, 8, 10	Table 4.1-16, Appendix H
Conca et al. 1993 [DIRS 170709]	Figure 2	Diffusion coefficients for granular materials	2 (e)	3, 8, 10	Table 4.1-16, Appendix H
Turner and Sassman 1996 [DIRS 179618]	Tables 1 and 3	Surface Complexation Constants	5 (a)	3, 10	Table 4.1-17, p. 4-29, Appendix J, Tables J-2 and J-3
Wang et al. 2001 [DIRS 176816]	Tables 3 and 4	Surface Complexation Constants	5 (a)	3, 10	Table 4.1-17, p. 4-29, Appendix J, Tables J-2 and J-3
Pepper et al.2006 [DIRS 179622]	Table 2	Surface Complexation Constants	5 (a)	3, 10	Table 4.1-17, p. 4-29, Appendix J, Tables J-2 and J-3
Cromières et al. 1998 [DIRS 179616]	Table 4	Surface Complexation Constants	5 (a)	3, 10	Table 4.1-17, p. 4-29, Appendix J, Tables J-2 and J-3
Appelo et al. 2002 [DIRS 168168]	Table 2	Surface Complexation Constants	5 (a)	3, 10	Table 4.1-17, p. 4-29, Appendix J, Table J-2
LaVerne and Tandon 2003 [DIRS 178303]	Figure 1	Water Vapor Adsorption Isotherms for UO_2 and CeO_2	5 (a)	3, 10	Table 4.1-18, p. 4-30, Section 6.3.4.6.1, Figure 6.3-42, output DTN: SN0703PAEBSRTA.001 [DIRS 185343], file *CSNF Isotherm Compilation 7-19-2007.xls*
	p. 13624	Specific surface area for UO_2 and CeO_2	5 (a)	3, 10	Table 4.1-18, p. 4-30, Section 6.3.4.6.1, Table 6.3-12
Gammage et al. 1970 [DIRS 178304]	Figure 2 p. 4277	Water Vapor Adsorption Isotherm for ThO_2 Specific surface area for ThO_2	5 (a)	3, 10	Table 4.1-18, p. 4-30, Section 6.3.4.6.1, Figure 6.3-42, Table 6.3-12, output DTN: SN0703PAEBSRTA.001 [DIRS 185343], file *CSNF Isotherm Compilation 7-19-2007.xls*
Holmes et al. 1974 [DIRS 154379]	Figure 3	Water Vapor Adsorption Isotherm for ZrO_2	5 (a)	3, 10	Table 4.1-18, p. 4-30, Section 6.3.4.6.1, Figure 6.3-42, output DTN: SN0703PAEBSRTA.001 [DIRS 185343], file *CSNF Isotherm Compilation 7-19-2007.xls*
	p. 368	Specific surface area for ZrO_2	5 (a)	3, 10	Table 4.1-18, p. 4-30, Section 6.3.4.6.1, Table 6.3-12

Table 1. Data Qualification for External Source Data Qualified for Intended Use in Document ANL-WIS-PA-000001 REV 03 (Continued)

Input	Source	Description	Method[1] (Rationale)[2]	Attribute[3]	Locations within AMR Where Data Are Listed and Where Qualification Is Documented or Corroboration Is Demonstrated
Stakebake 1971 [DIRS 178302]	Figure 8	Water Vapor Adsorption Isotherm for PuO_2	5 (a)	3, 10	Table 4.1-18, p. 4-30, Section 6.3.4.6.1, Figure 6.3-42, output DTN: SN0703PAEBSRTA.001 [DIRS 185343], file *CSNF Isotherm Compilation 7-19-2007.xls*
	p. 253	Specific surface area for PuO_2	5 (a)	3, 10	Table 4.1-18, p. 4-30, Section 6.3.4.6.1, Table 6.3-12
Stakebake and Dringman 1968 [DIRS 178840]	Figure 3, Figure 4	Water Vapor Adsorption Isotherm for PuO_2	5 (a)	3, 10	Table 4.1-18, p. 4-30, Section 6.3.4.6.1, Figure 6.3-42, output DTN: SN0703PAEBSRTA.001 [DIRS 185343], file *CSNF Isotherm Compilation 7-19-2007.xls*
	Table 1	Specific surface area for PuO_2	5 (a)	3, 10	Table 4.1-18, p. 4-30, Section 6.3.4.6.1, Table 6.3-12
Paffett et al. 2003 [DIRS 178712]	Figure 8	Water Vapor Adsorption Isotherm for PuO_2	5 (a)	3, 10	Table 4.1-18, p. 4-30, Section 6.3.4.6.1, Figure 6.3-42, output DTN: SN0703PAEBSRTA.001 [DIRS 185343], file *CSNF Isotherm Compilation 7-19-2007.xls*
	Table 1	Specific surface area for PuO_2	5 (a)	3, 10	Table 4.1-18, p. 4-30, Section 6.3.4.6.1, Table 6.3-12
Kandori and Ishikawa 1991 [DIRS 178680]	Figure 2	Water Vapor Adsorption Isotherm for amorphous ferric oxide hydroxide	5 (a)	3, 10	Table 4.1-19, p. 4-33, Section 6.3.4.3.2, p. 6-72, Figure 6.3-34, output DTN: SN0703PAEBSRTA.001 [DIRS 185343], file *Corrosion Products Composite Isotherm 7-19-2007.xls*
Koch and Møller 1987 [DIRS 173784]	Figures 5 and 6	Water Vapor Adsorption Isotherms for goethite	5 (a)	3, 10	Table 4.1-19, p. 4-33, Section 6.3.4.3.2, p. 6-72, Figure 6.3-34, output DTN: SN0703PAEBSRTA.001, file *Corrosion Products Composite Isotherm 7-19-2007.xls*
	Table 1	Goethite specific surface area	5 (a)	7, 10	Table 4.1-19, pp. 4-13 through 4-15, Section 6.3.4.3.3, Appendix K, Figure K-5, output DTN: SN0703PAEBSRTA.001 [DIRS 185343], file *Goethite specific surface area 7-12-2007.xls*
Carruthers et al. 1971 [DIRS 178656]	Figure 7	Water Vapor Adsorption Isotherms for chromium oxide gel	5 (a)	3, 10	Table 4.1-19, p. 4-33, Section 6.3.4.3.2, p. 6-72, Figure 6.3-34, output DTN: SN0703PAEBSRTA.001 [DIRS 185343], file *Corrosion Products Composite Isotherm 7-19-2007.xls*
	Table IV	Specific surface area for chromium oxide gel	5 (a)	3, 10	Table 4.1-19, p. 4-33, Section 6.3.4.3.3, Table 6.3-7

Table 1. Data Qualification for External Source Data Qualified for Intended Use in Document ANL-WIS-PA-000001 REV 03 (Continued)

Input	Source	Description	Method[1] (Rationale)[2]	Attribute[3]	Locations within AMR Where Data Are Listed and Where Qualification Is Documented or Corroboration Is Demonstrated
Morimoto et al. 1969 [DIRS 162877]	Figures 3 and 4 (adsorption isotherms) and Table I (monolayer capacity)	Water Vapor Adsorption Isotherms and monolayer capacity for α-Fe_2O_3	5 (a)	3, 10	Table 4.1-19, p. 4-33, Section 6.3.4.3.2, p. 6-72, Figure 6.3-34, output DTN: SN0703PAEBSRTA.001 [DIRS 185343], file *Corrosion Products Composite Isotherm 7-19-2007.xls*
Harju et al. 2005 [DIRS 178670]	Figure 4a (adsorption isotherm) and Table 6 (monolayer volume)	Water Vapor Adsorption Isotherm and monolayer volume for Cr_2O_3	5 (a)	3, 10	Table 4.1-19, p. 4-33, Section 6.3.4.3.2, p. 6-72, Figure 6.3-34, output DTN: SN0703PAEBSRTA.001 [DIRS 185343], file *Corrosion Products Composite Isotherm 7-19-2007.xls*
Rice et al. 1980 [DIRS 178725]	Figure 2	Water Vapor Adsorption Isotherms for NiO	5 (a)	3, 10	Table 4.1-19, p. 4-33, Section 6.3.4.3.2, p. 6-72, Figure 6.3-34, output DTN: SN0703PAEBSRTA.001 [DIRS 185343], file *Corrosion Products Composite Isotherm 7-19-2007.xls*
Nagao et al. 1995 [DIRS 162878]	Figure 1b	Water Vapor Adsorption Isotherm for Cr_2O_3	5 (a)	3, 10	Table 4.1-19, p. 4-33, Section 6.3.4.3.2, p. 6-72, Figure 6.3-34, output DTN: SN0703PAEBSRTA.001 [DIRS 185343], file *Corrosion Products Composite Isotherm 7-19-2007.xls*
	p. 222	Specific surface area for Cr_2O_3	5 (a)	3, 10	Table 4.1-19, p. 4-33, Section 6.3.4.3.3, Table 6.3-7
Kuwabara et al. 1987 [DIRS 178682]	Figure 1	Water Vapor Adsorption Isotherm for α-Fe_2O_3	5 (a)	3, 10	Table 4.1-19, p. 4-33, Section 6.3.4.3.2, p. 6-72, Figure 6.3-34, output DTN: SN0703PAEBSRTA.001 [DIRS 185343], file *Corrosion Products Composite Isotherm 7-19-2007.xls*
Kittaka et al. 1984 [DIRS 178830]	Figure 6a (adsorption isotherm) and p. 459 (monolayer covereage)	Water Vapor Adsorption Isotherm and monolayer coverage for α-$HCrO_2$	5 (a)	3, 10	Table 4.1-19, p. 4-33, Section 6.3.4.3.2, p. 6-72, Figure 6.3-34, output DTN: SN0703PAEBSRTA.001 [DIRS 185343], file *Corrosion Products Composite Isotherm 7-19-2007.xls*
	Table 1	Specific surface area for α-$HCrO_2$	5 (a)	3, 10	Table 4.1-19, p. 4-33, Section 6.3.4.3.3, Table 6.3-7

Table 1. Data Qualification for External Source Data Qualified for Intended Use in Document ANL-WIS-PA-000001 REV 03 (Continued)

Input	Source	Description	Method[1] (Rationale)[2]	Attribute[3]	Locations within AMR Where Data Are Listed and Where Qualification Is Documented or Corroboration Is Demonstrated
Kittaka et al. 1983 [DIRS 178681]	Figure 6, Figure 7 (adsorption isotherms) and Table 1 (monolayer capacity)	Water Vapor Adsorption Isotherms and monolayer capacity for Cr_2O_3	5 (a)	3, 10	Table 4.1-19, p. 4-33, Section 6.3.4.3.2, p. 6-72, Figure 6.3-34, output DTN: SN0703PAEBSRTA.001 [DIRS 185343], file *Corrosion Products Composite Isotherm 7-19-2007.xls*
	Table 1	Specific surface area for Cr_2O_3	5 (a)	3, 10	Table 4.1-19, p. 4-33, Section 6.3.4.3.3, Table 6.3-7
Micale et al. 1976 [DIRS 179136]	Figure 3 (adsorption isotherms) and p. 542 (statistical monolayer)	Water Vapor Adsorption Isotherms and statistical monolayer for $Ni(OH)_2$	5 (a)	3, 10	Table 4.1-19, p. 4-33, Section 6.3.4.3.2, p. 6-72, Figure 6.3-34, output DTN: SN0703PAEBSRTA.001 [DIRS 185343], file *Corrosion Products Composite Isotherm 7-19-2007.xls*
	p. 541 and 542	Specific surface area for $Ni(OH)_2$	5 (a)	3, 10	Table 4.1-19, p. 4-33, Section 6.3.4.3.3, Table 6.3-7
Micale et al. 1985 [DIRS 173785]	Figures 2 and 3 (adsorption isotherms) and Table 1 (monolayer coverage)	Water Vapor Adsorption Isotherm for α-Fe_2O_3 and γ-FeOOH	5 (a)	3, 10	Table 4.1-19, p. 4-33, Section 6.3.4.3.2, p. 6-72, Figure 6.3-34, output DTN: SN0703PAEBSRTA.001 [DIRS 185343], file *Corrosion Products Composite Isotherm 7-19-2007.xls*

Table 1. Data Qualification for External Source Data Qualified for Intended Use in Document ANL-WIS-PA-000001 REV 03 (Continued)

Input	Source	Description	Method[1] (Rationale)[2]	Attribute[3]	Locations within AMR Where Data Are Listed and Where Qualification Is Documented or Corroboration Is Demonstrated
Jurinak 1964 [DIRS 154381]	Figures 5 and 6	Water Vapor Adsorption Isotherms for α-Fe_2O_3 and FeOOH	5 (a)	3, 10	Table 4.1-19, p. 4-33, Section 6.3.4.3.2, p. 6-72, Figure 6.3-34, output DTN: SN0703PAEBSRTA.001 [DIRS 185343], file *Corrosion Products Composite Isotherm 7-19-2007.xls*
	Table 1	Specific surface area for α-Fe_2O_3 and FeOOH	5 (a)	3, 10	Table 4.1-19, p. 4-33, Section 6.3.4.3.3, Table 6.3-7

[1] Method from SCI-PRO-001, *Qualification of Unqualified Data*, Attachment 2.
[2] The rationale is that (a) it is the most suitable considering the data, the intended use, and availability of corroborating data; (b) it is the most suitable considering the use in similar applications; (c) it is the most suitable considering the data and available documentation of the QA program; (d) it is the most suitable considering the data and the existing documentation regarding the data and the data originator; (e) corroborating data are available for comparison with the unqualified data set and any inferences drawn to corroborate the unqualified data can be clearly identified, justified and documented.
[3] Attributes from SCI-PRO-001, *Qualification of Unqualified Data*, Attachment 3.

Table 2. DIRS Changes to Correct Indirect/Direct Classification and Miscellaneous Related Changes

Input	Source	Description	DIRS Changes Required
McCafferty and Zettlemoyer 1970 [DIRS 154382]	Figure 3	Water vapor adsorption Isotherms for α-Fe_2O_3	In 3rd DIRS entry, change "Steel Corrosion Products" to "Fe2O3" under Input Description. Change input usage to "Direct Input" Change "N/A" to "Data" under Input Category.
	p. 453	Specific surface area of Fe_2O_3	In 2nd DIRS entry, delete "Entire," under Specifically Used From; delete "Sections 6.3.4.3.1, 6.3.4.3.2;" under Specifically Used In; delete ", adsorption isotherm for water vapor on Fe2O3" under Input Description.
	p. 454	Water molecule cross-sectional area, A_w	In 1st DIRS entry, change "6.3.4.3.3" to "6.3.4.3.2" under Specifically Used From;
Cornejo et al. 1984 [DIRS 178660]	Table 1	Specific surface area for HFO	Change input usage to "Direct Input" Change "N/A" to "Data" under Input Category.
Cornejo 1987 [DIRS 178659]	Table 1	Specific surface area for HFO	Change input usage to "Direct Input" Change "N/A" to "Data" under Input Category.
Schwertmann et al. 2004 [DIRS 178734]	Table 1	Specific surface area for HFO	Change input usage to "Direct Input" Change "N/A" to "Data" under Input Category.
Mitov et al. 2002 [DIRS 178686]	Table 5	Specific surface area for HFO	Change input usage to "Direct Input" Change "N/A" to "Data" under Input Category.
Clausen and Fabricius 2000 [DIRS 178655]	Table 2	Specific surface area for HFO	Change input usage to "Direct Input" Change "N/A" to "Data" under Input Category.
O'Reilly and Hochella 2003 [DIRS 178704]	Table 1	Specific surface area for HFO	Change input usage to "Direct Input" Change "N/A" to "Data" under Input Category.
Sani et al. 2004 [DIRS 178727]	p. 2640	Specific surface area for HFO	Change input usage to "Direct Input" Change "N/A" to "Data" under Input Category.
Hofmann et al. 2004 [DIRS 173783]	Table 1	Specific surface area for HFO	Change input usage to "Direct Input" Change "N/A" to "Data" under Input Category.
	Figure 8	Water Vapor Adsorption Isotherms for HFO	Delete 1st DIRS entry (Input Description: "Comparison of Adsorption Isotherms..."). In 3rd DIRS entry, add "Figure 6.3-23" under Specifically Used In; change "Steel Corrosion Products" to "HFO;" change input usage to "Direct Input" Change "N/A" to "Data" under Input Category.
	p. 167	Density of HFO	Change input usage to "Indirect Input." Change "Data" to "N/A" under Input Category.

Input	Source	Description	DIRS Changes Required

Table 2. DIRS Changes to Correct Indirect/Direct Classification and Miscellaneous Related Changes (Continued)

Input	Source	Description	DIRS Changes Required
Sauvé et al. 2000 [DIRS 178732]	Table 1	Specific surface area for HFO	Change input usage to "Direct Input" Change "N/A" to "Data" under Input Category.
Weidler 1997 [DIRS 178741]	Table 1	Specific surface area for HFO	Change input usage to "Direct Input" Change "N/A" to "Data" under Input Category.
Guzman et al. 1994 [DIRS 178669]	Table 1	Specific surface area for HFO	Change input usage to "Direct Input" Change "N/A" to "Data" under Input Category.
Larsen and Postma 2001 [DIRS 178683]	Table 2	Specific surface area for HFO	Change input usage to "Direct Input" Change "N/A" to "Data" under Input Category.
Leone et al. 2001 [DIRS 178684]	p. 1317	Specific surface area for HFO	Change input usage to "Direct Input" Change "N/A" to "Data" under Input Category.
Davis and Leckie 1978 [DIRS 125591]	p. 95	Specific surface area for HFO	Change input usage to "Direct Input" Change "N/A" to "Data" under Input Category.
Liaw et al. 1989 [DIRS 178685]	Table 1	Specific surface area for HFO	Change input usage to "Direct Input" Change "N/A" to "Data" under Input Category.
Crosby et al. 1983 [DIRS 178662]	Table II	Specific surface area for HFO	Change input usage to "Direct Input" Change "N/A" to "Data" under Input Category.
Axe and Anderson 1995 [DIRS 178654]	p. 159	Specific surface area for HFO	Change input usage to "Direct Input" Change "N/A" to "Data" under Input Category.
Van der Giessen 1966 [DIRS 178740]	Table 1	Specific surface area for HFO	Change input usage to "Direct Input" Change "N/A" to "Data" under Input Category.
Davies-Colley et al. 1984 [DIRS 178666]	p. 492	Specific surface area for HFO	Change input usage to "Direct Input" Change "N/A" to "Data" under Input Category.
Tipping 1981 [DIRS 178737]	Table 1	Specific surface area for HFO	Change input usage to "Direct Input" Change "N/A" to "Data" under Input Category.
Carlson and Schwertmann 1981 [DIRS 142788]	Table 1	Specific surface area for HFO	Change input usage to "Direct Input" Change "N/A" to "Data" under Input Category.
Eggleton and Fitzpatrick 1988 [DIRS 173878]	Table 1	Specific surface area for HFO	Change input usage to "Direct Input" Change "N/A" to "Data" under Input Category.
Turner and Sassman 1996 [DIRS 179618]	Tables 1 and 3	Surface Complexation Constants	Change input usage to "Direct Input" Change "N/A" to "Data" under Input Category.
Wang et al. 2001 [DIRS 176816]	Tables 3 and 4	Surface Complexation Constants	Change input usage to "Direct Input" Change "N/A" to "Data" under Input Category.

Input	Source	Description	DIRS Changes Required
Pepper et al.2006 [DIRS 179622]	Table 2	Surface Complexation Constants	Change input usage to "Direct Input" Change "N/A" to "Data" under Input Category.
Cromières et al. 1998 [DIRS 179616]	Table 4	Surface Complexation Constants	Change input usage to "Direct Input" Change "N/A" to "Data" under Input Category.
Appelo et al. 2002 [DIRS 168168]	Table 2	Surface Complexation Constants	Change input usage to "Direct Input" Change "N/A" to "Data" under Input Category.
LaVerne and Tandon 2003 [DIRS 178303]	Figure 1	Water Vapor Adsorption Isotherms for SNF Waste Form Materials	Change input usage to "Direct Input" Change "N/A" to "Data" under Input Category.
	p. 13624	Specific surface area for UO_2 and CeO_2	Change input usage to "Direct Input" Change "N/A" to "Data" under Input Category.
Gammage et al. 1970 [DIRS 178304]	Figure 2, p. 4277	Water Vapor Adsorption Isotherm and specific surface area for SNF waste form materials	Add "Specific surface area of ThO2" to Input Description. Change input usage to "Direct Input" Change "N/A" to "Data" under Input Category.
Holmes et al. 1974 [DIRS 154379]	Figure 3	Water Vapor Adsorption Isotherm for SNF waste form materials	In 1st DIRS entry, add "Sections 4.1.2, 6.3.4.3.2" under Specifically Used In. In 2nd DIRS entry, delete "p. 368" under Specifically Used From; delete "Sections 4.1.2, 6.3.4.3.2; Tables 6.3-7, 6.3-12" under Specifically Used In; delete "Cross sectional area of a water molecule. Specific surface area of ZrO2." under Input Description; and change input usage to "Direct Input." Change "N/A" to "Data" under Input Category.
	p. 368 (specific surface area)	Specific surface area of ZrO_2.	In 3rd DIRS entry, delete "Fig. 3 (adsorption isotherm)" under Specifically Used From; add "Tables 6.3-7, 6.3-12" under Specifically Used In; delete "Water Vapor Adsorption Isotherms for SNF Waste Form Materials" and add "Specific surface area of ZrO2" under Input Description; and change input usage to "Direct Input." Change "N/A" to "Data" under Input Category.
Stakebake 1971 [DIRS 178302]	Figure 8	Water Vapor Adsorption Isotherm for SNF waste form materials	In 1st DIRS entry, delete ",p. 253 (specific surface area)" under Specifically Used From; add "Figure 6.3-38" under Specifically Used In; add "(PuO2)" under Input Description; change input usage to "Direct Input" Change "N/A" to "Data" under Input Category.

Input	Source	Description	DIRS Changes Required
	p. 253	Specific surface area of PuO_2.	In 2nd DIRS entry, add "(specific surface area)" under Specifically Used From; add "Table 4.1-18" under Specifically Used In; add "(specific surface area of PuO_2)." under Input Description; change input usage to "Direct Input" Change "N/A" to "Data" under Input Category. Delete 3rd DIRS entry (entire row).
Stakebake and Dringman 1968 [DIRS 178840]	Figure 3, Figure 4, Table 1	Water Vapor Adsorption Isotherm and specific surface area for SNF waste form materials	Change input usage to "Direct Input" Change "N/A" to "Data" under Input Category.
Paffett et al. 2003 [DIRS 178712]	Figure 8, Table 1	Water Vapor Adsorption Isotherm and specific surface area for SNF waste form materials	Change input usage to "Direct Input" Change "N/A" to "Data" under Input Category.
Kandori and Ishikawa 1991 [DIRS 178680]	Figure 2	Water Vapor Adsorption Isotherm for amorphous ferric oxide hydroxide	Change input usage to "Direct Input" Change "N/A" to "Data" under Input Category.
Koch and Møller 1987 [DIRS 173784]	Figures 5 and 6	Water Vapor Adsorption Isotherms for goethite	In 2nd DIRS entry, delete "; Table 1 (specific surface area)" under Specifically Used From; add "Figures 6.3-21, 6.3-22" under Specifically Used In; add " (Goethite)" under Input Description; Change input usage to "Direct Input" Change "N/A" to "Data" under Input Category.
	Table 1	Goethite specific surface area	In 3rd DIRS entry, delete "Figures 5 and 6" and add "Table 1 (specific surface area)" under Specifically Used From; delete "Figures 6.3-21, 6.3-22" and add "Table 4.1-19" under Specifically Used In; delete "Water Vapor Adsorption Isotherm for Goethite" and add "Specific surface area of goethite" under Input Description; change input usage to "Direct Input" Change "N/A" to "Data" under Input Category.
Carruthers et al. 1971 [DIRS 178656]	Figure 7	Water Vapor Adsorption Isotherms for chromium oxide gel	In 1st DIRS entry, change input usage to "Direct Input" Change "N/A" to "Data" under Input Category.
	Table IV	Specific surface area for chromium oxide gel	In 1st DIRS entry, add "Specific surface area of chromium oxide gel." under Input Description;

Input	Source	Description	DIRS Changes Required
Morimoto et al. 1969 [DIRS 162877]	Figures 3 and 4 (adsorption isotherms) and Table I (monolayer capacity)	Water Vapor Adsorption Isotherms and monolayer capacity for α-Fe_2O_3	Change input usage to "Direct Input" Change "N/A" to "Data" under Input Category.
Harju et al. 2005 [DIRS 178670]	Figure 4a (adsorption isotherm) and Table 6 (monolayer volume)	Water Vapor Adsorption Isotherm and monolayer volume for Cr_2O_3	Change input usage to "Direct Input" Change "N/A" to "Data" under Input Category.
Rice et al. 1980 [DIRS 178725]	Figure 2	Water Vapor Adsorption Isotherms for NiO	Change input usage to "Direct Input" Change "N/A" to "Data" under Input Category.
Nagao et al. 1995 [DIRS 162878]	Figure 1b, p. 222	Water Vapor Adsorption Isotherm and specific surface area for Cr_2O_3	Change input usage to "Direct Input" Change "N/A" to "Data" under Input Category.
Kuwabara et al. 1987 [DIRS 178682]	Figure 1	Water Vapor Adsorption Isotherm for α-Fe_2O_3	Change input usage to "Direct Input" Change "N/A" to "Data" under Input Category.
Kittaka et al. 1984 [DIRS 178830]	Figure 6a (adsorption isotherm) and p. 459 (monolayer covereage)	Water Vapor Adsorption Isotherm and monolayer coverage for α-$HCrO_2$	Change input usage to "Direct Input" Change "N/A" to "Data" under Input Category.
	Table 1	Specific surface area for α-$HCrO_2$	Change input usage to "Direct Input" Change "N/A" to "Data" under Input Category.
Kittaka et al. 1983 [DIRS 178681]	Figure 6, Figure 7 (adsorption isotherms) and Table 1 (monolayer capacity)	Water Vapor Adsorption Isotherms and monolayer capacity for Cr_2O_3	Change input usage to "Direct Input" Change "N/A" to "Data" under Input Category.
	Table 1	Specific surface area for Cr_2O_3	Change input usage to "Direct Input" Change "N/A" to "Data" under Input Category.
Micale et al. 1976 [DIRS 179136]	Figure 3 (adsorption isotherms) and p. 542 (statistical monolayer)	Water Vapor Adsorption Isotherms and statistical monolayer for $Ni(OH)_2$	Change input usage to "Direct Input" Change "N/A" to "Data" under Input Category.
	p. 541 and 542	Specific surface area for $Ni(OH)_2$	Change input usage to "Direct Input" Change "N/A" to "Data" under Input Category.
Micale et al. 1985 [DIRS 173785]	Figures 2 and 3 (adsorption isotherms) and Table 1 (monolayer coverage)	Water Vapor Adsorption Isotherm for α-Fe_2O_3 and γ-FeOOH	Change input usage to "Direct Input" Change "N/A" to "Data" under Input Category.
Bear 1988 [DIRS 101379]	p. 116	Exponents used in Archie's law	Change input category to "Established Fact"
Langmuir 1997 [DIRS 100051]	Table 10.2	Specific surface area of hematite	Change input category to "Established Fact"
Cornell and Schwertmann 2003 [DIRS 173037]	Entire	Density of HFO	Change input usage to "Indirect Input" Change "Data" to "N/A" under Input Category.

Input	Source	Description	DIRS Changes Required
Christl and Kretzschmar 1999 [DIRS 173811]	p. 2929	Site densities can be measured or estimated through fitting in a SCM.	Change input usage to "Indirect Input" Change "Data" to "N/A" under Input Category.
Hofmann et al. 2005 [DIRS 173711]	Table 2	Surface area and site density for HFO.	Change input usage to "Indirect Input" Change "Data" to "N/A" under Input Category.
Reimus et al. 2002 [DIRS 163008]	p. 2.25, Equation 2.5	Diffusion coefficient for saturated whole rock samples of tuff.	Delete "Table 4.1-19," and change "Sections 4.1.2, 6.5.3.6, 6.6.4.2" to "Section 6.6.4.2." Change input usage to "Indirect Input" Change "Data" to "N/A" under Input Category.
Jurinak 1964 [DIRS 154381]	Figures 5 and 6	Water Vapor Adsorption Isotherms for α-Fe_2O_3 and FeOOH	In 1st DIRS entry, replace "p. 480" with "pp. 479-480" under Specifically Used From; delete "Figures 6.3-7 & 7.2-1" under Specifically Used In; replace "Water adsorption isotherm on Fe2O3" with "Water molecule cross sectional area" under Input Description; change input usage to "Indirect Input." Change "Data" to "N/A" under Input Category. In 2nd DIRS entry, change "Figure 6" to "Figures 5 and 6" under Specifically Used From; change "Figure 6.3-20" to "Figures 6.3-19 and 6.3-20" under Specifically Used In; delete "Water molecule cross sectional area; specific surface area of Fe2O3" and "goethite specific surface area" and replace "Goethite water adsorption isotherm" with "Goethite and Fe2O3 water adsorption isotherms" under Input Description; change input usage to "Direct Input" Change "N/A" to "Data" under Input Category.
	Table I	Specific surface area for α-Fe_2O_3 and FeOOH	In 3rd DIRS entry, change "Fig. 5" to "Table I" under Specifically Used From; delete "; Figure 6.3-19" under Specifically Used In; change "Water Vapor Adsorption Isotherms for Steel Corrosion Products" to "Specific surface area of Fe2O3 and goethite" under Input Description; change input usage to "Direct Input" Change "N/A" to "Data" under Input Category. Delete 4th DIRS entry (Input Description "'Close-packed' monolayer of water").

Input	Source	Description	DIRS Changes Required
Dzombak and Morel 1990 [DIRS 105483]	Table 5.3	Sorption density and specific surface area data for ferrihydrite	Change input category to "Established Fact"
	Table 10.5	Surface Complexation Constants	Change input usage to "Direct Input" and input category to "Established Fact"
Briand et al. 2001 [DIRS 161617]	Table 4	Specific surface area of Fe_2O_3	Change input category to "Indirect Input" Change "Data" to "N/A" under Input Category.
Mills 1973 [DIRS 133392]	Table III	Self-diffusion coefficient of water	Change input category to "Indirect input" Change "Data" to "N/A" under Input Category.

V. CR 13657 Resolution

CR 13657 is resolved by correcting references in Figures 7.2-13 and 7.2-14 and providing specific locations of data in the sources:

1. In Figure 7.2-13, change the reference in the "Sources" notation from "EPA 2004 [DIRS 170376]" to "EPA 2004 [DIRS 172215], Table 5.22" and change the reference in the figure title from "EPA 1999 [DIRS 170376]" to "EPA 2004 [DIRS 172215], Table 5.22."

2. In Figure 7.2-14, change the reference in the "Sources" notation from "EPA 2004 [DIRS 170376]" to "EPA 2004 [DIRS 172215], Table 5.6."

None of the changes in response to CR 13657 impacts the conclusions of ANL-WIS-PA-000001 REV 03, and no downstream usage—neither the LA nor other project documents—is impacted.

VI. CR 13740 Resolution

CR 13740 is resolved by changing the word "highest" to "lowest" in describing the concentration of competing cations in the validation of the competitive surface complexation model in ANL-WIS-PA-000001 REV 03, Section 7.2.3:

1. p. 7-37, last 2 lines, and p. 7-38, 1st line: Change "The higher K_ds from the C-SCM are typically calculated when multiple extrema of the model are sampled (e.g., the highest surface areas, the lowest values, the highest concentration of competing cations)" to "The higher K_ds from the C-SCM are typically calculated when multiple extrema of the model are sampled (e.g., the highest surface areas, the lowest P_{CO_2} values, the lowest concentration of competing cations)."

2. p. 7-40, 1st paragraph under **Neptunium** heading, next-to-last sentence: Change "The higher K_ds from the C-SCM are calculated when multiple extrema of the model are sampled (e.g., the highest surface areas, the lowest P_{CO_2} values, the highest concentration of competing cations)" to "The higher K_ds from the C-SCM are calculated when multiple extrema of the model are sampled (e.g., the highest surface areas, the lowest P_{CO_2} values, the lowest concentration of competing cations)."

3. p. 7-41, lines 6-8: Change "The higher Am K_ds are calculated when multiple extrema of the model are sampled (e.g., the highest surface areas, the lowest P_{CO_2} values, the highest concentration of competing cations)" to "The higher Am K_ds are calculated when multiple extrema of the model are sampled (e.g., the highest surface areas, the lowest P_{CO_2} values, the lowest concentration of competing cations)."

These statements are only utilized as discussion of the information and are not used to constrain the values utilized within the safety analysis. None of the changes in response to CR 13740 impacts the conclusions of ANL-WIS-PA-000001 REV 03 and no downstream usage—neither the LA nor other project documents—is impacted.

VII. CR 13678 Resolution

CR 13678 is resolved by replacing Figures 6.5-10 and 6.5-11, in which image resolution is poor and figure and axis labels are illegible, with the following figures having better resolution and legible figure and axis labels. (Note that the thick bands in Figure 6.5-10 are the result of the density and orientation of data points and are not an indication of low resolution in the plots.)

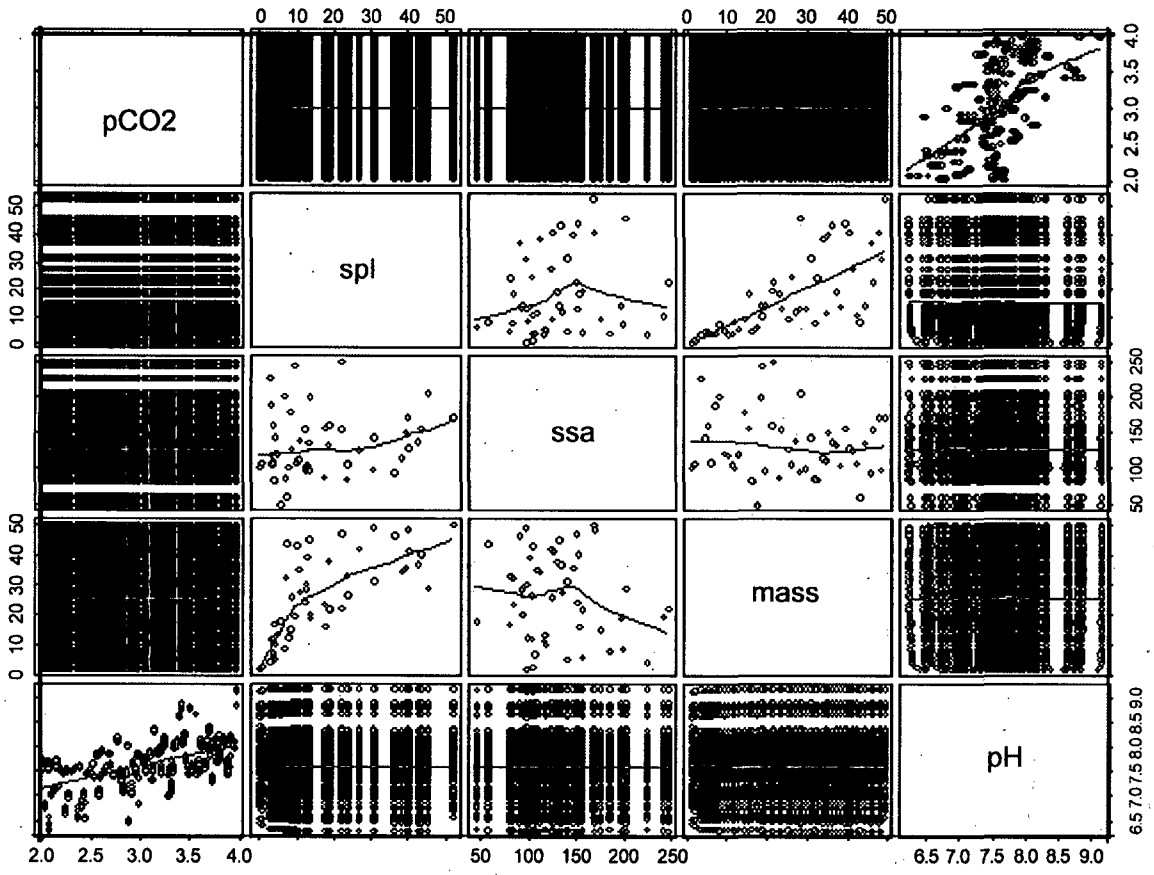

Source: S-PLUS plot of data in output DTN: SN0703PAEBSRTA.002

Figure 6.5-10. Scatter Plot Matrix of First 5 Predictors Versus the pH Response

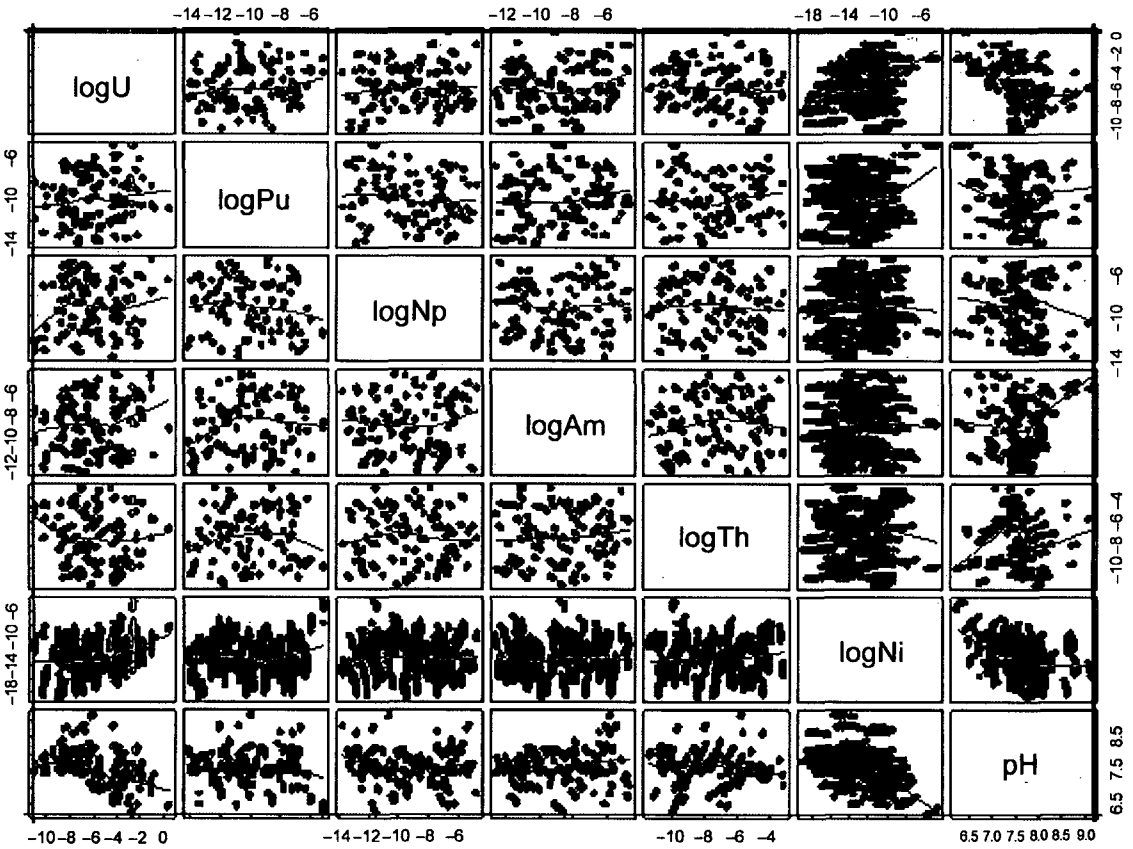

Source: S-PLUS plot of data in output DTN: SN0703PAEBSRTA.002

Figure 6.5-11. Scatter Plot Matrix of 6 Dissolved Concentration Predictors Versus the pH Response

None of the changes in response to CR 13678 impacts the conclusions of ANL-WIS-PA-000001 REV 03 and no downstream usage—neither the LA nor other project documents—is impacted.

VIII. CR 13643 Resolution

CR 13643 is resolved by correcting Eq. 6.5.1.2-9, which makes it consistent with the correct implementation in the TSPA-LA. In addition, the text describing Eq. 6.5.1.2-9 is corrected and revised to provide a clearer explanation of the concentration term. This correction also affects Eqs. 6.5.1.2-39 and 6.5.1.2-47 in Section 6.5.1.2 along with text and Eqs. 6.5.2.5-10 to 6.5.2.5-12 in Section 6.5.2.5.

None of the changes in response to CR 13643 impacts the conclusions of ANL-WIS-PA-000001 REV 03 and no downstream usage—neither the LA nor other project documents—is impacted.

CR 13643 is resolved by the following changes (in which underlining indicates the original text to be changed and the revised text):

1. p. 6-149, Eq. 6.5.1.2-9 and associated text: Change:

The term Q_{icm}^{embed} is the rate of mass conversion from dissolved state to embedded state onto waste form colloids for radionuclide species *i*. Radionuclides become embedded only in waste form colloids, not in iron oxyhydroxide or groundwater colloids. The conversion rate to embedded species is represented by a first order conversion of the species in solution:

$$Q_{icm}^{embed} = \theta_w \lambda_i^{embed} C_i, \qquad \text{(Eq. 6.5.1.2-9)}$$

where λ_i^{embed} is the first order rate constant (s^{-1}) for mass conversion from the dissolved state to the embedded state onto waste form colloids for radionuclide species *i*.

to:

For the waste form colloids generated during the degradation of the HLW glass and CSNF matrix, some mass of plutonium and americium is considered to be "embedded" within the waste form colloids at the time of generation and thereby considered as an intrinsic part of the colloid, not in equilibrium with the aqueous system. The term Q_{icm}^{embed} is the rate of conversion of mass of species *i* from degradation of the waste form to the embedded state associated the waste form colloids. The conversion rate to the embedded state is represented by a first order conversion:

$$Q_{icm}^{embed} = \theta_w \lambda_i^{embed} C_i^*, \qquad \text{(Eq. 6.5.1.2-9)}$$

where λ_i^{embed} is the first order rate constant (s^{-1}) for conversion of degraded mass of species *i* to the embedded mass associated with waste form colloids and the concentration term, C_i^*, is the concentration based on the mass of radionuclide species *i* made available from the degradation of the waste form per unit volume of water. This equation is discussed further in Section 6.5.2.5, where discretization of the mass balance equations and implementation in the TSPA are described. Radionuclides are considered to be embedded only in waste form colloids, not in iron oxyhydroxide or groundwater colloids.

2. p. 6-157, Eq. 6.5.1.2-39: Change:

$$\begin{aligned}\frac{\partial}{\partial t}\left[\theta_w R_{fi} C_i\right] = {} & \nabla\cdot\left(\theta_w D_i \nabla C_i\right) \\ & + \nabla\cdot\left\{\theta_w D_c \nabla\left[\left(K_{dicWF}C_{cWF} + K_{dicFeO}C_{cFeO} + K_{dicGW}C_{cGW}\right)C_i\right]\right\} \\ & - \nabla\cdot\left[\boldsymbol{q}_w\left(1 + K_{dicWF}C_{cWF} + K_{dicFeO}C_{cFeO} + K_{dicGW}C_{cGW}\right)C_i\right] \\ & \pm Q_{idp} - \left(\rho_b \bar{s}_{CP} + \theta_w C_{cFeO}\bar{s}_{cFeO}\right)k_{if}C_i + \rho_b \bar{s}_{CP} k_{ir}\hat{C}_{iCP} - \theta_w \lambda_i^{embed} C_i \\ & + \theta_w\left[\lambda_i^p r_{Mi}^p R_{fi}^p C_i^p - \lambda_i R_{fi} C_i\right],\end{aligned} \qquad \text{(Eq. 6.5.1.2-39)}$$

to:

$$\begin{aligned}\frac{\partial}{\partial t}\left[\theta_w R_{fi} C_i\right] = {} & \nabla\cdot\left(\theta_w D_i \nabla C_i\right) \\ & + \nabla\cdot\left\{\theta_w D_c \nabla\left[\left(K_{dicWF}C_{cWF} + K_{dicFeO}C_{cFeO} + K_{dicGW}C_{cGW}\right)C_i\right]\right\} \\ & - \nabla\cdot\left[q_w\left(1 + K_{dicWF}C_{cWF} + K_{dicFeO}C_{cFeO} + K_{dicGW}C_{cGW}\right)C_i\right] \\ & \pm Q_{idp} - \left(\rho_b \bar{s}_{CP} + \theta_w C_{cFeO}\bar{s}_{cFeO}\right)k_{if}C_i + \rho_b \bar{s}_{CP} k_{ir}\hat{C}_{iCP} - \theta_w \lambda_i^{embed} C_i^* \\ & + \theta_w\left[\lambda_i^p r_{Mi}^p R_{fi}^p C_i^p - \lambda_i R_{fi} C_i\right],\end{aligned} \qquad \text{(Eq. 6.5.1.2-39)}$$

[Note: The only change is in the last term in the 4th line, where C_i is replaced with C_i^*.]

3. <u>p. 6-159, Eq. 6.5.1.2-47: Change:</u>

$$\begin{aligned}\frac{\partial}{\partial t}\left[\theta_w R_{fi} C_i\right] = {} & \frac{\partial}{\partial z}\left(\theta_w D_i \frac{\partial C_i}{\partial z}\right) \\ & + \frac{\partial}{\partial z}\left(\theta_w D_c \frac{\partial}{\partial z}\left[\left(K_{dicWF}C_{cWF} + K_{dicFeO}C_{cFeO} + K_{dicGW}C_{cGW}\right)C_i\right]\right) \\ & - \frac{\partial}{\partial z}\left[q_{wz}\left(1 + K_{dicWF}C_{cWF} + K_{dicFeO}C_{cFeO} + K_{dicGW}C_{cGW}\right)C_i\right] \\ & \pm Q_{idp} - \left(\rho_b \bar{s}_{CP} + \theta_w C_{cFeO}\bar{s}_c\right)k_{if}C_i + \rho_b \bar{s}_{CP} k_{ir}\hat{C}_{iCP} - \lambda_i^{embed} C_i \\ & + \theta_w\left[\lambda_i^p r_{Mi}^p R_{fi}^p C_i^p - \lambda_i R_{fi} C_i\right].\end{aligned} \qquad \text{(Eq. 6.5.1.2-47)}$$

<u>to:</u>

$$\begin{aligned}\frac{\partial}{\partial t}\left[\theta_w R_{fi} C_i\right] = {} & \frac{\partial}{\partial z}\left(\theta_w D_i \frac{\partial C_i}{\partial z}\right) \\ & + \frac{\partial}{\partial z}\left(\theta_w D_c \frac{\partial}{\partial z}\left[\left(K_{dicWF}C_{cWF} + K_{dicFeO}C_{cFeO} + K_{dicGW}C_{cGW}\right)C_i\right]\right) \\ & - \frac{\partial}{\partial z}\left[q_{wz}\left(1 + K_{dicWF}C_{cWF} + K_{dicFeO}C_{cFeO} + K_{dicGW}C_{cGW}\right)C_i\right] \\ & \pm Q_{idp} - \left(\rho_b \bar{s}_{CP} + \theta_w C_{cFeO}\bar{s}_c\right)k_{if}C_i + \rho_b \bar{s}_{CP} k_{ir}\hat{C}_{iCP} - \lambda_i^{embed} C_i^* \\ & + \theta_w\left[\lambda_i^p r_{Mi}^p R_{fi}^p C_i^p - \lambda_i R_{fi} C_i\right].\end{aligned} \qquad \text{(Eq. 6.5.1.2-47)}$$

[Note: The only change is in the last term in the 4th line, where C_i is replaced with C_i^*.]

4. <u>p. 6-220, 2nd paragraph from bottom: Change:</u>

Within the waste form domain, some part of the <u>dissolved</u> mass of plutonium and americium made available from the degradation of HLW glass and CSNF is converted to "embedded" mass <u>on</u> the waste form colloids. This <u>conversion is required to satisfy the condition that some mass of plutonium and americium is "embedded" as</u> an intrinsic part of the colloid and is <u>not in equilibrium with the aqueous system, when generated from the degradation of HLW glass and</u>

CSNF. This mass is thus transported separately as a distinct species [*Waste Form and In-Drift Colloids-Associated Radionuclide Concentrations: Abstraction and Summary* (BSC 2005 [DIRS 177423], Sections 6.3.1 & 6.3.3.3)]. The mass rate of conversion per unit volume of water is modeled as a first order reaction given by $\lambda_i^{embed} C_i$, where λ_i^{embed} is the linear rate constant, and concentration C_i is the dissolved concentration of plutonium and americium species in the waste form domain. The conversion rate λ_i^{embed} is calculated at each time step in the waste form domain. Its calculation is discussed below.

to:

Within the waste form domain, some part of the mass of plutonium and americium made available from the degradation of HLW glass and CSNF is converted to "embedded" mass associated with the waste form colloids. This "embedded" mass is considered to be an intrinsic part of the colloids and is assumed to be available to the waste form colloids as long as there is plutonium and americium present in the waste form domain. This mass is thus transported separately as a distinct species [*Waste Form and In-Drift Colloids-Associated Radionuclide Concentrations: Abstraction and Summary* (BSC 2005 [DIRS 177423], Sections 6.3.1 & 6.3.3.3)]. The mass rate of conversion per unit volume of water is modeled as a first order reaction given by $\lambda_i^{embed} C_i^*$ (Eq. 6.5.1.2-9), where λ_i^{embed} is the linear rate constant, and the concentration C_i^* is the mass of radionuclide species *i* in the waste form domain per unit volume of water. The conversion rate λ_i^{embed} is calculated at each time step in the waste form domain. Its calculation is discussed below.

5. p. 6-221, Eqs. 6.5.2.5-10 to 6.5.2.5-12: Change:

$$\frac{\partial\left(\theta_w C_i^{embed}\right)}{\partial t} = -Q_{adv/diff}^{wfc} \frac{C_i^{embed}}{C_{cWF}} + \lambda_i^{embed} \theta_w C_i \,. \qquad \text{(Eq. 6.5.2.5-10)}$$

Discretization of this equation gives:

$$\frac{(\theta_w C_i^{embed})^{n+1} - (\theta_w C_i^{embed})^n}{t^{n+1} - t^n} = -\left(Q_{adv/diff}^{wfc} \frac{C_i^{embed}}{C_{cWF}}\right)^n + \lambda_i^{embed} (\theta_w C_i)^n \,. \text{(Eq. 6.5.2.5-11)}$$

This equation is solved for the conversion rate:

$$\lambda_i^{embed} = \frac{\dfrac{\left(\theta_w C_i^{embed}\right)^{n+1} - \left(\theta_w C_i^{embed}\right)^n}{\Delta t} + \left(Q_{adv/diff}^{wfc} \dfrac{C_i^{embed}}{C_{cWF}}\right)^n}{\left(\theta_w C_i\right)^n} \,. \qquad \text{(Eq. 6.5.2.5-12)}$$

to:

$$\frac{\partial\left(\theta_w C_i^{embed}\right)}{\partial t} = -Q_{adv/diff}^{wfc}\frac{C_i^{embed}}{C_{cWF}} + \lambda_i^{embed}\theta_w C_i^{*}. \qquad \text{(Eq. 6.5.2.5-10)}$$

Discretization of this equation gives:

$$\frac{(\theta_w C_i^{embed})^{n+1} - (\theta_w C_i^{embed})^{n}}{t^{n+1} - t^{n}} = -\left(Q_{adv/diff}^{wfc}\frac{C_i^{embed}}{C_{cWF}}\right)^{n} + \lambda_i^{embed}(\theta_w C_i^{*})^{n}. \text{(Eq. 6.5.2.5-11)}$$

This equation is solved for the conversion rate:

$$\lambda_i^{embed} = \frac{\dfrac{\left(\theta_w C_i^{embed}\right)^{n+1} - \left(\theta_w C_i^{embed}\right)^{n}}{\Delta t} + \left(Q_{adv/diff}^{wfc}\dfrac{C_i^{embed}}{C_{cWF}}\right)^{n}}{\left(\theta_w C_i^{*}\right)^{n}}. \qquad \text{(Eq. 6.5.2.5-12)}$$

[Note: The only changes are in the terms $\theta_w C_i$ (last term on the right in Eqs. 6.5.2.5-10 and 6.5.2.5-11 and in the denominator in Eq. 6.5.2.5-12), where C_i is replaced with C_i^*.]

6. Appendix A Notation, p. A-2, following definition of C_i: Add:

C_i^*	Concentration of radionuclide species *i* based on total mass of radionuclide species *i* in all states present in the waste form	kg m^{-3}	Eq. 6.5.1.2-9

IX. References

This section lists references that are used to resolve CRs in this ERD. References that are associated with a CR issue but are not used to resolve a CR, such as those in Tables 1 and 2, are not listed in this section.

IX.1. Documents Cited

169988 BSC (Bechtel SAIC Company) 2004. *Defense HLW Glass Degradation Model.* ANL-EBS-MD-000016 REV 02. Las Vegas, Nevada: Bechtel SAIC Company. ACC: DOC.20041020.0015; DOC.20050922.0002; LLR.20080408.0271; DOC.20081021.0002; DOC.20090323.0002.

111028 Ebert, W.L.; Hoburg, R.F.; and Bates, J.K. 1991. "The Sorption of Water on Obsidian and a Nuclear Waste Glass." *Physics and Chemistry of Glasses, 32,* (4), 133-137. Sheffield, England: Society of Glass Technology. TIC: 246078.

111034 Hagymassy, J., Jr.; Brunauer, S.; and Mikhail, R.Sh. 1969. "Pore Structure Analysis by Water Vapour Absorption. Part 1. T-Curves for Water Vapour." *Journal of Colloid and Interface Science, 29,* (3), 485-491. New York, New York: Academic Press. TIC: 246076.

177407 SNL (Sandia National Laboratories) 2007. *EBS Radionuclide Transport Abstraction.* ANL-WIS-PA-000001 REV 03. Las Vegas, Nevada: Sandia National Laboratories. ACC: DOC.20071004.0001; LLR.20080414.0023.

183478 SNL 2008. *Total System Performance Assessment Model /Analysis for the License Application.* MDL-WIS-PA-000005 REV 00 AD 01. Las Vegas, Nevada: Sandia National Laboratories. ACC: DOC.20080312.0001; LLR.20080414.0037; LLR.20080507.0002; LLR.20080522.0113; DOC.20080724.0005.

IX.2. Software Codes

182102 EXDOC_LA V. 2.0. 2007. WINDOWS XP, WINDOWS 2000 & WINDOWS 2003. STN: 11193-2.0-00.

184387 GoldSim V. 9.60.300. 2008. WIN 2000, WINXP, WIN2003. STN: 10344-9.60-03.

181049 MView V. 4.0. 2007. WINDOWS XP. STN: 10072-4.0-01.

185868 PHREEQC V. 2.11.01. 2008. WIN 2000. STN: 10068-2.11-01.

IX.3. Source Data, Listed by Data Tracking Number

185343 SN0703PAEBSRTA.001. Inputs Used in the Engineered Barrier System (EBS) Radionuclide Transport Abstraction. Submittal date: 04/10/2008.

IX.4. Output Data

MO0812TSPAOSIA.000. Over Sorption Impact Assessment for ERD-02 to ANL-WIS-PA-000001, Rev 03. Submittal date: 12/08/2008.

Attachment I – New DIRS Entries

Input Document			4. Specifically Used In:	5. Input Description	6. Input Usage	7. Input Category	8. Q Status	9. TBV/TBD Status
2a.	2. Technical Product Input Source Title and Identifier(s) with Version	3. Specifically Used From:						
352	SNL (Sandia National Laboratories) 2007. *Total System Performance Assessment Data Input Package for Requirements Analysis for Subsurface Facilities.* TDR-TDIP-PA-000001 REV 00. Las Vegas, Nevada: Sandia National Laboratories. ACC: DOC.20070921.0007. 179466	Table 4-1; Parameter 01-10	Appendix I.1	Drift diameter	Indirect Input	N/A	N/A	N/A
353	SNL (Sandia National Laboratories) 2007. *Total System Performance Assessment Data Input Package for Requirements Analysis for Transportation Aging and Disposal Canister and Related Waste Package Physical Attributes Basis for Performance Assessment.* TDR-TDIP-ES-000006 REV 00. Las Vegas, Nevada: Sandia National Laboratories. ACC: DOC.20070918.0005; LLR.20080328.0012. 179394	Tables A-1 and A-3	Section 6.3.4.3.4.2; Table 6.3-10	Typical measurements and surface areas for 21-PWR TAD waste package components	Indirect Input	N/A	N/A	N/A
	SNL (Sandia National Laboratories) 2008. *Total System Performance Assessment Model /Analysis for the License Application.* MDL-WIS-PA-000005 REV 00 AD 01. Las Vegas, Nevada: Sandia National Laboratories. ACC: DOC.20080312.0001; LLR.20080414.0037; LLR.20080507.0002; LLR.20080522.0113; DOC.20080724.0005. 183478	Section 4[a]	ERD 02, Section II.1	Inputs to the models run for the analysis of over-prediction of sorption	Direct Input	Data	N/A	N/A
		Section 3[a]	ERD 02, Section II.2	Software used for the analysis of over-prediction of sorption is same as used in TSPA-LA	Indirect Input	N/A	N/A	N/A
	EXDOC_LA V. 2.0. 2007. WINDOWS XP, WINDOWS 2000 & WINDOWS 2003. STN: 11193-2.0-00. 182102	Entire	ERD 02, Section II.2	Used to calculate expected values for quantities of interest.	Direct Input	Qualified Software	N/A	N/A
	GoldSim V. 9.60.300. 2008. WIN 2000, WINXP, WIN2003. STN: 10344-9.60-03. 184387	Entire	ERD 02, Section II.2	Used to query TSPA baseline simulations and to perform sensitivity analyses with the TSPA model.	Direct Input	Qualified Software	N/A	N/A
	MView V. 4.0. 2007. WINDOWS XP. STN: 10072-4.0-01. 181049	Entire	ERD 02, Section II.2	Used for performing regression analyses based on TSPA results.	Direct Input	Qualified Software	N/A	N/A
	PHREEQC V. 2.11.01. 2008. WIN 2000. STN: 10068-2.11-01. 185868	Entire	ERD 02, Section II.2	Used to perform geochemical modeling and to evaluate the effects of major ions that compete for sorption sites.	Direct Input	Qualified Software	N/A	N/A
	Hagymassy, J., Jr.; Brunauer, S.; and Mikhail, R.Sh. 1969. "Pore Structure Analysis by Water Vapour Absorption. Part 1. T-Curves for Water Vapour." *Journal of Colloid and Interface Science, 29*, (3), 485-491. New York, New York: Academic Press. TIC: 246076 111034	p. 489	ERD 02, Section IV	Isotherm for water on silica and quartz.	Indirect Input	N/A	N/A	N/A

INTENTIONALLY LEFT BLANK

LLYMP9011250B

NNA.900329.0142
NNA.19900329.0142

PNL-7170
UC-802

Results from NNWSI Series 3 Spent Fuel Dissolution Tests

C. N. Wilson

June 1990

Prepared for
the U.S. Department of Energy
Office of Civilian Radioactive Waste Management,
Yucca Mountain Project
under Contract DE-AC06-76RLO 1830

Pacific Northwest Laboratory
Operated for the U.S. Department of Energy
by Battelle Memorial Institute

00794 13340

PNL-7170

3 0 7 9 4 1 3 4 1

DISCLAIMER

This report was prepared as an account of work sponsored by an agency of the United States Government. Neither the United States Government nor any agency thereof, nor Battelle Memorial Institute, nor any of their employees, makes **any warranty, expressed or implied, or assumes any legal liability or responsibility for the accuracy, completeness, or usefulness of any information, apparatus, product, or process disclosed, or represents that its use would not infringe privately owned rights.** Reference herein to any specific commercial product, process, or service by trade name, trademark, manufacturer, or otherwise, does not necessarily constitute or imply its endorsement, recommendation, or favoring by the United States Government or any agency thereof, or Battelle Memorial Institute. The views and opinions of authors expressed herein do not necessarily state or reflect those of the United States Government or any agency thereof.

PACIFIC NORTHWEST LABORATORY
operated by
BATTELLE MEMORIAL INSTITUTE
for the
UNITED STATES DEPARTMENT OF ENERGY
under Contract DE-AC06-76RLO 1830

Printed in the United States of America

Available to DOE and DOE contractors from the
Office of Scientific and Technical Information, P.O. Box 62, Oak Ridge, TN 37831;
prices available from (615) 576-8401. FTS 626-8401.

Available to the public from the National Technical Information Service,
U.S. Department of Commerce, 5285 Port Royal Rd., Springfield, VA 22161.

NTIS Price Codes, Microfiche A01

Printed Copy

Price Code	Page Range
A02	1- 10
A03	11- 50
A04	51- 75
A05	76-100
A06	101-125
A07	126-150
A08	151-175
A09	176-200
A10	201-225
A11	226-250
A12	251-275
A13	276-300
A14	301-325

Price Code	Page Range
A15	326-350
A16	351-375
A17	376-400
A18	401-425
A19	426-450
A20	451-475
A21	476-500
A22	501-525
A23	526-550
A24	551-575
A25	576-600
A99	601-Up

PNL-7170
UC-802

RESULTS FROM NNWSI SERIES 3 SPENT FUEL DISSOLUTION TESTS

C. N. Wilson

June 1990

Prepared for
the U.S. Department of Energy
Office of Civilian Radioactive Waste Management,
Yucca Mountain Project
under Contract DE-AC06-76RLO 1830

Pacific Northwest Laboratory
Richland, Washington 99352

9 0 7 9 4 1 3 4 2

SUMMARY

The dissolution and radionuclide release behavior of spent fuel in groundwater is being studied by the Yucca Mountain Project (YMP), formerly the Nevada Nuclear Waste Storage Investigations (NNWSI) Project. Specimens prepared from pressurized water reactor fuel rod segments were tested in sealed stainless steel vessels in Nevada Test Site J-13 well water at 85°C and 25°C. The test matrix included three specimens of bare-fuel particles plus cladding hulls, two fuel rod segments with artificially defected cladding and watertight end fittings, and an undefected fuel rod section with watertight end fittings. Periodic solution samples were taken during test cycles with the sample volumes replenished with fresh J-13 water. Test cycles were periodically terminated and the specimens restarted in fresh J-13 water. The specimens were run for three cycles for a total test duration of 15 months.

Actinide concentrations (uranium, plutonium, americium, curium, and neptunium) peaked early in Cycle 1 of the bare-fuel tests and then declined to steady-state levels. Isotopes of plutonium and americium account for about 98% of the activity in spent fuel at 1,000 yr. Actinide concentrations rapidly reached stable steady-state values during Cycles 2 and 3. Steady-state activities on the order of 100 pCi/mL were measured for $^{239+240}Pu$, ^{241}Am, and ^{244}Cm at 25°C, and much lower activities on the order of 1 pCi/mL were measured for these radionuclides at 85°C. Even using the higher 25°C values, the steady-state concentrations indicated for all of the actinide elements were at least three orders of magnitude below those required to meet the Nuclear Regulatory Commission (NRC) 10 CFR 60.113 controlled release requirements for any realistic water flow rate through the repository. Calcium-uranium-silicate phases that may have contributed to the control of uranium concentrations were identified in the 85°C tests. Secondary phases controlling neptunium, plutonium, americium, and curium concentrations were not identified.

Concentrations of the more soluble fission product and activation product radionuclides generally tended to increase continuously with time. An exception was ^{90}Sr, which tended to reach maximum concentrations in the 85°C tests. Continuous release rates measured for ^{99}Tc, ^{137}Cs, and ^{129}I were

90794 1343

generally in the 10^{-4} to 10^{-3} of inventory per year range, but the rate for ^{129}I was lower at 25°C. Preferential release of ^{14}C continued through all three test cycles for a total release of about 1% of the ^{14}C specimen inventory. Comparison of ^{14}C releases in tests conducted in sealed and unsealed vessels indicated that ^{14}C was released to the atmosphere, most likely as CO_2. Although soluble radionuclides were released at rates in excess of the NRC limit of 10^{-5} of inventory per year in the current tests, additional data are needed to predict long-term release rates. The degree to which soluble radionuclides are preferentially released in such tests, and the degree to which the fuel will be degraded in the repository by processes such as oxidation, are not presently known.

9 0 7 9 4 1 3 4 4

ACKNOWLEDGMENTS

This report was prepared by Yucca Mountain Project (YMP) participants as part of the Civilian Radioactive Waste Management Program. The YMP is managed by the Yucca Mountain Project Office of the U.S. Department of Energy (DOE), Nevada Operations Office. YMP work is sponsored by the DOE Office of Civilian Radioactive Waste Management. The YMP is the former Nevada Nuclear Waste Storage Investigations (NNWSI) Project. The reported work was managed through the YMP (and NNWSI) Waste Package Task by Lawrence Livermore National Laboratory (LLNL) under Contract No. W-7405-ENG-48. The NNWSI title is used in this document to avoid changing the title of tests that were conducted prior to the project name change.

The NNWSI Series 3 Spent Fuel Dissolution Tests were conducted at the Hanford Engineering Development Laboratory, which was operated for the DOE by Westinghouse Hanford Company (WHC) under Contract No. DE-AC06-76FF02170. The NNWSI work along with most of the personnel involved were transferred from WHC to Pacific Northwest Laboratory (PNL) on June 29, 1987, as part of the DOE Hanford Site consolidation. PNL is operated for the DOE by Battelle Memorial Institute under Contract DE-AC06-76RLO 1830. Laboratory activities associated with the Series 3 tests were in general completed prior to transfer to PNL. Much of the data evaluation and preparation of this report occurred after transfer to PNL. Many people were involved in different aspects of the NNWSI Series 3 Spent fuel Dissolution Tests. The following list identifies the principal contributors.

Specimen Preparation

M. E. Freed
N. H. Larson

Setup, Sampling, and Test Operations

R. T. Steele
D. V. Archer

Sample Analyses

A. C. Leaf, Radiochemistry Team Leader
G. E. Meadows
D. L. Bellafatto

9 0 7 9 4 1 3 4 5

M. R. Eastman
J. M. Ruggles
A. M. Kozelisky

R. S. Strebin, ^{129}I
R. W. Strommatt, IC and Carbon
R. Ko, ICP
M. C. Burt, ICP
D. L. Baldwin, Fuel and Cladding ^{14}C Inventory
W. Y. Matsumoto, Burnup and Measured Nuclide Inventories

B. Mastel, SEM and XRD Specimen Preparation
B. P. Van der Cook, XRD

Management

V. M. Oversby, LLNL
H. F. Shaw, LLNL
R. L. Knecht, WHC

Others

J. R. Stuart, Data and Records Management
D. G. Farwick, Quality Assurance

9 0 7 9 4 1 3 4 6

CONTENTS

SUMMARY iii

ACKNOWLEDGMENTS v

ACRONYMS xv

1.0 BACKGROUND 1.1

2.0 TEST DESCRIPTION 2.1

2.1 TEST SPECIMENS 2.1

2.2 FUEL CHARACTERISTICS AND HISTORY 2.5

2.3 TEST SAMPLES AND ANALYSES 2.10

2.3.1 Starting J-13 Water 2.10

2.3.2 Periodic Solution Samples 2.10

2.3.3 Final Solution Samples 2.11

2.3.4 Rinse Samples 2.11

2.3.5 Acid Strip Samples 2.12

2.3.6 Ceramographic Samples 2.12

2.3.7 Rinse Filters 2.12

2.3.8 Coarse Rinse Sediments 2.13

2.4 CHEMISTRY 2.13

2.4.1 Radiochemistry 2.13

2.4.2 Solution Chemistry 2.16

2.5 TEST CYCLE RESTART 2.16

3.0 RESULTS AND DISCUSSION BY ELEMENT 3.1

3.1 GENERAL COMMENTS ON DATA PRESENTATION 3.1

3.1.1 Plotted Solution Sample Activity Data 3.1

3.1.2 "Quantities Measured" Tables 3.2

907941347

3.1.3 Qualifications for Certain Data Uses 3.3
3.2 URANIUM 3.4
3.2.1 Uranium in Solution Samples 3.5
3.2.2 Vessel Effects 3.7
3.2.3 Uranium Quantities in Sample Types 3.11
3.3 SECONDARY PHASE CHARACTERIZATION 3.13
3.4 PLUTONIUM 3.19
3.5 AMERICIUM 3.24
3.6 CURIUM 3.29
3.7 NEPTUNIUM 3.32
3.8 TECHNETIUM 3.37
3.9 CESIUM 3.42
3.10 STRONTIUM 3.44
3.11 IODINE 3.48
3.12 TIN-126 . . . . . 3.51
3.13 CARBON-14 . . . . . 3.52
3.14 COBALT-60 . . . . . 3.57
4.0 GENERAL DISCUSSION AND SUMMARY 4.1
4.1 THE ACTINIDES 4.2
4.1.1 Summary of Actinide Results 4.2
4.1.2 Comparisons with EQ3/6 Predictions 4.4
4.1.3 Actinide Release 4.7
4.2 FISSION AND ACTIVATION PRODUCTS 4.9
4.3 ADDITIONAL INFORMATION NEEDS 4.15
5.0 CONCLUSIONS 5.1
6.0 REFERENCES 6.1

9 0 7 9 4 1 3 4 8

APPENDIX A - RADIONUCLIDE INVENTORY AND RADIOCHEMICAL DATA A.1
APPENDIX B - SOLUTION CHEMISTRY DATA B.1
APPENDIX C - X-RAY DIFFRACTION INDEXING DATA C.1
APPENDIX D - PROCEDURES D.1
APPENDIX E - SURFACE AREA E.1

90794 1349

FIGURES

2.1 Series 3 Test Configurations 2.4

2.2 Ceramographic Section at Laser-Drilled Hole Defect Through the Cladding 2.6

2.3 Ceramographic Mosaic of As-Polished Specimen Section at Laser-Drilled Hole Defect Showing Postirradiation Fuel Cracking 2.7

3.1 Uranium Concentrations Measured in 0.4-μm Filtered Samples . . . 3.5

3.2 Comparison of Uranium Concentrations Measured in 0.4-μm Filtered Samples from the Three Series 3 and Two Series 2 Bare-Fuel Tests 3.7

3.3 SEM Photograph Showing Flocs on 0.4-μm Filter Disk Used to Filter the 119-Day Sample from Cycle 1 of the HBR/BF-85 Test 3.9

3.4 Metallographic Section of Bottom Weld in Specimen Basket from Cycle 1 of the HBR/BF-85 Test Etched with 10% Oxalic Acid 3.10

3.5 SEM Photograph and EDX Spectrum of Calcium-Uranium-Silicate Phase with Acicular Crystal Morphology on Rinse Filter from TP/BF-85 Cycle 1 Test 3.14

3.6 SEM Photograph and EDX Spectrum of Calcium-Uranium-Silicate Phase with Massive Flake Morphology on Rinse Filter from TP/BF-85 Cycle 2 Test 3.15

3.7 XRD Pattern of Rinse Filter from HBR/BF-85 Cycle 2 Test 3.17

3.8 XRD Pattern of Rinse Filter from TP/BF-85 Cycle 1 Test 3.18

3.9 XRD Pattern of Rinse Filter from TP/BF-85 Cycle 2 Test 3.19

3.10 Activity of $^{239+240}Pu$ in 0.4-μm Filtered Solution Samples 3.21

3.11 Comparison of $^{239+240}Pu$ Activities Measured in 0.4-μm Filtered Samples from the Three Series 3 and Two Series 2 Bare-Fuel Tests 3.22

3.12 Effects of Filtration on Measured $^{239+240}Pu$ Activity in Solution Samples from the Bare-Fuel Tests 3.23

3.13 Activity of ^{241}Am Measured in 0.4-μm Filtered Solution Samples 3.26

9 0 7 9 4 1 3 5 0

3.14 Comparison of ^{241}Am Activities Measured in 0.4-μm Filtered Samples from the Three Series 3 and Two Series 2 Bare-Fuel Tests 3.27

3.15 Effects of Filtration on Measured ^{241}Am Activity in Solution Samples from the Bare-Fuel Tests 3.28

3.16 Activity of ^{244}Cm Measured in 0.4-μm Filtered Solution Samples . 3.31

3.17 Comparison of ^{244}Cm Activities Measured in 0.4-μm Filtered Samples from the Three Series 3 and Two Series 2 Bare-Fuel Tests 3.32

3.18 Effects of Filtration on Measured ^{244}Cm Activity in Solution Samples from the Bare-Fuel Tests 3.33

3.19 Activity of ^{237}Np Measured in 0.4-μm Filtered Solution Samples from the Bare-Fuel Tests 3.35

3.20 Effects of Filtration on Measured ^{237}Np Activity in Solution Samples from the Bare-Fuel Tests 3.36

3.21 Technetium-99 Activities Measured in Unfiltered Samples from the Series 3 Bare-Fuel Tests and the Series 2 HBR Bare-Fuel Test 3.39

3.22 Activity of ^{137}Cs in 0.4-μm Filtered Solution Samples 3.43

3.23 Activity of ^{90}Sr in Unfiltered Solution Samples 3.46

3.24 Activities of ^{129}I Measured by Neutron Activation Analysis in Unfiltered Solution Samples 3.49

3.25 Activities of ^{14}C Measured in Unfiltered Solution Samples 3.54

4.1 Activity Levels of Fission Products and ^{14}C Levels Measured in the HBR/BF-25 and TP/BF-85 Tests 4.10

4.2 Inventory Fractions of ^{137}Cs, ^{90}Sr, ^{99}Tc, ^{129}I, and ^{14}C Measured in Solution During the HBR/BF-25 Test 4.12

4.3 Inventory Fractions of ^{137}Cs, ^{90}Sr, ^{99}Tc, ^{129}I, and ^{14}C Measured in Solution During the HBR/BF-85 Test 4.13

4.4 Inventory Fractions of ^{137}Cs, ^{90}Sr, ^{99}Tc, ^{129}I, and ^{14}C Measured in Solution During the TP/BF-85 Test 4.14

9 0 7 9 4 1 3 5 1

TABLES

2.1 Test Specimens 2.2

2.2 Characteristics of H. B. Robinson Unit 2 and Turkey Point Unit 3 Fuels 2.8

2.3 Specimen Radionuclide Inventories 2.9

2.4 Summary of Radiochemistry Methods 2.14

2.5 Pressurized Water Reactor Spent Fuel Radionuclide Inventories at 1,000 Years 2.15

3.1 Quantities of Uranium Measured in Samples 3.12

3.2 Residues Collected on Rinse Filters 3.13

3.3 Probable Phases Indicated by XRD on Bare-Fuel Rinse Filters . . . 3.17

3.4 Quantities of $^{239+240}Pu$ Measured in Samples 3.25

3.5 Quantities of ^{241}Am Measured in Samples 3.30

3.6 Quantities of ^{244}Cm Measured in Samples 3.34

3.7 Quantities of ^{237}Np Measured in Samples 3.38

3.8 Quantities of ^{99}Tc Measured in Samples 3.41

3.9 Percent Nuclide Fractions in Acid Strip Samples Attributed to Previously Undissolved Fuel Fines Based on ^{99}Tc Data 3.42

3.10 Quantities of ^{137}Cs Measured in Samples 3.45

3.11 Quantities of ^{90}Sr Measured in Samples 3.47

3.12 Quantities of ^{129}I Measured in Samples 3.50

3.13 ^{129}I Inventory Fractions in Series 2 and Series 3 Final Solution Samples 3.51

3.14 Quantities of ^{126}Sn Measured in Samples 3.53

3.15 Quantities of ^{14}C Measured in Samples 3.55

3.16 ^{14}C Inventory Fraction in Series 2 and Series 3 Final Solution Samples 3.56

3.17 Quantities of ^{60}Co Measured in Samples 3.57

9 0 7 9 4 1 3 5 2

4.1 Approximate STEADY-STATE Actinide Concentrations in the Bare-Fuel Tests 4.2

4.2 Comparison of Measured and EQ3/6 Predicted Actinide Concentrations 4.5

4.3 Annual Actinide Releases as a Fraction of the 1,000-Year Inventories 4.8

4.4 Continuous Annual Release Rates Measured for Soluble Fission Products as inventory Fraction Times 100,000 . . . . . 4.15

9 0 7 9 4 1 3 5 3

ACRONYMS

ATM	approved testing material
BWR	boiling water reactor
BCL	Battelle Columbus Laboratories
cpm	counts per minute
dpm	disintegrations per minute
EDX	energy dispersive X-ray analysis
EPA	U.S. Environmental Protection Agency
HBR	H. B. Robinson Reactor
IC	ion chromatography
ICP	inductive couple plasma
JCPDS	Joint Committee on Powder Diffraction Standards
LLNL	Lawrence Livermore National Laboratory
MCC	Materials Characterization Center
MTHM	metric tons heavy metal
NAA	neutron activation analysis
NEA	Nuclear Energy Agency
NNWSI	Nevada Nuclear Waste Storage Investigations
NRC	U.S. Nuclear Regulatory Commission
ORNL	Oak Ridge National Laboratory
PCI	pellet-cladding interaction
PNL	Pacific Northwest Laboratory
ppb	parts per billion (mass basis)
ppm	parts per million (mass basis)
PWR	pressurized water reactor
SCC	stress corrosion cracking
SEM	scanning electron microscopy
TP	Turkey Point Reactor
WBS	work breakdown structure
Westinghouse Hanford	Westinghouse Hanford Company
XRD	X-ray diffraction

9 0 7 9 4 1 3 5 4

1.0 BACKGROUND

The Yucca Mountain Project, formerly the Nevada Nuclear Waste Storage Investigations (NNWSI) Project, is investigating the suitability of the Topopah Spring Tuff at Yucca Mountain, Nevada, for potential use as a disposal site for spent nuclear fuel and other high-level waste forms. The repository horizon under study lies ~200 to 400 m above the water table in the unsaturated zone. Contact of the spent fuel by liquid water will not occur until the repository has cooled to below the 95°C boiling temperature at the repository elevation. At that time, which is predicted to be hundreds of years after disposal, a limited quantity of water infiltrating the rock could potentially enter a failed waste container and contact the spent fuel where cladding failures have also occurred. Migration of a limited quantity of such water from a failed waste container is considered to be the most probable mechanism for radionuclide release. In addition, there is the potential that ^{14}C (as CO_2) and possibly ^{129}I (as I_2) may migrate in the vapor phase.

Lawrence Livermore National Laboratory (LLNL) is the lead contractor for the Waste Package Task of the NNWSI Project. Westinghouse Hanford Company (Westinghouse Hanford) has been a subcontractor to LLNL, assisting them in determining the requirements for successful disposal of spent fuel at the Yucca Mountain Site.[a] The work at Westinghouse Hanford focused primarily on hot cell testing of spent fuel materials. Areas of investigation included leaching/dissolution behavior, cladding corrosion, and spent fuel low-temperature oxidation behavior. In the Spent Fuel Leaching/Dissolution Task at Westinghouse Hanford, three laboratory test series were conducted with pressurized water reactor (PWR) spent fuel specimens to characterize radionuclide release under NNWSI-relevant conditions.

In the Series 1 tests,[1] specimens prepared from Turkey Point (TP) Reactor Unit 3 fuel were tested in deionized distilled water in unsealed fused silica vessels under ambient hot cell air and temperature (25°C) conditions. Four specimen configurations were tested: 1) undefected fuel rod segments

---

(a) This work was transferred from the Westinghouse Hanford Company to the Pacific Northwest Laboratory on July 1, 1987, as part of the U.S. Department of Energy's Hanford Site Consolidation.

9 0 7 9 4 1 3 5 5

with water-tight end fittings, 2) fuel rod segments containing small laser-drilled holes through the cladding and with water-tight end fittings, 3) fuel rod segments with a machined slit through the cladding and water-tight end fittings, and 4) bare-fuel particles removed from the cladding plus the cladding hulls. A "semistatic" test procedure was developed in which periodic solution samples were taken with the sample volume replenished with fresh deionized distilled water. A constant water volume (250 mL) was maintained during all test cycles. Cycle 1 of the Series 1 tests was started during July 1983 and was 240 d in duration. At the end of the first cycle, the tests were sampled, the vessels stripped in 8 M HNO_3, and the specimens restarted in fresh deionized distilled water for a second cycle. Cycle 2 of the Series 1 tests was terminated at 128 d in July 1984.

The Series 2 tests were similar to the Series 1 tests except that: 1) the Series 2 tests were run in NNWSI reference J-13 well water, 2) each of the four specimen configurations was duplicated using both the TP and H. B. Robinson (HBR) Reactor PWR spent fuels, and 3) a vessel and specimen rinse procedure was added to the cycle termination procedures. Filtration of the collected rinse solution provided solids residues that were later examined for secondary-phase formation. Cycle 1 of the Series 2 tests was started in June 1984. All eight Series 2 specimens were run for a second cycle. Results from Cycles 1 and 2 of the Series 2 tests are reported in Reference 2. The two bare-fuel specimens were continued for Cycles 3, 4, and 5 for a total five-cycle testing time of 34 mo. Summary results for all five cycles of the Series 2 bare-fuel tests are given in References 3 and 4. A detailed report of the Series 2 bare-fuel test results is in preparation.

The Series 3 tests that are the subject of the current report used sealed stainless steel vessels and J-13 well water and were run at 85°C (one specimen at 25°C). The four specimen configurations tested in the Series 1 and Series 2 tests were also used in the Series 3 tests. The vessels used in Cycle 1 were fabricated from 304 stainless steel. New 304L stainless steel vessels were substituted in Cycles 2 and 3. During the time period of the Series 3 tests, 304L stainless steel was the NNWSI reference spent fuel container material. The Series 3 tests were started during February 1986 and

9 0 7 9 4 1 3 5 6

were run for three cycles for a total testing time of 15 mo. The purpose of this report is to provide detailed documentation of the NNWSI Series 3 Spent Fuel Dissolution Tests.

This work has been conducted under NNWSI work breakdown structure (WBS) element number 1.2.2.3.1.1.L and activity D-20-42 of the Scientific Investigation Plan for NNWSI Waste Form Testing.[5] Except where noted, this work has been conducted at Quality Level Assignment I.

90794 1357

2.0 TEST DESCRIPTION

A detailed description of the Series 3 tests is provided by the test plan[6] and in technical procedures that are identified in Appendix D. The intent of this section is to provide the reader with sufficient information about the test methods and fuel specimens to follow the discussion of results and calculation of the radionuclide fractional release values.

2.1 TEST SPECIMENS

The test matrix included six specimens that are identified in Table 2.1. All specimens were prepared from 5-in.-long fuel rod sections. The four specimen configurations tested are identical to those tested in the Series 1 and Series 2 tests and represent a range of potential degrees of cladding failure as follows.

- Undefected specimen with intact cladding and water-tight end fittings was run as a control specimen to indicate the amount of radionuclide release originating from residual cladding surface contamination and cladding crud deposits.

- Hole-defects specimen contained two small (~200-μm diameter) laser-drilled holes through the cladding near the center of the specimen. The ends of the hole-defects specimen were sealed with water-tight end fittings. The hole-defects specimen was intended to be representative of fuel rods containing small breaches, such as may result from pellet-cladding interaction (PCI) or stress corrosion cracking (SCC) cladding failures.

- Slit-defect specimen contained a 0.006-in. wide by 1-in. long machined slit through the cladding near the specimen center and was sealed at the ends with water-tight end fittings. The slit-defect specimen was intended to represent a more severe cladding failure, such as may occur if an SCC defect progressed to a relatively large crack or cladding cracks that may result from postirradiation handling.

- Bare-fuel specimens were prepared by machining axial slits through the cladding from end-to-end on opposite sides of the specimens, opening the split cladding, and removing the bare-fuel particles from the cladding. The cladding hulls are included with the fuel particles in these tests as part of the test specimen. The bare-fuel specimens are intended to represent the worst-case cladding failure, where the cladding has split open and the fuel has fallen out.

90794 1358

TABLE 2.1. Test Specimens

Test ID	Rod Section ID	Fuel Configuration[a]	Temp. (°C)	Fuel Weight[b] (g)
HBR/BF-25	C5C-I	HBR Bare Fuel	25	86.17 84.85 83.66
TP/BF-85	F6-2B	TP Bare Fuel	85	85.55 84.33 83.64
HBR/BF-85	C5C-K	HBR Bare Fuel	85	80.70 79.39 78.67
HBR/SD-85	C5B-D	HBR Slit Defect	85	85.77
HBR/HD-85	C5B-B	HBR Hole Defects	85	80.16
HBR/UD-85	C5B-A	HBR Undefected	85	85.07
HBR/BF-2-25	C5C-H	HBR Bare Fuel[c]	25	83.10 82.92 81.45
TP/BF-2-25	I9-24	TP Bare Fuel[c]	25	27.21 26.66 26.14

(a) HBR = H. B. Robinson.
TP = Turkey Point.
(b) Three weights given for bare-fuel tests are for Cycles 1, 2, and 3, respectively. Cladding weight was assumed to be 16.4 g for all specimens.
(c) Series 2 tests,[2] which are discussed in this report for comparison.

9 0 7 9 4 1 3 5 9

The Series 3 tests were conducted in sealed stainless steel vessels as shown in Figure 2.1, with different vessel internal configurations for bare-fuel specimens versus the clad fuel specimens with water-tight end fittings. One HBR fuel specimen in each of the four configurations was tested at 85°C. A bare-fuel specimen prepared from TP fuel was also tested at 85°C for comparison with the HBR fuel. The temperature was controlled at 85 ± 2°C using a constant-temperature oil bath. The 85°C temperature may be near the temperature at which liquid water could first form in a failed waste package under an air-steam atmosphere as the repository cools after several hundred years postclosure.[7] An additional HBR bare-fuel specimen was tested at 25°C to correlate dissolution behavior with temperature. The 25°C test also provides for correlation of results from Series 3 tests in sealed stainless steel vessels with those from unsealed silica vessels used in the Series 2 tests. Both vessel materials were relevant to the repository system; 304L stainless steel was the reference container material when the Series 3 tests were started and silica is chemically more similar to the tuff rock outside the container.

An important part of the specimen preparation procedures was the removal from the cladding exterior surface of fine particulate contamination that results from sectioning and handling in contaminated hot cells. Such contamination would seriously bias the test results if not removed. One purpose of the undefected test specimens in the test matrix was to provide an indication of the released radioactivity originating from residual contamination on the cladding exterior surface. Another purpose for the undefected specimen was to verify integrity of the O-ring seal in the end fittings used on the clad specimens. Before installing end fitting hardware on the undefected, hole-defects (laser-drilled), and slit-defect specimens, the cladding surface was decontaminated to less than 50 cpm smearable alpha and less than detectable beta/gamma above the Hanford 327 Building background (~150 cpm in a lead-shielded cave). The cladding exterior of the bare-fuel specimens was also decontaminated to less than 50 cpm smearable alpha before the cladding was axially split to remove the bare fuel.

The ends of the undefected, laser-drilled, and slit-defect specimens were sealed using water-tight end fittings fabricated from modified Cajon

9 0 7 9 4 1 3 6 0

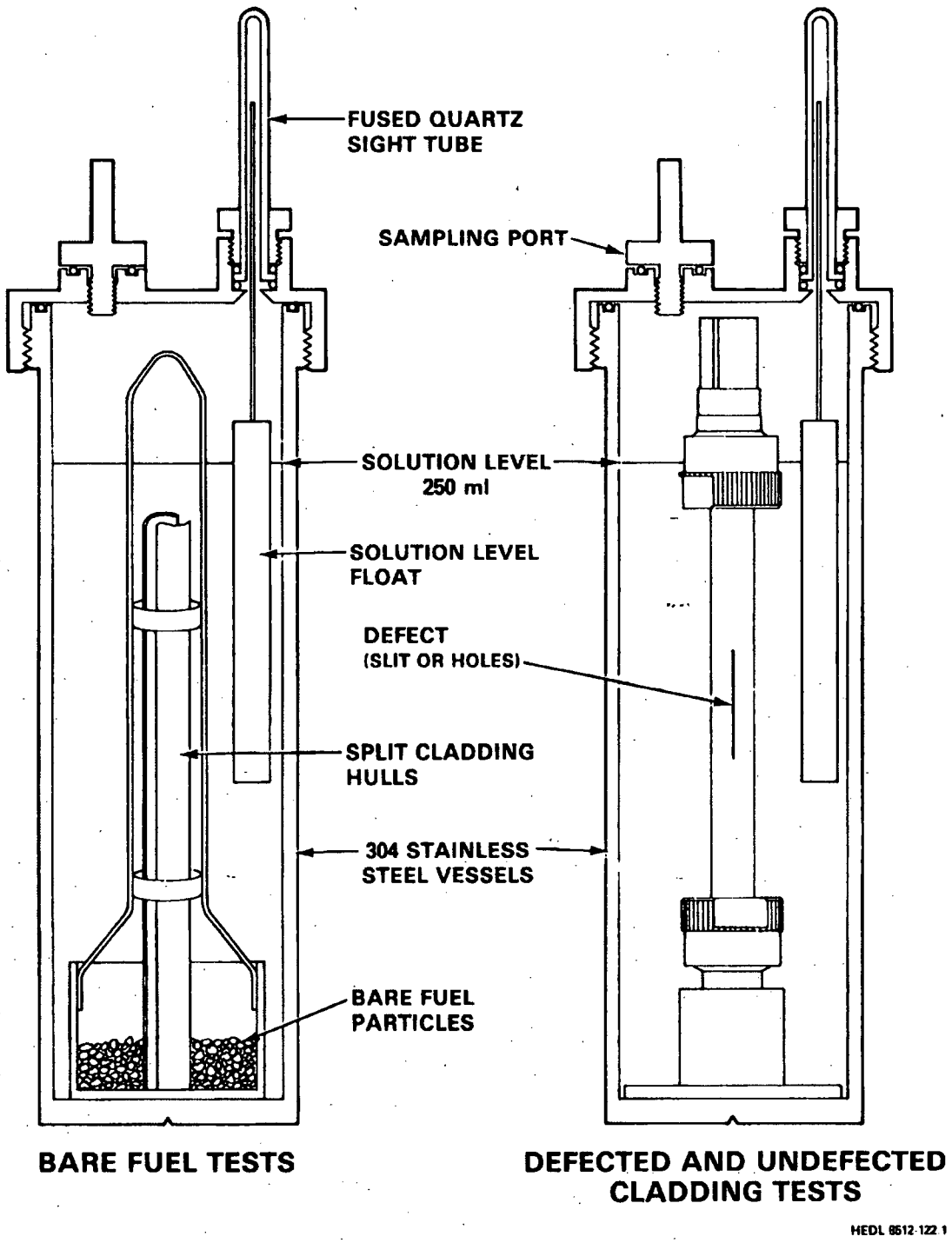

FIGURE 2.1. Series 3 Test Configurations (Neg. 8600029-1)

9 0 7 9 4 1 3 6 1

Model SS-8-UT-A-10 Ultra Torr[a] vacuum adaptors. The end-fitting seal was made using ethylene propylene O-rings chosen for their radiation resistance and water compatibility. The top fittings of both the hole-defects and slit-defect specimens contained a small vent hole above the test solution level to allow the defected cladding specimens to fill with solution to the external test solution level.

A ceramographic section showing a laser-drilled hole defect through the cladding of a TP fuel specimen (Series 1) is shown in Figure 2.2. A mosaic photograph showing the entire section in the as-polished condition is shown in Figure 2.3. The postirradiation thermal cracking pattern shown in Figure 2.3 is typical of that for the HBR and TP fuels used in the Series 3 tests and is indicative of the size of the resulting particles used in the bare-fuel tests.

2.2 FUEL CHARACTERISTICS AND HISTORY

The two fuel types used in the test matrix were similar PWR fuels, as indicated by the relevant fuel characteristics listed in Table 2.2. Both fuels were low-gas-release PWR fuels from the same vendor and approximately the same vintage.

The HBR fuel was obtained through the Pacific Northwest Laboratory (PNL) Materials Characterization Center (MCC) as an "approved testing material" (ATM) for geological repository testing and was identified by PNL-MCC as ATM-101.[8] The ATM-101 Rod C5 was cut into three sections during Spring 1983. The two HBR bare-fuel specimens were sectioned from the C5C center section of Rod C5. The slit-defect, hole-defects, and undefected specimens were sectioned from the top end of the C5B bottom section of Rod C5. The Series 2 HBR specimens were taken from the top portion of rod segment C5C. Other sections taken from the C5C and C5B segments were used for ^{14}C, burnup, and ceramographic analyses and examinations.

The TP specimen was sectioned from the center of a previously sectioned 24-in.-long rod segment identified as Section 2 from Rod F6. Axial location of the specimen is from 34 to 39 in. from the bottom of Rod F6. The original

---

(a) Ultra Torr is a trademark of Cajon Company, Macedonia, Ohio.

9 0 7 9 4 1 3 6 2

FIGURE 2.2. Ceramographic Section at Laser-Drilled Hole Defect Through the Cladding (Neg. 8307376-8)

TURKEY POINT ROD SPECIMEN J-8-19,
B-17 ASSEMBLY
LASER-DRILLED, LEACHED 60 DAYS

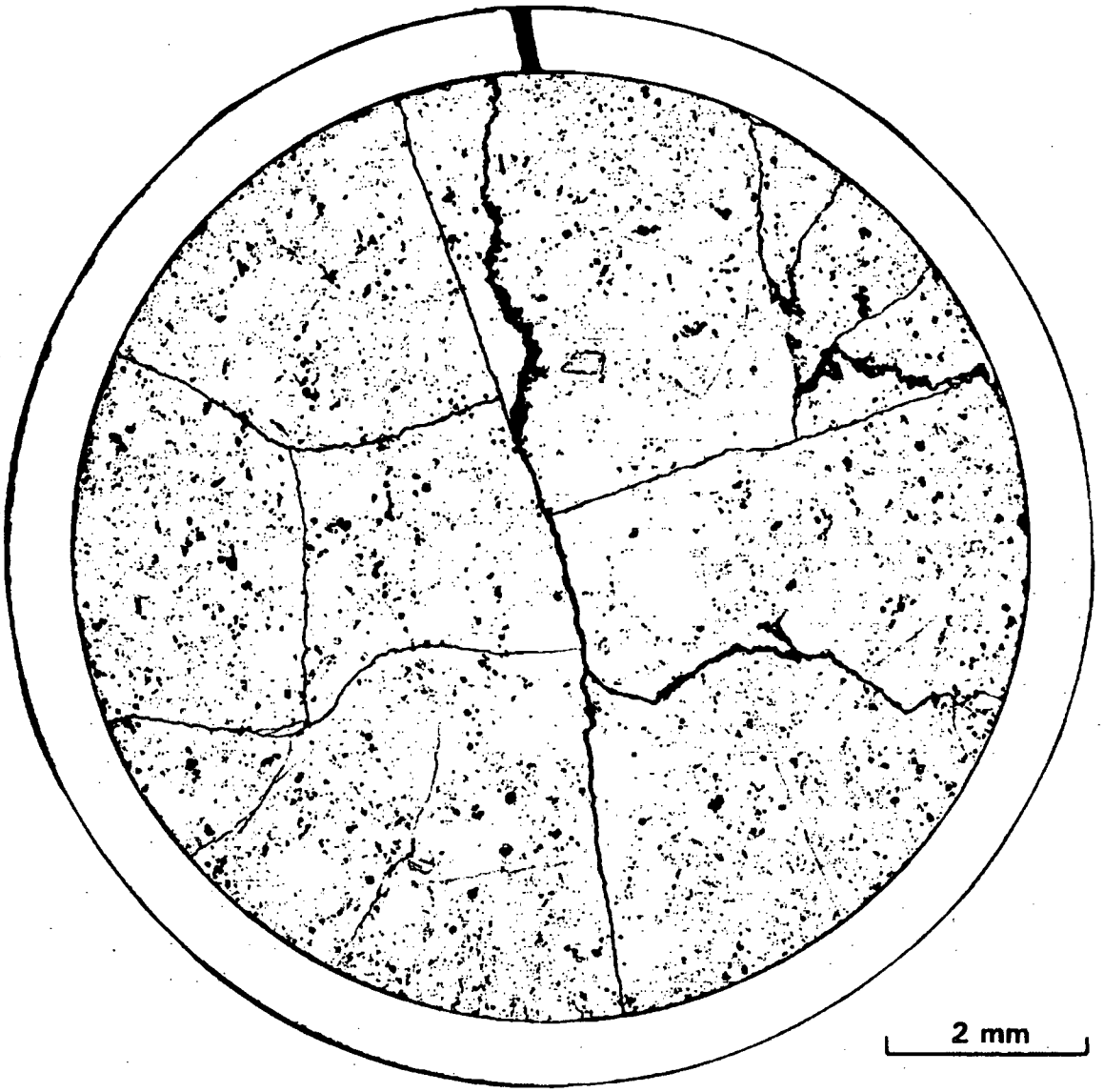

FIGURE 2.3. Ceramographic Mosaic of As-Polished Specimen Section at Laser-Drilled Hole Defect Showing Postirradiation Fuel Cracking. (Particle size in the bare-fuel tests were approximately that indicated by the postirradiation cracking.) (Neg. 8307465-1)

907794 1364

TABLE 2.2. Characteristics of H. B. Robinson Unit 2 and Turkey Point Unit 3 Fuels

Characteristic	H. B. Robinson	Turkey Point
Fuel Type	PWR 15 x 15	PWR 15 x 15
Assembly Identification	BO-5	B-17
Rod Identification	C5	F6
Discharge Date	May 6, 1974	November 25, 1975
Nominal Burnup	30 MWd/kgU	27 MWd/kgU
Fission Gas Release	0.2%	0.3%
Initial Enrichment	2.55 wt% ^{235}U	2.559 wt% ^{235}U
Initial Pellet Density	92% TD (UO_2)	92% TD (UO_2)
Initial Fuel Grain Size	~6 μm	~25 μm
Initial Rod Diameter	10.7 mm OD	10.7 mm OD
Cladding Material	Zircaloy-4	Zircaloy-4
Cladding Thickness	0.62 mm	0.62 mm
PNL-MCC Identification	ATM-101	--

rod sectioning was performed at Battelle Columbus Laboratories (BCL) in 1979 and is documented along with characterization data on Rods G7, G8, J8, I9, and H6 of Assembly B-17 in Reference 9.

Fuel rod sectioning diagrams for the C5B, C5C, and F6-2 rod segments used for the Series 3 specimens are contained in the test plan.[6] Axial locations for all specimens were chosen to avoid regions of nonuniform burnup that occur near spacer grid locations and towards the top and bottom ends of the fuel rod.

Inventories for the radionuclides analyzed were calculated from ORIGEN-2 data tabulated in Appendix E of Reference 8. The calculated inventory values along with radiochemically measured values on an HBR fuel sample are given in Table 2.3. The average times from discharge assumed (12 yr for HBR and 10.5 yr for TP) correspond to midway through Cycle 1. Linear interpolation was used to adjust the tabulated ORIGEN-2 data for burnup and time from discharge. Fractional release calculations for this report use a single ORIGEN-2 based inventory value for each radionuclide and are not corrected for changes in inventory during the 15-mo testing time. Of the principal radionuclides

9 0 7 9 4 1 3 6 5

TABLE 2.3. Specimen Radionuclide Inventories (μCi/g of fuel except as indicated)

Nuclide	H. B. Robinson ORIGEN-2[a]	H. B. Robinson Measured[b]	Turkey Point ORIGEN-2[a]
Burnup (MWd/kgM)	30.2[b]	30.2	27.5[c]
Uranium (μg/g of fuel)	8.45×10^5	--	8.48×10^5
^{244}Cm	1.28×10^3	1.43×10^3[d]	9.90×10^2
^{241}Am	1.77×10^3	1.63×10^3	1.51×10^3
$^{239+240}Pu$	7.44×10^2	7.16×10^2	7.04×10^2
^{237}Np	2.43×10^{-1}	2.35×10^{-1}	2.18×10^{-1}
^{137}Cs	6.37×10^4	6.57×10^4	6.04×10^4
^{129}I	2.65×10^{-2}	--	2.42×10^{-2}
^{126}Sn	6.74×10^{-1}	--	6.11×10^{-1}
^{99}Tc	1.05×10^1	8.34×10^0	9.74×10^0
^{90}Sr	4.17×10^4	--	4.03×10^4
^{14}C	--	(e)	

(a) Calculated from ORIGEN-2 data in PNL-5109,[8] assuming 12 yr from discharge for H. B. Robinson and 10.5 yr from discharge for Turkey Point.
(b) Radiochemically determined (September 1985) from Sample C5C-D.
(c) Reported burnup for Sample G7-15.[9]
(d) Actually $^{243+244}Cm$ since both isotopes have similar alpha energies; ORIGEN-2 data indicate that ^{243}Cm is ~1% of $^{243+244}Cm$.
(e) ^{14}C average of values measured on Samples C5C-J and C5B-C: Fuel = 0.49 μCi/g; Cladding = 0.53 μCi/g.

discussed, ^{244}Cm (with 5% decay in the 15 mo) showed the greatest inventory change. The specimen inventories used in fractional release calculations were obtained by multiplying the per gram inventories in Table 2.3 times the specimen weights given in Table 2.1. Progressive decreases in weights of the bare-fuel samples in successive cycles is due to removal of particles for characterization, losses because of dissolution, and losses of spalled grains from the particle surfaces during terminal specimen rinsing.

9 0 7 9 4 1 3 6 6

2.3 TEST SAMPLES AND ANALYSES

Each test cycle was started, sampled, terminated, and the samples were analyzed following approved procedures identified in Appendix D. The sampling schedule and specified analyses for Cycle 1 are given in the test plan.[6] Similar sampling schedules and analyses were specified for Cycles 2 and 3 with the more significant changes noted below.

2.3.1 Starting J-13 Water

At the beginning of each test cycle, the J-13 water used to start the cycle was analyzed (Appendix B). The following analyses were performed: pH, inductive coupled plasma (ICP) emission spectrometry for cations, ion chromatography (IC) for anions, and inorganic carbon for bicarbonate ion concentration calculation.

2.3.2 Periodic Solution Samples

Periodic solution samples were taken through the sampling port (see Figure 2.1) using preleached 20-mL plastic syringes with 6-in.-long stainless steel needles. The sampling depth was slightly higher than the upper lip of the internal bare-fuel sample basket, which is shown to scale in Figure 2.1. The 85°C test vessels remained in the oil bath during sampling so the samples were taken at temperature. Before drawing the sample, ~50 mL of air were bubbled through the vessel from the syringe at the sampling depth. The original purpose of the bubbling in the Series 1 and 2 tests was to provide for a small amount of convection or mixing effect just prior to sampling. Although this procedure is probably of questionable value for mixing, it was retained so that the sampling procedure would be consistent in all test series. Periodic solution sample volumes ranged from 10 to 30 mL, depending on the analyses that were to be performed. After the samples were removed, the sample volumes were replenished with fresh J-13 well water so that a constant water volume of 250 mL was maintained in the test vessels.

Solution samples were placed in preleached glass vials and capped in the hot cell. The samples were removed from the hot cell to a glovebox and aliquots prepared for analysis, usually within an hour of sampling. The first step when the sample vial was opened was to measure pH on an aliquot from the vial. Aliquots were also taken and placed in sealed vials for ^{14}C and ^{129}I

9 0 7 9 4 1 3 6 7

analyses if specified. The remaining sample was then usually separated into aliquots for the unfiltered, 0.4-μm filtered, and 18-Å filtered[a] fractions. Analysis of 18-Å filtered solution samples was deleted starting with the fifth sample (Day 62) of Cycle 2. Uranium, alpha (for $^{239+240}Pu$), gamma (for ^{137}Cs), ^{241}Am, ^{237}Np, ^{126}Sn, and ^{99}Tc analyses were routinely performed on all three filtered fractions; and ^{129}I, ^{90}Sr, and ^{14}C analyses were routinely performed on the unfiltered fractions. Solution chemistry (ICP, IC, and inorganic carbon) analyses were performed on the 0.4-μm filtered fraction, when specified. For sampling schedules, volumes and analyses performed refer to the radiochemistry and solution chemistry data tables in Appendices A and B.

2.3.3 Final Solution Samples

A final solution sample was taken immediately before termination of a test cycle on the termination day. The procedure for the final solution sampling is identical to that for the periodic solution samples, except that the sample volume was not replenished with fresh J-13 well water. For the purposes of data evaluation, the volume of the final solution sample is assumed to be the entire 250 mL of solution in the test.

2.3.4 Rinse Samples

After the final solution sample was taken, the vessels were removed from the constant temperature bath for cycle termination. The bare-fuel particles were removed to a 250-mL beaker, and the remaining final solution was decanted off. The fuel particles were rinsed in the 250-mL beaker with J-13 water (~50 mL), rocking the breaker from side to side ten times and allowing the particles to tumble in the bottom of the beaker. The bare-fuel rinse water was then decanted into a 1,000-mL beaker, and the bare-fuel rinse was repeated four more times. The bare-fuel rinse solution routinely became dark and turbid in appearance during the first few rinse cycles as surface grains (loosened by grain boundary dissolution) and sediment from the test became

---

(a) The 18-Å filtered fraction referred to in this report is a sample fraction centrifuge filtered through an Amicon Corporation type CF25 Centriflo membrane filter cone. Centriflo is a trademark of the Amicon Corporation, Lexington, Massachusetts.

9 0 7 9 4 1 3 6 8

temporarily suspended. Clad specimens with end fittings, cladding hulls from bare-fuel tests, specimen baskets or pedestals, floats, and the interior vessel surfaces were thoroughly rinsed with J-13 water from a squirt bottle with the rinse water draining into the 1,000-mL beaker. The rinse water volumes in the 1,000-mL beakers were made up to 600 mL after specimen and component rinsing by addition of fresh J-13 well water and then were left covered overnight to settle. A sample was removed from the top of the settled rinse solutions the next morning using a syringe and preleached sample vials. Routine requested analyses for the rinse solution samples included uranium, alpha spectrometry, gamma spectrometry, ^{241}Am, ^{237}Np, ^{99}Tc, ^{90}Sr, and ^{14}C. Rinse samples from bare-fuel tests were 0.4-μm filtered prior to analyses.

2.3.5 Acid Strip Samples

After rinsing, the internal components less the actual specimens were placed back in their respective vessels, and 300 mL of 8 M HNO_3 were added. The caps were replaced and the vessels rolled on their sides so that the interiors would be completely washed with the acid. The next day the acid was poured into a bottle, back into the vessel, and then back into the bottle again. The acid strip solution in the bottles was then sampled for analyses. Requested analyses routinely included uranium, alpha spectrometry, gamma spectrometry, ^{241}Am, ^{237}Np, ^{99}Tc, and ^{90}Sr.

2.3.6 Ceramographic Samples

Two random fuel particles were removed from the 250-mL beaker after cycle termination for later ceramographic examination. The particles were mounted in resin, ground to expose an internal section, polished, and examined in the as-polished condition. The intersection of the section plane with the particle surface was of primary interest and was examined for evidence of grain boundary dissolution or any other type of observable preferential dissolution.

2.3.7 Rinse Filters

After the rinse solution samples were taken, the remaining solutions in the 1,000-mL beakers were stirred to get the finer sediments back into suspension. The rinse solutions were then filtered through 0.4-μm filters, and the filtrate solutions were discarded. The filters were weighed to determine

9 0 7 9 4 1 3 6 9

the net amount of residue filtered from each rinse solution. The filters were later examined by scanning electron microscopy (SEM) and X-ray diffraction (XRD) to identify and characterize any secondary solid phases present.

2.3.8 Coarse Rinse Sediments

Coarser particles that would not remain in suspension long enough to be decanted off during filtration of the rinse solution were allowed to settle to the bottom of the 1,000-mL beakers. These sediments were allowed to dry and, if present in sufficient quantity (a few mg or more), removed and weighed. Samples of these coarse sediments were then examined in the SEM. The coarse rinse sediments consisted primarily of small particles of fuel.

2.4 CHEMISTRY

Chemical analyses of solution samples were divided into two types for the purposes of evaluation: the analyses of uranium and radionuclides originating from the fuel specimens (radiochemistry) and the analyses of species contained in the starting J-13 well water (solution chemistry).

2.4.1 Radiochemistry

A summary of the radiochemistry methods is given in Table 2.4. Principal radionuclides present in 1,000-year-old spent fuel were of primary interest and are summarized in Table 2.5. The 1,000-yr inventories are significant relative to the U.S. Nuclear Regulatory Commission (NRC) stated requirement that "release rate of any radionuclide from the engineered barrier system ... shall not exceed one part in 100,000 per year of the inventory of that radionuclide calculated to be present at 1,000 years."[11] Approximately 99% of the 1,000-yr activity is from plutonium and americium isotopes plus ^{99}Tc. Other long-lived nuclides analyzed were ^{237}Np, ^{14}C, ^{126}Sn, and ^{129}I. Shorter half-life radionuclides including fission products ^{137}Cs (30.2 yr), ^{134}Cs (2.2 yr), ^{90}Sr (28.6 yr), and ^{244}Cm (18.1 yr) and activation product ^{60}Co (5.3 yr) were also analyzed, since they represent a major fraction of the activity in spent fuel during the first few hundred years. Selenium-79 was dropped from the Series 3 analytical schedule, since attempts to measure it by liquid scintillation following separation in the Series 2 tests failed.[2] Possibly the most significant radionuclide listed in Table 2.5 that was not

90794 1370

TABLE 2.4. Summary of Radiochemistry Methods

Radionuclide	Method	Detection Limits (pCi/mL)	Detection Limits (ppb)	10^{-5} Inventory (pCi/mL)[a]
^{244}Cm	α-spectrometry	0.2	3×10^{-6}	4100
^{241}Am	α-spectrometry following separation	0.1	3×10^{-5}	5700
$^{239+240}Pu$	α-spectrometry	0.2	0.003	2380
^{237}Np	α-spectrometry following separation	0.1	0.14	0.8
^{137}Cs	γ-spectrometry	200	0.002	2.0×10^{5}
^{129}I	Neutron activation analysis	10^{-5}	0.0001	0.08
^{126}Sn	GeLi well γ-spectrometry following separation	0.2	0.02	2.2
^{99}Tc	β-proportional counting following separation	10	0.6	34
^{90}Sr	β-proportional counting following separation	20	0.0001	1.3×10^{5}
^{60}Co	γ-spectrometry	200	0.0002	(b)
^{14}C	Liquid scintillation counting following separation	20	0.004	2
U	Fluorescence	--	1	(3 ppm)

(a) Assumes 10^{-5} of H. B. Robinson test specimen inventory dissolved in 250 mL.
(b) ^{60}Co inventory is unknown.

90794 1371

TABLE 2.5. Pressurized Water Reactor Spent Fuel Radionuclide Inventories at 1,000 Years[a]

Radionuclide[b]	Half-Life (yr)	Ci/1,000 MTHM	1,000-Year Activity (% of Total)	Cumulative Activity (%)
^{241}Am	432	894,500	51.33	51.33
^{243}Am	7,380	31,080[c]	1.78[c]	53.11
^{240}Pu	6,569	476,900	27.37	80.48
^{239}Pu	24,130	304,700	17.45	97.96
^{242}Pu	375,800	1,755	0.10	98.07
^{238}Pu	88	967	0.06	98.12
^{99}Tc	213,000	13,030	0.75	98.87
^{59}Ni	80,000	5,150	0.295	
^{63}Ni	100	354	0.020	
^{93}Zr	1.53E+06	1,933	0.111	
^{93m}Nb	15	1,836	0.105	
^{94}Nb	20,300	1,240	0.071	
^{14}C	5,730	1,372	0.079[d]	
^{234}U	244,500	1,984	0.114	
^{238}U	2.47E+09	317	0.016	
^{236}U	2.34E+07	271	0.018	
^{237}Np	2.14E+06	1,000	0.057	
^{126}Sn	100,000	772	0.044	
^{79}Se	65,000	405	0.023	
^{135}Cs	3.00E+06	345	0.020	
^{151}Sm	90	163	0.009	
^{107}Pd	6.50E+6	112	0.006	
^{129}I	1.57E+07	32	0.0018	

(a) Based on ORIGEN-2 data in ORNL/TM-7431[10] for 33,000 MWd/MTM burnup PWR spent fuel, actinides plus fission products plus activation products.
(b) Radionuclides with 1,000-yr activity less than ^{129}I or half-life less than 1 yr omitted.
(c) Includes activity of ^{239}Np daughter product.
(d) ^{14}C activity may vary considerably depending on as-fabricated nitrogen impurities.

90794 1372

analyzed was activation product ^{59}Ni, which is primarily associated with fuel assembly structural components, which were not included in these tests.

The approximate detection limits for each radionuclide are compared in Table 2.4 to the activity that would result if 10^{-5} of the specimen inventory were to be dissolved in the 250 mL of test solution. In the Series 1 and 2 tests, actinide concentrations in solution tended to stabilize at values near or below concentrations corresponding to 10^{-5} of inventory in solution. The Table 2.4 radionuclides for which the detection limits were just adequate or borderline for the bare-fuel tests and not adequate for the lower release defected cladding tests were ^{237}Np, ^{126}Sn, and ^{99}Tc.

A discussion of detection limits and relative errors precedes the tabulated results of the radiochemistry analyses in Appendix A. Summaries of the principal radiochemistry procedures are contained in Appendix D.

9 0 7 9 4 1 3 7 3

2.4.2 Solution Chemistry

Solution chemistry measurements included pH, ICP for cations, IC for anions, and inorganic carbon. Bicarbonate (HCO_3^-) concentration in μg/mL was calculated by multiplying the inorganic carbon results (also in μg/mL) by 5.0833 to correct for molecular weight. For certain analyses, organic carbon and total carbon were also reported. The detection limits of the solution chemistry analyses were generally on the order of 0.1 μg/mL, which was adequate for following the concentrations of ionic species in J-13 well water in order to determine if these species were being precipitated during the tests. Other purposes for the solution chemistry data were to indicate if significant corrosion of the vessels occurred or if test or sample contamination with nonradioactive species occurred.

2.5 TEST CYCLE RESTART

Experience in the Series 2 tests indicated that the fuel should be restarted for subsequent cycles as soon as possible and not allowed to dry between cycles, or an oxidized surface film could form on the fuel leading to enhanced dissolution and supersaturation of uranium early in the following cycle. New vessels and internal components were fabricated for Cycle 2, and the tests were restarted in the new vessels on the same day (within a few

hours) of Cycle 1 termination. When Cycle 2 was terminated, the vessels were reused for Cycle 3, requiring an extra day between cycles while the vessels were being stripped, neutralized, rinsed, and reassembled with new sight tubes and O-rings. The time between Cycle 2 termination and Cycle 3 start is estimated to be ~30 hours, during which time the bare-fuel specimens remained wet covered in the 250-mL beakers, and the cladding hulls and clad specimens were stored wet in plastic bags.

As in the Series 2 tests, only the bare-fuel specimens were originally to have been run for Cycle 3 of the Series 3 tests. However, for the purpose of not changing test geometry (and possibly the bath-to-vessel internal temperature gradient), it was decided to restart all the specimens for Cycle 3 but only sample the bare-fuel specimens. Since the duration of Cycle 3 was then shortened and the number of solution samples reduced, the budget at termination allowed a final solution sample from all the vessels. (The purpose for shortening Cycle 3 was to complete Quality Assurance Level I laboratory testing activities prior to their transfer from Westinghouse Hanford to PNL.)

90794 1374

3.0 RESULTS AND DISCUSSION BY ELEMENT

3.1 GENERAL COMMENTS ON DATA PRESENTATION

A complete tabulation of radiochemical results reported in pCi activity units (μg units for uranium) is contained in Appendix A. A complete tabulation of the nonradioactive water chemistry data for each test is contained in Appendix B. A detailed discussion of the results organized by element and radionuclide is contained in this chapter. Results for the actinides, whose concentrations and activities in solution were limited by their relatively low solubility, are presented before those of the more soluble fission and activation produce elements. A discussion of results from the characterization of secondary phases found in filtered solids residues follows the uranium results. Results from the bare-fuel tests are emphasized in most of the discussions.

A more general discussion of the bare-fuel test results is contained in the following chapter. The actinide results are compared to solubilities predicted by the EQ3/6 geochemical modeling code, and results for both the actinides and the more soluble fission and activation products are discussed relative to NRC release limits in that chapter.

3.1.1 Plotted Solution Sample Activity Data

Solution sample data for the various nuclides are plotted in composite plots showing data for the three sequential test cycles in adjacent boxes along the X-axis. Data reported as "less than" values are plotted with downward arrows with the plotted point representing the estimated detection limit for the particular measurement. A reference level is shown in the Cycle 3 box of many of the plots indicating the level that would result if the indicated fraction of the specimen inventory dissolved in the 250 mL of test solution. The same symbol is used for data from the same test in different plots, except for plots comparing filter fractions where the same symbols are used for the same filter fractions. Open symbols are used for Series 3 data, and closed (filled-in) symbols are used for Series 2 data that are included in some plots for comparison. Data are plotted as concentration (μg/mL for uranium) or activity (pCi/mL) measured in solution samples in this chapter.

9 0 7 9 4 1 3 7 5

Specimen inventory fractions of ^{137}Cs, ^{90}Sr, ^{99}Tc, ^{129}I, and ^{14}C measured in solution are plotted together for each of the three bare-fuel tests in the following chapter. Each data point in these plots represents the inventory fraction in the 250 mL of test solution on the sample date plus the inventory fractions estimated to have been removed in previous samples taken during the test cycle.

3.1.2 "Quantities Measured" Tables

Tables of the quantities of nuclides measured in the various types of liquid samples were compiled for each nuclide. The "periodic samples" values given in these tables are the sum of sample activities times sample volume for each periodic solution sample (excluding the final solution sample) in which detectable activities were measured. Since not all nuclides were measured in every sample, the periodic sample values may be in some cases less than the actual total quantity removed in periodic samples. In the case of ^{129}I, where only a single periodic sample was analyzed, that value was assumed as an estimate of the ^{129}I in all periodic samples. The "final solution" value is the quantity of the nuclide determined to be in the 250 mL of test solution at the end of a test cycle. For the actinides and ^{137}Cs, the "periodic solution" and "final solution" values are based on 0.4-μm filtered data. For ^{99}Tc, ^{90}Sr, ^{129}I, ^{126}Sn, and ^{14}C, the "periodic solution" and "final solution" values are based on unfiltered data. Concentration of the nuclide in the final solution is given in parentheses below the "final solution" value in the indicated units.

The "rinse" value is the quantity of the nuclide determined to be dissolved in the 600-mL rinse solutions when sampled the day after cycle termination. Rinse solution samples from bare-fuel tests were 0.4-μm filtered prior to analysis, while rinse solution samples from the clad-fuel tests were unfiltered. The "acid strip" value is the quantity of the nuclide determined to be dissolved in the 300 mL of 8 M HNO_3 used to strip the internal vessel hardware components at cycle termination. The "cycle total" values are the sum of the periodic samples, final solution, rinse, and acid strip values. The "$\div 10^{-5}$ Inv." value is the cycle total value divided by 10^{-5} of the inventory of that nuclide calculated to be present in the initial spent fuel test specimen. The "% in solution" value is the sum of the periodic samples plus

9 0 7 9 4 1 3 7 6

the final solution values divided by the cycle total value times 100. "Less than" symbols indicate either: 1) the value was reported as below detection limits for the particular sample or 2) the value is a sum in which greater than 5% is based on "less than" values. A double dash (--) indicates that a value was not measured.

3.1.3 Qualifications for Certain Data Uses

The tabulated quantities of nuclides measured should not, in general, be directly related to release or amounts of actual fuel dissolution without considering certain qualifications. There is, in particular, a question of the significance of actinide quantities measured in the rinse and acid strip solutions from the bare-fuel tests where these data account for the majority of the nuclide content in the cycle total values.

Rinse Samples--Grains of undissolved fuel and quantities of precipitated secondary-phase materials were removed from the bare-fuel tests with the rinse solution. These phases partially dissolved in the fresh J-13 well water rinse solution during the day between cycle termination and rinse solution sampling. Actinide concentrations in the bare-fuel rinse solutions were usually equal to and often greater than in the final solution samples. Because of the relatively large (600-mL) volume, nuclide quantities measured in rinse solutions were, in some cases, a significant portion of the total cycle measured quantities.

Acid Strip--Ideally from a data evaluation point of view, the acid strip would contain all nuclides dissolved from the fuel that plated, precipitated, or otherwise did not remain in solution. However, in the bare-fuel tests, much of the precipitated secondary-phase material ended up undissolved in the rinse solution residue. An effort was made to remove all visible particles of fuel from the vessel components prior to stripping, but it is possible that microscopic particles of undissolved spent fuel were dissolved in the acid strip solution. In the Cycle 3 HBR/BF-85 acid strip sample, a rather large fuel particle was evidently dissolved.

10^{-5} Inventory--The tabulated "cycle total" values for the various nuclides were normalized to inventory by dividing by 10^{-5} of the ORIGEN-2 based specimen inventory for comparison. In the data discussions, the

90794 1377

resulting values are in some instances loosely referred to as "fractional release." Similarly for comparison, the solution activity level that would result if 10^{-5} of the specimen inventory were in solution is shown on various plots of the periodic solution sample data. The purpose of normalizing tabulated data to inventory and indicating relative inventory fraction levels on plots was to provide a means for comparison of these data. These values cannot be directly compared to the NRC release rate limit of one part in 10^5 per year of the 1,000-yr inventory (10 CFR 60.113).[11] For solubility-limited radionuclides, an assessment of the fractional release rate in the repository requires, at a minimum, knowledge of the amount of water that contacts the waste in a given year.

3.2 URANIUM

Except for a limited portion of certain fission products that diffuse out of the fuel matrix during irradiation, activation products associated primarily with cladding and fuel assembly structural components, and somewhat higher concentrations as a result of higher local burnup at the outer edge of the fuel pellets (rim effect), most of the radionuclide inventory in spent fuel is thought to be rather uniformly distributed in the UO_2 fuel matrix phase. In particular, the alpha-emitting actinides that account for the majority of the postcontainment period activity, and for which the most stringent U.S. Environmental Protection Agency (EPA) releases limits[12] apply, are thought to be contained in solid solution with the UO_2 matrix phase. In addition to dissolution from the fuel matrix phase, water soluble nuclides may be preferentially dissolved from sources such as grain boundaries where they may concentrate during irradiation. It was not possible to determine the relative amounts of matrix release versus preferential release for water soluble nuclides, or the amounts of fuel matrix dissolution, in the present tests because of the limited solubility of uranium and the other actinides. It has yet to be demonstrated that any of the nuclides that remain fully in aqueous solution after release from the fuel are not preferentially dissolved relative to the fuel matrix phase during such tests so as to provide a quantitative measure for matrix dissolution.

90794 1378

3.2.1 Uranium in Solution Samples

Uranium concentrations measured in 0.4-μm filtered solution samples from the six Series 3 tests are compared in Figure 3.1. In Cycle 1 of the bare-fuel tests, uranium concentrations reached a maximum in the initial samples at values on the order of about 10 mg/mL and then decreased to about 0.4 μg/mL in the TP/BF-85 test and about 0.2 μg/mL in the HBR/BF-25 test. The anomalous behavior exhibited during Cycle 1 of the HBR/BF-85 test is discussed later in Section 3.2.2 on vessel effects. Lower initial concentrations were observed in Cycles 2 and 3 of the bare-fuel tests. The initial Cycle 1 concentration peaks are thought to result from the dissolution of more readily dissolved oxidized fuel phases that form on the fuel surface as a result of handling and storing in air prior to testing. The oxidized surface film was apparently depleted by dissolution during Cycle 1, and very little additional surface oxidation appears to have occurred between cycles during which time the fuel was not allowed to dry.

9 0 7 9 4 1 3 7 9

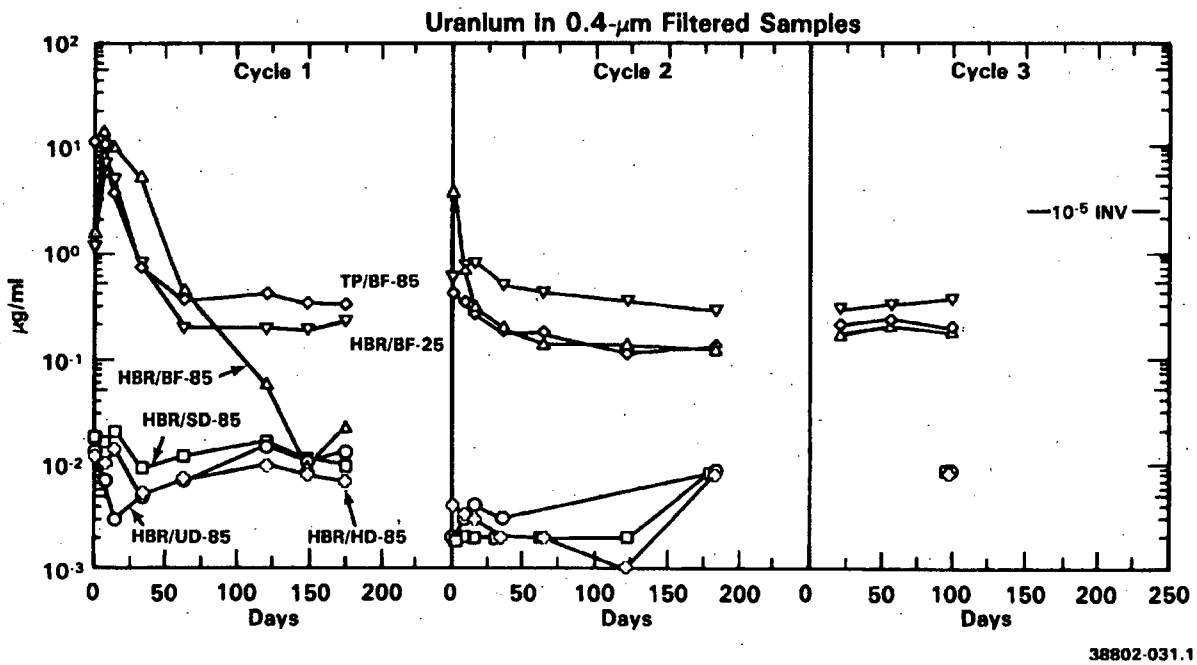

FIGURE 3.1. Uranium Concentrations Measured in 0.4-μm Filtered Samples

During both Cycles 2 and 3, the HBR/BF-25 test exhibited higher uranium concentrations than did the HBR/BF-85 and TP/BF-85 tests, which is the reverse of the temperature effect observed in Cycle 1, where the TP/BF-85 test showed higher uranium concentration than the HBR/BF-25 test. In later Cycle 2 samples and in Cycle 3 samples from the bare-fuel tests, uranium concentrations reached apparent steady-state values of about 0.1 to 0.2 μg/mL in the 85°C tests versus about 0.3 to 0.4 μg/mL in the 25°C test.

Much lower uranium concentrations were measured with the slit-defect and hole-defects specimens than with the bare-fuel specimens. In fact, no significant differences in uranium concentrations were observed for the HBR/SD-85, HBR/HD-85 or HBR/UD-85 specimens, suggesting the uranium release measured in these tests originated primarily from residual surface contamination on the cladding and not from the fuel within the specimens. A decrease in uranium concentrations measured initially in Cycle 2 of these three tests may be due to a depletion of soluble residual contamination on the cladding surface during Cycle 1. An increase in uranium concentrations in these three tests at the end of Cycle 2 and during Cycle 3 (only final solution samples were analyzed in Cycle 3) back to levels observed in Cycle 1 may be related to a degradation of the O-ring seals in the end-fittings. (End-fitting seal degradation was indicated by accelerated ^{137}Cs release from the undefected specimen starting with the 34-d Cycle 2 sample.)

Substantial reductions in uranium concentration as a result of filtration occurred in only a few samples, suggesting that uranium in most samples was in true solution and not present in fine suspended particles or colloidal phases. Uranium concentration measured in the unfiltered, 0.4-μm filtered, and 18-Å filtered fractions of the 119-d HBR/BF-85 Cycle 1 sample were 0.12, 0.055, and 0.028 μg/mL, respectively. This sample exhibited anomalous behavior in other respects and is discussed below under "Vessel Effects." A reduction from 1.67 μg/mL in the unfiltered aliquot to 0.41 μg/mL in the 0.4-μm filtered aliquot in the Day 1 sample from Cycle 2 of the TP/BF-85 test is another notable exception. One qualification for this data is that the laser fluorimetry method does not measure uranium contained in suspended solids. After filtration, the sample aliquots are acidified to 1% HNO_3 prior to analysis in order to dissolve any plate-out, colloids, or suspended

90794 1380

particles. There may be some question as to whether or not all suspended particles, such as undissolved fuel fines or uranium-containing secondary phases, are completely dissolved by this acidification step prior to analysis.

3.2.2 Vessel Effects

The 0.4-μm filtered uranium data from the Series 3 bare-fuel tests in sealed stainless steel vessels are compared to that from the Series 2 bare-fuel tests in unsealed silica vessels in Figure 3.2. After the initial Cycle 1 peak, lower uranium concentrations were observed in the Series 3 bare-fuel tests in comparison to those observed in the Series 2 bare-fuel tests. Local reactions between the stainless steel vessels and solution may be reducing U^{+6} to U^{+4} and limiting uranium solubility. Since the quantity of uranium in solution is not great, a small amount of vessel element oxidation may have a significant effect on uranium concentration. However, considering the low concentration of multivalent ions in J-13 water capable of providing effective Eh buffering, redox equilibrium was probably not well established in the Series 3 tests.

90794 1381

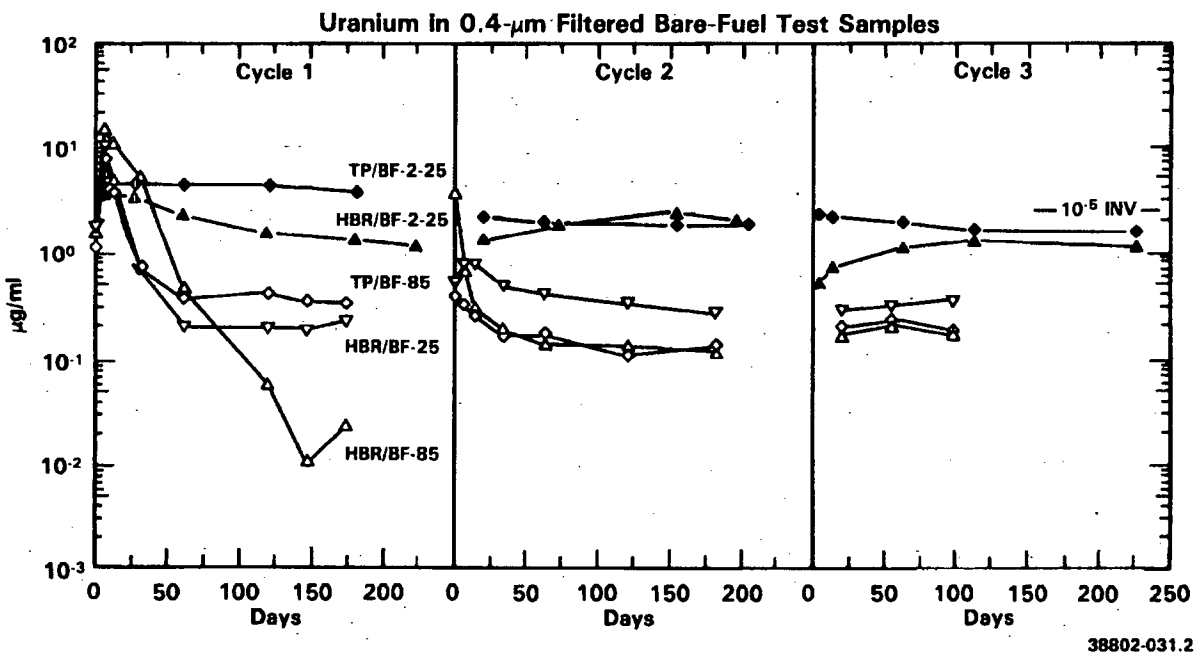

FIGURE 3.2. Comparison of Uranium Concentrations Measured in 0.4-μm Filtered Samples from the Three Series 3 and Two Series 2 Bare-Fuel Tests

The fact that stainless steel vessels are not completely inert relative to solutions containing Eh buffers was noted by Gray, who observed color changes with ZoBell's solution (an Eh standard based on the Fe^{+2}/Fe^{+3} reaction) in stainless steel containers, while no change was observed for the same ZoBell's solution in silica containers.[13] The $KMnO_4$ titration of equimolar $K_3Fe(CN)_6$ plus $K_4Fe(CN)_6$ solutions contained in 316 stainless steel under argon atmosphere for 3 days indicated that twice as much Fe^{+2} was present as in the starting solution, while no significant change in Fe^{+2}/Fe^{+3} ratio was observed for solutions contained in silica vessels. The additional Fe^{+2} in stainless steel resulted from reduction of the Fe^{+3}, from corrosion of the vessel (which contained a welded bottom), or from a combination of both.

The HBR/BF-85 Cycle 1 test exhibited anomalous behavior with uranium concentration decreasing to a minimum value of 0.01 μg/mL in the 147-d sample. The drop in uranium concentration (and also a drop in ^{99}Tc activity) is attributed to a combination of reduced solution oxygen potential in response to corrosion occurring within the vessel and scavenging of these elements by iron-bearing precipitates. A slight yellow turbidity was observed in the 119-d sample from this test, which was notable since solution samples are normally clear. The ICP data indicated 0.14 μg/mL Fe in 0.4-μm filtered solution on Day 33, increased to 0.45 μg/mL on Day 147, and dropped to 0.03 μg/mL on Day 174 at cycle termination. The 147-d sample was added in response to the observations on the 119-d sample from the HBR/BF-85 test. As indicated in Figure 3.3, the turbidity in the 119-d HBR/BF-85 sample appears to have been caused by the formation of iron-silicon containing flocs. The weld joining the bottom of the bare-fuel specimen basket to its cylindrical sides was considered a likely corrosion site, and several metallographic sections of this weld were examined after Cycle 1 termination. Figure 3.4(A) shows the etched microstructure at the boundary of the weld heat-affected zone and the bottom plate near the outer basket surface. This region would have been in a crevice region at the bottom of the narrow gap between the vessel and specimen basket. The more heavily etched appearance near the outer surface of the heat-affected zone suggests that some degree of intergranular corrosion may have occurred at this location. A stress crack shown in Figure 3.4(B) occurred at the weld intersection with the inner crevice

9 0 7 9 4 1 3 8 2

90794 1383

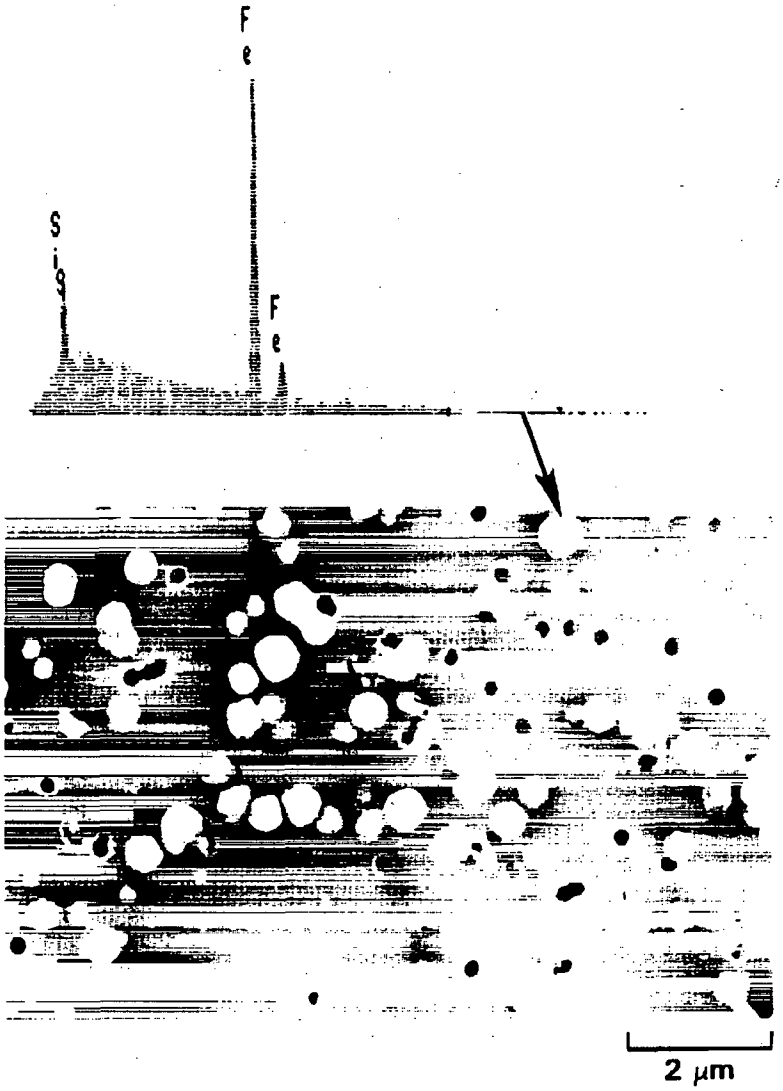

FIGURE 3.3. SEM Photograph Showing Flocs on 0.4-μm Filter Disk Used to Filter the 119-Day Sample from Cycle 1 of the HBR/BF-85 Test. (Accompanying EDX spectra indicates an iron-silicate floc composition.)

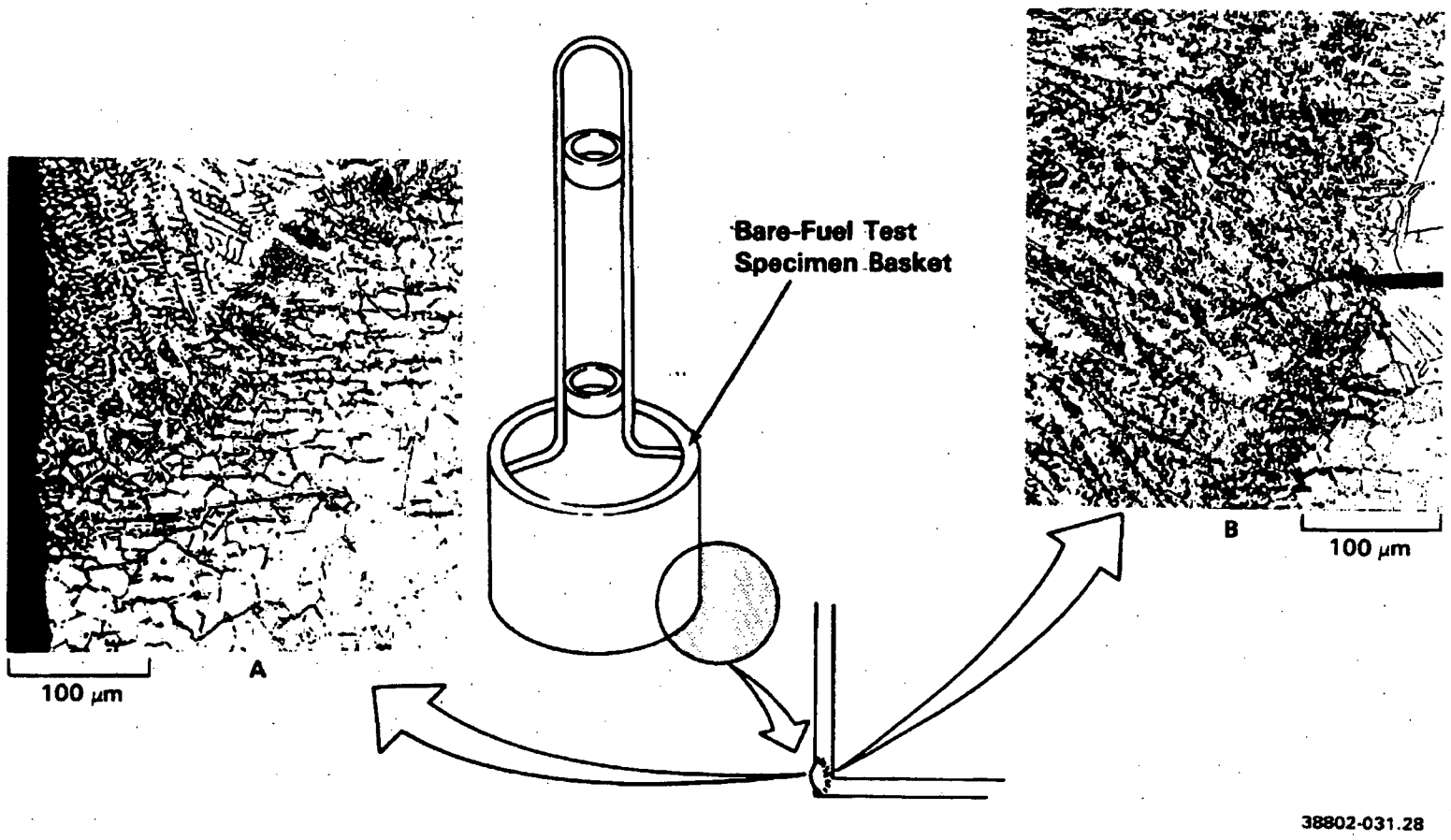

FIGURE 3.4. Metallographic Section of Bottom Weld in Specimen Basket from Cycle 1 of the HBR/BF-85 Test Etched with 10% Oxalic Acid (Neg. 8802279-1)

9 0 7 9 4 1 3 8 4

between the basket bottom plate and cylindrical side. Stress corrosion associated with this region may have been another source for iron dissolution.

Temperature/time conditions that allow precipitation of chromium-carbide phases at the grain boundaries may occur near the weld margins in austenitic stainless steel alloys such as 304. Transformation of the chromium-depleted austenitic stainless steel near the grain boundary to ferritic phase then sensitizes the grain boundaries to corrosion. Based on the apparent corrosion occurring in the 304 stainless steel HBR/BF-85 Cycle 1 vessel, it was decided to fabricate new vessels using 304L stainless steel for Cycle 2. Less of a tendency for such intergranular corrosion should occur with the lower carbon content 304L stainless steel. Data from Cycles 2 and 3 (especially ^{99}Tc data) suggest that corrosion-induced effects comparable to those observed in the HBR/BF-85 Cycle 1 test did not occur with the 304L stainless steel vessels.

3.2.3 Uranium Quantities in Sample Types

The quantities of uranium measured in the various liquid sample types are given in Table 3.1. The largest effect shown by these data is the much greater apparent release from bare-fuel in comparison to that from fuel still tightly confined in defected cladding. Much of the difference comes from the uranium measured in the rinse and strip samples in the bare-fuel tests that, as previously discussed in Section 3.1.3, are of questionable significance, since the portion of precipitated secondary uranium phases undissolved in the rinse solutions and the quantity of previously undissolved fuel fines dissolved in the strip solutions are not known. There was no evidence that grains of undissolved fuel or significant amounts of nuclide-containing secondary-phase particles were contained in the rinse or strip solutions from the three clad-specimen tests. Another observation on the bare-fuel rinse and strip sample data is that a greater portion of the measured uranium in these samples was contained in the rinse samples at 25°C in comparison to the 85°C tests. This correlation was also noted for the other actinides. This effect is explained by the hypothesis that actinides precipitated from the 85°C tests transformed to more stable crystalline phases exhibiting lower solubility in the rinse solution versus the 25°C test where less secondary-phase formation occurred, and the phases that did form may not have completely transformed to the more stable mineral states.

9 0 7 9 4 1 3 8 5

TABLE 3.1. Quantities of Uranium Measured in Samples (μg)

	HBR/BF-25	TP/BF-85	HBR/BF-85	HBR/SD-85	HBR/HD-85	HBR/UD-85
Cycle 1						
Periodic Samples	485	263	643	2.02	1.30	1.21
Final Solution	57.5	82.5	5.5	2.50	1.75	3.25
[U (ppm)]	(0.23)	(0.33)	(0.02)	(0.010)	(0.007)	(0.013)
Rinse	396	108	330	<0.6	66	0.6
Acid Strip	405	6330	4950	30	4.8	2.4
Cycle Total	1343	6784	5928	35.1	74	7.5
+ 10^{-5} Inv.	1.86	9.35	8.75	0.05	0.11	0.01
% in Solution	40.4	5.1	10.9	12.9	4.1	59.8
Cycle 2						
Periodic Samples	76.9	29.6	90.0	0.26	0.32	0.29
Final Solution	70.0	32.5	30.0	2.25	2.00	2.00
[U (ppm)]	(0.28)	(0.13)	(0.12)	(0.009)	(0.008)	(0.008)
Rinse	576	66	78	4.2	2.4	3.6
Acid Strip	159	810	1860	3.9	3.3	3.6
Cycle Total	882	938	2058	10.6	8.0	9.5
+ 10^{-5} Inv.	1.24	1.31	3.09	0.015	0.012	0.013
% in Solution	16.7	6.6	5.8	23.7	28.9	24.1
Cycle 3						
Periodic Samples	15.8	10.8	9.5	--	--	--
Final Solution	95.0	47.5	45.0	2.25	2.25	2.00
[U (ppm)]	(0.38)	(0.19)	(0.18)	(0.009)	(0.009)	(0.008)
Rinse	660	78	84	--	--	--
Acid Strip	24.9	480	(a)	--	--	--
Cycle Total	769	616	(a)	--	--	--
+ 10^{-5} Inv.	1.13	0.87	(a)	--	--	--
% in Solution	13.9	9.5	(a)	--	--	--
Sum of Cycles 1, 2 & 3						
Σ Cycle Totals	3021	8338	>8125	45.7[b]	82[b]	17[b]
+ 10^{-5} Inv.	4.23	11.53	>12.04	0.063[b]	0.12[b]	0.023[b]

(a) Cycle 3 HBR/BF-85 acid strip appears to have been contaminated by fuel particles.
(b) Cycles 1 and 2 only.
NOTE: Periodic samples, final solution and bare fuel rinse values are based on 0.4-μm filtered data. Other values are based on unfiltered data.

90794 1386

The acid strip solution from Cycle 3 of the HBR/BF-85 test in particular was anomalous in its high nuclide content. On first analysis, 18.3 mg of uranium were indicated as being dissolved in this solution. A second aliquot taken and analyzed a few weeks later indicated that 116 mg of uranium had dissolved in this solution. Since the average bare-fuel particle in the test weighed 100 to 200 mg, it appears likely that one of these particles was left in the vessel when it was acid-stripped and was not yet completely dissolved when the first aliquot was taken for analysis.

3.3 SECONDARY PHASE CHARACTERIZATION

After removing the rinse solution sample for analysis, the remaining rinse solution was stirred to get settled particles temporarily into suspension and then filtered through a 0.4-μm filter. The weights of solid residues collected on the filters are given in Table 3.2 along with identification of the filters that were examined by SEM and XRD. The SEM examination included energy dispersive X-ray (EDX) analysis of observed particles and residues. The most abundant phase observed on rinse filters from the bare-fuel tests was individual grains or small particles of fuel. Grains at the fuel particle surfaces were apparently loosened as a result of grain boundary dissolution during the tests and removed by the rinsing procedure.

Quantities of acicular crystalline phases (Figure 3.5) indicated by EDX analyses to have a calcium-uranium-silicate composition were observed on rinse filters from Cycles 1 and 2 of the TP/BF-85 test and on the rinse filter from Cycle 2 of the HBR/BF-85 test. Flakes of material indicated as having different calcium-uranium-silicate composition richer in silicon (Figure 3.6)

TABLE 3.2. Residues Collected on Rinse Filters (mg)

Cycle	HBR/BF-25	TP/BF-85	HBR/BF-85	HBR/SD-85	HBR/HD-85	HBR/UD-85
1	6.1	10.0s,x	8.8s	0.4	0.8	1.2s
2	4.7s	20.8s,x	11.5s,x	1.2	0.7	1.9s
3	6.2	9.9	8.5			

s = examined by SEM
x = examined by XRD

9 0 7 9 4 1 3 8 7

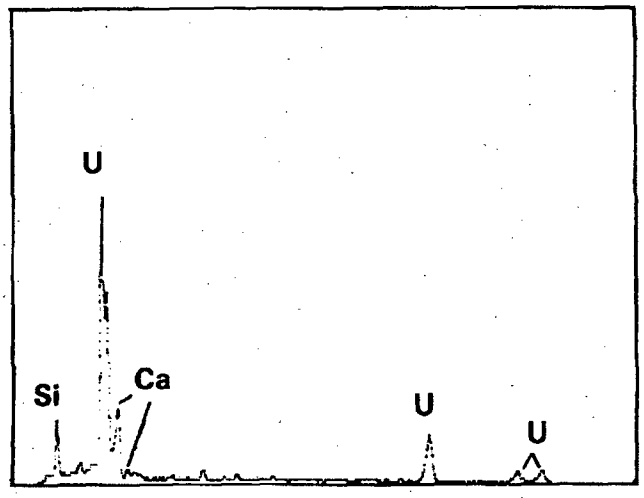

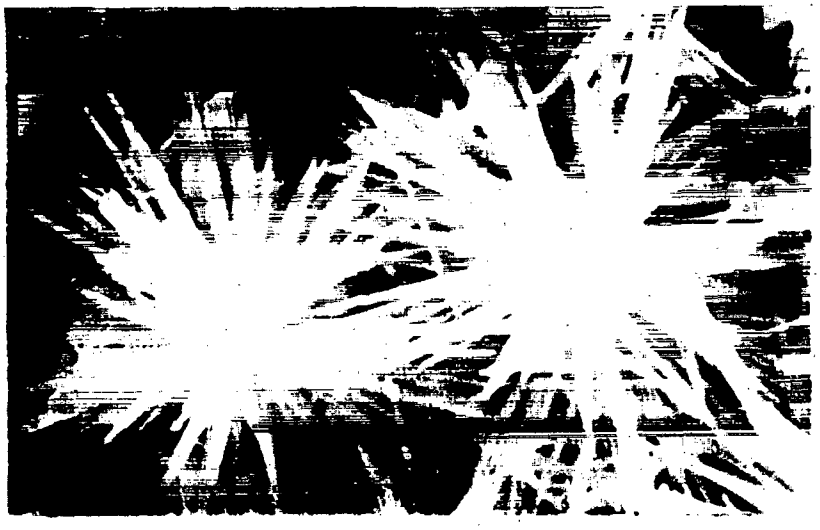

Neg 3085

5 µm

FIGURE 3.5. SEM Photograph and EDX Spectrum of Calcium-Uranium-Silicate Phase with Acicular Crystal Morphology on Rinse Filter from TP/BF-85 Cycle 1 Test (SEM Neg. 3085)

90794 1388

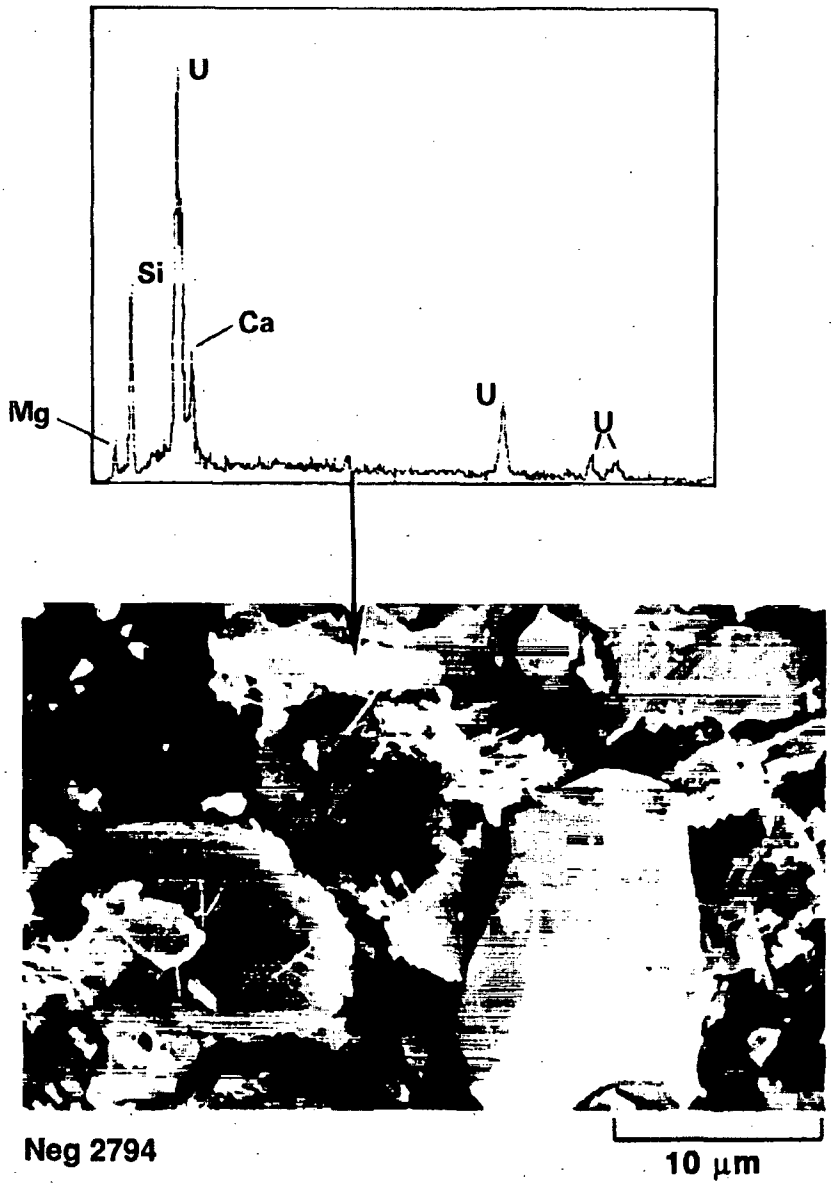

FIGURE 3.6. SEM Photograph and EDX Spectrum of Calcium-Uranium-Silicate Phase with Massive Flake Morphology on Rinse Filter from TP/BF-85 Cycle 2 Test (SEM Neg. 2794)

90794 1389

were also observed. The XRD patterns from these three rinse filters were extensively compared with reference Joint Committee on Powder Diffraction Standards (JCPDS) powder diffraction patterns for identification of possible uranium-containing secondary phases. Indexing data for lines identified in the XRD patterns by the diffractometer computer are tabulated in Appendix C. Confirmed and other possible uranium phases indicated by the XRD data are identified in Table 3.3. The acicular crystalline phase shown in Figure 3.5 is most likely uranophane and the higher silicon content phase shown in Figure 3.6 is likely a haiweeite phase.

The XRD pattern obtained from a piece of the HBR/BF-85 Cycle 2 rinse filter is shown in Figure 3.7 with reference stick patterns for uranophane and UO_2. The UO_2 lines are identified by a "U" and the uranophane lines by a "UP" in the sample pattern, providing an excellent match for all but one of the significant lines. The weak low-angle line identified as "H" was best matched by the 100% intensity 002 line (d = 9.30 Å) of the JCPDS No. 13-118 ranquilite pattern and was next closely matched by the 100% intensity line (d = 9.26 Å) in the JCPDS No. 12-721 haiweeite pattern. The symbol "H" was given to this low angle peak since ranquilite was renamed as haiweeite in the 1987 JCPDS files, and three of the four "haiweeite" patterns in the 1987 files have their most intense peak near this location.

The XRD pattern from the TP/BF-85 Cycle 1 rinse filter shown in Figure 3.8 was the weakest of the three patterns. There are two strong non-UO_2 lines in this pattern. The lower angle line identified as "H" is at the same position as the "H" line discussed above in the HBR/BF-85 Cycle 2 rinse filter pattern and is most closely matched by the 002 line of the JCPDS No. 13-118 ranquilite pattern. The position of the higher angle non-UO_2 line corresponds to a lattice spacing of d = 3.36 Å. Possible matches for this line are the 30% intensity 042 line of the JCPDS 13-118 ranquilite pattern and the 80% intensity 220 line in the JCPDS 26-1392 soddyite pattern, both with d = 3.34 Å. Another possible match is the 100% intensity line at d = 3.38 Å in the JCPDS 17-462 calcium-ursilite pattern. Major lines in all of these patterns are, however, missing from the sample pattern. A possible explanation for the missing lines would be preferred orientation on the filter

2 0 7 9 4 1 3 9 0

TABLE 3.3. Probable Phases Indicated by XRD on Bare-Fuel Rinse Filters

Mineral Name	Chemical Formula	JCPDS No.[a]	Status[b]
Uraninite	UO_2	5-550[i]	C
Uranophane	$CaO \cdot 2UO_3 \cdot 2SiO_2 \cdot 6H_2O$	8-442[i]	C
Ranquilite[c]	$1.5CaO \cdot 2UO_3 \cdot 5SiO_2 \cdot 12H_2O$	13-118[i]	L
Haiweeite	$CaO \cdot 2UO_3 \cdot 6SiO_2 \cdot 5H_2O$	12-721[o]	P
Ursilite[c]	$2CaO \cdot 2UO_3 \cdot 5SiO_2 \cdot 9H_2O$	17-462[o]	P
Soddyite	$2UO_3 \cdot SiO_2 \cdot 2H_2O$	26-1392*	P

(a) JCPDS data quality ratings: * = Best, i = Intermediate, o = Low.
(b) C = Confirmed, L = Likely, P = Possible.
(c) Renamed as haiweeite in the 1987 JCPDS files.

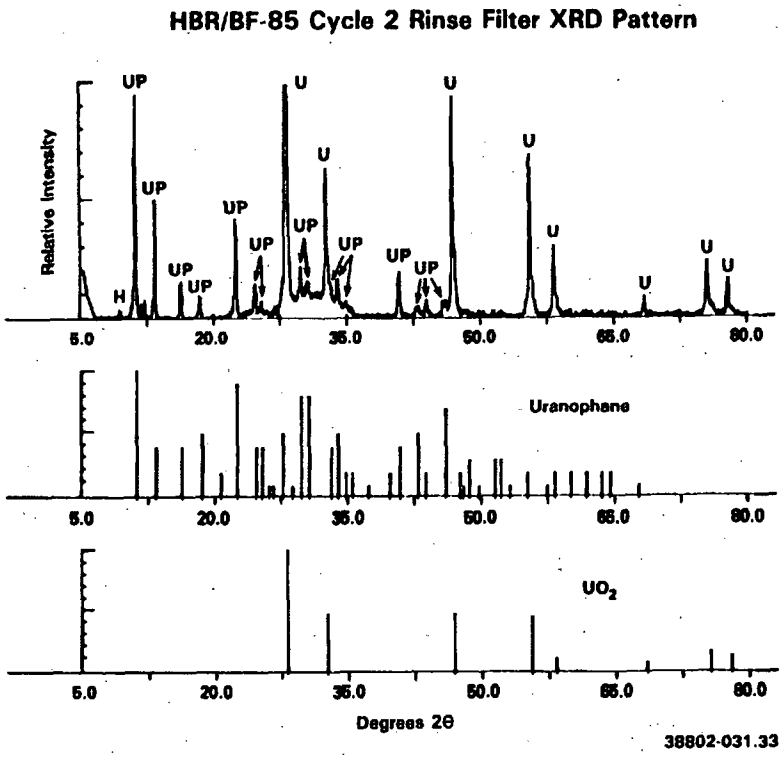

FIGURE 3.7. XRD Pattern of Rinse Filter from HBR/BF-85 Cycle 2 Test. (UP = Uranophane, U = UO_2, and H = Haiweeite.) (Neg. 90032144-14)

90794 1391

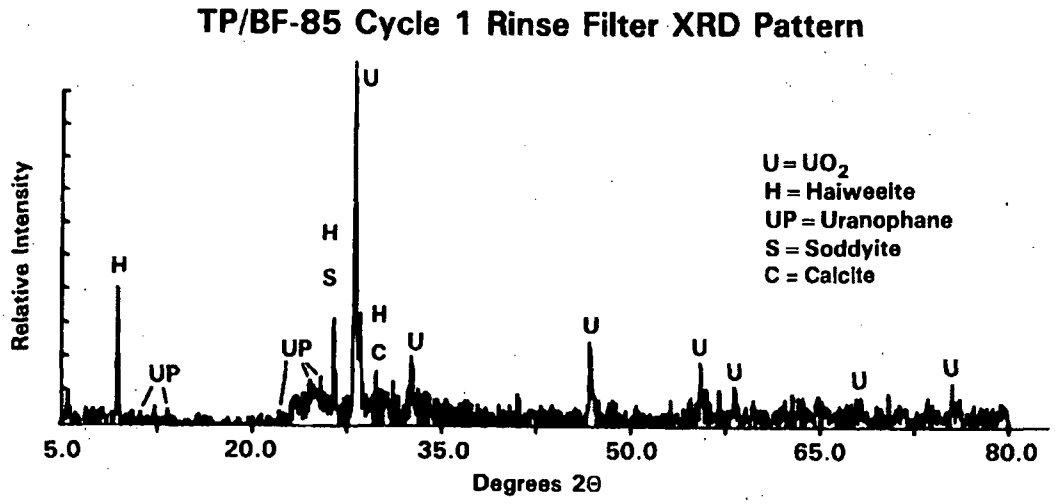

FIGURE 3.8. XRD Pattern of Rinse Filter from TP/BF-85 Cycle 1 Test. (UO_2 lines are identified as "U" and a haiweeite line as "H". The "HS" line may be haiweeite and/or soddyite.) (Neg. 90032144-16)

sample. The higher angle line has tentatively been labeled "H" and "S" because it could result from one of the "haiweeite" phases, soddyite, or some combination of these phases. Soddyite formation in this test would correlate with the lower solution calcium concentrations measured (1.1 μg/mL) and may explain why uranium concentrations stabilized at higher levels than in Cycles 2 and 3. A weaker non-UO_2 line identified at d = 3.121 Å could be a haiweeite or calcite line. The location of possible uranophane lines too weak for identification by the diffractometer computer are also shown.

The XRD pattern from the TP/BF-85 Cycle 2 rinse filter is shown in Figure 3.9. The same low angle "haiweeite" line observed in the HBR/BF-85 Cycle 2 and TP/BF-85 Cycle 1 rinse filters is present. Three other weak lines marked "H" correspond to line positions in the JCPDS 13-118 ranquilite pattern. Most of the remaining significant lines appear to be from uranophane or UO_2. In general, the XRD evidence for haiweeite formation in the 85°C bare-fuel tests is not as convincing as that for uranophane.

90794 1392

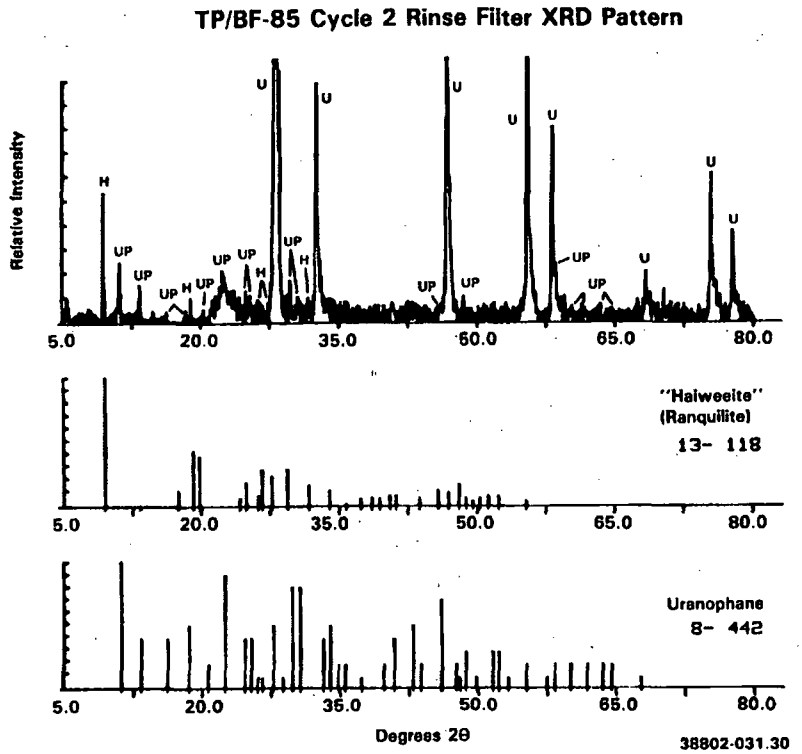

FIGURE 3.9. XRD Pattern of Rinse Filter from TP/BF-85 Cycle 2 Test. (UO_2 lines are identified as "U", uranophane lines as "UP," and haiweeite lines tentatively as "H." JCPDS patterns for uranophane and the "haiweeite" mineral ranquilite are shown below.) (Neg. 90032144-13)

Other phases such as calcite, dolomite, and SiO_2 (possibly as amorphous gel) also appear to be likely in all the rinse filters based on the SEM data and probably account for most of the rinse filter residue mass in the three clad fuel-specimen tests. White scale formation at the waterline was noted in all of the 85°C tests at cycle termination. No waterline scale formation was observed in the HBR/BF-25 test. As indicated by the solution chemistry data tabulated in Appendix B, significant drops in calcium, magnesium, silicon, and HCO_3 concentrations occurred in the five 85°C tests but not in the HBR/BF-25 test.

Formation of the secondary phases dolomite, calcite, quartz, haiweeite, and soddyite during spent-fuel dissolution in J-13 well water has been

90794 1393

predicted by the EQ3/6 geochemical model.[14] Thermodynamic properties of uranophane need yet to be determined for addition to the EQ3/6 database. There was no evidence in the examined rinse filters of schoepite ($UO_3 \cdot 2H_2O$) formation, which is predicted to occur eventually as fuel dissolution progresses. Further depletion of silicon concentration followed by increasing uranium concentration (expected prior to schoepite formation) was not observed. The observed uranium concentrations, solution chemistry data, and secondary-phase formation data are relatively consistent with EQ3/6 predictions. However, the solids characterizations data to date are considered limited. In particular, phases containing other important nuclide elements such as plutonium, americium, and curium, which either did not dissolve or dropped out of solution, have not been confirmed or identified.

90794 1394

3.4 PLUTONIUM

Plutonium isotopes account for about 45% of the ORIGEN-2 calculated activity of spent fuel at 1,000 yr and about 90% of the activity at 10,000 yr. Plutonium is thought to be in solid solution at a concentration on the order of 1% in the spent fuel UO_2 matrix phase. The principal isotopes accounting for most of the postcontainment period plutonium alpha activity are ^{239}Pu (24,000-yr half-life) and ^{240}Pu (6,570-yr half-life) that, because of their very similar alpha decay energies, are measured together as $^{239+240}Pu$ activity. In the relatively young spent fuel used in the current testing, ^{241}Pu (14.4-yr half-life) accounts for about 92% of the total actinide activity and about 22% of the total actinide plus fission product activity.

Activities of $^{239+240}Pu$ measured in 0.4-μm filtered solution samples are plotted in Figure 3.10. During Cycle 1 of the bare-fuel tests, plutonium rapidly reached maximum activities and then dropped out of solution, with the greatest decreases in activity occurring in the 85°C tests. Relatively stable steady-state activities on the order of 100 pCi/mL (~1 ppb or $10^{-8.4}$ M plutonium) were measured at 25°C in Cycles 2 and 3 of the bare-fuel tests versus much lower activities on the order of 1 pCi/mL (~0.01 ppb or $10^{-10.4}$ M plutonium) measured at 85°C. Lower actinide activities in solution at 85°C are attributed to faster kinetics for formation of solubility-limiting secondary phases at the higher temperature. Even lower activities ranging from about

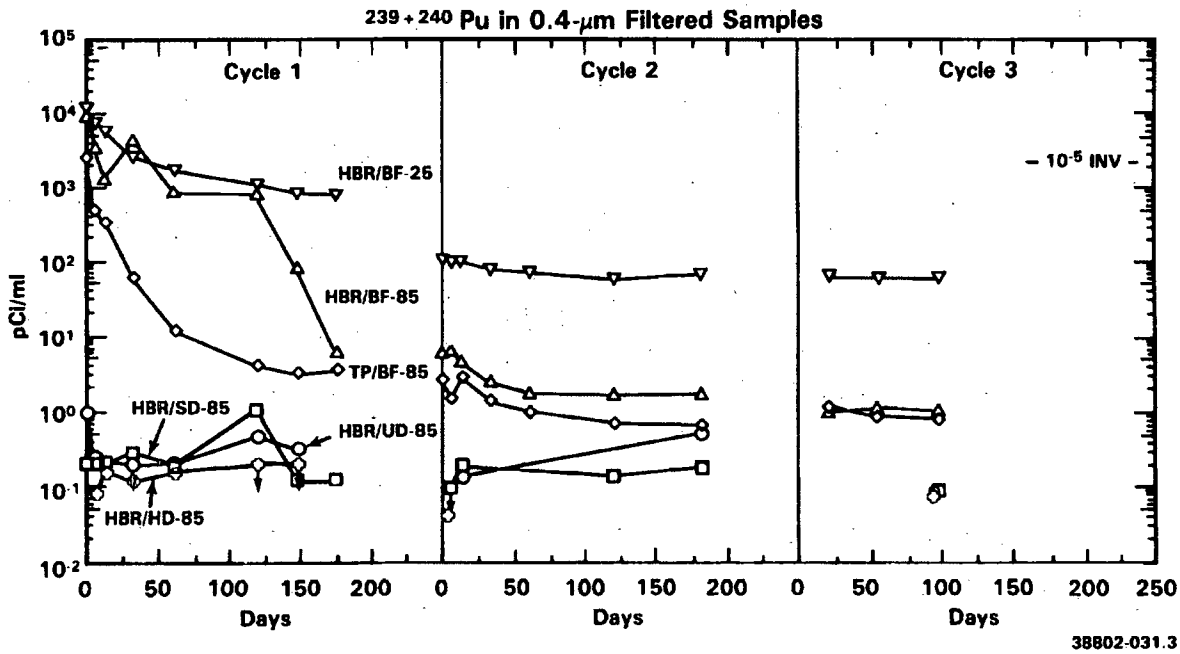

FIGURE 3.10. Activity of $^{239+240}Pu$ in 0.4-μm Filtered Solution Samples

0.1 to 1 pCi/mL, which were not much above the $^{239+240}Pu$ detection limit, were measured in the 85°C tests using fuel in defected cladding and undefected cladding.

The 0.4-μm filtered $^{239+240}Pu$ solution sample data from the Series 3 bare-fuel tests are compared to that from the Series 2 bare-fuel tests in Figure 3.11. The effects of sealed stainless steel versus unsealed silica vessels are relatively small compared to the effect of temperature. Activities measured near the end of each cycle of three 25°C bare-fuel tests ranged from about 900 pCi/mL ($10^{-7.4}$ M plutonium) in Cycle 1 of the Series 3 test down to about 30 pCi/mL ($10^{-8.9}$ M plutonium) in Cycle 2 of the HBR Series 2 test. These results agree very well with those reported by Rai and Ryan[15], who measured the solubility of PuO_2 and hydrous $PuO_2 \cdot xH_2O$ in deionized water suspensions aged for up to 1,300 d at 25°C. At a pH of 8, which was the extrapolated lower limit of their data and the approximate pH in the Series 2 and 3 tests, they report that plutonium concentration ranged from about

90794 1395

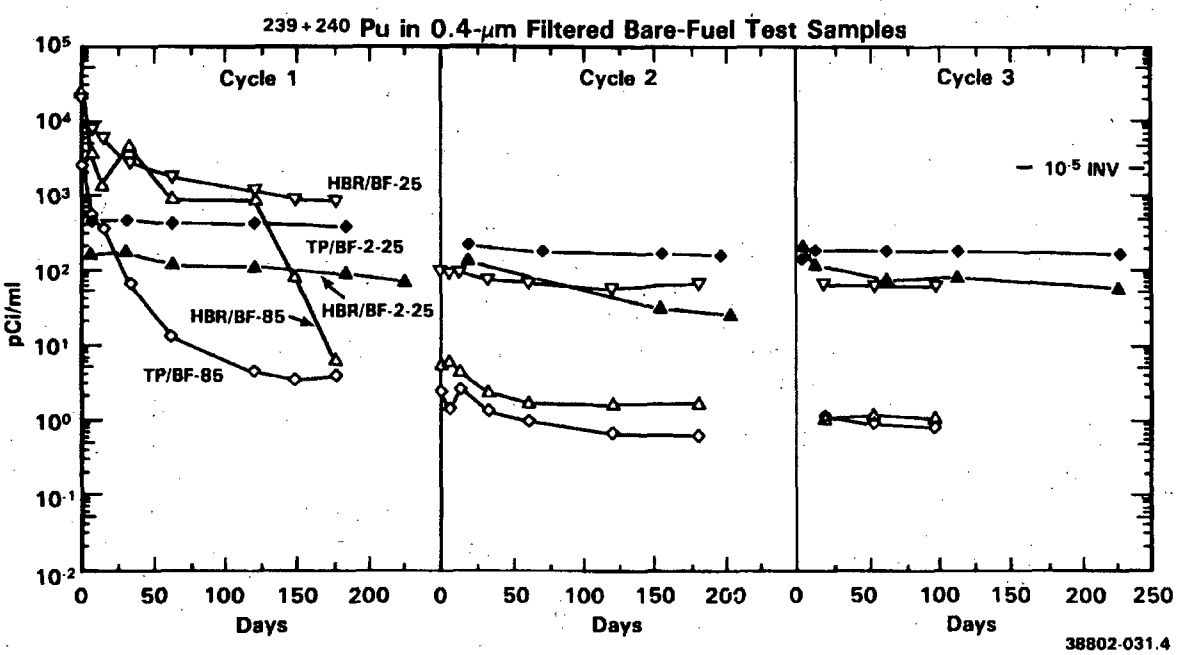

FIGURE 3.11. Comparison of $^{239+240}Pu$ Activities Measured in 0.4-μm Filtered Samples from the Three Series 3 and Two Series 2 Bare-Fuel Tests

$10^{-7.4}$ M, where amorphous $PuO_2 \cdot xH_2O$ was thought to be controlling concentration, down to about 10^{-9} M, where aging to a more crystalline PuO_2 was thought to reduce Pu concentration. Samples were 0.015 μm or 18-Å filtered.

The effect of sample filtration on $^{239+240}Pu$ activities measured in solution samples from the bare-fuel tests are shown in Figure 3.12. The effect of 0.4-μm filtration was generally slight, except in Cycle 3 of the 85°C tests, where the effect diminished with time. The 18-Å filtration was conducted only through the 34-d Cycle 2 sample. Approximately 80% of the activity in the later HBR/BF-25 Cycle 1 0.4-μm filtered samples was retained by the 18-Å filters, with this percentage dropping to about 40% in Cycle 2. The greatest filtration effect was observed during the HBR/BF-85 Cycle 1 test, where 99.86% of the 0.4-μm filtered activity in the 119-d sample was retained by the 18 Å filter, which may be another anomaly of the vessel corrosion that occurred in this test. Plutonium may have been adsorbed on a finely dispersed iron-silica phase that formed in this test, floccules of which were shown in Figure 3.3. An order of magnitude reduction in activity was also observed for

9 0 7 9 4 1 3 9 6

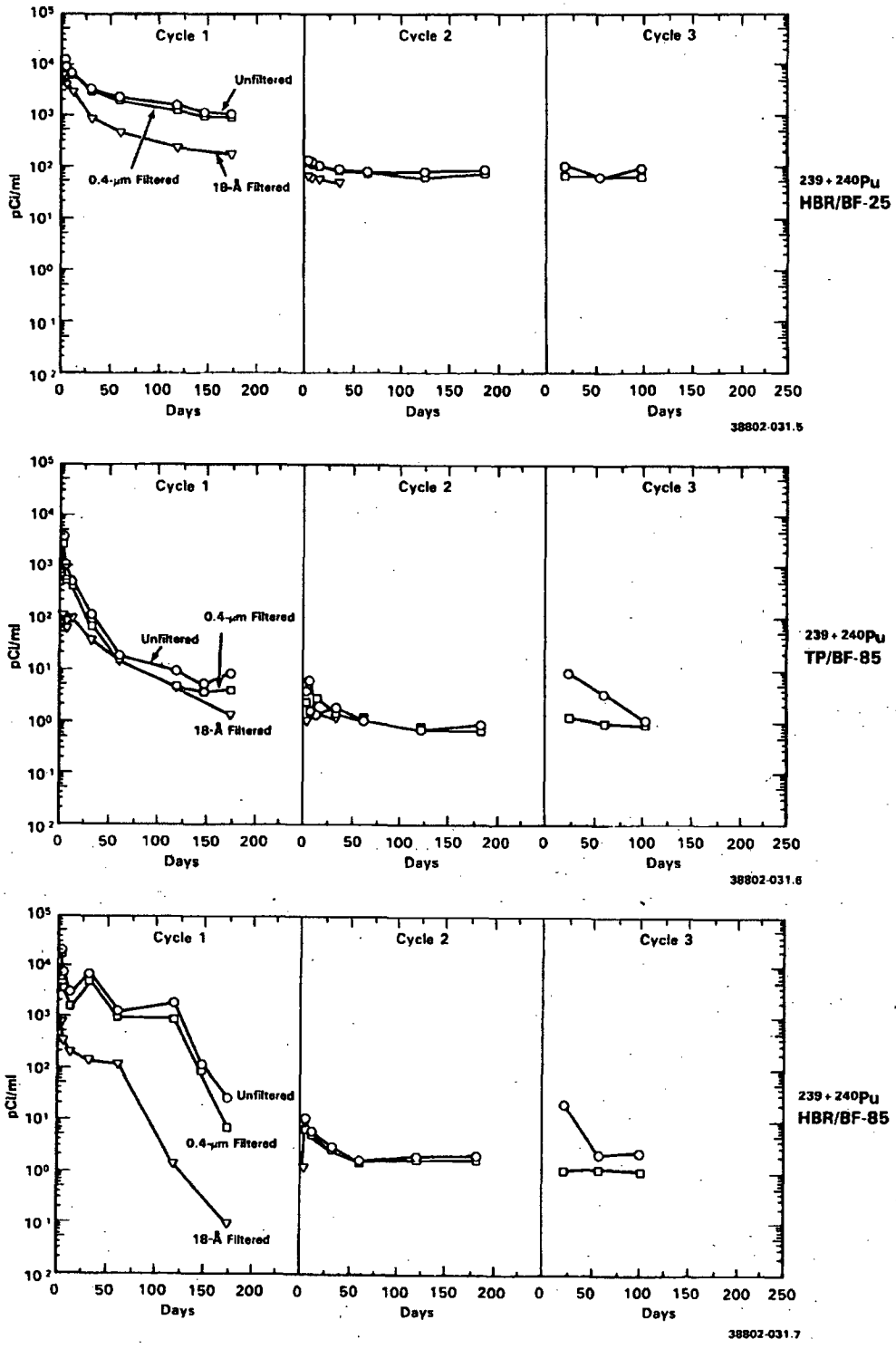

FIGURE 3.12. Effects of Filtration on Measured $^{239+240}Pu$ Activity in Solution Samples from the Bare-Fuel Tests

90794 1397

the initial 18-Å filtered samples from the TP/BF-85 Cycle 1 test. Except as noted, the effects of filtration on measured plutonium activities were in general relatively small. The filtration effects were particularly small during Cycle 2.

Although stable plutonium colloid formation in aqueous systems has been well documented,[15,16] the filtration data do not strongly support colloid formation as a primary factor contributing to solution plutonium content over an extended period. The actual quantities of plutonium released by fuel dissolution during Cycles 2 and 3 were probably on the order of a few micrograms. This relatively small amount of plutonium could have been incorporated in the uranium secondary phases as they formed or may have been associated with other phases that either precipitated or plated out of solution. The data given in Table 3.4 indicate that the majority of the plutonium was measured in the acid strip samples. The greater quantities of plutonium in acid strip solutions from the 85°C bare-fuel tests relative to the 25°C test are probably indicative of a greater amount of fuel dissolution and actinide precipitation at the higher temperature.

9 0 7 9 4 1 3 9 8

3.5 AMERICIUM

At 1,000 yr, ^{241}Am accounts for about half of the gross activity in spent fuel. Americium-241 activity in spent fuel increases during the first ~100 yr after discharge as a result of ^{241}Pu decay and then decreases by alpha decay (432-yr half-life) to ^{237}Np. By 10,000 yr, the only remaining significant americium isotope is ^{243}Am, which accounts for ~3% (including a short-lived ^{239}Np daughter) of the gross 10,000-yr activity. Americium concentration in the spent fuel matrix phase is ~6 x 10^{-4} g per g of fuel, which is thought to be in solid solution with the matrix phase.

Activity of ^{241}Am measured in 0.4-μm filtered solution samples is plotted in Figure 3.13. The effect of temperature on americium activity in solution is even greater than with plutonium. Relatively stable steady-state ^{241}Am activities on the order of 100 pCi/mL were measured during Cycles 2 and 3 of the 25°C bare-fuel test, which is about the activity level measured for $^{239+240}Pu$ in this test. Activity levels during Cycles 2 and 3 of the 85°C bare-fuel tests dropped to an approximate range of about 0.1 to 0.5 pCi/mL,

TABLE 3.4. Quantities of $^{239+240}Pu$ Measured in Samples (nCi)

	HBR/BF-25	TP/BF-85	HBR/BF-85	HBR/SD-85	HBR/HD-85	HBR/UD-85
Cycle 1						
Periodic Samples	629	57.1	580	<0.078	<0.022	<0.038
Final Solution	229	1.01	1.7	0.034	<0.056	~0.05
[Pu (pg/mL)]	(9660)	(43.2)	(71.4)	(1.43)	(<2.4)	(~2)
Rinse	188	24.3	97	0.081	0.01	~0.6
Acid Strip	1527	3554	5392	37.3	6.0	7.8
Cycle Total	2573	3636	6071	37.5	6.0	8.0
+ 10^{-5} Inv.	4.01	6.04	10.11	0.059	0.01	0.013
% in Solution	33.3	1.60	9.6	0.03	<1.2	~1
Cycle 2						
Periodic Samples	11.2	0.22	0.46	~0.01	--	--
Final Solution	17.7	0.16	0.43	0.045	<0.02	0.135
[Pu (pg/mL)]	(747)	(6.7)	(18.1)	(1.90)	(<1)	(5.7)
Rinse	216	17.0	33.5	0.054	0.08	0.054
Acid Strip	430	1224	1581	6.76	2.4	7.30
Cycle Total	675	1242	1615	6.87	2.5	7.49
+ 10^{-5} Inv.	1.07	2.09	2.74	0.011	0.004	0.012
% in Solution	4.3	0.03	0.05	0.79	--	>1.8
Cycle 3						
Periodic Samples	3.24	0.05	0.06	--	--	--
Final Solution	16.1	0.20	0.26	0.022	0.022	0.022
[Pu (pg/mL)]	(681)	(8.6)	(11.0)	(0.95)	(0.95)	(0.95)
Rinse	233	30.8	26.5	--	--	--
Acid Strip	511	819	(a)	--	--	--
Cycle Total	573	850	(a)	--	--	--
+ 10^{-5} Inv.	1.21	1.44	(a)	--	--	--
% in Solution	2.6	0.03	(a)	--	--	--
Sum of Cycles 1, 2 & 3						
Σ Cycle Totals	4000	5728	>7713	44.3[b]	9.1[b]	15.4[a]
+ 10^{-5} Inv.	6.29	9.57	>12.89	0.07[b]	0.02[b]	0.025[a]

(a) Cycle 3 HBR/BF-85 acid strip appears to have been contaminated by fuel particles.
(b) Cycles 1 and 2 only.
NOTE: Periodic samples, final solution and bare fuel rinse values are based on 0.4-μm filtered data. Other values are based on unfiltered data.

907941399

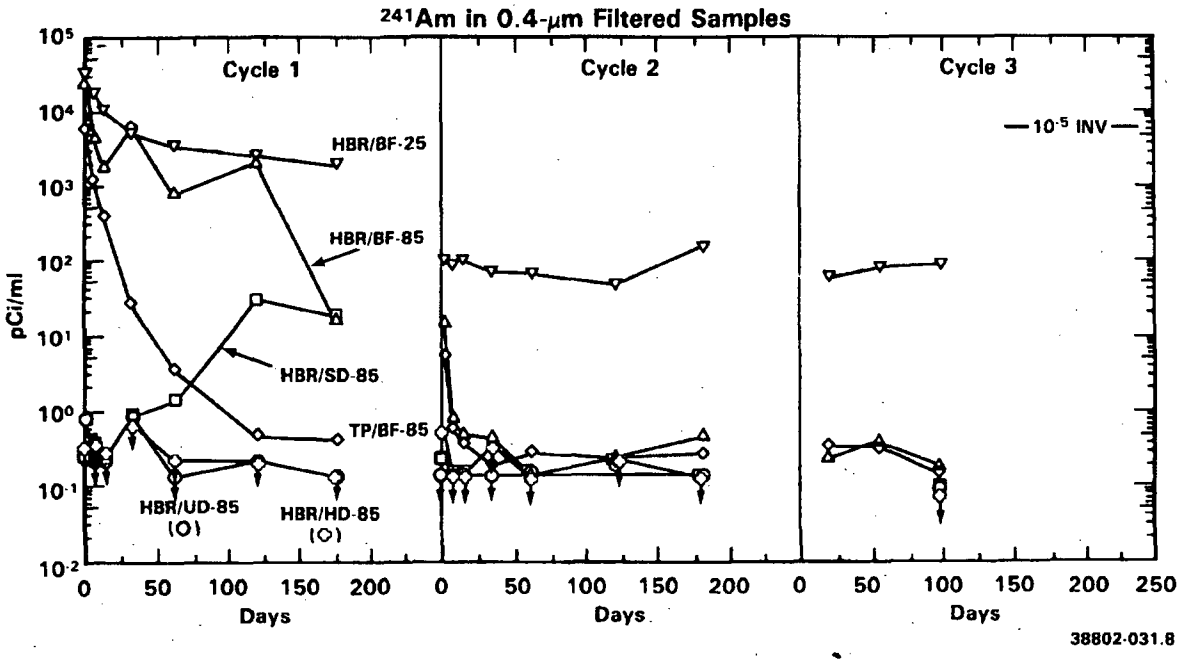

FIGURE 3.13. Activity of ^{241}Am Measured in 0.4-μm Filtered Solution Samples

which was barely above the detection limit. Except for Cycle 1 of the slit-defect test, ^{241}Am activities were generally below detection in the slit-defect, hole-defects, and undefected clad fuel tests. Activity in the slit-defect test reached a maximum value of 31 pCi/mL in the 119-d Cycle sample. Most of this activity was apparently present in solution as fine suspended particles since the 18-Å filtered activity increased only to a barely detectable 0.45 pCi/mL during Cycle 1 of this test.

The 0.4-μm filtered ^{241}Am solution sample data from the Series 3 bare-fuel tests are compared to that from the Series 2 bare-fuel tests in Figure 3.14. As with the plutonium data, these data show very little effect of sealed stainless steel versus unsealed silica vessels on the 25°C americium activity. However, the effect of temperature is again clearly shown. Although relatively stable steady-state activities appeared to be established during individual test cycles at 25°C, these activity levels varied from about 2,000 pCi/mL at the end of Cycle 1 of the Series 3 test down to 11 pCi/mL at the end of Cycle 2 of the Series 2 HBR test. Excluding the Cycle 1 data and the Series 2 Cycle 2 HBR data, the 25°C activities tended to stabilize at

90794 1400

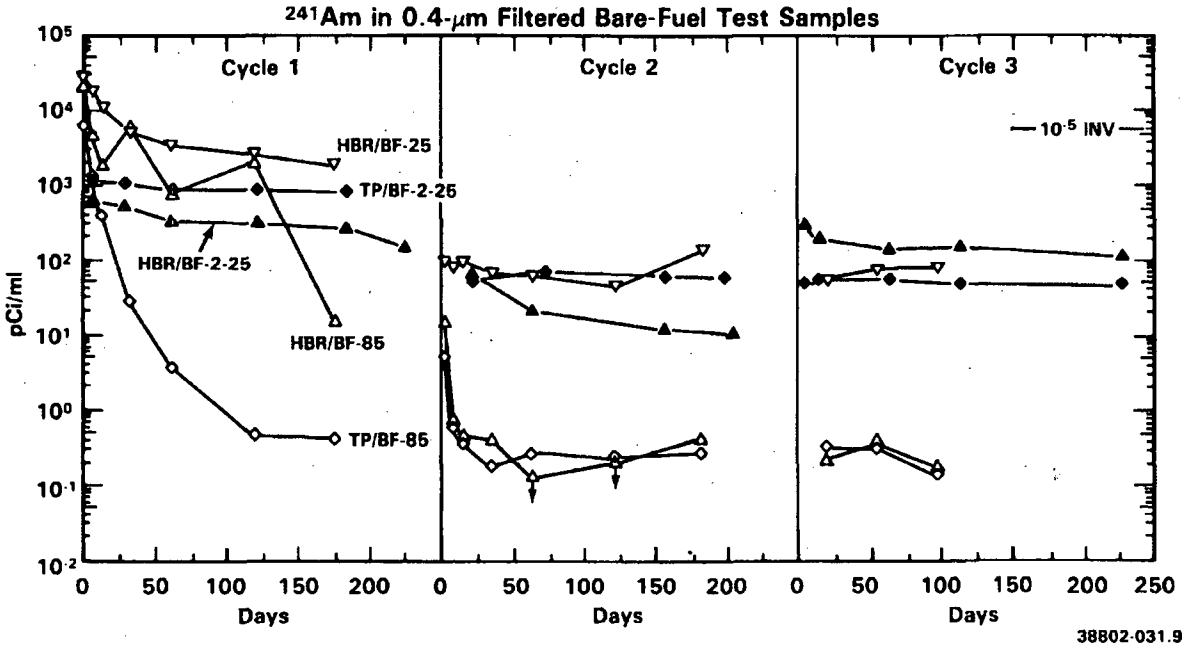

FIGURE 3.14. Comparison of ^{241}Am Activities Measured in 0.4-μm Filtered Samples from the Three Series 3 and Two Series 2 Bare-Fuel Tests

levels on the order of 100 pCi/mL, which corresponds to an americium concentration of $10^{-9.8}$ M. The 85°C activities during Cycles 2 and 3 tended to stabilize at more consistent levels around 0.2 pCi/mL, corresponding to an americium concentration of $10^{-12.5}$ M.

The effects of filtration on ^{241}Am activity measured in solution samples are shown in Figure 3.15 for the bare-fuel tests. The effects of 0.4-μm filtration were small in the 25°C test. However, only a few percent of the 0.4-μm filtered activity was passed by the 18-Å filters in the 25°C test, suggesting that ^{241}Am may have been associated with a colloidal phase at 25°C. The generally much lower ^{241}Am activities reached in all filter fractions at 85°C suggest that a different mechanism may be controlling americium concentrations in the 85°C tests. Americium association with a colloidal phase is also suggested for Cycle 1 of the HBR/BF-85 test in which vessel corrosion anomalies were indicated. Differences between unfiltered and 0.4-μm filtered data in the other 85°C test cycles could indicate formation of low-density suspended floccules or gel structures.

90794 1401

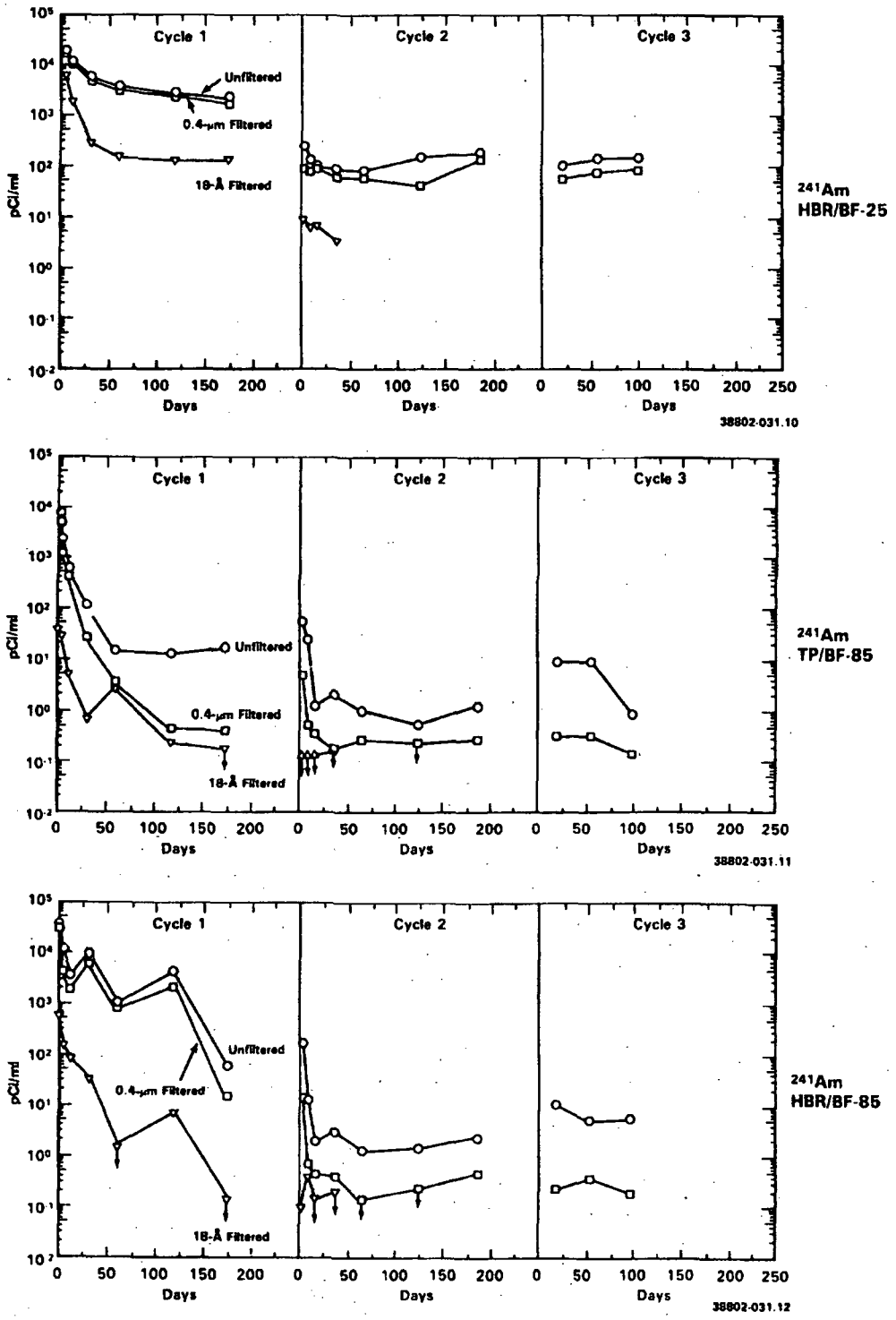

FIGURE 3.15. Effects of Filtration on Measured ^{241}Am Activity in Solution Samples from the Bare-Fuel Tests

90794 1402

The data for quantities of ^{241}Am activity measured in the various liquid sample types tabulated in Table 3.5 are somewhat similar in appearance to the data for uranium and $^{239+240}Pu$. Greater ^{241}Am activity was measured in periodic, final solution, and rinse solution samples from the HBR/BF-25 test than in the same samples from the 85°C bare-fuel tests. Lower actinide concentrations in solution at 85°C are attributed primarily to kinetic factors involved in the nucleation and precipitation of stable secondary phases or colloids. The amount of ^{241}Am measured in the HBR/BF-85 Cycle 1 acid strip (15,811 nCi, the largest quantity of ^{241}Am measured) corresponds to only ~5 μg of americium (the americium content of ~9 mg of fuel). Due to the small quantities involved, separation and characterization of secondary phases containing americium in a high concentration would be difficult. If americium is contained in dilute concentration in the more abundant uranium secondary phases, it may be possible to measure ^{241}Am activity in these phases, if they can be separated. The 102 nCi of ^{241}Am measured in the HBR/SD-85 Cycle 1 acid strip indicates that some precipitation or plate-out did occur in response to the increasing ^{241}Am activity observed in unfiltered and 0.4-μm samples in Cycle 1 of this test.

90794 1403

3.6 CURIUM

Curium-244 is one of the five principal alpha-emitting nuclides (along with ^{241}Am, ^{238}Pu, ^{239}Pu, and ^{240}Pu) in the spent fuel specimens tested. One other high-activity actinide isotope in young spent fuel is ^{241}Pu, which beta-decays with a 14.4-yr half-life to ^{241}Am. Of these six principal actinide nuclides occurring in young spent fuel, ^{244}Cm is the second shortest lived, decaying with a 18.1-yr half-life to ^{240}Pu. (Plutonium-238 is the next shortest lived, decaying with a 88-yr half-life to ^{234}U.) After ^{244}Cm has decayed out, the alpha activity contributed by other curium isotopes is minor in comparison to that contributed by americium and plutonium decay. The curium concentration (93% ^{244}Cm) in the spent fuel specimens was about 2×10^{-5} g/g of fuel.

The activity of ^{244}Cm measured in 0.4-μm filtered solution samples is plotted in Figure 3.16. The 0.4-μm filtered ^{244}Cm data from the bare-fuel tests are compared to those from the two Series 2 bare-fuel tests in

TABLE 3.5. Quantities of ^{241}Am Measured in Samples (nCi)

	HBR/BF-25	TP/BF-85	HBR/BF-85	HBR/SD-85	HBR/HD-85	HBR/UD-85
Cycle 1						
Periodic Samples	1241	114.0	926	<0.88	<0.05	<0.06
Final Solution	492	0.10	13.72	4.62	<0.034	<0.034
[Am (pg/mL)]	(724)	(0.15)	(5.5)	(6.8)	(<0.05)	(<0.05)
Rinse	243	47.0	151	0.19	0.14	0.19
Acid Strip	8365	9757	15811	102	5.0	3.5
Cycle Total	10341	9918	16892	107	5.2	3.8
+ 10^{-5} Inv.	6.78	7.68	11.83	0.071	0.004	0.003
% in Solution	16.8	1.15	5.5	5.1	<1.6	<2.4
Cycle 2						
Periodic Samples	10.2	0.104	0.27	<0.027	<0.032	<0.013
Final Solution	38.7	0.068	0.11	<0.034	<0.034	<0.034
[Am (pg/mL)]	(57)	(0.10)	(0.17)	(<0.05)	(<0.05)	(<0.05)
Rinse	239	28.6	63.8	0.24	0.16	0.16
Acid Strip	2027	2784	4608	2.84	2.43	2.7
Cycle Total	2315	2813	4672	3.14	2.66	2.9
+ 10^{-5} Inv.	1.54	2.21	3.32	0.002	0.002	0.002
% in Solution	2.1	0.006	0.008	<2	<2.5	<1.6
Cycle 3						
Periodic Samples	3.42	0.016	0.015	--	--	--
Final Solution	22.0	0.034	0.045	<0.02	<0.022	<0.022
[Am (pg/mL)]	(32)	(0.05)	(0.07)	(<0.03)	(<0.03)	(<0.03)
Rinse	319	61.1	62.7	--	--	--
Acid Strip	1635	1811	(a)	--	--	--
Cycle Total	1979	1872	(a)	--	--	--
+ 10^{-5} Inv.	1.34	1.48	(a)	--	--	--
% in Solution	1.3	0.003	(a)	--	--	--
Sum of Cycles 1, 2 & 3						
& Cycle Totals	14635	14602	<21627	110[b]	7.8[b]	6.7[b]
+ 10^{-5} Inv.	9.66	11.37	>15.20	0.073[b]	0.006[b]	0.004[b]

(a) Cycle 3 HBR/BF-85 acid strip appears to have been contaminated by fuel particles.
(b) Cycles 1 and 2 only.
NOTE: Periodic samples, final solution and bare fuel rinse values are based on 0.4-μm filtered data. Other values are based on unfiltered data.

90794 1404

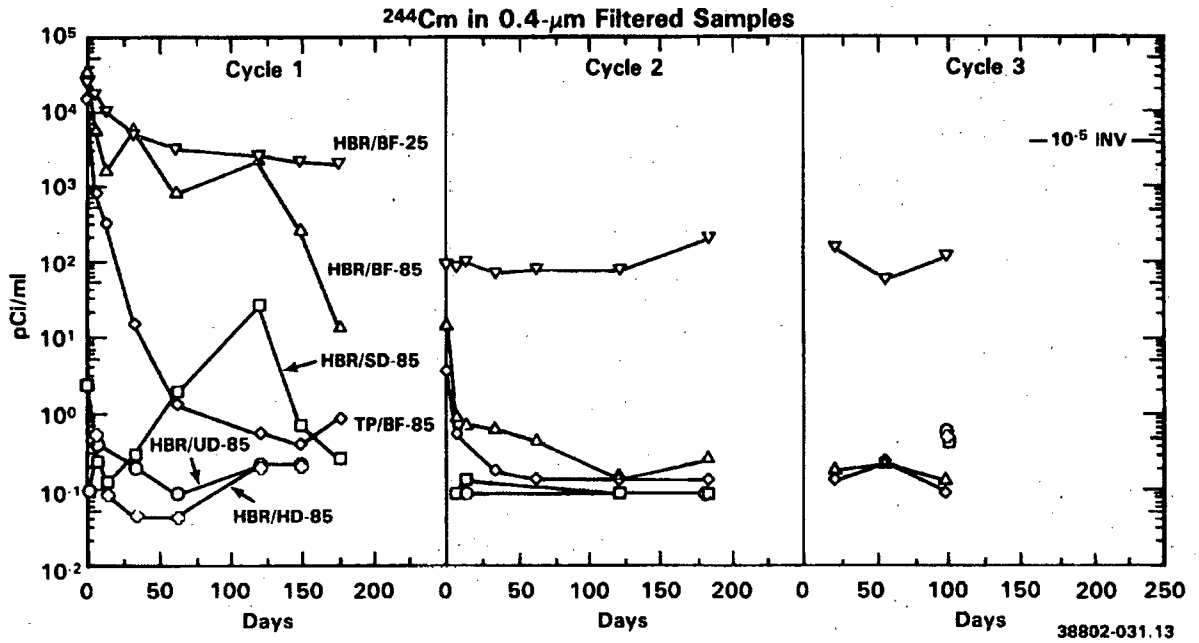

FIGURE 3.16. Activity of ^{244}Cm Measured in 0.4-μm Filtered Solution Samples

Figure 3.17. The effects of filtration on ^{244}Cm measured in solution samples from the bare-fuel tests are shown in Figure 3.18. Quantities of ^{244}Cm measured in different liquid sample types are tabulated in Table 3.6. In terms of activity levels, the ^{244}Cm data are quite similar in appearance to the ^{241}Am data. However, equivalent ^{244}Cm activities correspond to much lower concentrations in comparison to ^{241}Am. During Cycles 2 and 3 of the 25°C bare-fuel tests, ^{244}Cm activity tended to stabilize at levels on the order of 100 pCi/mL, corresponding to a curium concentration of about $10^{-11.1}$ M. At 85°C, ^{244}Cm activity dropped to about 0.1 pCi/mL, corresponding to a curium concentration of about $10^{-14.3}$ M.

During the HBR/SD-85 Cycle 1 test, the 0.4-μm filtered ^{244}Cm activity peaked in the 119-d sample at about 28 pCi/mL and then dropped to about 0.3 pCi/mL by the end of Cycle 1. The 0.4-μm filtered ^{241}Am activity similarly increased during this test but showed much less drop after the 119-d sample. However, the 18-Å filtered activities for both ^{241}Am and ^{244}Cm remained below 0.5 pCi/mL during all of Cycle 1, suggesting that americium and

9 0 7 9 4 1 4 0 5

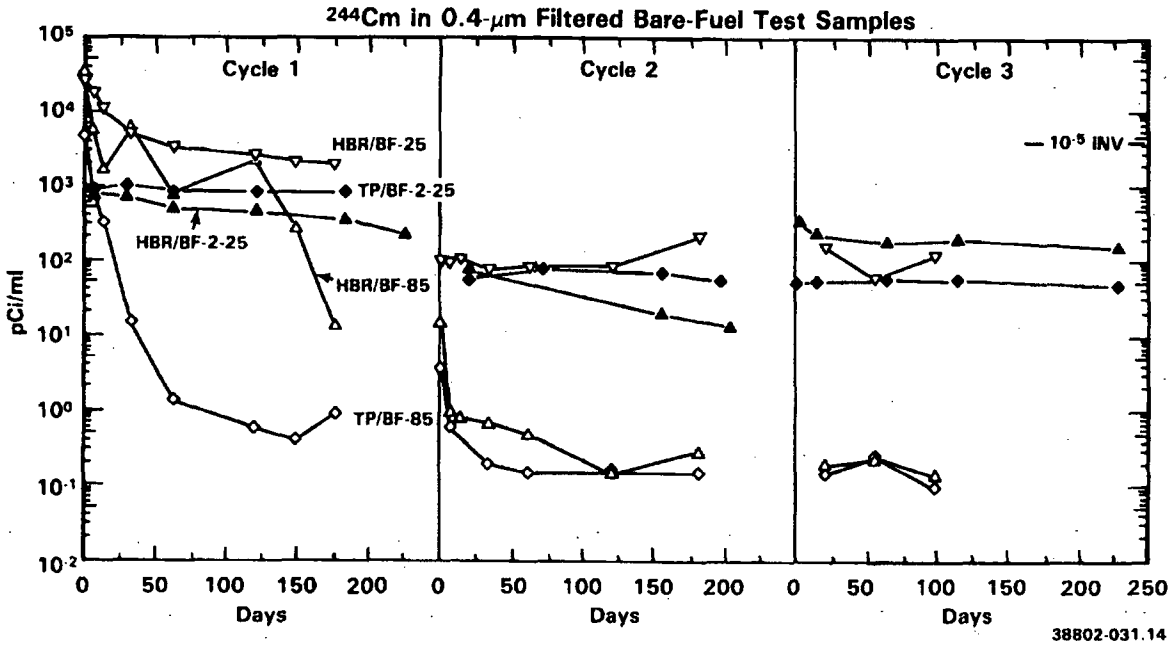

FIGURE 3.17. Comparison of ^{244}Cm Activities Measured in 0.4-μm Filtered Samples from the Three Series 3 and Two Series 2 Bare-Fuel Tests

curium may have been associated with separate finely suspended phases since only ^{244}Cm dropped out in the 0.4-μm filtered samples. In most other respects, the ^{244}Cm data were remarkably similar to the ^{241}Am data.

3.7 NEPTUNIUM

The primary neptunium isotope of concern for repository storage of spent fuel is ^{237}Np. Concentration of neptunium in spent fuel is about 4×10^{-4} g/g of fuel and, at this low concentration, likely remains in solid solution with the fuel matrix phase. With a 2,140,000-yr half-life, ^{237}Np activity is initially relatively low (about 0.24 μCi/g in the test specimens) but increases with time for several thousand years as the product of ^{241}Am decay (432-yr half-life). At 1,000 yr, ^{237}Np activity increases to about 1 μCi/g and accounts for about 0.06% of the total Ci activity in spent fuel. At 10,000 yr, ^{237}Np accounts for about 0.25% of total activity of spent fuel. Neptunium-239 represents a larger fraction of the spent fuel total activity (~0.9 % at 1,000 yr and ~1.4% at 10,000 yr). However, ^{239}Np, with its short

90794 1406

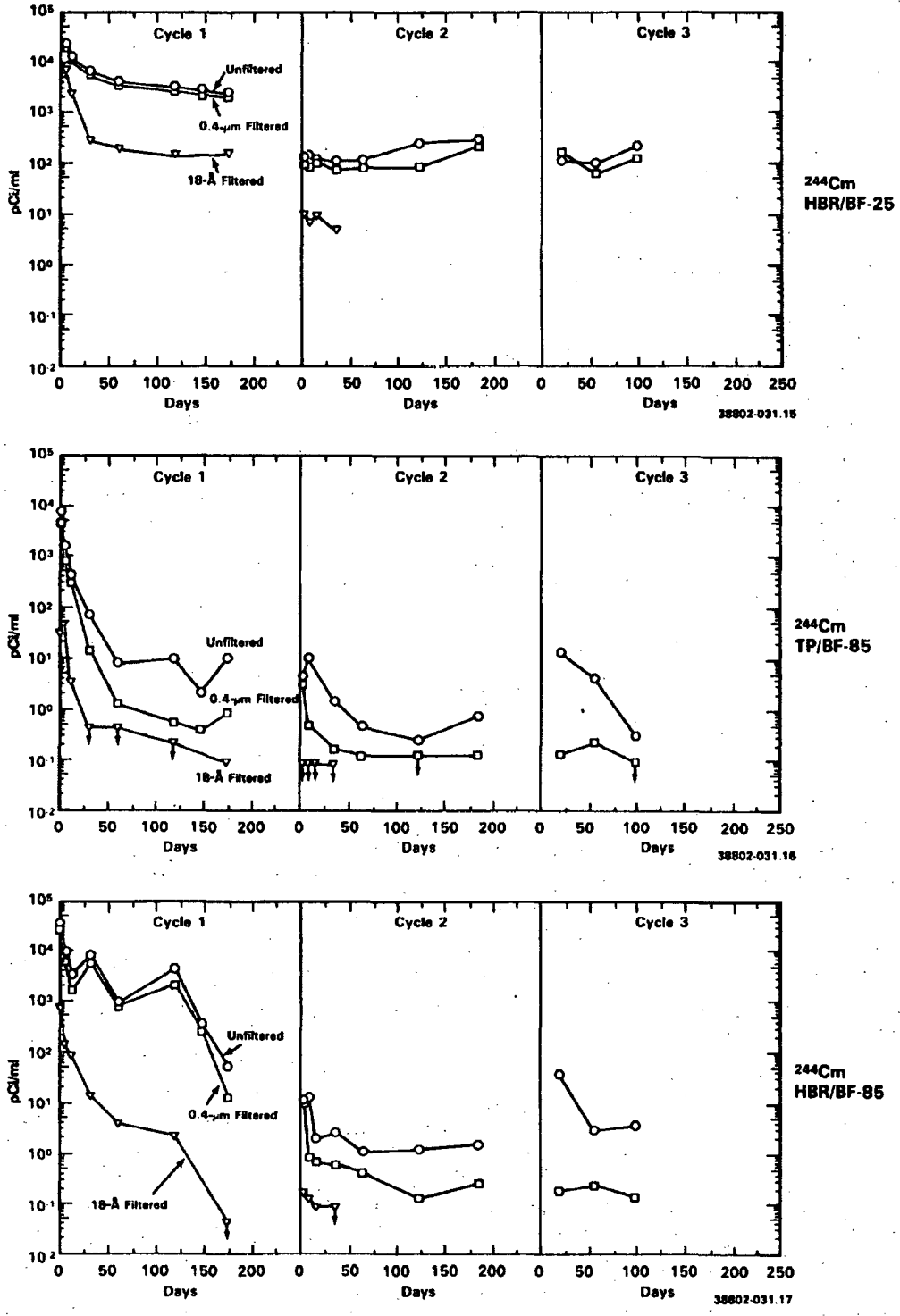

FIGURE 3.18. Effects of Filtration on Measured ^{244}Cm Activity in Solution Samples from the Bare-Fuel Tests

9 0 7 9 4 1 4 0 7

TABLE 3.6. Quantities of ^{244}Cm Measured in Samples (nCi)

	HBR/BF-25	TP/BF-85	HBR/BF-85	HBR/SD-85	HBR/HD-85	HBR/UD-85
Cycle 1						
Periodic Samples	1272	97.9	911	0.81	<0.02	<0.03
Final Solution	512	0.225	3.49	0.068	<0.034	<0.03
[Cm (pg/mL)]	(26)	(0.012)	(0.18)	(0.003)	(<0.002)	(<0.002)
Rinse	243	29.5	134	0.11	0.054	--
Acid Strip	9095	7622	15541	99	4.2	2.8
Cycle Total	11122	7949	16589	100	4.3	2.9
+ 10^{-5} Inv.	10.08	9.15	16.06	0.091	0.004	0.003
% in Solution	16.0	1.27	5.5	0.88	<1.2	<1.7
Cycle 2						
Periodic Samples	11.5	0.138	0.29	<0.007	--	--
Final Solution	53.8	0.034	0.068	<0.023	--	<0.023
[Cm (pg/mL)]	(2.8)	(0.002)	(0.003)	(<0.001)	--	(<0.001)
Rinse	189	22.2	63	0.054	0.1	0.054
Acid Strip	2284	2162	4324	2.84	1.8	2.57
Cycle Total	2538	2184	4388	2.92	1.9	2.64
+ 10^{-5} Inv.	2.34	2.62	4.32	0.0027	~0.002	0.0024
% in Solution	2.6	0.008	0.008	<1	--	<0.85
Cycle 3						
Periodic Samples	5.5	0.009	0.010	--	--	--
Final Solution	31.0	<0.023	0.034	0.11	0.13	0.146
[Cm (pg/mL)]	(1.6)	(<0.001)	(0.002)	(0.006)	(0.007)	(0.008)
Rinse	273	42.2	52.7	--	--	--
Acid Strip	1554	1239	(a)	--	--	--
Cycle Total	1863	1281	(a)	--	--	--
+ 10^{-5} Inv.	1.74	1.55	(a)	--	--	--
% in Solution	2.0	<0.003	(a)	--	--	--
Sum of Cycles 1, 2 & 3						
Σ Cycle Totals	15524	11215	21030	102[b]	6.2[b]	5.5[b]
+ 10^{-5} Inv.	14.16	13.32	20.43	0.094	0.006[b]	0.005[b]

(a) Cycle 3 HBR/BF-85 acid strip appears to have been contaminated by fuel particles.
(b) Cycles 1 and 2 only.
NOTE: Periodic samples, final solution and bare fuel rinse values are based on 0.4-μm filtered data. Other values are based on unfiltered data.

9 0 7 9 4 1 4 0 8

half-life (~2 d), is a transient state in the ^{243}Am to ^{239}Pu decay chain. Although a small portion of the total activity, neptunium is of concern because it has been predicted to be the most soluble of the alpha-emitting actinides under NNWSI repository conditions[17] and will be present for a very long time.

Activities of ^{237}Np measured in 0.4-μm filtered samples from the three bare-fuel tests are plotted in Figure 3.19. The effects of filtration on ^{237}Np activity are shown in Figure 3.20. Only data from the bare-fuel tests are plotted, since ^{237}Np activities were generally below detection in the tests using clad fuel. After an initial apparent supersaturation in Cycle 1, ^{237}Np activity drops to a range of about 0.1 to 0.5 pCi/mL during Cycles 2 and 3. The solution activity data do not show a significant dependence on temperature or filtration. Scatter in the data shown in Figures 3.19 and 3.20 is attributed primarily to counting statistics for the low activities being measured. A ^{237}Np activity of 0.2 pCi/mL, which is about the middle of the range measured in Cycles 2 and 3, corresponds to a neptunium concentration of

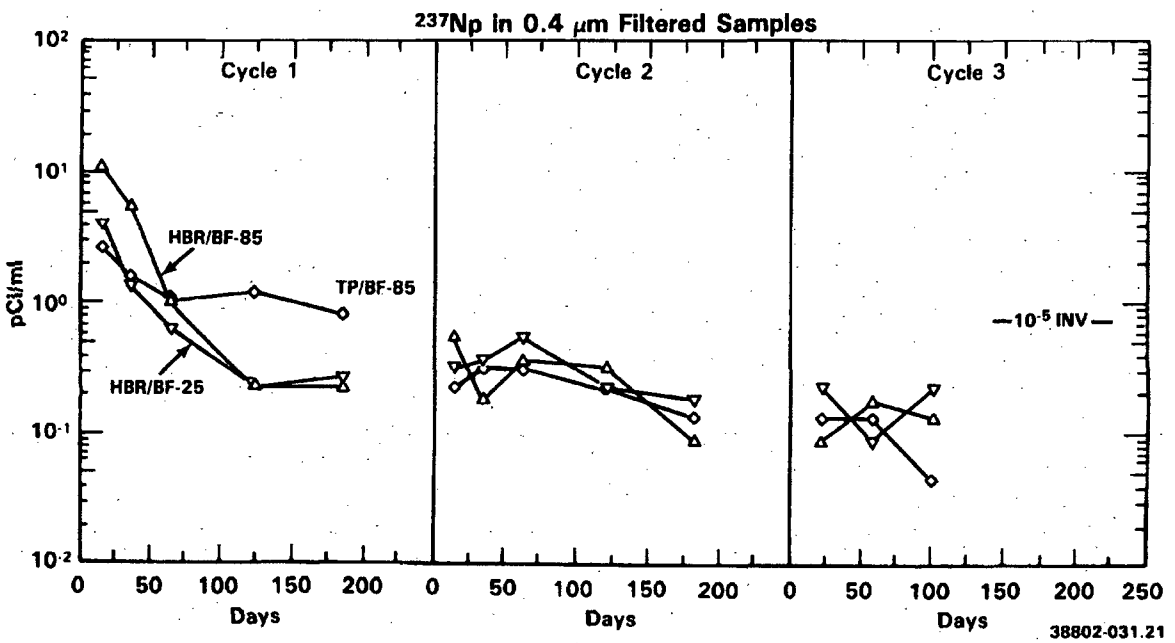

FIGURE 3.19. Activity of ^{237}Np Measured in 0.4-μm Filtered Solution Samples from the Bare-Fuel Tests

90794 1409

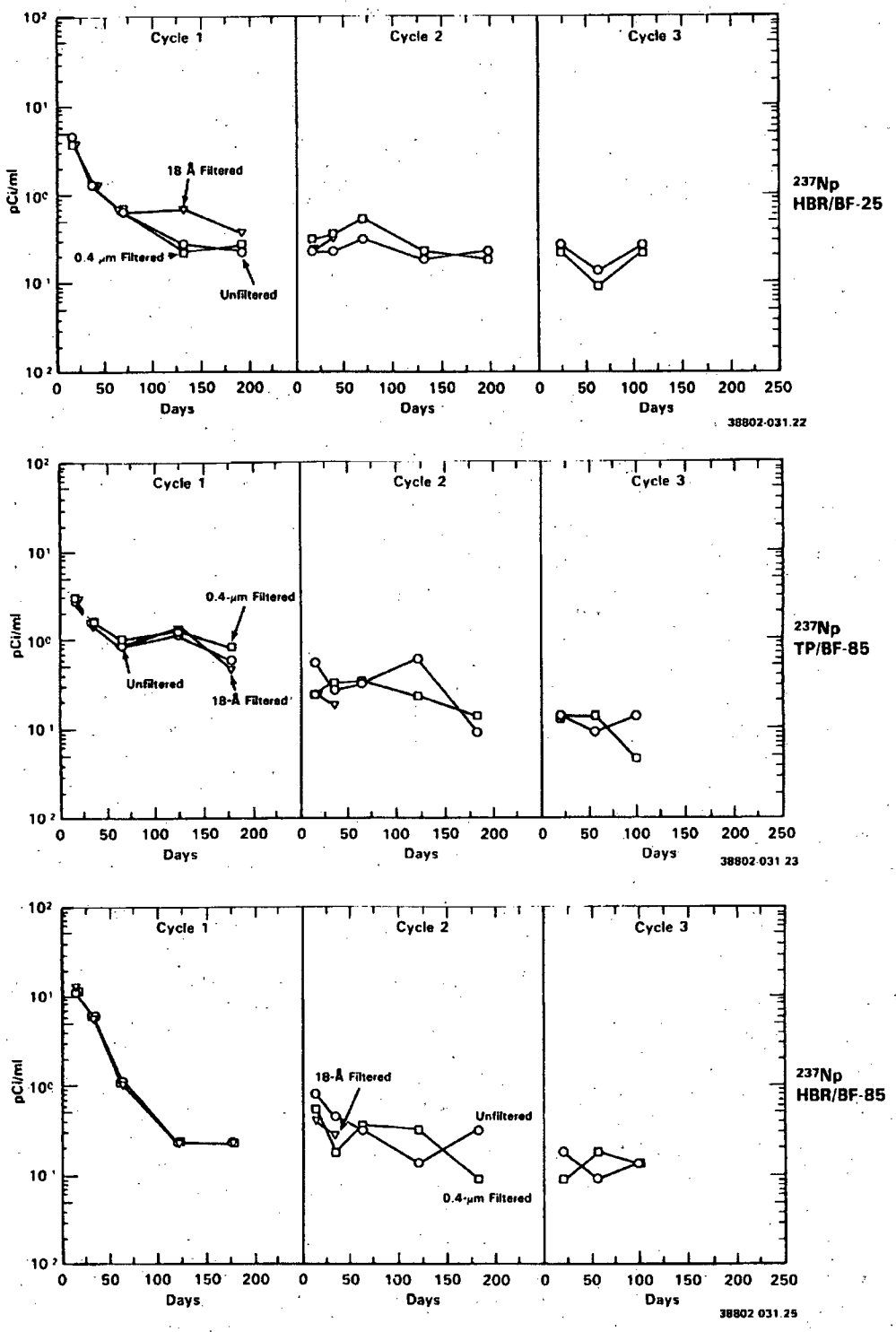

FIGURE 3.20. Effects of Filtration on Measured ^{237}Np Activity in Solution Samples from the Bare-Fuel Tests

90794 1410

about $10^{-8.9}$ M. The absense of significant effects of filtration on the activities of ^{237}Np measured in solution samples indicate that neptunium was not present as colloids or suspended phases in these samples.

Quantities of ^{237}Np measured in the various liquid sample types from the bare-fuel tests are tabulated in Table 3.7. (Note that these data are tabulated in pCi units whereas the $^{239+240}Pu$, ^{241}Am, and ^{244}Cm data were tabulated in nCi units.) As with the other actinides, it appears that neptunium-containing secondary phases from the 25°C tests redissolved in the rinse solutions to a greater extent than those from the 85°C tests. Generally larger quantities of ^{237}Np in acid strip solutions at 85°C is consistent with data for the other actinides suggesting greater fuel dissolution and subsequent removal of species from solution occurred at the higher temperature. The percentages of ^{237}Np measured in solution samples are generally somewhat higher than for the other actinides and much higher than measured for $^{239+240}Pu$, ^{241}Am, and ^{244}Cm in Cycles 2 and 3 of the 85°C bare-fuel tests.

3.8 TECHNETIUM

Technetium-99, which beta-decays with a 213,000-yr half-life, accounts for about 0.75% of the total activity of spent fuel at 1,000 yr and about 3% of the activity at 10,000 yr. Technetium is expected to be soluble as TcO_4^- in air-equilibrated water and may reach relatively high activities in water that contacts substantially degraded fuel. Only ^{99}Tc data from the bare-fuel tests are discussed in this report because ^{99}Tc activities in the other tests were generally below the detection limit.

Activities of ^{99}Tc measured in unfiltered samples from the three Series 3 bare-fuel tests and the Series 2 HBR bare-fuel tests are plotted as a linear plot in Figure 3.21. The most significant aspect of this data is that, with the exception of Cycle 1 of the HBR/BF-85 test, the ^{99}Tc activity in solution increases continuously with time and is not limited by solubility. At the beginning of Cycle 1, there was a rapid release on the order of 0.01% of the specimen inventory. In the TP/BF-85 test, the rapid release was followed by a continuous release of about 5×10^{-6} of specimen inventory per day. Most of the ^{99}Tc initially released to solution in the HBR/BF-85 test dropped out of solution following the 62-d sample, which was probably a result of

90794 1411

TABLE 3.7 Quantities of ^{237}Np Measured in Samples (pCi)

	HBR/BF-25	TP/BF-85	HBR/BF-85	HBR/SD-85	HBR/HD-85	HBR/UD-85
Cycle 1						
Periodic Samples	143	163	415	For these tests ^{237}Np activity was below the detection limit.		
Final Solution	68	203	<68			
[Np (ppb)]	(0.38)	(1.15)	(<0.32)			
Rinse	162	<135	<135			
Acid Strip	135	1243	1486			
Cycle Total	508	<1744	<2104			
+ 10^{-5} Inv.	2.43	<9.3	<10.7			
% in Solution	41.5	~21.0	~23			
Cycle 2						
Periodic Samples	36	<27	35			
Final Solution	45	34	22.5			
[Np (ppb)]	(0.26)	(0.19)	(0.13)			
Rinse	189	<54	<54			
Acid Strip	81	500	662			
Cycle Total	351	<615	<774			
+ 10^{-5} Inv.	1.70	<3.4	<4.0			
% in Solution	23.0	~10	~7.5			
Cycle 3						
Periodic Samples	7.9	6.8	6.8			
Final Solution	56.3	11.3	33.8			
[Np (ppb)]	(0.32)	(0.06)	(0.20)			
Rinse	216	27	<27			
Acid Strip	95	149	(a)			
Cycle Total	375	194	(a)			
E 10^{-5} Inv.	1.85	1.06	(a)			
% in Solution	17.1	9.3	(a)			
Sum of Cycles 1, 2 & 3						
Σ Cycle Totals	1234	<2553	2945[b]			
+ 10^{-5} Inv.	5.97	<13.7	~15.1[b]			

(a) Cycle 3 HBR/BF-85 acid strip appears to have been contaminated by fuel particles.
(b) Cycles 1 and 2 only.
NOTE: Periodic samples, and final solution and rinse values are based on 0.4-μm filtered data.

9 0 7 9 4 1 4 1 2

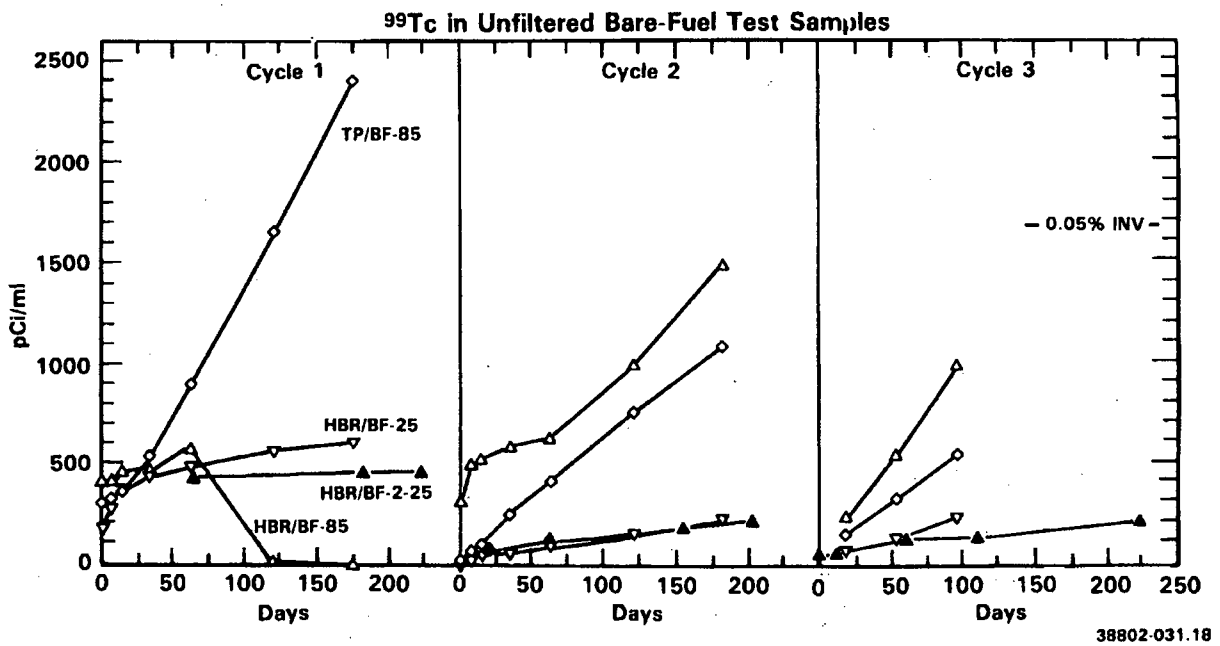

FIGURE 3.21. Technetium-99 Activities Measured in Unfiltered Samples from the Series 3 Bare-Fuel Tests and the Series 2 HBR Bare-Fuel Test

reducing conditions caused by the vessel corrosion anomaly indicated to have occurred in this test, and also correlates with the drop in uranium concentration observed in this test. There was an enhanced initial release from this test in Cycle 2, which likely resulted from dissolution of technetium-bearing phases (TcO_2, technetium adsorbed on precipitates, etc.) that precipitated during Cycle 1 and were not completely removed from the fuel surface during the cycle termination rinsing procedure. The ^{99}Tc continuous release rate showed a significant dependence on temperature.

During Cycles 2 and 3, ^{99}Tc was continuously released at a rate of about 2.5×10^{-6} of specimen inventory per day in both the HBR/BF-85 and TP/BF-85 tests. Continuous release rate during Cycle 2 of both the HBR/BF-25 and HBR/BF-2-25 tests was about 5×10^{-7} of specimen inventory per day. The continuous ^{99}Tc release to solution with time is presumably the additive result of congruent dissolution of the fuel matrix plus preferential release from grain boundaries (or other phases) where technetium may be concentrated. However, the relative contributions of these two sources of release could not

90794 1413

be determined. Technetium-99, which segregates from the fuel matrix during irradiation, is known to combine with fission products molybdenum, ruthenium, rhodium, and palladium forming finely dispersed "five metal" particles in the fuel. These particles are very difficult to dissolve even in nitric acid and may remain undissolved even during fuel reprocessing. Therefore, the mechanism by which ^{99}Tc would be preferentially released during dissolution tests in water is uncertain.

Quantities of ^{99}Tc measured in the different sample types are tabulated in Table 3.8. Except for the HBR/BF-85 Cycle 1 test, most of the measured ^{99}Tc (>90%) was in solution. The ^{99}Tc fractional releases represented by the Cycle Total values divided by 10^{-5} of specimen inventory were generally much greater than those for the actinides, indicating either a large component of preferential release of ^{99}Tc or a large amount of actinide secondary phase material unaccounted for in the rinse and strip samples. The 708 nCi of ^{99}Tc measured in solution in the TP/BF-85 Cycle 1 test would correspond to about 62 mg of congruent uranium dissolution if ^{99}Tc were not preferentially released. The fact that only about 6.8 mg of uranium was accounted for in the Cycle Total value, and that only 10 mg of material was retained on the rinse filter (most of which was undissolved fuel grains), implies that about 50 mg uranium in secondary phase material was not accounted for in this test if ^{99}Tc was not preferentially released. By the same estimate, about 20 mg of secondary phase uranium would have been missed in Cycle 2 of the TP/BF-85 test. That such quantities of secondary phases remained attached to the fuel particle surfaces, or otherwise escaped observation, is unlikely but possible. These data support the hypothesis that preferential release from grain boundaries or other secondary fuel phases is likely a significant component of the ^{99}Tc release. Unfortunately, the data are not sufficient to derive quantitative estimates of the relative fractions of ^{99}Tc (or any other nuclide) release originating from congruent matrix dissolution versus preferential dissolution.

By assuming that all of the ^{99}Tc measured in acid strip samples originates from previously undissolved fuel fines, one can estimate the portion of other nuclides in the acid strip samples originating from previously undissolved fuel fines. The percentages of uranium, $^{239+240}Pu$, ^{241}Am, ^{237}Np, ^{137}Cs, and ^{90}Sr in acid strip samples thereby calculated to have originated

90794 1414

TABLE 3.8. Quantities of ^{99}Tc Measured in Samples (nCi)

	HBR/BF-25	TP/BF-85	HBR/BF-85	HBR/SD-85	HBR/HD-85	HBR/UD-85
Cycle 1						
Periodic Samples	60.1	109	54	<2.4	<1.7	<1.5
Final Solution	153	599	<2	<2.3	<2.3	<2.3
[Tc (ppb)]	(36)	(141)	(<0.5)	(<0.5)	(<0.5)	(<0.5)
Rinse	10.3	24	22.4	<5.4	<12.2	<5.4
Acid Strip	4.6	12.3	24.3	<2.7	<2.7	<2.7
Cycle Total	228	745	103	<12.7	<18.9	<11.8
+ 10^{-5} Inv.	25.2	89.4	12.2	<1.4	<2.2	<1.3
% in Solution	93.5	95.1	54.6	--	--	--
Cycle 2						
Periodic Samples	8.4	34.2	78	In Cycles 2 and 3 these values were below the detection limit.		
Final Solution	56.3	270	372			
[Tc (ppb)]	(13)	(63)	(87)			
Rinse	4.0	6.5	11.9			
Acid Strip	<1.4	6.5	10.1			
Cycle Total	70.1	317	471			
+ 10^{-5} Inv.	7.9	38.6	56.5			
% in Solution	~93	95.9	95.3			
Cycle 3						
Periodic Samples	4.8	11.8	19.4			
Final Solution	58.6	135	248			
[Tc (ppb)]		(32)	(58)			
Rinse	<5.4	<54	10.8			
Acid Strip	<2.7	5.4	(a)			
Cycle Total	<71.5	158	278			
+ 10^{-5} Inv.	<8.1	19.4	33.7			
% in Solution	>88.7	93.1	>96			
Sum of Cycles 1, 2 & 3						
Σ Cycle Total	370	1220	852			
+ 10^{-5} Inv.	41.2	147.4	102.2			

(a) Cycle 3 HBR/BF-85 acid strip appears to have been contaminated by fuel particles.

NOTE: Bare fuel test rinse samples were 0.4-μm filtered. All other values are based on unfiltered data.

9 0 7 9 4 1 4 1 5

from previously undissolved fuel fines are given in Table 3.9 for test cycles in which significant ^{99}Tc values were measured in the acid strip samples. The relatively high fraction of the uranium in the Cycle 1 HBR/BF-25 acid strip sample attributed to previously undissolved fuel fines and is consistent with the observation that very little uranium-bearing secondary phase material was found in rinse filter residues from this test. The fact that the Table 3.9 values are not particularly high for the HBR/BF-85 Cycle 1 test indicates that little of the ^{99}Tc that dropped out of solution in this test remained attached to the vessel components after the rinse procedure. An interesting result is the portions of ^{137}Cs and ^{90}Sr measured in acid strip solutions that would appear to originate from plate-out or precipitated secondary phases.

3.9 CESIUM

The fission product cesium nuclides, ^{134}Cs (2.06-yr half-life) and ^{137}Cs (30.2-yr half-life), plus ^{137m}Ba (short-lived ^{137}Cs daughter), account for about 38% of the total activity of the tested fuel and for a significant portion of the decay heat during the thermal period. The longer lived ^{135}Cs nuclide (2,300,000-yr half-life) had a much lower inventory (0.3 μCi/g versus 6×10^4 μCi/g for ^{137}Cs) and was not measured in the current tests. Cesium is relatively mobile under temperature and oxygen potential conditions present in the fuel during irradiation due to its ~670°C boiling point in the metallic

TABLE 3.9. Percent Nuclide Fractions in Acid Strip Samples Attributed to Previously Undissolved Fuel Fines Based on ^{99}Tc Data[a]

Test	Cycle	U	$^{239+240}Pu$	^{241}Am	^{237}Np	^{137}Cs	^{90}Sr
HBR/BF-25	1	90.9	21.3	9.3	78.9	32.4	49.4
TP/BF-85	1	16.9	25.0	19.5	22.1	3.1	4.6
	2	69.9	38.4	36.2	29.1	48.6	34.0
HBR/BF-85	1	39.3	31.9	25.9	37.8	8.9	15.7
	2	43.4	45.3	36.9	35.3	42.8	8.9

(a) Assumes 100% of ^{99}Tc measured in acid strip samples was from previously undissolved fuel fines.

90794 1416

state. As a result, the cesium inventory fraction in the gap may approach that of fission gases xenon and krypton.

The ^{137}Cs activities measured in 0.4-μm filtered solution samples are plotted in Figure 3.22. Gap releases of 0.66% in the HBR/BF-25 test, 0.84% in the HBR/BF-85 test, and 0.36% in the TP/BF-85 test were measured in the 1-d Cycle 1 solution samples. The Cycle 2 bare-fuel releases were on the order of a few percent of those measured in Cycle 1. Release from the HBR/HD-85 specimen was much slower than from the HBR/SD-85 and bare-fuel specimens, and release of a portion of the ^{137}Cs gap inventory from this specimen appears to have been delayed into Cycle 2.

The O-ring in the end fittings of the HBR/UD-85 test specimen apparently started leaking after the 14-d Cycle 2 sample. The O-ring seals in this test appear to have substantially failed during Cycle 3 with most of the initial gap inventory being released during this cycle. The O-ring failure was likely a result of radiation exposure and simultaneous O-ring failure in the HBR/HD-85 and HBR/SD-85 tests is likely. The O-ring failures did not appear

90794 1417

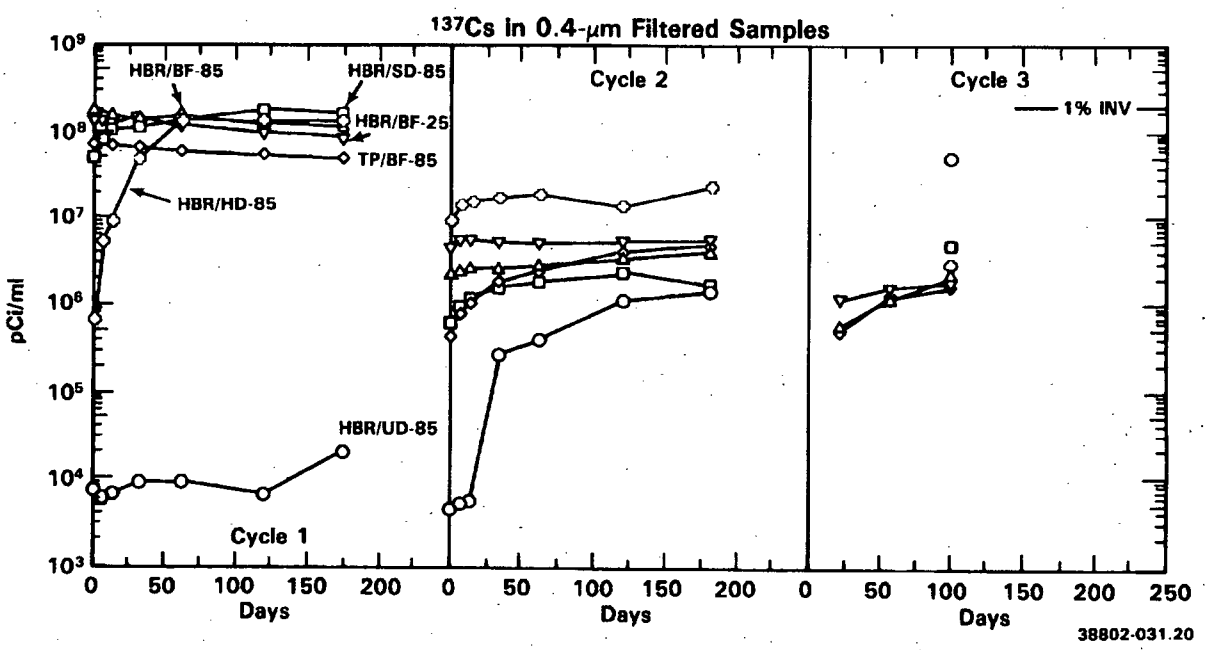

FIGURE 3.22. Activity of ^{137}Cs in 0.4-μm Filtered Solution Samples

to be a significant factor in the delayed release of nuclides other than ^{137}Cs. The fact that the O-rings seals did not fail over two complete test cycles in the Series 2 tests may be related to the lower 25°C temperature of these tests.

The quantities of ^{137}Cs measured in the various sample types are tabulated in Table 3.10. The total measured fractional releases for Cycles 1, 2, and 3 from the HBR specimens were about 1% at 85°C and about 0.8% at 25°C. The total measured fractional release for the TP specimen at 85°C was about 0.5%. If the assumption is valid that all the ^{99}Tc in the acid strip samples originated from previously undissolved fuel fines, the Table 3.9 data suggest that much of the ^{137}Cs in acid strip solutions (particularly in Cycle 1 of the 85°C tests) was associated with plate-out or other secondary phases. Cesium may have been adsorbed onto colloids or by silica gel that dropped from solution in these tests. However, cesium association with any particular phase has not been confirmed.

3.10 STRONTIUM

Strontium-90 beta-decays (28.6-yr half-life) to a short-lived ^{90}Y daughter, which then beta-decays (64-hour half-life) to stable ^{90}Zr. Strontium-90 plus ^{90}Y activity accounts for about 28% of the total activity of the specimens tested and, along with ^{137}Cs and its ^{137m}Ba daughter, account for a substantial portion of the decay heat during the repository thermal period.

Analyses for ^{90}Sr were conducted on selected samples during Cycles 1 and 2 and on all Cycle 3 solution samples. Only unfiltered aliquots were analyzed for ^{90}Sr, except for the Cycle 3 final solution samples from the bare-fuel tests, where unfiltered and 0.4-μm filtered aliquots were also analyzed. No significant differences were found between the unfiltered and the 0.4-μm filtered results in the three samples on which both filter fractions were analyzed. The ^{90}Sr activities measured in the unfiltered samples are plotted in Figure 3.23. Quantities of ^{90}Sr measured in different sample types are given in Table 3.11.

Strontium-90 was rapidly released to solution in Cycle 1 of the bare-fuel tests but then appeared to saturate and drop out of solution. Solution

9079414 8

TABLE 3.10. Quantities of ^{137}Cs Measured in Samples (μCi)

	HBR/BF-25	TP/BF-85	HBR/BF-85	HBR/SD-85	HBR/HD-85	HBR/UD-85
Cycle 1						
Periodic Samples	17718	8820	19908	15858	9019	1.1
Final Solution	21734	11712	27590	39640	31419	5.3
[Cs (ppb)]	(2521)	(1359)	(3200)	(4600)	(3645)	(0.6)
Rinse	1368	719	1084	381	473	1
Acid Strip	86	2446	1649	70	45	0.14
Cycle Total	40906	23696	50230	55949	40956	7.6
+ 10^{-5} Inv.	745	459	977	1024	802	0.14
% in Solution	96.5	86.6	94.6	99.2	98.7	84.7
Cycle 2						
Periodic Samples	686	239	352	192	1966	8.6
Final Solution	1329	1239	1032	418	5709	367
[Cs (ppb)]	(154)	(144)	(120)	(48)	(662)	(42.6)
Rinse	128	55	56	78	130	36.2
Acid Strip	22	83	143	0.3	23	0.29
Cycle Total	2166	1616	1582	688	7828	412
+ 10^{-5} Inv.	40.1	37.7	31.3	12.6	153	7.61
% in Solution	93.0	91.5	87.4	88.7	98.1	91.2
Cycle 3						
Periodic Samples	70	42	45	--	--	--
Final Solution	476	428	528	1227	698	12950
[Cs (ppb)]	(55)	(50)	(61)	(142)	(81)	(1502)
Rinse	64	32	26	--	--	--
Acid Strip	22	57	(a)	--	--	--
Cycle Total	633	559	600	1227	698	12950
+ 10^{-5} Inv.	11.9	11.1	12.0	23	13.7	240
% in Solution	86.4	84.1	<95.6	--	--	--
Sum of Cycles 1, 2 & 3						
Σ Cycle Totals	43704	25871	52412	57864	49482	13370
+ 10^{-5} Inv.	797	501	1020	1059	969	248

(a) Cycle 3 HBR/BF-85 acid strip appears to have been contaminated by fuel particles.

NOTE: Periodic samples, final solution and bare fuel rinse values are based on 0.4-μm filtered data. Other values are based on unfiltered data.

90794 1419

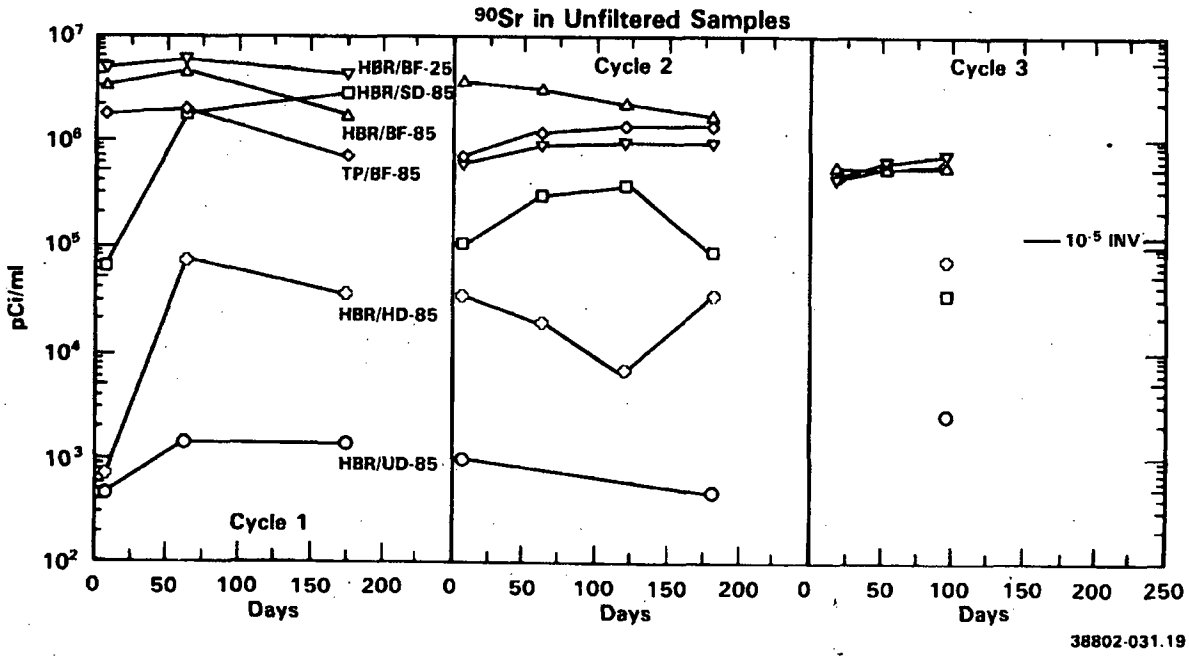

FIGURE 3.23. Activity of ^{90}Sr in Unfiltered Solution Samples

activities in the 174-d Cycle 1 samples from both the HBR/BF-85 and TP/BF-85 tests were only about 40% as high as measured in the 62-d samples. A significant drop in ^{90}Sr activity also occurred during Cycle 2 of the HBR/BF-85 test. That ^{90}Sr is controlled to a degree by secondary phases in these test cycles is supported by the relatively small fraction of the ^{90}Sr activity in the acid strip samples calculated to have originated from previously undissolved fuel fines (see Table 3.9). Strontium may be partially substituting for calcium in secondary phases such as uranophane, haiweeite, calcite, or dolomite at concentrations below those that would have been detected during SEM-EDX examination of solid residues from these tests.

The calculated "fractional release" values for ^{90}Sr (+ 10^{-5} Inv. values in Table 3.11) were significantly greater than those for calculated for the actinides, suggesting that ^{90}Sr is preferentially released. The fractional release values were particularly greater in the HBR/SD-85 test. Although release was delayed in the HBR/SD-85 test, by the end of Cycle 1, the ^{90}Sr level in solution in this test was greater than that in the two 85°C bare-fuel

9 0 7 9 4 1 4 2 0

TABLE 3.11. Quantities of ^{90}Sr Measured in Samples (μCi)

	HBR/BF-25	TP/BF-85	HBR/BF-85	HBR/SD-85	HBR/HD-85	HBR/UD-85
Cycle 1						
Periodic Samples	254	86	51	56	2.3	<0.05
Final Solution	1089	180	441	707	8.7	0.33
[Sr (ppb)]	(56.4)	(9.4)	(23)	(36)	(0.45)	(0.02)
Rinse	92	104	119	22	13.9	0.22
Acid Strip	37	1116	615	48	1.1	0.135
Cycle Total	1472	1486	1366	834	26.0	0.725
+ 10^{-5} Inv.	41.0	43.1	40.6	23.3	0.78	0.02
% in Solution	91.3	17.9	46.2	91.5	42.3	~50
Cycle 2						
Periodic Samples	50	62	162	15.5	1	--
Final Solution	248	348	419	22.8	8.67	0.11
[Sr (ppb)]	(12.8)	(18.1)	(21.7)	(1.15)	(0.45)	(0.006)
Rinse	31.3	41	71	2.03	1	<0.27
Acid Strip	14.5	79	450	0.72	5.77	<0.11
Cycle Total	343	530	1102	40.5	16.5	<0.49
+ 10^{-5} Inv.	12.8	15.6	33.3	1.13	0.49	<0.02
% in Solution	86.7	77.3	52.8	93.2	58.9	--
Cycle 3						
Periodic Samples	28.1	25	28	--	--	--
Final Solution	196	157	153	8.9	18.2	0.63
[Sr (ppb)]	(10.2)	(8.1)	(7.9)	(0.46)	(0.94)	(0.033)
Rinse	23.3	24	23	--	--	--
Acid Strip	15.7	84	(a)	--	--	--
Cycle Total	263	290	205	>8.9	>18.2	>0.63
+ 10^{-5} Inv.	7.5	8.6	6.2	>0.25	>0.55	>0.01
% in Solution	85.2	62.6	>88.6	--	--	--
Sum of Cycles 1, 2 & 3						
Σ Cycle Total	2078	2307	2673	883	60.7	1.85
+ 10^{-5} Inv.	58.2	67.3	80.1	24.7	1.82	~0.03

(a) Cycle 3 HBR/BF-85 acid strip appears to have been contaminated by fuel particles.

NOTE: Bare fuel test rinse samples were 0.4-μm filtered. All other values are based on unfiltered data.

90794 1421

tests. Another indication that ^{90}Sr may be present as gap inventory, or otherwise concentrated in the fuel so as to be available for preferential release, is that the inventory fractions in solution early in Cycle 1 of HBR/BF-25 and HBR/BF-85 tests were significantly greater than that of ^{99}Tc, whose activity did not appear to be solubility limited. (This is shown in the following chapter where fission inventory fractions in solution are compared in the same plot.) Although the release and solubility control mechanisms are not clear, ^{90}Sr appears to be initially released preferentially and then subject to some form of solution concentration control.

3.11 IODINE

Iodine-129 beta-decays with a 17,000,000-yr half-life to stable ^{129}Xe. With an inventory of about 0.025 μCi/g of fuel (~30 Ci/1,000 MTHM) in the tested specimens, ^{129}I was the lowest activity nuclide measured and required neutron activation analysis for its detection. Although ^{129}I has a relatively low activity inventory in spent fuel, it is relatively soluble, may possibly be mobile in the vapor phase as I_2 (although the present data do not support this), and has a potential for incorporation into the biosphere.

Iodine-129 analyses were made only on single midcycle and final solution samples from each cycle, plus the Cycle 1 acid strip and Cycle 3 rinse samples. Only bare-fuel test samples were analyzed for ^{129}I during Cycle 3. Activities of ^{129}I measured in unfiltered solution samples are plotted in Figure 3.24. Quantities of ^{129}I measured in the different sample types are tabulated in Table 3.12. Since only one periodic solution sample from each cycle was analyzed for ^{129}I, the result of this analysis was assumed for all periodic samples in calculating the "periodic samples" values in Table 3.12. The greatest ^{129}I releases were observed in the two 85°C bare-fuel tests and Cycle 1 of the slit-defect test. Although the acid strip and rinse sample data are limited, these data indicate that most of the ^{129}I was in solution.

Relatively large fractional releases of ^{129}I of about 0.1%, 0.3%, and 0.4% were measured during Cycle 1 of the TP/BF-85, HBR/BF-85, and HBR/SD-85 tests, respectively. Such large releases probably result from dissolution of a fission product phase formed in the gap. However, the mechanism and phases

9 0 7 9 4 1 4 2 2

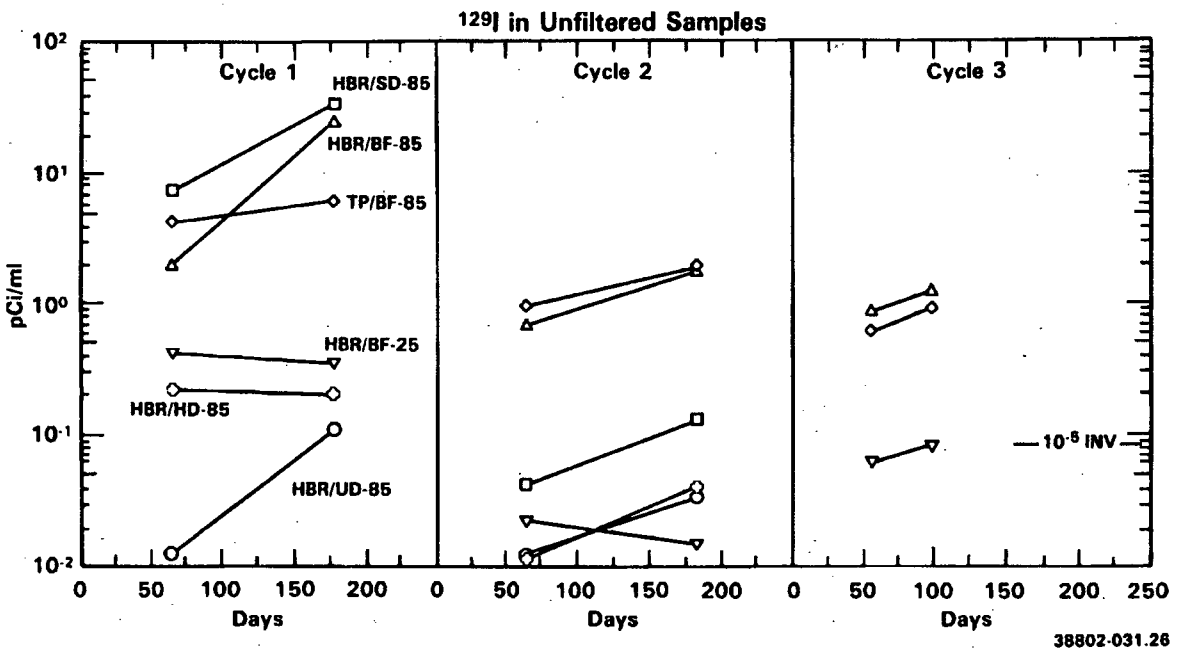

FIGURE 3.24. Activities of ^{129}I Measured by Neutron Activation Analysis in Unfiltered Solution Samples

involved would appear to be different than those involved in the gap release of ^{137}Cs. Cycle 1 fractional releases of ^{137}Cs in these tests were 0.46% in the TP/BF-85 test and about 1.0% in both the HBR/BF-85 and HBR/SD-85 tests. The greatest difference, however, was temperature dependence, with only about 0.076% of the ^{129}I inventory versus 0.75% of the ^{137}Cs inventory being released during Cycle 1 of the HBR/BF-25 test. Also, ^{129}I release appeared to be less rapid than that of ^{137}Cs, particularly in the HBR/BF-85 test where most of the ^{129}I release occurred between the interim 62-d sample and the final 174-d sample. In the HBR/HD-85 test, about 0.8% of the ^{137}Cs inventory was released in Cycle 1, while only about 0.0044% of ^{129}I inventory was released in Cycles 1 and 2 combined. The ^{137}Cs gap inventory appears to be associated with more readily soluble phases that rapidly dissolve at 25°C as well as 85°C, while ^{129}I may be associated with a phase that is only slowly dissolved at the lower temperature. One possibility may be that fission product iodine reacts with and penetrates the cladding inner surface from which it is only slowly dissolved at 25°C.

9 0 7 9 4 1 4 2 3

TABLE 3.12. Quantities of ^{129}I Measured in Samples (pCi)

	HBR/BF-25	TP/BF-85	HBR/BF-85	HBR/SD-85	HBR/HD-85	HBR/UD-85
Cycle 1						
Periodic Samples[a]	62.1	615	290	1058	31.9	1.81
Final Solution	86.7	1522	6200	8375	49.8	27.75
[I (ppb)]	(2.8)	(49)	(200)	(270)	(1.6)	(0.9)
Rinse	--	--	--	--	--	--
Acid Strip	25.8	75	64	4.8	1.2	0.02
Cycle Total	174.6	2212	6554	9438	82.9	29.58
+ 10^{-5} Inv.	7.65	107	306	415	3.9	1.31
% in Solution	85.2	96.6	99.0	99.9	98.6	99.9
Cycle 2						
Periodic Samples[a]	2.9	121	88	5.6	1.5	--
Final Solution	3.7	467	430	32.2	10.0	8.48
[I (ppb)]	(0.12)	(15)	(14)	(1.0)	(0.32	(0.3)
Rinse	--	--	--	--	--	--
Acid Strip	--	--	--	--	--	--
Cycle Total	6.6	589	518	37.8	11.5	8.48
+ 10^{-5} Inv.	0.29	29	24.6	1.66	0.54	0.38
% in Solution	--	--	--	--	--	--
Cycle 3						
Periodic Samples[a]	3.0	30	41			
Final Solution	20.7	229	310			
[I (ppb)]	(0.67)	(7.4)	(10)			
Rinse	8.0	8.9	7.3			
Acid Strip	--	--	--			
Cycle Total	31.7	267	358			
+ 10^{-5} Inv.	1.43	13.2	17.2			
% in Solution	74.6	96.7	98.0			
Sum of Cycles 1, 2 & 3						
Σ Cycle Total	213	3069	7429	9476[b]	94.4[b]	38.1[b]
+ 10^{-5} Inv.	9.4	149	348	417[b]	4.4[b]	1.7[b]

(a) Activity in the single periodic sample analyzed for ^{129}I times total volume of all periodic samples in the cycle.
(b) Cycles 1 and 2 only.
NOTE: Bare fuel test rinse samples were 0.4-μm filtered. All other values are based on unfiltered data.

9 0 7 9 4 1 4 2 4

During Cycles 2 and 3 of the HBR/BF-85 and TP/BF-85 tests, ^{129}I was continuously released at a rate of about 1.2×10^{-6} of inventory per day, which is somewhat less (35 to 66%) than the continuous fractional release measured for ^{99}Tc in these test cycles and similar to or slightly greater than that measured for ^{137}Cs. However, the ^{129}I continuous release rates were much lower than those of the other soluble fission products during Cycles 2 and 3 of the HBR/BF-25 test. Implications of these continuous release rates are further discussed in the following chapter.

The ^{129}I inventory fractions in solution at cycle termination are compared for the Series 2 and Series 3 tests in Table 3.13. The purpose of this comparison is to indicate if significant portions of the released ^{129}I escaped in the vapor phase from the unsealed Series 2 vessels. If anything, these data show the reverse, with less ^{129}I in solution at 25°C in the HBR/BF-25 test using a sealed stainless steel vessel than in the Series 2 tests using unsealed silica vessels. The data do not provide evidence to support the theory that ^{129}I may be released as I_2 and transported in the vapor phase. These data also again show the temperature dependence of ^{129}I release in the Series 3 tests.

90794 1425

3.12 TIN-126

Tin-126 beta-decays with a 100,000-yr half-life to ^{126}Sb, which decays with a 12.5-d half-life to stable ^{126}Te. The ^{126}Sn inventory at about 0.7 μCi/g of fuel (~770 Ci/1,000 MTHM) is the next lowest activity nuclide after ^{129}I to be analyzed.

TABLE 3.13. ^{129}I Inventory Fractions in Series 2 and Series 3 Final Solution Samples (parts per 100,000)

Test	Cycle 1	2	3	4	5
HBR/BF-2-25	8.2	5.4	5.4	3.2	2.6
TP/BF-2-25	22.4	8.5	5.5	4.7	2.6
HBR/BF-25	3.8	0.17	0.93		
HBR/BF-85	290	20.4	14.9		
TP/BF-85	73.5	22.9	11.3		

The activity of ^{126}Sn in solution samples was not plotted because of the limited number of samples showing detectable activities. Significant ^{126}Sn activities were measured in several solution samples and acid strip samples from the bare-fuel tests. Quantities of ^{126}Sn measured in samples from the bare-fuel tests are tabulated in Table 3.14. Most of the significant ^{126}Sn measured was in the acid strip samples. The total fractional releases measured are slightly less than, but on the order of, those measured for the actinides, suggesting that ^{126}Sn may have been congruently released with the actinides. At less than 10^{-4} g/g fuel concentration in spent fuel, tin may possibly be soluble in the matrix phase and congruently released as the matrix dissolves. However, the current data are somewhat limited for support of such a conclusion.

9 0 7 9 4 1 4 2 6

3.13 CARBON-14

Carbon-14 (5730-yr half-life) is an activation product formed during irradiation by the (n,p) reaction on nitrogen impurities, and from the (n,α) reaction on ^{17}O.[18] ORIGEN calculations for ^{14}C inventories in spent fuel depend on assumed values for initial ^{14}N impurity levels in the fuel and cladding, which are not generally well known and may vary significantly between individual fuel samples. Also, ORIGEN predictions of ^{14}C inventory do not include the possibility of the incorporation of ^{14}C produced by (n,α) reaction on ^{17}O in the cooling water into exterior assembly and cladding surfaces. Carbon-14 was radiochemically measured on two fuel and cladding samples taken from the HBR C5 rod. The average of the two analyses gave 0.49 μCi/g for fuel and 0.53 μCi/g for cladding. This level of ^{14}C corresponds to about 530 Ci/1,000 MTHM. Carbon-14 is of particular concern because it is mobile in the vapor phase [18,19] as CO_2 and in groundwater as HCO_3^- and has a high potential for incorporation into the biosphere.

The ^{14}C activities measured in unfiltered solution samples are plotted in Figure 3.25. The 10^{-5} inventory level shown in Figure 3.25 is based on the ^{14}C results obtained for the HBR C5 rod samples that were analyzed for ^{14}C inventory. Quantities of ^{14}C measured in the different sample types are tabulated in Table 3.15. Fractional release values (+ 10^{-5} Inv.) are not

TABLE 3.14. Quantities of ^{126}Sn Measured in Samples (pCi)

	HBR/BF-25	TP/BF-85	HBR/BF-85	HBR/SD-85	HBR/HD-85	HBR/UD-85
Cycle 1						
Periodic Samples[a]	78.4	<<	57	For these tests ^{126}Sn activity was below the detection limit.		
Final Solution	90.1	<68	<56			
[^{126}Sn (pg/mL)]	(12.7)	(<9.5)	(<7.9)			
Rinse	<135	<135	<135			
Acid Strip	365	2297	1622			
Cycle Total	<668	<2500	<1870			
+ 10^{-5} Inv.	<1.15	<4.78	<3.44			
% in Solution	~30	~3	~5			
Cycle 2						
Periodic Samples[a]	<<	15	<<			
Final Solution	<34	<68	<68			
[^{126}Sn (pg/mL)]	(<4.8)	(<9.5)	(<9.5)			
Rinse	<162	<135	<135			
Acid Strip	162	1297	1270			
Cycle Total	<358	<1515	<1473			
+ 10^{-5} Inv.	<0.63	<2.94	<2.75			
Cycle 3						
Periodic Samples[a]	<<	6.8	<<			
Final Solution	<34	<34	<34			
[^{126}Sn (pg/mL)]	(<4.8)	(<4.8)	(<4.8)			
Rinse	<81	<81	<81			
Acid Strip	230	811	(b)			
Cycle Total	<345	<932	<115?			
+ 10^{-5} Inv.	<0.61	<1.82	<0.22?			
Sum of Cycles 1, 2 & 3						
Σ Cycle Total	<1371	<4947	<3457			
+ 10^{-5} Inv.	<2.4	<9.55	<6.4?			

(a) Periodic sample values are total quantities in unfiltered samples for which detectable levels were reported. << indicates all samples analyzed were reported as "less than" values.
(b) Acid strip sample appeared to be contaminated by fuel particles.

9 0 7 9 4 1 4 2 7

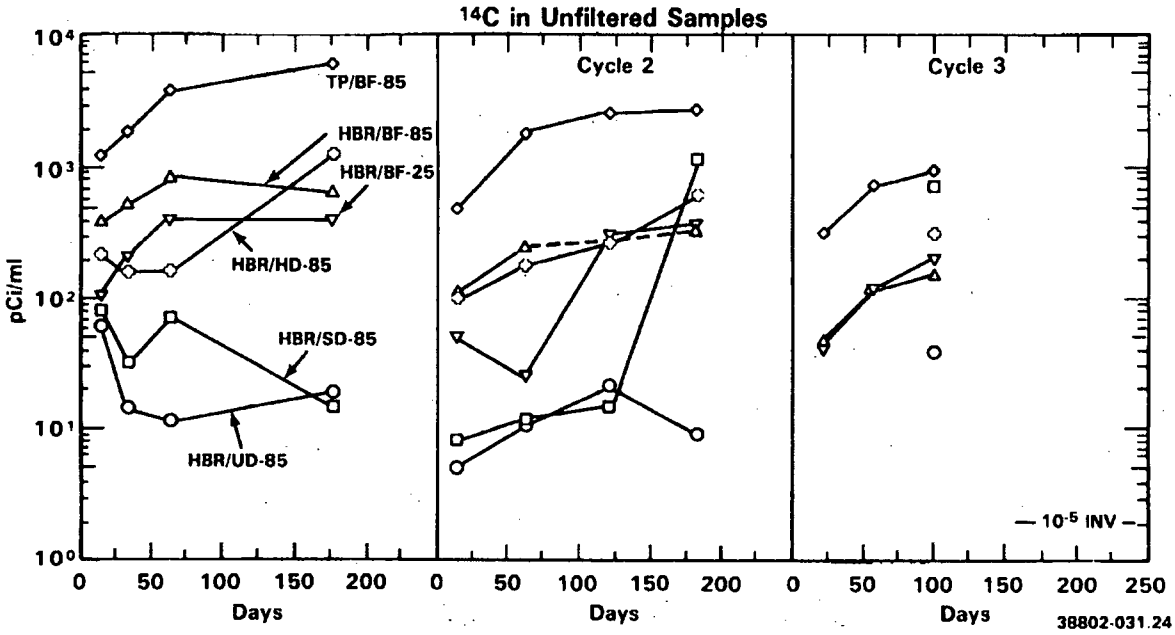

FIGURE 3.25. Activities of ^{14}C Measured in Unfiltered Solution Samples

calculated for the cycle total values in the TP/BF-85 test, since ^{14}C inventory was not determined for the TP fuel. Significantly greater ^{14}C activities measured in the TP/BF-85 test, in comparison to any of the other tests using the HBR fuel, is probably the result of significantly higher ^{14}C inventory for the TP fuel specimen. Comparison of the results from the HBR/BF-25 and HBR/BF-85 tests suggests that the aqueous release of ^{14}C is not strongly dependent on temperature.

Presumably, some of the ^{14}C released to solution in the 85°C tests dropped out of solution along with that portion of HCO_3^- originally in J-13 water that was observed to drop out. It was not possible to determine ^{14}C in the acid strip solution, since it was immediately lost to the atmosphere from any precipitated carbonate phases upon first contact by the 8 M HNO_3. The Cycle 3 rinse solutions from the three bare-fuel tests were analyzed for ^{14}C and were found to contain 4.5 to 6.9% of the total ^{14}C measured in Cycle 3. The "% in solution" values given for Cycle 3 are maximum values and are preceded by a

9 0 7 9 4 1 4 2 8

TABLE 3.15. Quantities of ^{14}C Measured in Samples (nCi)

	HBR/BF-25	TP/BF-85	HBR/BF-85	HBR/SD-85	HBR/HD-85	HBR/UD-85
Cycle 1						
Periodic Samples[a]	20.5	188	49.4	4.8	14.4	2.1
Final Solution	99.0	1486	164	3.7	317.6	4.8
[$^{14}CO_3$ (ppb)]	(0.44)	(6.7)	(0.73)	(0.02)	(1.42)	(0.02)
Rinse	--	--	--	--	--	--
Acid Strip	--	--	--	--	--	--
Cycle Total	119.6	1674	213	8.5	332	6.9
+ 10^{-5} Inv.	235	--	442	16.7	692	13.7
% in Solution	--	--	--	--	--	--
Cycle 2						
Periodic Samples[a]	8.0	99	8.5	0.8	12.0	0.3
Final Solution	89.0	664	84.5	281.5	157.7	<2.3
[$^{14}CO_3$ (ppb)]	(0.40)	(3.0)	(0.38)	(1.26)	(0.71)	(<0.01)
Rinse	--	--	--	--	--	--
Acid Strip	--	--	--	--	--	--
Cycle Total	97.0	763	93.0	282.3	170	<2.6
+ 10^{-5} Inv.	193	--	195	557	353	<5.1
% in Solution	--	--	--	--	--	--
Cycle 3						
Periodic Samples[a]	4.1	26	4.1	--	--	--
Final Solution	51.8	236	39.4	184	78.8	9.7
[$^{14}CO_3$ (ppb)]	(0.23)	(1.1)	(0.18)	(0.82)	(0.35)	(0.04)
Rinse	3.8	12.4	3.2	--	--	--
Acid Strip	--	--	--	--	--	--
Cycle Total	59.7	275	46.7	184	78.8	9.7
+ 10^{-5} Inv.	120	--	99.0	362	164	19.2
% in Solution	<93.7	<95.5	<93.1	--	--	
Sum of Cycles 1, 2 & 3						
Σ Cycle Total	276	2712	353	475	581	<19.2
+ 10^{-5} Inv.	548	--	736	936	1209	<38

(a) Total of quantities in periodic samples for which detectable levels were reported.

NOTE: All values are based on data for unfiltered samples, except for the Cycle 3 rinse samples which were 0.4-μm filtered.

9 0 7 9 4 1 4 2 9

< symbol because some ^{14}C likely precipitated in carbonate phases along with the HCO_3^- originally in the J-13 water and was lost during the acid stripping procedure.

The ~1.2% total measured fractional release (Σ Cycle Totals ÷ 10^{-5} Inv. = 1209) indicated for ^{14}C in the HBR/HD-85 test is the largest fractional release value indicated for any nuclide in the Series 3 tests. The somewhat lower fractional release values for the slit-defect and bare-fuel tests may be due to pretest loss of $^{14}CO_2$ from the more severely defected specimens. The small ^{14}C release values measured in the HBR/UD-85 test indicate that most of the measured release in the other Series 3 tests originated from the fuel or from the gap inventory and not from the cladding exterior. This is a different result than previously reported for the Series 2 tests, where measured ^{14}C releases were not much greater in the defected cladding and bare-fuel tests than in the undefected test.[2] The ^{14}C inventory fractions measured in final solution samples from the Series 2 and Series 3 test cycles using the HBR fuel are compared in Table 3.16. The much higher activities measured in the bare-fuel and defected cladding specimens in the sealed Series 3 vessels indicate that most of the ^{14}C released from the specimens in the Series 2 tests was probably lost to the atmosphere as $^{14}CO_2$. The magnitude of the ^{14}C

TABLE 3.16. ^{14}C Inventory Fraction[a] in Series 2 and Series 3 Final Solution Samples (parts per 100,000)

Test	Cycle 1	Cycle 2	Cycle 3	Cycle 4	Cycle 5
HBR/BF-2-25	13.0	12.4	13.0	13.9	11.0
HBR/SD-2-25	27.5	33.9			
HBR/HD-2-25	48.1	22.3			
HBR/UD-2-25	10.1	3.7			
HBR/BF-25	194	177	104		
HBR/BF-85	339	178	84		
HBR/SD-85	7.3	555	362		
HBR/HD-85	662	329	164		
HBR/UD-85	9.6	<4.5	19.2		

(a) Based on ^{14}C measured in HBR fuel (0.49 μCi/g) and cladding (0.53 μCi/g).

90794 1430

releases measured in the Series 3 tests suggest that ^{14}C was preferentially released from sources of concentration such as the fuel-cladding gap or grain boundaries.

3.14 COBALT-60

Cobalt-60 is an activation product produced by neutron activation of ^{59}Co and (n,p) reaction on ^{60}Ni. Cobalt-60 is produced in fuel assembly structural components and may also occur in "crud" deposits on the cladding surface where its inventory is variable. With a 5.26-yr half-life, ^{60}Co will decay away during the repository containment period. However, the relatively high-gamma energy (1.3 MeV) associated with its decay requires heavy shielding for attenuation, making ^{60}Co activity a concern during fuel handling and emplacement.

Quantities of ^{60}Co measured in final solution, acid strip, and rinse samples are given in Table 3.17. Cobalt-60 activities were generally less than detectable and were not reported for solution samples from the four 85°C tests using the HBR fuel. Most of the ^{60}Co measured in the 85°C tests was in the acid strip samples. In the 25°C test, most of the ^{60}Co appeared to remain in solution. The TP fuel specimen appeared to release much more ^{60}Co than did the HBR fuel specimens.

TABLE 3.17. Quantities of ^{60}Co Measured in Samples (μCi)

	HBR/BF-25	TP/BF-85	HBR/BF-85	HBR/SD-85	HBR/HD-85	HBR/UD-85
Cycle 1						
Final Solution	5.22	<	<	<	<	<
Rinse	<	1.3	<	<	<	<
Acid Strip	0.68	154	5.46	2.01	0.34	0.34
Cycle 2						
Final Solution	0.52	<	<	<	<	<
Rinse	<	0.14	<	<	<	<
Acid Strip	<	12.9	0.33	0.10	0.12	0.04
Cycle 3						
Final Solution	<	<	0.29			
Rinse	<	0.18	<			
Acid Strip	0.08	3.0	<			

907941431

4.0 GENERAL DISCUSSION AND SUMMARY

Nonvolatile radionuclides present in spent nuclear fuel (or vitrified high-level waste) will require dissolution or suspension in water to be transported from a failed waste package in the repository in the absence of a major geological event such as volcanism. The repository horizon under study at Yucca Mountain lies in the unsaturated zone above the water table, and contact of the spent fuel by water that may infiltrate the rock will not occur until the repository has cooled to below the 95°C boiling temperature of water at the repository elevation. This is predicted to be several hundred years after disposal. Results from the Series 3 tests are summarized and discussed in this chapter relative to their implications for spent fuel storage in the repository during the postthermal period. Except as noted, the following discussions focus on results from the three bare-fuel tests. Areas where additional information would be useful are also identified.

The present results indicate that the radionuclides of interest in spent fuel fall into three general categories relative to potential release mechanisms under predicted Yucca Mountain repository conditions. The first category is radionuclides whose release will be limited by low solubility. The actinides, which account for most of the long-term radioactivity of spent nuclear fuel, are the primary radionuclides of interest in this first category. The second category is the more soluble radionuclides for which dissolution rates from the fuel may be an important factor in predicting potential release. Long-lived fission and activation product radionuclides are of primary concern in this category. The third category is radionuclides that may be mobile in the vapor phase and do not require water contact for release. The primary long-lived radionuclide in spent fuel known to be transported in the vapor phase is ^{14}C. There is also a potential for vapor transport of ^{129}I as I_2 that has not been clearly defined.

90794 1432

4.1 THE ACTINIDES

4.1.1 Summary of Actinide Results

Actinide concentrations (uranium, neptunium, plutonium, americium, and curium) measured in solution samples rapidly reached maximum levels during the first test cycle and then generally dropped to lower steady-state levels in Cycles 2 and 3. The approximate steady-state concentrations measured for the actinides in the bare-fuel tests are summarized in Table 4.1. The data for 0.4-μm filtered solutions are considered the most relevant for release estimates, since particles of greater size would likely settle out, and finer colloidal particles that could remain in suspension and be transported with water movement would be retained by the 18-Å filters. The data for 25°C 18-Å filtered solutions given for americium and curium suggest that most of the

TABLE 4.1. Approximate Steady-State Actinide Concentrations[a] in the Bare-Fuel Tests

Actinide	25°C 0.4 μm	25°C 18 Å	85°C (0.4 μm)
Uranium			
μg/mL	0.3	--	0.15
Log M	-5.9	--	-6.2
Neptunium			
^{237}Np (pCi/mL)	0.2	--	0.14
Log M	-8.9	--	-9.1
Plutonium			
$^{239+240}$Pu (pCi/mL)	100	--	1.0
Log M	-8.4	--	-10.4
Americium			
^{241}Am (pCi/mL)	100	3.6	0.1
Log M	-9.8	-11.3	-12.3
Curium			
^{244}Cm (pCi/mL)	100	4.5	0.1
Log M	-11.3	-12.6	-14.3

(a) Estimated, based on plotted Cycles 2 and 3 data for 0.4-μm filtered solutions and the Cycle 2 34-d data for 18-Å filtered solutions.

9 0 7 9 4 1 4 3 3

activity in the 0.4-μm filtered ^{241}Am and ^{244}Cm solution samples was associated with suspended phases in the 25°C test. A portion of the plutonium measured in unfiltered and 0.4-μm filtered solution samples also appears to be associated with suspended phases, but this fraction was much less than measured for americium and curium. No significant filtration effects were noted for uranium or neptunium.

Approximate steady-state uranium concentrations measured during Cycles 2 and 3 of the Series 3 bare-fuel tests (about 0.3 μg/mL at 25°C and 0.15 μg/mL at 85°C) were somewhat lower than the 1 to 2 μg/mL range measured in unsealed silica vessels in the Series 2 tests. Significantly lower uranium concentrations, on the order of 0.01 μg/mL or less, were measured for the slit-defect and holes-defect tests. Calcium-uranium-silicate mineral phases identified as uranophane (confirmed) and haiweeite (likely) were characterized in rinse filter residues from the 85°C bare-fuel tests. Formation of these phases likely controlled or influenced the uranium concentrations in these tests. Phases controlling the concentrations of the other actinide elements were not identified. Detection and characterization of such secondary phases may be difficult because of the extremely small masses of these actinides involved.

The steady-state solution activities measured for nuclides of plutonium, americium, and curium were much lower at 85°C than at 25°C. Kinetic factors involved in the nucleation and growth of secondary phases that limit the concentration of these elements were probably key factors in accounting for the lower concentrations at 85°C. Therefore, lower actinide concentrations may eventually occur at 25°C. Uranium and plutonium concentrations were lower in the slit-defect and holes-defect tests were than in the bare-fuel tests, but americium and curium concentrations during Cycles 2 and 3 were not greatly affected by specimen type. The neptunium data were not greatly affected by temperature.

90794 1434

4.1.2 Comparisons With EQ3/6 Predictions[a]

Spent fuel dissolution in J-13 well water was simulated using the geochemical modeling code EQ3/6[20] to determine whether steady-state actinide concentrations measured in the laboratory dissolution tests could be related to the precipitation of actinide-bearing solids. Version 3245 of the EQ3/6 code and version 3270R13 of the supporting thermodynamic database were used to simulate spent fuel dissolution at 25°C and 90°C assuming atmospheric CO_2 gas fugacity and two different O_2 fugacities, $10^{-0.7}$ (atmospheric) and 10^{-12} bars. The lower 10^{-12} bar oxygen fugacity value was initially chosen because its use resulted in a predicted neptunium concentration at 25°C that matched the experimentally measured neptunium concentration. The simulation process is described in more detail in Reference 14. The computer simulations predict the sequence of solid precipitates that form to sequester elements released via spent fuel dissolution, and the corresponding elemental concentrations in solution. Approximate steady-state actinide concentrations measured at 25°C and 85°C in the Series 3 tests are compared in Table 4.2 to concentrations of actinides in equilibrium with the listed solids as calculated in the EQ3/6 simulations.

The concentrations of uranium in the EQ3/6 simulation vary not only as the precipitates vary, but also during the precipitation of a single mineral, such as soddyite, because of changes in the pH and overall chemical characteristics of the solution. As previously discussed, uranophane, haiweeite, and possibly soddyite were indicated in the 85°C Series 3 tests. Unfortunately, reliable thermodynamic data for uranophane are not available, which complicates comparison of the laboratory test results to the calculated solubility limits. Haiweeite, a calcium-uranium-silicate, as is uranophane, is predicted to precipitate at uranium concentrations that are lower than the measured steady-state values. In the absence of thermodynamic data for

(a) The EQ3/6 calculations were performed at LLNL to Quality Assurance Level III under the direction of C. J. Bruton. This section, including Tables 4.2 and 4.3, is excerpted from Reference 17 with editorial changes for adaptation to the present report.

9 0 7 9 4 1 4 3 5

TABLE 4.2. Comparison of Measured and EQ3/6 Predicted Actinide Concentrations (Log M)

Actinide	Measured[a] 25°C	Measured[a] 85°C	EQ3/6[b] 25°C -0.7	EQ3/6[b] 25°C -12.0	EQ3/6[b] 90°C -0.7	EQ3/6[b] 90°C -12.0	Phase
U	-5.9	-6.2	-7.2/7.0[c]	7.1/-6.9	-8.8/-7.6	-8.5/-7.5	H
			-7.0/-6.9	-6.9/-6.8	-7.6	-7.5	H + S
			-6.9/-4.3	-6.8/-4.2	-7.6/-6.0	-7.5/-5.9	S
			-4.3	-4.2	-6.0	-5.9	S + Sch
			-4.2	-4.1	-6.0/-5.8	-5.8/-5.6	Sch
Np	-8.9	-9.1	-6.2	-9.0	-5.2	-8.0	NpO_2
Pu	-8.4	-10.4	-12.4	-13.8	-11.9	-14.6	PuO_2
			-4.3	-5.7	-4.2	-6.9	$Pu(OH)_4$
Am	-9.8	-12.3	-8.3	-8.3	--	--	$Am(OH)CO_3$
			--	--	-8.4	-8.4	$Am(OH)_3$
Cm	-11.3	-14.2	Cm not in thermodynamic database				

(a) Series 3 tests, 0.4-μm filtered.
(b) At oxygen fugacities log f_{O2} = -0.7 (atmospheric) and log f_{O2} = -12.0 with solubility control by precipitated secondary phases as listed. H = haiweeite; S = soddyite; Sch = schoepite. All phases are in crystalline state except $Pu(OH)_4$, which is amorphous.
(c) -7.2/-7.0 refers to a range in concentration from -7.2 to -7.0.

9 0 7 9 4 1 4 3 6

uranophane, the measured uranium concentrations appear to be consistent with the precipitation of soddyite at both 25°C and 90°C in the simulations.

Neptunium concentration is controlled by equilibrium with NpO_2 in the simulations. However, the predicted concentration of neptunium is highly dependent on solution Eh and pH[21]. Changing the O_2 fugacity from $10^{-0.7}$ bars to 10^{-12} bars in the simulations results in good agreement between measured and predicted concentrations of neptunium at 25°C, but over estimates neptunium concentrations at 90°C. The experimental data do not reflect predicted increases in neptunium concentration with temperature, which indicates a needto critically evaluate the thermodynamic data for neptunium at elevated temperatures. The Eh was not measured during the laboratory tests, and redox equilibrium may not have been established among various phases within the sealed stainless steel vessels considering that J-13 water has very little capacity to buffer Eh.

Plutonium concentrations measured at both temperatures were greater than predicted based on equilibration with crystalline PuO_2 at either oxygen fugacity, but were less than predicted based on precipitation of amorphous $Pu(OH)_4$. The $10^{-8.4}$ M concentration measured at 25°C is in the range reported by Rai and Ryan[15], who (as previously discussed) measured the solubility of PuO_2 and hydrous $PuO_2 \cdot xH_2O$ in water over periods of up to 1,300 d at 25°C. At a pH of 8, which was the extrapolated lower limit of their data and the approximate pH in the Series 2 and 3 tests, they reported that plutonium concentrations ranged from about $10^{-7.4}$ M, where an amorphous $PuO_2 \cdot xH_2O$ was thought to control concentration, down to about 10^{-9} M, where aging of the amorphous material produced a more (but incompletely) crystalline PuO_2 that was thought to control concentration.

The measured americium concentrations were lower than predicted in the EQ3/6 simulations based on precipitation of $Am(OH)CO_3$ at 25°C or $Am(OH)_3$ at 90°C. A possible explanation for this difference is that americium, and likely curium, may have precipitated from solution with the lanthanides. The chemistry of trivalent americium and curium can be expected to be very similar to that of light lanthanide fission product elements, which are present in spent fuel at much greater concentrations than are americium and curium and have similar ionic radii in the trivalent state. The transuranic actinides

9 0 7 9 4 1 4 3 7

may also be precipitating at low concentrations in the uranium-bearing precipitates. Sorption of actinides on colloids or other surfaces such as the fuel or test hardware may have also controlled some aspects of solution concentration not considered in the geochemical simulations.

Comparisons between experimental results and predictions in Table 4.2 are predicated on the assumption that solid phases as listed precipitate from solution and exert control on solution composition. Except for some uranium-bearing minerals, no minerals containing actinide radionuclides have been identified in the laboratory tests. Detection and characterization of actinide-bearing secondary phases may be difficult because of the extremely small masses involved. Precipitates limiting actinide concentrations in the laboratory tests may also be amorphous, colloidal, or in some other less than perfectly crystalline state. The concentrations of the affected actinides would therefore gradually decrease as aging progressed. It is not currently reasonable to expect a geochemical model to accurately predict the effects of all potential concentration-controlling processes over time spans of thousands of years. However, neither is it practical to conduct long-term dissolution tests for all potential fuel and solution chemistry states in the repository. Identification of phases and processes controlling solution concentrations, and obtaining reliable thermodynamic data for these phases and processes, are important data needs if geochemical models are to be used to predict potential radionuclide concentrations.

4.1.3 Actinide Release

The fact that all of the actinides rapidly reached maximum concentrations in tests where the water-to-fuel ratio and recharge rates are large relative to those likely to occur in a failed waste package in the repository suggests that actinide release will be solubility limited. That is, the release rate will be limited by individual actinide element solubilities and the amount of water moving through the repository and will not depend on the actual dissolution rate of the fuel. The logarithms of the approximate steady-state actinide concentrations (0.4-μm filtered) measured at 25°C and

9079414138

resulting annual fractional releases are given in Table 4.3. A water flow rate of 20 L/yr per waste package containing 3140 kg of 33,000 MWd/MTM PWR fuel is assumed.

The actinide releases given in Table 4.3 are all at least three orders of magnitude less than the 10^{-5} per year of 1,000-yr inventory limit specified by the NRC in 10 CFR 60.113[11] and indicate that the NRC requirement should be met for any realistic water flow rate. The plutonium and americium release values are of particular significance because isotopes of these two actinides account for about 98% of the total activity of spent fuel at 1,000 yr (see Table 2.5). These values are probably conservative since the concentrations assumed are based on $^{239+240}Pu$ and ^{241}Am activity levels of 100 pCi/mL measured at 25°C, while much lower activities on the order of 1 pCi/mL or less were measured at 85°C. Kinetic factors involved in the nucleation and growth of secondary phases that control plutonium and americium concentrations may eventually allow lower solution activities to occur at 25°C and over longer time periods relevant to the repository. Lower $^{239+240}Pu$ and ^{241}Am activities on the order of 10 pCi/mL were measured during Cycles 4 and 5 of the Series 2 tests. The calculated releases assume maintenance of steady values for

TABLE 4.3. Annual Actinide Releases as a Fraction of the 1,000-Year Inventories

Actinide	Concentration Log(M)	Log(Release)
U	-5.9	-8.6
Np	-8.9	-8.8
Pu	-8.4	-9.0
Am	-9.8	-9.1

NOTE: Assumes water flow rate of 20 L/yr per waste package transporting actinides at the indicated concentrations. Each waste package is assumed to contain 3140 kg of 33,000 MWd/MTM burnup PWR fuel. The concentrations are approximate steady-state concentrations reached in 0.4-μm filtered solution in Cycles 2 and 3 of the HBR-3-25 test.

9 0 7 9 4 1 4 3 9

actinide concentrations over time, whereas the geochemical simulations suggest that actinide concentrations, and uranium concentrations in particular, may vary with time as different solubility-controlling solid phases form. Confidence in such release predictions will be greatly increased when the chemical mechanisms of solubility control are identified and successfully modeled.

4.2 FISSION AND ACTIVATION PRODUCTS

Analyses were conducted to measure the activities of the fission products ^{137}Cs, ^{134}Cs, ^{90}Sr, ^{99}Tc, ^{129}I, and ^{126}Sn and the activation products ^{14}C and ^{60}Co. Of these, ^{137}Cs, ^{134}Cs, ^{90}Sr, and ^{60}Co will decay away during the thermal (containment) period and will not be present for dissolution after the waste packages have cooled sufficiently to allow water contact with the fuel. The inventories of the principal radionuclides remaining in spent fuel at 1,000 yr were tabulated in Table 2.5. After the actinides, ^{99}Tc at about 0.77% accounts for the next greatest portion of the 1,000-yr inventory. Depending on factors such as initial nitrogen impurity levels in the original fuel, ^{14}C will probably account for about 0.01 to 0.1% of the activity at 1,000 yr. Discounting the actinides, ^{99}Tc and ^{14}C, all other fission and activation product radionuclides account for a little less than 1% of the total 1,000-yr radionuclide inventory in spent fuel. Of those not measured, nickel activation products in hardware components represent the greatest portion (~0.3 %) of the 1,000-yr inventory. Analysis of ^{79}Se was deleted from the Series 3 tests, since it was not detectable in the Series 2 tests.

The range of activities measured for fission and activation product radionuclides is shown in Figure 4.1 for the HBR/BF-25 and TP/BF-85 tests. The activity of ^{135}Cs calculated to be in solution based on the ^{137}Cs data adjusted for ORIGEN-2 calculated yields is plotted as a dashed line. Tin-126 was detected at an activity level of about 1 pCi/mL in some of the Cycle 1 solution samples, but it was not detectable by direct counting methods in Cycles 2 and 3. Iodine-129, which accounts for only about 0.002% of the 1,000-yr inventory, was the lowest level radionuclide measured and required neutron activation analysis for its measurement. The isotopes ^{99}Tc, ^{14}C,

9 0 7 9 4 1 4 4 0

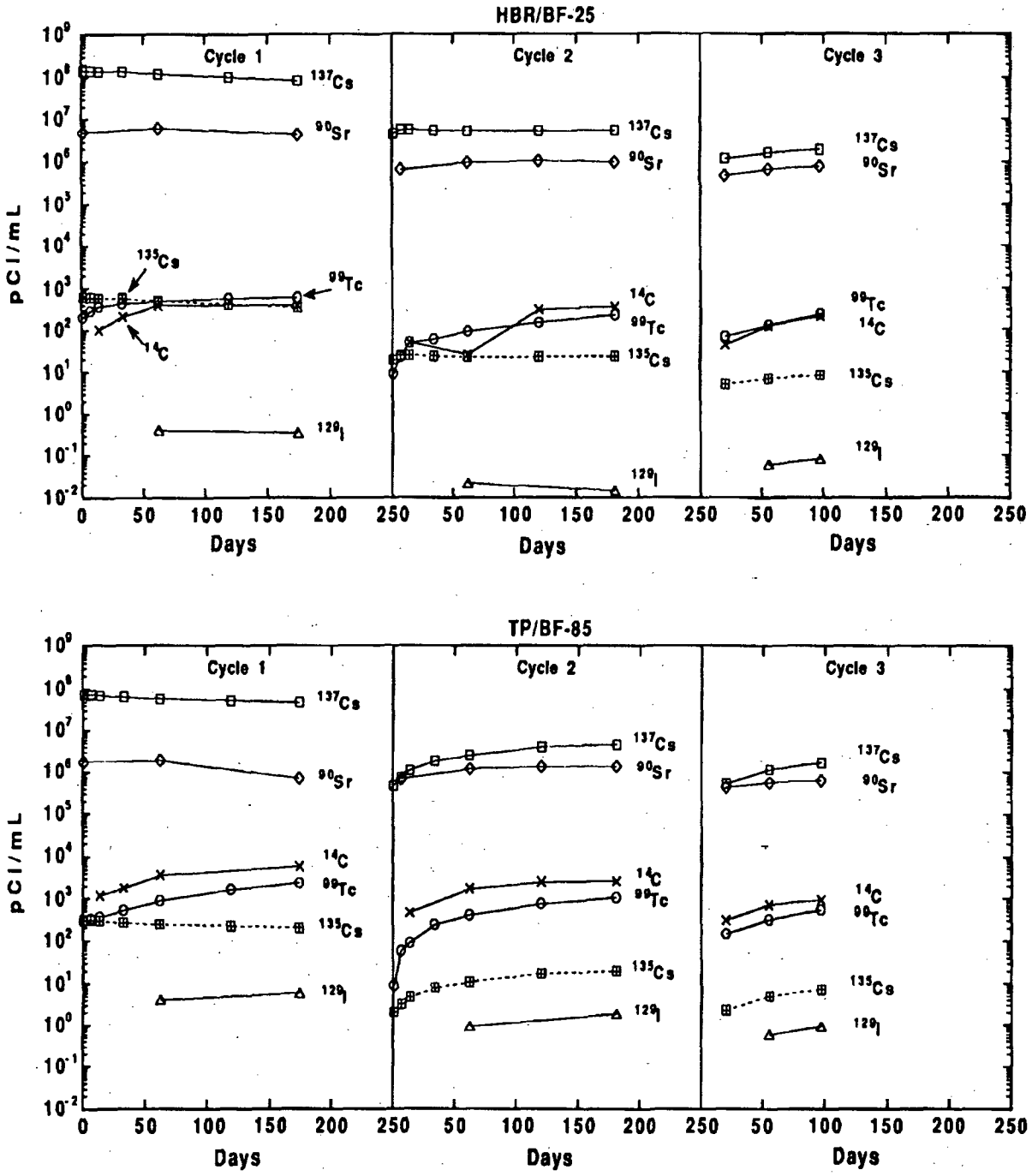

FIGURE 4.1. Activity Levels of Fission Products and ^{14}C Levels Measured in the HBR/BF-25 (above) and TP/BF-85 (below) Tests. (^{135}Cs levels shown are calculated based on the ^{137}Cs data.)

9 0 7 9 4 1 4 4 1

^{135}Cs, ^{129}I, and ^{126}Sn are the only nonactinide radionuclides that will be present during the postthermal period for which significant activities were measured or calculated.

The inventory fractions of ^{137}Cs, ^{90}Sr, ^{99}Tc, ^{129}I, and ^{14}C measured in solution in the three bare-fuel tests are plotted in Figures 4.2 through 4.4. Each data point in these plots includes the inventory fraction in solution on the sampling day plus the inventory fractions estimated to have been removed in previous samples during the test cycle. (Carbon-14 is not included in Figure 4.4 for the TP/BF-85 test because ^{14}C inventory was not measured on the TP fuel.) The initial preferential releases of ^{137}Cs from gap inventory during Cycle 1 of the three tests are shown in expanded scale plots (upper plots in Figures 4.2 to 4.4). The activity of ^{90}Sr in solution appears to be solubility limited, particularly in the 85°C tests. Significant preferential release of ^{14}C during all three cycles of the HBR/BF-25 and HBR/BF-85 tests is indicated. The fractional inventories of ^{14}C plotted were normalized to the inventory value measured for the fuel (0.49 μCi/g). Normalizing the data to the inventories measured in the fuel plus cladding would only drop the plotted ^{14}C inventory fraction levels by 18%.

The reduced scale plots in Figures 4.2 through 4.4 clearly show continuous release of soluble fission products during Cycles 2 and 3. The apparent limited solubility of strontium in the tests is also shown. The continuous release rates measured during Cycles 2 and 3, expressed as annual fractional release times 10^5, are given for ^{99}Tc, ^{137}Cs, and ^{129}I in Table 4.4. These values indicate a dissolution rate for the spent fuel by itself that is too high to meet the requirements of 10 CFR 60.113[11] for the soluble radionuclides if significant portions of the indicated releases result from fuel matrix dissolution. If these release rates are primarily the result of preferential release from grain boundaries, they may become lower over time as exposed grain boundary inventories are depleted and the release rates approach a lower fuel matrix dissolution rate. However, matrix dissolution rates may increase over time as wettable surface area increases as a result of grain boundary dissolution and/or general fuel degradation by oxidation. Physical degradation of the fuel as a result of reaction with the repository

9 0 7 9 4 1 4 4 2

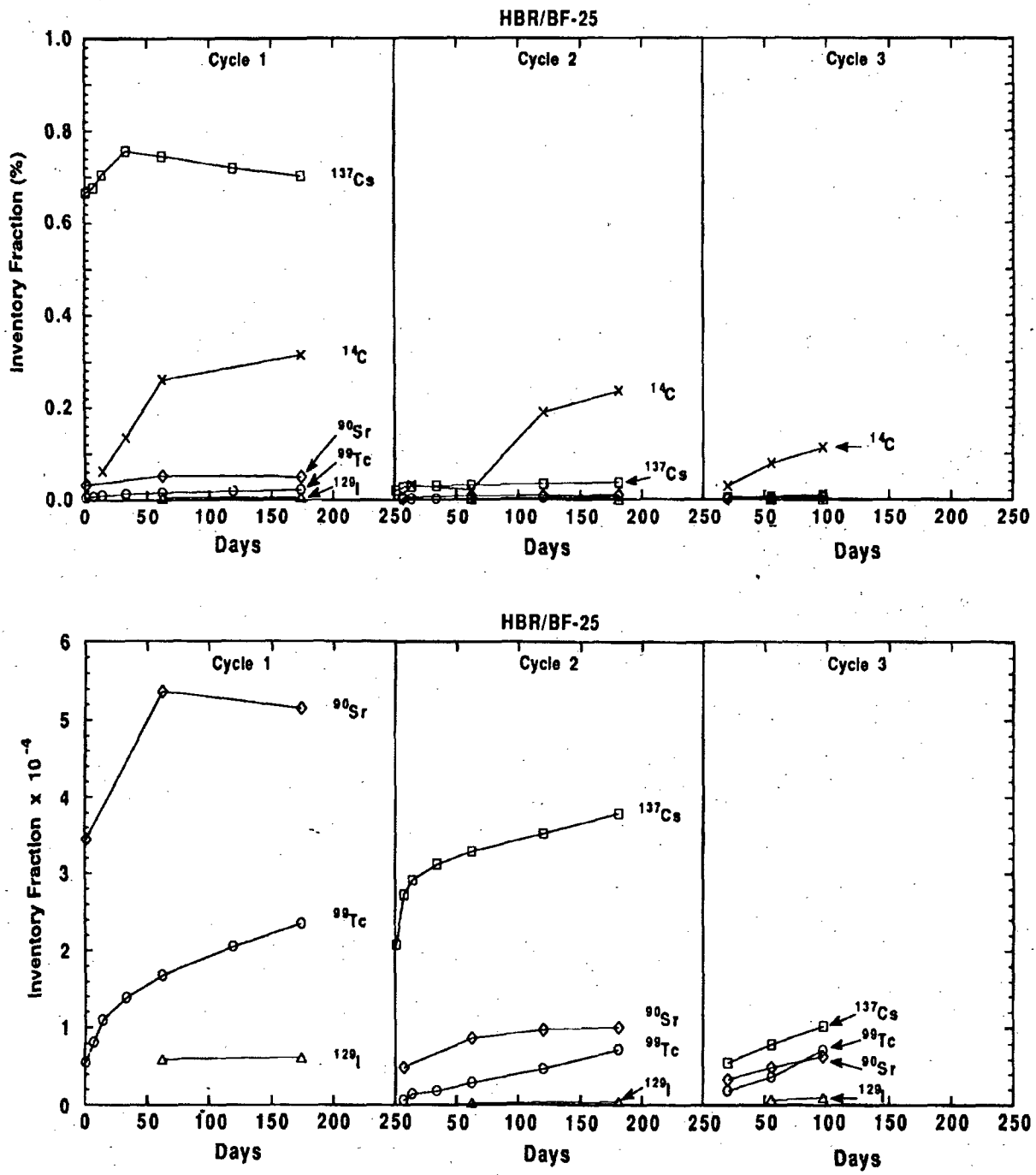

FIGURE 4.2. Inventory Fractions of ^{137}Cs, ^{90}Sr, ^{99}Tc, ^{129}I, and ^{14}C Measured in Solution During the HBR/BF-25 Test

9 0 7 9 4 1 4 4 3

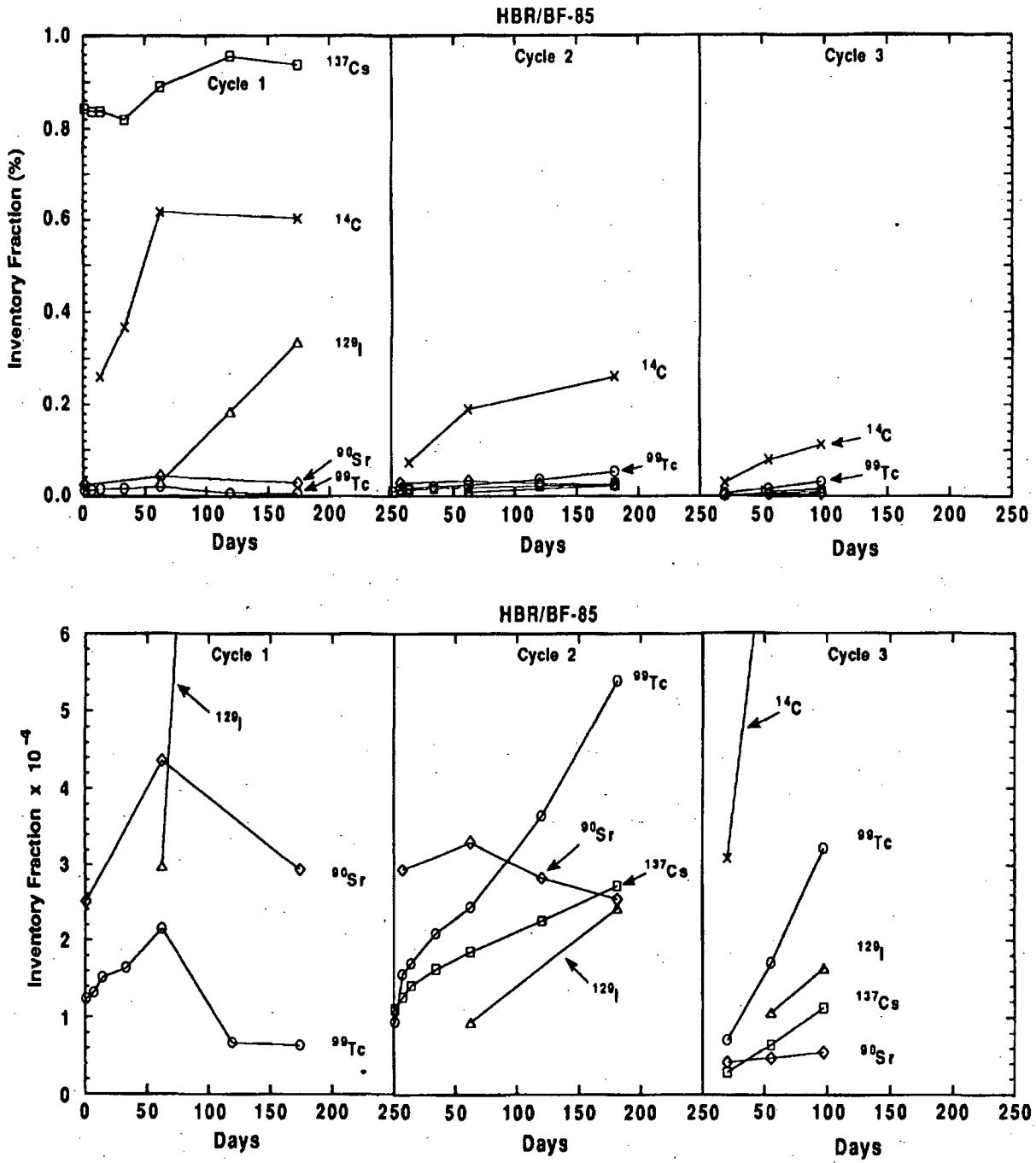

FIGURE 4.3. Inventory Fractions of ^{137}Cs, ^{90}Sr, ^{99}Tc, ^{129}I, and ^{14}C Measured in Solution During the HBR/BF-85 Test

9 0 7 9 4 1 4 4 4

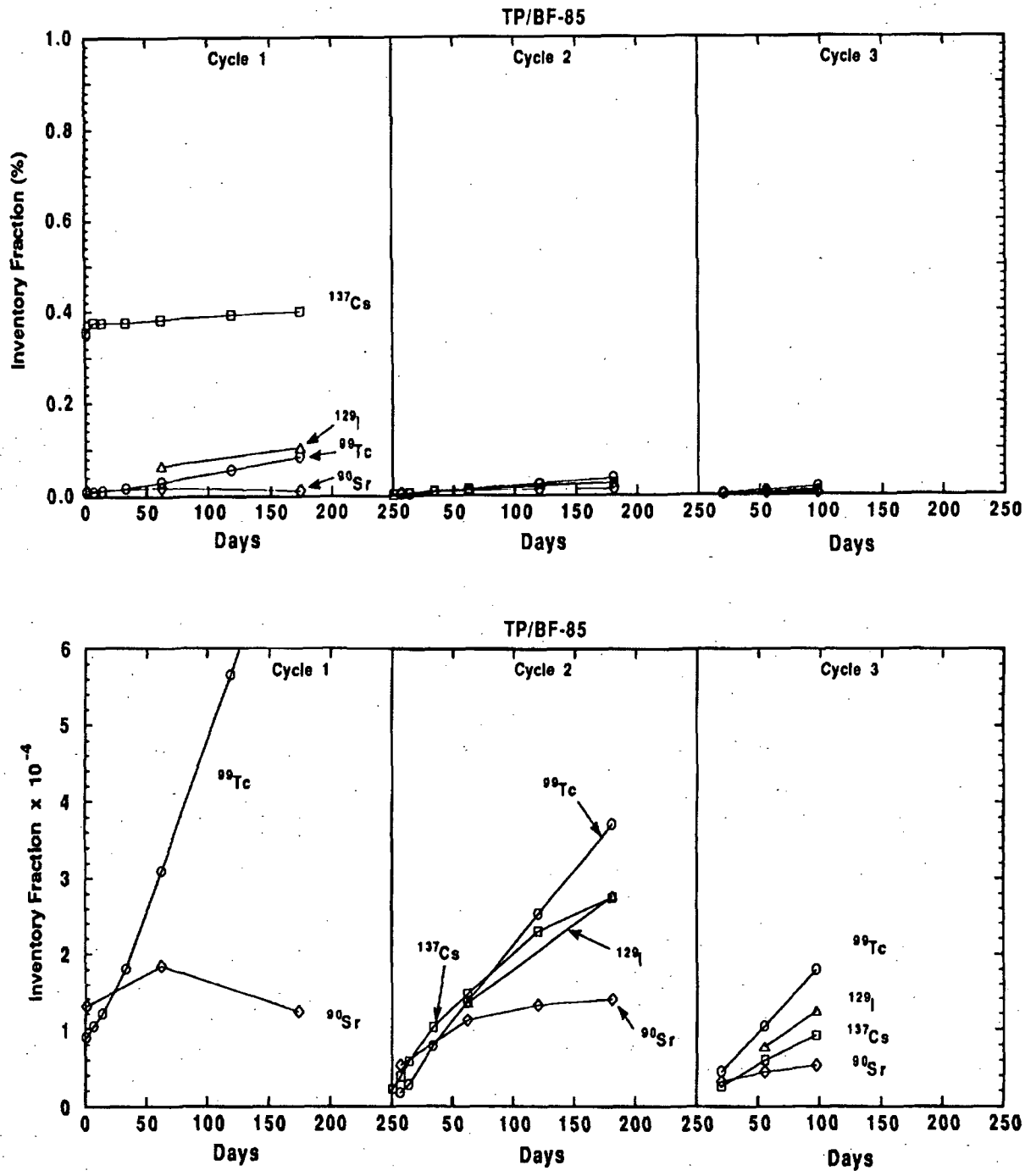

FIGURE 4.4. Inventory Fractions of ^{137}Cs, ^{90}Sr, ^{99}Tc, ^{129}I, and ^{14}C Measured in Solution During the TP/BF-85 Test

9 0 7 9 4 1 4 4 5

TABLE 4.4. Continuous Annual Release Rates Measured for Soluble Fission Products as Inventory Fraction Times 100,000

Test/FP	Cycle 2[a]	Cycle 3[b]
HBR/BF-25		
^{99}Tc	13	25
^{137}Cs	17	22
^{129}I	0.6	2.8
HBR/BF-85		
^{99}Tc	90[c]	120
^{137}Cs	27	40
^{129}I	45	49
TP/BF-85		
^{99}Tc	73	64
^{137}Cs	43	31
^{129}I	44	41

(a) 34 to 174 d.
(b) 20 to 97 d.
(c) 62 to 174 d.

atmosphere may also free soluble nuclides contained in the fuel matrix phase, allowing them to be more rapidly dissolved when contacted by water.

It may be possible to determine the degree to which the soluble nuclides were preferentially released in the present tests by retesting the fuel specimens in a flow-through test apparatus using flow rates sufficient to prevent uranium saturation. However, a better understanding of potential degradation of the fuel in the repository environment, along with some data on the dissolution behavior of degraded fuel states, are also needed to define effectiveness of the fuel itself as a barrier to the release of soluble-radionuclides. Modeling the dissolution behavior of spent fuel requires a time-dependent model for the state of the fuel, which will likely be much more difficult to establish and validate than will the dissolution behavior of a given fuel state.

4.3 ADDITIONAL INFORMATION NEEDS

Evaluation of the Series 3 test results has indicated a need for additional information in the following areas.

90794 1446

1. Preferential Versus Matrix Dissolution - Most of the inventory of soluble radionuclides is presumably contained in the fuel matrix phase. However, the relative contributions of matrix dissolution versus preferential release from locations such as grain boundaries where soluble radionuclides may concentrate have generally not been determined in dissolution experiments to date. It may be possible to determine the degree to which the soluble radionuclides were preferentially released, and therefore determine the static test fuel matrix dissolution rates, by retesting the fuel specimens in a flow-through test apparatus using flow rates sufficient to prevent uranium saturation.

2. Fuel Oxidation - Under real Yucca Mountain repository conditions, fuel in a failed waste package may be exposed to air for a considerable time before contacting water. Slow oxidation of the UO_2 fuel matrix in the repository environment may cause significant physical degradation of the fuel. The dissolution behavior of slowly oxidized fuel has not been investigated. Several spent fuel specimens from on-going Long-Term, Low-Temperature Oxidation Studies[22] are available for dissolution testing.

3. Secondary Phases - Knowledge of the secondary phases that control nuclide concentrations and quality thermodynamic data for these phases are required for valid geochemical modeling. With the exception of uranium, secondary phases controlling the concentrations of sparingly soluble nuclides were not identified in the present tests. Characterization of the phases that controlled plutonium, americium, and neptunium concentrations would be most useful, since these actinides account for the major portion of spent fuel activity for several thousand years. Small quantities of phases containing these nuclides may be present in currently archived filter residue samples. Special techniques will need to be developed for isolation and analysis of these phases.

4. Fuel Type Variables - The effects on dissolution behavior of variables represented in the spent fuel population may be worth testing. In addition to burnup and gas release variables, fuels

9 0 7 9 4 1 4 4 7

containing gadolinia as a burnable poison may be worth testing. Comparison of typical boiling water reactor (BWR) and PWR fuels under the same test conditions should also be considered.

5. Other Material Variables - Effects of vessel type and anomalies due to localized corrosion were observed in the Series 3 tests. Spent fuel dissolution tests in vessels representative of new candidate container materials should be considered when these materials are identified. Dissolution tests that include representative rock with posttest examination of the rock for nuclide absorption may also be worthwhile.

6. Surface Area - Dissolution rates measured for soluble radionuclides were normalized to specimen inventories for this report. Such dissolution rates are expected vary with the exposed surface area of the fuel, which will depend on the state of degradation of the fuel. Because of the unknown effects of grain boundaries and other porosity, it was not possible to normalize the data to surface area so as to obtain dissolution rates that are independent of particle size and morphology. However, geometric surface areas are calculated for the HBR and TP fuel specimens in Appendix E.

9 0 7 9 4 1 4 4 8

5.0 CONCLUSIONS

The following conclusions and observations are made based on the results of the NNWSI Series 3 Spent Fuel Dissolution Tests.

1. Actinide concentrations (uranium, plutonium, americium, curium, and neptunium) generally appeared to reach steady-state levels in all three test cycles of the bare-fuel tests. Control of actinide concentrations at stable levels in solution was attributed to the achievement of a steady-state between fuel dissolution and secondary-phase formation or other mechanisms such as sorption.

2. Uranium-bearing secondary phases were found in significant amounts in filter residues from the 85°C bare-fuel tests. Formation of the calcium-uranium-silicate phase uranophane was confirmed, and haiweeite was tentatively identified. A possible indication of soddyite formation was also found in one of the filter residues. Secondary phases controlling plutonium, americium, curium, and neptunium concentrations were not identified.

3. Plutonium, americium, and curium activities measured in solution samples from the 85°C bare-fuel tests were from two to three orders of magnitude lower than those measured in unfiltered and 0.4-μm filtered samples from the 25°C test. Slightly lower uranium concentrations were also measured at 85°C in Cycles 2 and 3. Lower actinide concentrations at 85°C are attributed to faster kinetics for formation of solubility-limiting secondary phases at the higher 85°C temperature. Neptunium activities showed no significant dependence on temperature or filtration.

4. Plutonium, americium and curium activities measured in 18-Å filtered samples from the 25°C bare fuel test were significantly less than those measured in unfiltered and 0.4-μm filtered samples suggesting that these elements were present as colloids in this test. The effects of filtration were generally greater for americium and curium than for plutonium. Notable reductions in americium and curium activities also occurred with 0.4 μm filtration in the 85°C bare fuel tests.

90794 1449

5. Steady-state actinide concentrations measured in 0.4-μm filtered samples from the 25°C bare-fuel test were at least three orders of magnitude below those necessary to meet the NRC 10 CFR 60.113 controlled release requirements based on reasonable assumed water flow rates through the repository. This result is of particular significance, since plutonium and americium isotopes account for ~98% of the activity in spent fuel at 1,000 yr, and eventual plutonium and americium concentrations may be lower than those measured in 0.4-μm filtered samples from the 25°C tests.

6. Measured uranium concentrations were consistent with those predicted by the EQ3/6 geochemical modeling code for precipitation of soddyite. Good agreement between measured and predicted concentration was obtained for neptunium based on equilibration with NpO_2 at 25°C when the oxygen fugacity in the simulation was set at 10^{-12} bars. A broad range of concentrations that bracketed the measured values was predicted for plutonium depending upon the assumed oxygen fugacity and concentration-controlling phase. Measured americium concentrations were less than predicted based on data for equilibration with $Am(OH)CO_3$ or $Am(OH)_3$.

7. Actinide fractional releases from the bare-fuel tests were much greater than in the slit-defect or hole-defects tests. Actinide releases from the slit-defect test were somewhat greater than in the hole-defects test, with most of the difference accounted for in the Cycle 1 acid strip samples. Actinide releases in the hole-defects test were not significantly different from those measured in the undefected test.

8. The radionuclides ^{137}Cs, ^{90}Sr, ^{99}Tc, ^{129}I, and ^{14}C were continuously released in the bare-fuel tests at rates exceeding 10^{-5} of inventory per year. Of these radionuclides, only ^{90}Sr showed significant indications that its concentration was limited by solubility. Cesium-137 showed the greatest fractional release during Cycle 1, while ^{14}C showed the greatest fractional release during Cycles 2 and 3.

9079 4 1450

9. Iodine-129 release was much greater at 85°C than at 25°C. Comparison of the Series 3 test results to those from the Series 2 tests gave no indication that ^{129}I had been lost as I_2 from the unsealed Series 2 vessels. The ^{129}I release in the slit-defect test was equivalent to that in the bare-fuel test, but ^{129}I released in the hole-defects test was not significantly greater than in the undefected test.

10. Comparison of ^{14}C solution activity data measured in the sealed Series 3 tests to that measured in the unsealed Series 2 tests indicated that most of the ^{14}C released in the Series 2 tests was probably lost to the atmosphere as $^{14}CO_2$. The TP fuel appeared to have a much greater ^{14}C inventory (or gap inventory) than did the HBR fuel on which fuel and cladding ^{14}C inventory was radiochemically determined.

11. Long-term release rates for soluble nuclides are uncertain. The relative contributions of fuel matrix phase dissolution, versus preferential release from locations such as grain boundaries where soluble nuclides may be concentrated, was not determined. Preferential release would likely decrease as the inventory of soluble nuclides on exposed grain boundaries is depleted. However, there is reason to suspect that accelerated dissolution of soluble nuclides may eventually occur as a result of degradation of the fuel by oxidation in the repository air atmosphere.

12. A vessel corrosion anomaly occurred during Cycle 1 of the 85°C HBR bare-fuel test. The most significant effects associated with the apparent vessel corrosion were: 1) uranium concentration dropped to about 10 ppb, and 2) ^{99}Tc activity dropped to less than detectable. These effects are attributed to removal of uranium and technetium by coprecipitation with or sorption on iron-bearing precipitates, or to reduction of the soluble UO_2^{+2} and TcO_4^- species as a result of redox coupling with Fe^0 to Fe^{+2}/Fe^{+3} reactions.

13. Calcium, magnesium, silicon, and HCO_3^- precipitated from solution during all 85°C tests cycles, while the chemistry of the starting

90794 1451

J-13 well water remained essentially unchanged during the 25°C test. In addition to the calcium-uranium-silicate phases observed in the two 85°C bare-fuel tests, scale formation was observed at the waterline in all of the 85°C tests. The SEM-EDX examinations suggest that calcite, SiO_2 (possibly as a gel), and possibly dolomite were formed during the 85°C tests. A portion of the released ^{14}C is likely to be incorporated in the carbonate phases. A portion of the released ^{90}Sr is also likely to be incorporated in secondary phases, possibly as a partial substitute for calcium.

90794 1452

6.0 REFERENCES

1. Wilson, C. N. 1985. Results from NNWSI Series 1 Spent Fuel Leach Tests. HEDL-TME 84-30, Westinghouse Hanford Company, Richland, Washington. NNA.900216.0070.

2. Wilson, C. N. 1987. Results from Cycles 1 and 2 of NNWSI Series 2 Spent Fuel Dissolution Tests. HEDL-TME 85-22, Westinghouse Hanford Company, Richland, Washington. NNA.900216.0071.

3. Wilson, C. N. 1988. "Summary of Results from the Series 2 and Series 3 NNWSI Bare Fuel Dissolution Tests." In Proceedings from the Scientific Basis for Nuclear Waste Management XI, November 30 - December 5, 1987, Boston, Massachusetts, eds. M. J. Apted and R. E. Westerman. Mat. Res. Soc. Symp. Proc., Pittsburgh, Pennsylvania, Vol. 112, pp. 473-483. NNA.900306.0016.

4. Wilson, C. N. 1987. "Recent Results from NNWSI Spent Fuel Leaching/ Dissolution Tests." UCRL-21019, HEDL-SA-3700, Presented at the American Ceramic Society Annual Meeting, Pittsburgh, Pennsylvania; April 26-30, 1987. NNA.900306.0011.

5. Shaw, H. F. 1987. Plan for Spent Fuel Waste Form Testing for NNWSI. UCID-21272, Lawrence Livermore National Laboratory, Livermore, California. NN1.881209.0027.

6. Wilson, C. N. 1986. Test Plan for Series 3 NNWSI Spent Fuel Leaching/Dissolution Tests. HEDL-7577, Westinghouse Hanford Company, Richland, Washington. NNA.900216.0069.

7. Glassley, W. E. 1986. Reference Waste Package Environment Report. UCRL-53726, Lawrence Livermore National Laboratory, Livermore, California. HQS.880517.2445.

8. Barner, J. O. 1984. Characterization of LWR Spent Fuel MCC-Approved Testing Material ATM-101. PNL-5109, Pacific Northwest Laboratory, Richland, Washington. HQS.880517.2387.

9. Davis, R. B., and V. Pasupathi. 1981. Data Summary for the Destructive Examination of Rods G7, G9, J8, I9, and H6 from Turkey Point Fuel Assembly B17. HEDL-TME 80-85, Westinghouse Hanford Company, Richland, Washington. HQS.880517.2418.

10. Croff, A. G., and C. W. Alexander. 1980. Decay Characteristics of Once-Through LWR and LMFBR Spent Fuels, High-Level Wastes, and Fuel Assembly Structural Material Wastes. ORNL/TM-7431, Oak Ridge National Laboratory, Oak Ridge, Tennessee. NNA.870406.0442.

11. Code of Federal Regulations. 1983. "Disposal of High-Level Radioactive Wastes in Geological Repositories - Licensing Procedures." Title 10, Chapter 1, Part 60, Section 60.113. NNA.890715.0655.

90794 1453

12. Code of Federal Regulations. 1985. "Environmental Standards for the Management and Disposal of Spent Nuclear Fuel, High-Level, and Transuranic Radioactive Wastes," (40 CFR P191). Federal Register, Vol. 50, No. 182, pp. 38066-38089, U.S. Environmental Protection Agency, Washington, D.C. NNA.891018.0191.

13. Gray, W. J. 1988. "Effects of Radiation on the Oxidation Potential of Salt Brine." In Proceedings from the Scientific Basis for Nuclear Waste Management XI, November 30 - December 5, 1987, Boston, Massachusetts, eds. M. J. Apted and R. E. Westerman. Mat. Res. Soc. Symp. Proc., Pittsburgh, Pennsylvania, Vol. 112, pp. 405-413. NNA.900306.0014.

14. Bruton, C. J., and H. F. Shaw. 1988. "Geochemical Simulation of the Reaction Between Spent Fuel Waste Form and J-13 Water at 25°C and 90°C." In Proceedings from the Scientific Basis for Nuclear Waste Management XI, November 30 - December 5, 1987, Boston, Massachusetts, eds. M. J. Apted and R. E. Westerman. Mat. Res. Soc. Symp. Proc., Pittsburgh, Pennsylvania, Vol. 112, pp. 243-240. NNA.871113.0021.

15. Rai, D., and J. L. Ryan. 1982. "Crystallinity and Solubility of Pu(IV) Oxide and Hydrous Oxide in Aged Aqueous Suspensions." Radiochemica Acta, Vol. 30, pp. 213-216. NNA.900306.0013.

16. Rundberg, R. S., A. J. Mitchell, I. R. Triay, and B. Torstenfelt. 1988. "Size and Density of a 242Pu Colloid." In Proceedings from the Scientific Basis for Nuclear Waste Management XI, November 30 - December 5, 1987, Boston, Massachusetts, eds. M. J. Apted and R. E. Westerman. Mat. Res. Soc. Symp. Proc., Pittsburgh, Pennsylvania, Vol. 112, pp. 243-248. NNA.900306.0015.

17. Wilson, C. N., and C. J. Bruton. 1989. Studies on Spent Fuel Dissolution Behavior Under Yucca Mountain Repository Conditions. PNL-SA-16832 and UCRL-100223, paper presented at Fourth International Symposium on Ceramics in Nuclear Waste Management, American Ceramic Society Annual Meeting, Indianapolis, Indiana, April 23-27, 1989. (Proceedings in press.) NNA.890515.0196.

18. Campbell, D. O., and S. R. Buxton. 1976. "Hot Cell Studies of Light Water Reactor Fuel Reprocessing." CONF 761103-13, American Nuclear Society Meeting, Washington, D.C; November 15-19, 1976; Vol. 24, pp. 232-233. NNA.900306.0012.

19. Van Konynenburg, R. A., C. F. Smith, H. W. Culham, and C. H. Otto Jr. 1985. "Behavior of Carbon-14 in Waste Packages for Spent Fuel in a Repository in Tuff." In Proceedings from the Scientific Basis for Nuclear Waste Management VIII, November 26-29, 1984, Boston, Massachusetts, eds. C. M. Jantzen, J. A. Stone and R. C. Ewing. Mat. Res. Soc. Symp. Proc., Pittsburgh, Pennsylvania, Vol. 44, pp. 405-412. NNA.900320.0150.

90794 1454

20. Wolery, T. J. 1979. Calculation of Chemical Equilibrium Between Aqueous Solution and Minerals: The EQ3/6 Software Package. UCRL-52658, Lawrence Livermore National Laboratory, Livermore, California. HQS.880517.2586.

21. Lemire, R. J. 1984. An Assessment of the Thermodynamic Behavior of Neptunium in Water and Model Groundwater from 25°C to 150°C. AECL-781, Atomic Energy Commission of Canada, Ltd., Whiteshell Nucl. Res. Estbl., Pinawa, Manitoba, Canada. NNA.900320.0149.

22. Einziger, R. E. and H. C. Buchanan. 1988. Long-Term, Low-Temperature Oxidation of PWR Fuel; Interim Transition Report, WHC-EP-0070, Westinghouse Hanford Company, Richland, Washington. ~~NNA.910108.0113.~~ ~~BB 1-9-91~~ NNA.900620.0297 BB 2-7-91

90794 1455

APPENDIX A

RADIONUCLIDE INVENTORY AND RADIOCHEMICAL DATA

9 0 7 9 4 1 4 5 6

APPENDIX A

RADIONUCLIDE INVENTORY AND RADIOCHEMICAL DATA

A.1 RADIONUCLIDE INVENTORY DATA

Specimen radionuclide inventories used for most calculations in this report were calculated from ORIGEN-2 data given in PNL-5109[A1] for the ATM-101 H. B. Robinson Reactor (HBR) Unit 2 PWR fuel 12 yr after reactor discharge. Since the Turkey Point (TP) fuel was similar (same vendor, same design, similar vintage and same 2.55% ^{235}U initial enrichment), these ORIGEN-2 data were considered appropriate for both fuels. An age of 10.5 yr from discharge was used for the TP fuel. Linear interpolation was applied to correct the tabulated ORIGEN-2 data for age and burnup. A factor of 0.8815 was then used to convert the inventories from a "per gram metal" basis to a "per gram fuel" basis. The resulting per gram fuel radionuclide inventories are given in Table 2.3 of the text. Specimen weights required for calculating per specimen radionuclide inventories are contained in Table 2.1 of the text.

A.2 RADIOCHEMICAL DATA

Results from uranium analyses were generally reported in μg/mL (ppm) units. Results for other radiochemical analyses were generally reported as disintegrations per minute (dpm) per mL of solution. Rod sample results were reported as dpm/rod (μg/rod for uranium). Data were converted from dpm to pCi units using the conversion factor of 1 pCi = 2.2 dpm. Concentrations were calculated from the pCi/mL data using Equations (A.1) and (A.2). The μg/pCi and isotope/element conversion factors for Equation (A.1) are contained in Table A.1. The radiochemical results for all sample analyses in pCi units (μg units for uranium) are given for each cycle of both tests in Tables A.2 through A.7 of this appendix.

9079414 57

TABLE A.1. Activity-Concentration Conversion Factors

Radionuclide	(μg/pCi)	Turkey Point[a]	H. B. Robinson[a]
^{14}C	2.24 E-7	--	--
^{60}Co	8.82 E-10	--	--
^{90}Sr	7.07 E-9	0.546	0.546
^{99}Tc	5.87 E-5	1.000	1.000
^{126}Sn	3.52 E-7	0.30	0.30
^{129}I	6.13 E-3	0.76	0.76
^{137}Cs	1.16 E-8	0.40	0.40
^{237}Np	1.42 E-3	0.999	0.999
^{238}Pu	5.72 E-8	0.012	0.014
^{239}Pu	1.63 E-5	0.595	0.577
^{240}Pu	4.41 E-6	0.255	0.263
^{241}Am	3.09 E-7	0.863	0.840
^{244}Cm	1.20 E-8	0.930	0.926

(a) Isotope-to-element mass ratio based on ORIGEN-2 data in PNL-5109[A1] interpolated to 27.7 MWd/kgM for Turkey Point and 30.2 MWd/kgM for H. B. Robinson burnup, at 10.5 and 12 yr after discharge, respectively.

$$\text{Elemental Concentration } (\mu g/mL) = \frac{\text{Activity } (pCi/mL) \times (\mu g/pCi)}{\text{isotope/element}} \quad (A.1)$$

For conversion to molarity:

$$\text{Molarity } (mole/L) = \frac{\mu g/mL}{1000 \times \text{atomic mass}} \quad (A.2)$$

For calculation of plutonium concentration from $^{239+240}Pu$ pCi/mL data using Equation (A.1), the ^{239}Pu (or ^{240}Pu) pCi/mL value is needed. The $^{239}Pu/^{239+240}Pu$ activity ratio should be 0.374 for the HBR fuel and 0.389 for the TP fuel based on the PNL-5109[A1] ORIGEN-2 data.

9 0 7 9 4 1 4 5 8

TABLE A.2. HBR/BF-25 (C5C-I) Cycles 1, 2 & 3 (pCi)

DAY	SAMPLE TYPE	VOLUME ml	pH	U UNFILTER	U 0.4 um	U 10 A	Pu-239-Pu-240 UNFILTER	Pu-239-Pu-240 0.4 um	Pu-239-Pu-240 10 A	Am-241-Pu-238 UNFILTER	Am-241-Pu-238 0.4 um	Am-241-Pu-238 10 A	Am-241 UNFILTER	Am-241 0.4 um	Am-241 10 A	Cm-244 UNFILTER	Cm-244 0.4 um	Cm-244 10 A	Cs-137 UNFILTER	Cs-137 0.4 um	Cs-137 10 A	Cs-134 UNFILTER	Cs-134 0.4 um	Cs-134 10 A
1	Sol	15	8.63	1.38E-01	1.26E-01	1.29E-01	1.23E-04	1.23E-04	6.62E-03	5.99E-04	5.95E-04	3.07E-04	2.68E-04	2.72E-04	9.37E-03	2.74E-04	2.84E-04	1.17E-04	1.46E-06	1.46E-06	1.41E-06	4.95E-06	4.91E-06	4.86E-06
7	Sol	15	7.88	1.29E-01	1.18E-01	1.29E-01	9.48E-03	8.29E-03	3.98E-03	4.45E-04	4.17E-04	1.69E-04	1.92E-04	1.09E-04	6.38E-03	2.16E-04	1.98E-04	7.16E-03	1.48E-06	1.41E-06	1.35E-06	4.86E-06	4.95E-06	4.73E-06
14	Sol	29	7.53	5.06E-00	5.20E-00	5.70E-00	6.49E-03	6.48E-03	2.85E-03	2.06E-04	2.71E-04	9.99E-03	1.11E-04	1.65E-04	1.97E-03	1.18E-04	1.08E-04	2.38E-03	1.38E-06	1.37E-06	1.32E-06	4.96E-06	4.86E-06	4.64E-06
33	Sol	30	8.44	6.78E-01	7.30E-01	5.08E-01	3.24E-03	2.94E-03	8.56E-02	1.49E-04	1.31E-04	2.53E-03	6.17E-03	5.23E-03	3.06E-02	6.56E-03	5.36E-03	2.03E-02	1.38E-06	1.37E-06	1.31E-06	4.58E-06	4.58E-06	4.33E-06
62	Sol	30	7.65	2.00E-01	2.00E-01	1.78E-01	2.10E-03	1.91E-03	4.48E-02	9.56E-03	8.38E-03	1.34E-03	4.02E-03	3.45E-03	1.61E-02	4.09E-03	3.43E-03	2.13E-02	1.19E-06	1.29E-06	1.19E-06	3.63E-06	3.79E-06	3.86E-06
62	Syringe	15		1.18E-02			3.74E-01			1.86E-02			1.48E-02			1.86E-02								
119	Sol	30	7.85	2.30E-01	2.00E-01	1.08E-01	1.52E-03	1.23E-03	2.31E-02	6.94E-03	5.01E-03	6.03E-02	3.08E-03	2.64E-03	1.44E-02	3.23E-03	2.03E-03	1.47E-02	9.91E-07	9.02E-07	9.68E-07	3.84E-06	3.14E-06	3.84E-06
147	Sol	16	7.77	2.29E-01	1.90E-01		1.11E-03	9.64E-02		5.58E-03	4.58E-03					2.73E-03	2.25E-03							
174	Sol	250	7.95	2.68E-01	2.38E-01	2.08E-01	9.86E-02	9.14E-02	1.75E-02	4.01E-03	4.31E-03	6.17E-02	2.47E-03	1.97E-03	1.48E-02	2.46E-03	2.85E-03	1.62E-02	8.33E-07	8.69E-07	8.42E-07	2.42E-06	2.49E-06	2.45E-06
174	Strip	300		1.35E-00			5.09E-03			4.13E-04			2.79E-04			3.83E-04			2.05E-05			6.98E-03		
174	Rinse	600			6.68E-01			3.14E-02			1.18E-03			4.85E-02			4.85E-02			2.22E-00			8.49E-04	
CYCLE 2																								
1	Sol	15	8.33	6.00E-01	5.90E-01	3.70E-01	1.22E-02	1.00E-02	6.13E-01	4.32E-02	3.72E-02	1.08E-02	2.86E-02	9.95E-01	9.46E-00	1.38E-02	9.82E-01	9.91E-00	4.49E-06	4.40E-06	4.24E-06	1.24E-05	1.29E-05	1.19E-05
7	Sol	15	8.13	9.16E-01	8.30E-01	7.70E-01	1.14E-02	1.01E-02	6.04E-01	4.29E-02	3.44E-02	1.84E-02	1.57E-02	8.07E-01	6.76E-00	1.42E-02	9.23E-01	6.76E-00	5.63E-06	5.54E-06	5.27E-06	1.62E-05	1.53E-05	1.49E-05
14	Sol	30	8.31	8.00E-01	8.40E-01	8.10E-01	9.02E-01	1.02E-02	5.68E-01	3.50E-02	3.41E-02	1.55E-02	1.11E-02	1.02E-02	7.21E-00	1.23E-02	1.00E-02	9.46E-00	6.00E-06	5.63E-06	5.59E-06	1.84E-05	1.00E-05	1.56E-05
34	Sol	30	8.15	5.10E-01	5.00E-01	4.90E-01	8.51E-01	7.88E-01	4.68E-01	3.17E-02	2.60E-02	1.24E-02	9.91E-01	8.94E-01	3.68E-00	1.12E-02	7.43E-01	4.58E-00	5.45E-06	5.27E-06	5.32E-06	1.49E-05	1.45E-05	1.55E-05
62	Sol	29	8.00	4.10E-01	4.20E-01		7.70E-01	7.25E-01		2.90E-02	2.56E-02		9.19E-01	8.07E-01		1.18E-02	8.11E-01		5.10E-06	5.14E-06		1.48E-05	1.41E-05	
120	Sol	29	7.81	3.90E-01	3.56E-01		7.40E-01	5.90E-01		3.70E-02	1.99E-02		1.71E-02	4.73E-01		2.46E-02	8.29E-01		5.97E-06	5.80E-06		1.37E-05	1.46E-05	
181	Sol	250	8.04	2.90E-01	2.06E-01		8.24E-01	7.07E-01		4.02E-02	3.37E-02		2.06E-02	1.55E-02		2.85E-02	2.15E-02		5.41E-06	5.32E-06		1.30E-05	1.25E-05	
181	Rinse	600			9.68E-01			3.68E-02			1.19E-03			3.98E-02			3.15E-02			2.14E-05			4.77E-03	
181	Strip	300		5.30E-01			1.43E-03			1.05E-04			8.76E-03			7.61E-03			7.48E-04			1.02E-03		
CYCLE 3																								
28	Sol	25	8.01	2.90E-01	3.00E-01		1.02E-02	0.53E-01		3.63E-02	2.18E-02		1.08E-02	5.81E-01		1.19E-02	1.59E-02		1.19E-06	1.18E-06		2.08E-04	2.78E-04	
55	Sol	25	7.78	3.78E-01	3.38E-01		5.68E-01	6.44E-01		2.12E-02	1.08E-02		1.51E-02	7.68E-01		9.65E-01	6.99E-01		1.68E-06	1.61E-06		3.06E-04	3.75E-04	
97	Sol	250	7.92	3.00E-01	3.00E-01		9.18E-01	6.44E-01		3.02E-02	2.45E-02		1.55E-02	8.78E-01		2.13E-02	1.24E-02		1.92E-06	1.91E-06		4.09E-04	4.17E-04	
97	Rinse	600			1.18E-00			3.71E-02			1.46E-03			5.32E-02			4.65E-02			1.00E-05			2.38E-03	
97	Strip	300		8.38E-02			1.78E-03			9.28E-03			5.45E-03			5.18E-03			7.48E-04			1.71E-03		

DAY	SAMPLE TYPE	VOLUME ml	pH	Co-60 UNFILTER	Co-60 0.4 um	Co-60 10 A	SrY-90 UNFILTER	SrY-90 0.4 um	SrY-90 10 A	Np-237 UNFILTER	Np-237 0.4 um	Np-237 10 A	Tc-99 UNFILTER	Tc-99 0.4 um	Tc-99 10 A	Sn-126 UNFILTER	Sn-126 0.4 um	Sn-126 10 A	C-14 UNFILTER	C-14 0.4 um	C-14 10 A	I-129 UNFILTER	I-129 0.4 um	I-129 10 A
1	Sol	15	8.63										2.03E-02											
7	Sol	15	7.88				4.95E-06						2.04E-02											
14	Sol	29	7.53							4.50E-00	3.92E-00	3.78E-00	3.09E-02	3.42E-02	3.56E-02				1.02E-02					
33	Sol	30	8.44							1.26E-00	1.31E-00	1.72E-00	4.46E-02	4.50E-02	4.50E-02	9.01E-01	8.11E-01	(2.70E-01	2.14E-02					
62	Sol	30	7.65		2.45E-04		5.99E-00			8.31E-01	8.31E-01	8.31E-01	4.95E-02	4.95E-02	4.95E-02	1.00E-00	9.01E-01	(2.25E-01	4.63E-02			4.14E-01		
62	Syringe	15																						
119	Sol	30	7.85							2.70E-01	(2.25E-01	6.75E-01	5.72E-02	5.54E-02	5.54E-02	8.31E-01	7.66E-01	4.50E-01						
147	Sol	16	7.77											5.63E-02										
174	Sol	250	7.95	2.09E-04	1.95E-04		4.36E-06			2.25E-01	2.70E-01	3.60E-01	5.13E-02	5.04E-02	6.00E-02	3.06E-01	5.85E-01	4.85E-01	3.08E-02			3.47E-01		
174	Strip	300		2.26E-03			1.23E-05			4.50E-01			1.53E-01			1.72E-00						5.59E-02		
174	Rinse	600						1.53E-05			2.70E-01			1.71E-01			(2.25E-01							
CYCLE 2																								
1	Sol	15	8.33			4.38E-02							(9.01E-00											
7	Sol	15	8.13				6.58E-05						2.26E-01											
14	Sol	30	8.31			1.17E-03				(2.25E-01	3.15E-01	2.25E-01	4.95E-01	4.85E-01	4.23E-01	(2.25E-01	NC	NC	5.85E-01					
34	Sol	30	8.15	1.15E-03						2.25E-01	3.60E-01	3.15E-01	5.86E-01	5.41E-01	4.50E-01	(2.25E-01	NC	NC						
62	Sol	29	8.00	1.38E-03	1.52E-03		9.59E-05			3.15E-01	5.41E-01		9.91E-01	9.46E-01		(2.25E-01	NC		2.52E-01			2.22E-02		
120	Sol	29	7.81	2.13E-03	2.56E-03		1.04E-00			1.06E-01	2.25E-01		1.49E-02	1.68E-02		(2.25E-01	NC		3.02E-02					
181	Sol	250	8.04	2.07E-03	2.26E-03		9.91E-05			2.25E-01	1.00E-01		2.25E-02	2.25E-02		(1.35E-01	NC		3.56E-02			1.48E-02		
181	Rinse	600						5.23E-04			3.15E-01			6.76E-00			(2.70E-01							
181	Strip	300		5.77E-02			4.02E-04			2.70E-01			(4.50E-00			5.41E-01								
CYCLE 3																								
28	Sol	25	8.01		4.04E-02		4.73E-05			2.70E-01	2.25E-01		6.76E-01	6.76E-01		(2.25E-01	NC		4.32E-01					
55	Sol	25	7.78	8.51E-02	8.78E-02		6.53E-05			1.35E-01	9.01E-02		1.26E-02	1.35E-02		(2.25E-01	(2.25E-01		1.22E-02			6.04E-02		
97	Sol	250	7.92				7.84E-05	7.84E-05		2.70E-01	2.25E-01		2.34E-02	2.34E-02		(1.35E-01	NC		2.07E-02			6.20E-02		
97	Rinse	600						3.89E-04			3.60E-01			(9.01E-00			(1.35E-01			8.31E-00			1.34E-02	
97	Strip	300		1.92E-02			6.23E-04			3.15E-01			(9.01E-00			7.66E-01								

UNITS: In pCi/ml for all but Uranium, ug/ml for Uranium.

NC: Not counted because unfiltered fraction was less than detectable.

9 0 7 9 4 1 4 5 9

TABLE A.3. TP/BF-85 (F6-2B) Cycles 1, 2 & 3 (pCi)

DAY	SAMPLE TYPE	VOLUME ml	pH	U UNFILTER	U 0.4 um	U 18 A	Pu-239+Pu-240 UNFILTER	Pu-239+Pu-240 0.4 um	Pu-239+Pu-240 18 A	Am-241+Pu-238 UNFILTER	Am-241+Pu-238 0.4 um	Am-241+Pu-238 18 A	Am-241 UNFILTER	Am-241 0.4 um	Am-241 18 A	Cm-244 UNFILTER	Cm-244 0.4 um	Cm-244 18 A	Cs-137 UNFILTER	Cs-137 0.4 um	Cs-137 18 A	Cs-134 UNFILTER	Cs-134 0.4 um	Cs-134 18 A
1	Sol	15	0.84	1.18E-00	1.18E-00	1.18E-00	3.74E-03	2.69E-03	1.29E-02	1.78E-04	1.12E-04	2.08E-02	8.88E-03	5.01E-03	3.51E-01	8.08E-03	5.18E-03	3.33E-01	7.34E-07	7.39E-07	6.98E-07	3.02E-06	3.91E-06	3.54E-06
7	Sol	15	0.29	8.39E-00	8.08E-00	7.08E-00	1.08E-03	5.32E-02	6.68E-01	4.18E-03	2.12E-03	1.05E-02	2.98E-03	1.17E-03	2.05E-01	1.74E-03	8.51E-02	4.95E-01	7.34E-07	7.35E-07	6.99E-07	3.78E-06	3.72E-06	3.52E-06
14	Sol	29	0.15	3.98E-00	3.90E-00	3.18E-00	4.95E-02	3.08E-02	9.55E-01	1.68E-03	1.17E-03	1.65E-02	8.39E-02	4.19E-02	4.95E-00	4.73E-02	3.45E-02	3.08E-00	6.89E-07	6.88E-07	6.68E-07	3.52E-06	3.45E-06	3.41E-06
33	Sol	38	0.19	8.48E-01	7.39E-01	7.08E-01	1.13E-02	8.76E-01	3.68E-01	3.03E-02	1.44E-02	7.21E-01	1.17E-02	2.60E-01	8.78E-01	7.39E-01	1.49E-01	(4.58E-01	5.35E-07	5.48E-07	5.61E-07	3.14E-06	3.25E-06	2.89E-06
62	Sol	39	7.91	4.48E-01	3.09E-01	2.08E-01	1.08E-01	1.35E-01	1.44E-01	4.01E-01	2.39E-01	2.25E-01	1.49E-01	3.08E-00	2.78E-00	8.56E-00	1.35E-00	(4.58E-01	5.72E-07	5.88E-07	5.68E-07	2.76E-06	2.85E-06	2.74E-06
119	Sol	30	0.01	4.08E-01	4.28E-01	3.98E-01	9.46E-00	4.58E-00	4.23E-00	2.07E-01	0.01E-00	7.05E-00	1.31E-01	4.56E-01	(2.25E-01	1.04E-01	5.06E-01	(2.25E-01	5.27E-07	5.27E-07	5.65E-07	2.36E-06	2.43E-06	2.32E-06
147	Sol	10	0.02	4.06E-01	3.48E-01		4.95E-00	3.08E-00		9.91E-00	8.81E-00					2.25E-00	4.85E-01							
174	Sol	250	0.07	4.08E-01	3.38E-01	3.28E-01	8.56E-00	4.05E-00	1.35E-00	3.39E-01	8.11E-00	2.70E-00	1.76E-01	4.05E-01	1.08E-01	1.04E-01	9.01E-01	9.01E-02	4.77E-07	4.68E-07	4.68E-07	2.09E-06	2.12E-06	2.16E-06
174	Strip	300		2.11E-01			1.18E-04			5.58E-04			3.22E-04			2.54E-04			8.15E-00			3.08E-05		
174	Rinse	600			1.08E-01			4.65E-01			1.15E-02			7.84E-01			4.91E-01			1.29E-05			5.32E-04
CYCLE 2																								
1	Sol	15	0.36	1.67E-00	4.18E-01	2.29E-01	3.92E-00	2.39E-00	9.01E-01	1.31E-01	8.56E-00	1.08E-00	5.59E-01	4.95E-00	(1.35E-01	4.95E-00	3.51E-00	(9.01E-02	4.82E-05	4.80E-05	4.84E-05	2.62E-04	2.15E-04	2.81E-04
7	Sol	15	0.15	3.68E-01	9.38E-03	3.39E-01	8.31E-00	1.44E-00	1.56E-00	2.05E-01	8.39E-00	2.70E-00	2.48E-01	5.41E-01	(1.35E-01	1.08E-01	5.41E-01	(9.01E-02	7.78E-05	7.93E-05	7.43E-05	3.19E-04	3.31E-04	3.24E-04
14	Sol	30	7.95	2.68E-01	2.68E-01	2.08E-01	1.35E-00	2.79E-00	1.46E-00	3.39E-00	8.11E-00	2.25E-00	1.22E-00	3.08E-01	(1.35E-01	7.21E-01	2.38E-00	(9.01E-02	1.12E-05	1.18E-05	1.08E-05	4.77E-04	4.77E-04	4.59E-04
34	Sol	30	0.10	2.18E-01	1.79E-01	1.78E-01	1.08E-00	1.35E-00	1.13E-00	5.41E-00	2.25E-00	1.08E-00	2.13E-00	1.08E-01	(1.08E-01	1.68E-00	1.08E-01	(9.01E-02	1.88E-05	1.63E-05	1.78E-05	7.84E-04	7.84E-04	7.25E-04
62	Sol	29	0.23	1.08E-01	1.79E-01		9.91E-01	9.91E-01		2.39E-00	1.08E-00		9.91E-01	2.79E-01		4.05E-01	1.35E-01		2.58E-05	2.53E-05		1.65E-05	1.02E-05	
120	Sol	29	0.03	1.68E-01	1.18E-01		8.76E-01	8.76E-01		1.67E-00	1.08E-00		5.41E-01	(2.25E-01		2.70E-01	(1.35E-01		4.65E-06	4.00E-00		1.04E-05	1.55E-05	
181	Sol	250	0.30	1.28E-01	1.38E-01		8.56E-01	6.31E-01		2.70E-00	1.53E-00		1.17E-00	2.78E-01		8.11E-01	1.35E-01		4.64E-06	4.95E-05		1.78E-05	1.87E-05	
181	Rinse	600			1.18E-01			2.84E-01			1.92E-02			4.77E-01			3.89E-01			9.19E-04			3.45E-03	
181	Strip	300		2.78E-00			4.08E-03			1.09E-04			8.26E-03			7.21E-03			2.78E-05			9.65E-03		
CYCLE 3																								
29	Sol	25	0.21	2.38E-01	2.08E-01		8.56E-00	1.17E-00		3.38E-01	1.98E-00		9.01E-00	3.15E-01		1.35E-01	1.35E-01		5.38E-05	5.48E-05		1.93E-04	1.99E-04	
55	Sol	25	0.29	2.68E-01	2.38E-01		3.24E-00	9.01E-01		1.22E-01	1.94E-00		9.01E-00	3.15E-01		4.23E-00	2.25E-01		1.16E-00	1.15E-00		4.84E-04	3.81E-04	
97	Sol	250	0.33	2.08E-01	1.68E-01		9.01E-01	8.11E-01		2.34E-00	1.48E-00		8.56E-01	1.35E-01		3.15E-01	(9.01E-02		1.78E-00	1.71E-00		5.64E-04	6.77E-04	
97	Rinse	600			1.38E-01			5.14E-01			1.05E-02			1.02E-02			7.03E-01			5.38E-04			1.87E-03	
97	Strip	300		1.68E-00			2.73E-03			1.12E-04			8.04E-03			4.13E-03			1.98E-05			6.84E-03		

DAY	SAMPLE TYPE	VOLUME ml	pH	Co-60 UNFILTER	Co-60 0.4 um	Co-60 18 A	Sr-90 UNFILTER	Sr-90 0.4 um	Sr-90 18 A	Np-237 UNFILTER	Np-237 0.4 um	Np-237 18 A	Tc-99 UNFILTER	Tc-99 0.4 um	Tc-99 18 A	Sn-126 UNFILTER	Sn-126 0.4 um	Sn-126 18 A	C-14 UNFILTER	C-14 0.4 um	C-14 18 A	I-129 UNFILTER	I-129 0.4 um	I-129 18 A
1	Sol	15	0.84			2.27E-04							2.97E-02											
7	Sol	15	0.29	4.77E-04	5.64E-04	3.67E-04	1.68E-06						3.26E-02											
14	Sol	29	0.15							2.75E-00	2.61E-00	2.79E-00	3.61E-02	3.78E-02	3.38E-02				1.19E-03					
33	Sol	30	0.19							1.63E-00	1.63E-00	1.35E-00	5.36E-02	5.58E-02	5.27E-02	(2.78E-01	3.15E-01	(2.78E-01	1.01E-03					
62	Sol	30	7.91				1.95E-06			8.56E-01	9.91E-01	8.11E-01	9.01E-02	9.01E-02	9.01E-02	IS	IS	IS	3.85E-03			4.18E-00		
119	Sol	30	0.01							1.13E-00	1.17E-00	1.17E-00	1.65E-03	1.71E-03	1.64E-03	(2.70E-01	NC	NC						
147	Sol	10	0.02											1.95E-03										
174	Sol	250	0.07				7.21E-05			5.05E-01	6.11E-01	4.58E-01	2.48E-03	2.34E-03	2.43E-03	(2.78E-01	NC	NC	5.95E-03			6.09E-00		
174	Strip	300		5.14E-05			3.72E-00			4.14E-00			4.18E-01			7.05E-00						2.58E-01		
174	Rinse	600			2.23E-03			1.73E-05			(2.25E-01			4.03E-01			(2.25E-01							
CYCLE 2																								
1	Sol	15	0.36	1.92E-03	1.33E-03	1.07E-03							(9.01E-00											
7	Sol	15	0.15	2.01E-03	2.29E-03	1.84E-03	6.05E-05						5.61E-01											
14	Sol	30	7.95	2.19E-03	1.65E-03	1.43E-03				5.41E-01	2.25E-01	(2.25E-01	9.01E-01	9.01E-01	9.91E-01	(2.25E-01	(2.25E-01	NC	4.72E-02					
34	Sol	30	0.10	2.65E-03	2.76E-03	2.63E-03				2.78E-01	3.15E-01	1.08E-01	2.43E-02	2.34E-02	2.34E-02	3.15E-01	(2.25E-01							
62	Sol	29	0.23	1.35E-03	1.48E-03		1.21E-06			3.15E-01	3.15E-01		4.05E-02	4.05E-02		(2.25E-01	NC		1.73E-03			9.33E-01		
120	Sol	29	0.03	1.65E-03			1.38E-06			5.05E-01	(2.25E-01		7.67E-02	8.02E-02		2.78E-01	(1.35E-01		2.52E-03					
181	Sol	250	0.30				1.39E-06			9.01E-02	1.35E-01		1.83E-03	1.98E-03		(2.78E-01	NC		2.66E-03			1.87E-00		
181	Rinse	600			2.34E-02			6.68E-04			(9.01E-02			1.88E-01			(2.25E-01							
181	Strip	300		4.38E-04			2.65E-05			1.67E-00			2.16E-01			4.32E-00								
CYCLE 3																								
29	Sol	25	0.21	5.98E-02	4.68E-02		4.41E-05			1.35E-01	1.35E-01		1.46E-02	1.49E-02		2.78E-01	NC		3.11E-02					
55	Sol	25	0.29	5.68E-02			5.63E-05			(9.01E-02	1.35E-01		3.24E-02	3.38E-02		(2.25E-01	NC		7.21E-02			6.95E-01		
97	Sol	250	0.33				6.26E-05	6.35E-05		1.35E-01	4.68E-02		5.41E-02	5.41E-02		(1.35E-01	NC		9.46E-02			9.15E-01		
97	Rinse	600			2.97E-02			4.88E-04			4.68E-02			(9.01E-00			(1.35E-01			2.97E-01			1.49E-02	
97	Strip	300		9.95E-03			2.08E-05			4.95E-01			1.88E-01			2.78E-00								

UNITS: Solution samples (Sol) in dpm/ml for all but Uranium, ug/ml for Uranium.

NC: Not counted because unfiltered fraction was less than detectable.
IS: Insufficient Sample

90794 1460

TABLE A.4. HBR/BF-85 (C5C-K) Cycles 1, 2 & 3 (pCi)

DAY	SAMPLE TYPE	VOLUME ml	pH	U UNFILTER	U 0.4 um	U 10 A	Pu-239+Pu-240 UNFILTER	Pu-239+Pu-240 0.4 um	Pu-239+Pu-240 10 A	Am-241+Pu-239 UNFILTER	Am-241+Pu-239 0.4 um	Am-241+Pu-239 10 A	Am-241 UNFILTER	Am-241 0.4 um	Am-241 10 A	Cm-244 UNFILTER	Cm-244 0.4 um	Cm-244 10 A	Cs-137 UNFILTER	Cs-137 0.4 um	Cs-137 10 A	Cs-134 UNFILTER	Cs-134 0.4 um	Cs-134 10 A
1	Sol	15	8.02	1.60E-00	1.78E-00	1.78E-00	2.07E-04	1.97E-04	7.48E-02	9.06E-04	8.61E-04	2.64E-03	3.83E-04	3.03E-04	6.85E-02	3.77E-04	3.41E-04	8.15E-02	1.73E-00	1.74E-00	1.66E-00	6.17E-06	6.08E-06	6.90E-06
7	Sol	15	8.15	1.60E-01	1.56E-01	1.10E-01	7.30E-03	3.68E-03	3.18E-02	2.90E-04	1.62E-04	9.32E-02	1.11E-04	4.66E-03	1.68E-02	9.77E-03	5.77E-03	1.63E-02	1.02E-00	1.03E-00	1.03E-00	5.83E-06	5.72E-06	5.41E-06
14	Sol	29	7.91	1.16E-01	1.16E-01	8.29E-00	2.76E-03	1.45E-03	1.91E-02	1.05E-04	5.64E-03	5.08E-02	3.08E-03	1.08E-03	8.05E-01	3.63E-03	1.72E-03	9.19E-01	1.62E-00	1.48E-00	1.43E-00	5.36E-06	5.18E-06	4.01E-06
33	Sol	30	8.24	5.46E-00	5.25E-00	3.00E-00	6.85E-03	4.02E-03	1.40E-02	2.64E-04	1.06E-04	3.00E-02	9.55E-03	5.76E-03	3.34E-01	8.36E-03	6.04E-03	1.63E-01	1.30E-00	1.33E-00	1.29E-00	4.60E-06	4.45E-06	4.22E-06
62	Sol	30	8.15	4.90E-01	4.48E-01	4.00E-01	1.23E-03	9.28E-02	1.29E-02	4.03E-03	3.17E-03	3.29E-02	1.00E-03	8.00E-02	(1.35E-00	1.00E-03	8.50E-02	4.00E-00	1.35E-00	1.34E-00	1.22E-00	4.43E-06	4.35E-06	4.24E-06
62	Syringe	15		7.00E-03			1.04E-01			2.93E-01			1.00E-01			1.17E-01								
119	Sol	25	7.79	1.29E-01	5.50E-02	2.00E-02	1.02E-03	9.05E-02	1.31E-00	9.19E-03	4.55E-03	4.05E-00	4.46E-03	2.14E-03	6.70E-00	4.08E-03	2.29E-03	3.30E-00	1.22E-00	1.27E-00	1.25E-00	4.19E-06	3.92E-06	3.79E-06
147	Sol	18	7.67	1.29E-02	1.00E-02		1.17E-02	6.63E-01		6.71E-02	4.60E-02					3.83E-02	2.80E-02							
174	Sol	250	7.92	1.00E-02	2.20E-02	1.00E-02	2.42E-01	5.70E-00	9.01E-02	1.29E-02	3.02E-01	1.00E-01	6.85E-01	1.49E-01	(1.35E-01	5.77E-01	1.40E-01	(4.50E-02	1.12E-00	1.16E-00	1.10E-00	3.25E-06	3.22E-06	3.29E-06
174	Strip	300		1.65E-01			1.80E-04			9.50E-04			5.27E-04			5.16E-04			5.50E-06			1.52E-05		
174	Rinse	600			5.50E-01			1.02E-02			6.31E-02			2.52E-02			2.23E-02			1.61E-00			5.14E-04	
CYCLE 2																								
1	Sol	15	8.34	3.05E-00	3.02E-00	3.02E-00	9.91E-00	5.00E-00	1.17E-00	3.56E-01	3.15E-01	2.04E-00	1.73E-02	1.49E-01	9.01E-02	1.26E-01	1.49E-01	1.00E-01	2.25E-00	2.20E-00	2.20E-00	8.35E-04	8.53E-04	8.22E-04
7	Sol	15	8.20	7.00E-01	7.10E-01	6.50E-01	1.12E-01	8.31E-00	8.50E-00	3.03E-01	1.63E-01	1.70E-01	3.35E-01	7.21E-01	3.00E-01	1.35E-01	9.01E-01	1.35E-01	3.44E-00	2.40E-00	2.27E-00	8.00E-04	8.71E-04	8.35E-04
14	Sol	30	8.33	3.10E-01	3.00E-01	3.40E-01	5.00E-00	4.60E-00	4.90E-00	1.63E-01	1.25E-01	1.17E-01	2.03E-00	4.50E-01	(1.35E-01	2.07E-00	7.91E-01	9.01E-02	2.50E-00	2.50E-00	2.45E-00	7.83E-04	7.43E-04	8.71E-04
34	Sol	30	8.34	2.00E-01	1.90E-01	1.70E-01	2.97E-00	2.39E-00	2.40E-00	9.40E-00	6.31E-00	5.41E-00	3.11E-00	4.05E-01	(1.00E-01	2.75E-00	6.81E-01	(9.01E-02	2.71E-00	2.02E-00	2.50E-00	7.34E-04	7.30E-04	6.85E-04
62	Sol	29	8.30	1.40E-01	1.40E-01		1.62E-00	1.71E-00		6.31E-00	4.05E-00		1.31E-00	(1.35E-01		1.13E-00	4.50E-01		2.63E-00	2.79E-00		7.94E-04	7.25E-04	
120	Sol	29	8.02	1.10E-01	1.30E-01		1.04E-00	1.67E-00		5.00E-00	3.20E-00		1.44E-00	(2.25E-01		1.20E-00	1.35E-01		3.43E-00	3.49E-00		9.26E-04	8.00E-04	
181	Sol	250	8.17	1.10E-01	1.20E-01		2.07E-00	1.71E-00		6.31E-00	4.14E-00		2.25E-00	4.50E-01		1.53E-00	2.70E-01		4.00E-00	4.13E-00		9.77E-04	1.01E-05	
181	Rinse	600			1.30E-01			6.59E-01			2.46E-02			1.00E-02			1.05E-02			9.28E-04			2.22E-03	
181	Strip	300		8.20E-00			5.37E-03			2.71E-04			1.54E-04			1.44E-04			4.77E-06			1.17E-04		
CYCLE 3																								
20	Sol	25	8.19	1.70E-01	1.70E-01		2.12E-01	1.00E-00		9.19E-01	2.57E-00		1.04E-01	2.25E-01		3.65E-01	1.00E-01		5.05E-05	5.77E-05		1.43E-04	1.35E-04	
55	Sol	25	8.11	1.00E-01	2.10E-01		2.10E-00	1.13E-00		8.56E-00	2.70E-00		4.95E-00	3.00E-01		2.04E-00	2.25E-01		1.25E-05	1.24E-05		2.74E-04	2.77E-04	
97	Sol	250	8.35	1.00E-01	1.00E-01		2.43E-00	1.84E-00		9.40E-00	2.52E-00		5.41E-00	1.00E-01		3.56E-00	1.35E-01		2.09E-05	2.11E-05		4.77E-04	4.77E-04	
97	Rinse	600			1.40E-01			4.37E-01			2.16E-02			1.05E-02			8.70E-01			4.37E-04			9.56E-02	
97	Strip	300		8.10E-01			8.42E-04			3.07E-05			1.75E-05			1.16E-05			6.00E-05			1.33E-05		
97	Strip	Resample		4.34E-02						Alpha = 2.56E-05														

DAY	SAMPLE TYPE	VOLUME ml	pH	Co-60 UNFILTER	Co-60 0.4 um	Co-60 10 A	SrY-90 UNFILTER	SrY-90 0.4 um	SrY-90 10 A	Np-237 UNFILTER	Np-237 0.4 um	Np-237 10 A	Tc-99 UNFILTER	Tc-99 0.4 um	Tc-99 10 A	Sn-126 UNFILTER	Sn-126 0.4 um	Sn-126 10 A	C-14 UNFILTER	C-14 0.4 um	C-14 10 A	I-129 UNFILTER	I-129 0.4 um	I-129 10 A
1	Sol	15	8.02										4.19E-02											
7	Sol	15	8.15				3.30E-00						4.23E-02											
14	Sol	29	7.91							1.04E-01	1.00E-01	1.20E-01	4.04E-02	4.50E-02	4.23E-02				3.00E-02					
33	Sol	30	8.24							5.00E-00	5.41E-00	5.41E-00	4.00E-02	4.04E-02	4.77E-02	1.44E-00	1.25E-00	(2.25E-01	5.22E-02					
62	Sol	30	8.15				4.04E-00			1.13E-00	9.91E-01	1.04E-00	5.00E-02	5.00E-02	5.00E-02	(2.25E-01	4.05E-01	(2.70E-01	8.50E-02			1.03E-00		
62	Syringe	15																						
119	Sol	25	7.79							(2.25E-01	(2.25E-01	(2.25E-01	1.44E-01	9.01E-00	1.04E-01	4.50E-01	(2.70E-01							
147	Sol	18	7.67											(2.40E-01										
174	Sol	250	7.92				1.77E-00			(2.25E-01	(2.25E-01	(2.25E-01	(9.01E-00	(9.01E-00	(9.01E-00	(2.25E-01	NC	NC	8.55E-02			2.48E-01		
174	Strip	300		1.02E-04			2.00E-05			4.95E-00			8.11E-01			5.41E-00						2.13E-01		
174	Rinse	600						1.90E-05			(2.25E-01			3.74E-01			(2.25E-01							
CYCLE 2																								
1	Sol	15	8.34										3.15E-02											
7	Sol	15	8.20				3.07E-05						5.00E-02											
14	Sol	30	8.33							8.11E-01	5.41E-01	4.05E-01	5.10E-02	4.95E-02	4.00E-02	(2.25E-01	(2.25E-01	NC	1.00E-02					
34	Sol	30	8.34							4.00E-01	1.00E-01	2.70E-01	5.00E-02	5.00E-02	5.41E-02	(2.25E-01	NC	NC						
62	Sol	29	8.30				3.13E-00			3.15E-01	3.00E-01		8.31E-02	6.76E-02		(2.25E-01	NC		2.40E-02			6.75E-01		
120	Sol	29	8.02				2.24E-00			1.35E-01	3.15E-01		0.00E-02	1.03E-03		(2.25E-01	(1.35E-01		1.35E-01					
181	Sol	250	8.17				1.00E-00			3.15E-01	9.01E-02		1.49E-03	1.44E-03		(2.70E-01	NC		3.38E-02			3.72E-00		
181	Rinse	600						1.10E-05			(9.01E-02			1.90E-01			(2.25E-01							
181	Strip	300		1.10E-03			1.50E-00			2.21E-00			3.30E-01			4.23E-00								
CYCLE 3																								
20	Sol	25	8.19				5.50E-05			1.00E-01	9.01E-02		2.34E-02	2.43E-02		(2.25E-01	NC		4.77E-01					
55	Sol	25	8.11				5.72E-05			(9.01E-02	1.00E-01		5.41E-02	5.41E-02		(2.25E-01	NC		1.17E-02			0.16E-01		
97	Sol	250	8.35	1.10E-03	0.42E-02		0.13E-05	0.13E-05		1.35E-01	1.35E-01		9.01E-02	9.01E-02		(1.35E-01	NC		1.50E-02			1.74E-00		
97	Rinse	600						3.00E-04			(4.50E-02			1.00E-01			(1.35E-01			5.41E-00			1.22E-02	
97	Strip	300					4.05E-00			2.03E-01			6.31E-02			1.05E-01								

UNITS: In pCi/ml for all but Uranium, ug/ml for Uranium.

NC Not counted because unfiltered fraction was less than detectable.

90794 1461

TABLE A.5. Test Identification: HBR/SD-85 (C5B-D) Cycles 1, 2 & 3 (pCi)

DAY	SAMPLE TYPE	VOLUME ml	pH	U UNFILTER	U 0.4 um	U 10 A	Pu-239-Pu-240 UNFILTER	Pu-239-Pu-240 0.4 um	Pu-239-Pu-240 10 A	Am-241-Pu-238 UNFILTER	Am-241-Pu-238 0.4 um	Am-241-Pu-238 10 A	Am-241 UNFILTER	Am-241 0.4 um	Am-241 10 A	Cm-244 UNFILTER	Cm-244 0.4 um	Cm-244 10 A	Cs-137 UNFILTER	Cs-137 0.4 um	Cs-137 10 A	Cs-134 UNFILTER	Cs-134 0.4 um	Cs-134 10 A
1	Sol	15	8.72	1.40E-02	1.60E-02	1.38E-02	6.31E-01	1.40E-00		2.12E-00	5.56E-00	Alpha(.45	1.76E-00	9.01E-01	(2.25E-01	9.01E-01	2.67E-00		5.27E-07	5.38E-07	5.65E-07	1.75E-06	1.81E-06	1.74E-06
7	Sol	15	8.39	1.40E-02	1.60E-02	1.38E-02	4.65E-01	2.25E-01	2.25E-01	1.64E-00	3.16E-01	6.31E-01	0.76E-01	(2.25E-01	(4.50E-01	4.95E-01	2.78E-01	1.80E-01	8.51E-07	8.47E-07	8.15E-07	2.99E-06	2.94E-06	2.76E-06
14	Sol	20	8.34	1.60E-02	2.00E-02	1.50E-02	3.15E-01	2.25E-01		4.95E-01	6.31E-01	Alpha(.45	(2.25E-01	(2.70E-01	(2.70E-01	9.01E-02	1.35E-01		1.05E-06	1.04E-06	1.00E-06	3.55E-06	3.62E-06	3.45E-06
33	Sol	30	8.38	1.10E-02	9.00E-03	9.00E-03	2.67E-00	5.15E-01	(2.70E-01	9.01E-00	5.31E-00	(2.70E-01	5.31E-00	(9.01E-01	(2.70E-01	5.86E-00	3.15E-01	(2.70E-01	1.14E-06	1.13E-06	1.08E-06	3.77E-06	3.71E-06	3.47E-06
62	Sol	30	8.29	1.30E-02	1.20E-02	1.00E-02	3.42E-00	(2.25E-01		1.89E-01	1.25E-00	Alpha(.27	1.22E-01	1.40E-00	(1.35E-01	1.31E-01	1.08E-00		1.33E-06	1.32E-06	1.33E-06	4.34E-06	4.42E-06	4.41E-06
119	Sol	25	8.19	1.00E-02	1.60E-02	1.60E-02	4.65E-00	1.26E-00	2.70E-01	3.69E-01	2.16E-01	4.05E-01	3.11E-01	3.11E-01	4.50E-01	4.01E-01	2.75E-01	2.25E-01	1.78E-06	1.74E-06	1.69E-06	5.77E-06	5.86E-06	5.59E-06
147	Sol	10	8.13	1.10E-02	1.10E-02		2.70E-01	1.35E-01		2.63E-00	9.01E-01					2.25E-00	7.21E-01							
174	Sol	250	8.33	1.10E-02	1.00E-02	1.00E-02	7.86E-00	1.35E-01	1.35E-01	4.28E-01	2.70E-01	2.25E-01	1.05E-01	1.85E-01	4.50E-01	2.70E-01	2.70E-01	(9.01E-02	1.53E-06	1.50E-06	1.63E-06	4.64E-06	4.50E-06	4.77E-06
174	Strip	300		1.00E-01			1.24E-02			5.06E-02			3.39E-02			3.38E-02			2.33E-05			6.05E-03		
174	Rinse	500		(1.00E-03			1.35E-01			3.60E-01			3.16E-01			1.68E-01			0.35E-05			1.84E-04		
CYCLE 2																								
1	Sol	15	8.38	2.00E-03	2.00E-03	2.00E-03	1.00E-01			4.05E-01	Alpha(.27	Alpha(.27	(1.35E-01	(2.25E-01	(1.35E-01	2.25E-01			6.13E-05	6.12E-05	5.90E-05	1.00E-04	1.08E-04	1.00E-04
7	Sol	15	8.00	2.00E-03	2.00E-03	2.00E-03	9.01E-02	(9.01E-02	9.01E-02	2.70E-01	1.00E-01	1.00E-01	(1.35E-01	(1.35E-01	(1.35E-01	9.01E-02	(9.01E-02	(9.01E-02	9.46E-05	9.41E-05	8.66E-05	2.65E-04	2.60E-04	2.61E-04
14	Sol	30	8.12	2.00E-03	2.00E-03	2.00E-03		1.00E-01		Alpha(.23	4.05E-01	Alpha(.27	(1.35E-01	(1.35E-01	(1.35E-01		1.35E-01		1.17E-05	1.16E-05	1.16E-05	3.45E-04	3.34E-04	3.22E-04
34	Sol	30	8.29	2.00E-03	2.00E-03	2.00E-03			9.01E-02	Alpha(.23	Alpha(.32	4.05E-01	(4.50E-01	(3.60E-01	(1.80E-01			(4.50E-02	1.64E-05	1.64E-05	1.62E-05	4.73E-04	4.64E-04	4.55E-04
62	Sol	20	8.25	5.00E-03	2.00E-03					Alpha(.32	Alpha(.45		(1.80E-01	(1.35E-01					1.77E-04	1.05E-05		4.77E-04	4.06E-04	
120	Sol	20	8.15	2.00E-03	2.00E-03		1.35E-01	1.35E-01		3.60E-01	1.00E-01		(2.25E-01	(2.25E-01		(9.01E-02	(9.01E-02		2.34E-05	2.37E-05		5.95E-04	6.04E-04	
181	Sol	250	7.49	9.00E-03	9.00E-03		3.15E-01	1.00E-01		1.13E-00	4.50E-01		4.05E-01	(1.35E-01		5.86E-01	(9.01E-02		1.68E-05	1.67E-05		4.93E-04	4.87E-04	
181	Rinse	500		7.00E-03			9.01E-02			2.25E-01			4.05E-01			9.01E-02			1.29E-05			3.39E-03		
181	Strip	300		1.30E-02			2.25E-01			5.18E-01			9.45E-00			9.46E-00			9.86E-02					
CYCLE 3																								
97	Sol	250	7.92	9.00E-03	9.00E-03		1.80E-01	9.01E-02		9.91E-01	8.11E-01		3.16E-01	(9.01E-02		5.41E-01	4.50E-01		4.05E-06	4.91E-06		1.09E-05	1.09E-05	

DAY	SAMPLE TYPE	VOLUME ml	pH	Co-60 UNFILTER	Co-60 0.4 um	Co-60 10 A	SrY-90 UNFILTER	SrY-90 0.4 um	SrY-90 10 A	Np-237 UNFILTER	Np-237 0.4 um	Np-237 10 A	Tc-99 UNFILTER	Tc-99 0.4 um	Tc-99 10 A	Sn-126 UNFILTER	Sn-126 0.4 um	Sn-126 10 A	C-14 UNFILTER	C-14 0.4 um	C-14 10 A	I-129 UNFILTER	I-129 0.4 um	I-129 10 A
1	Sol	15	8.72										2.07E-01											
7	Sol	15	8.39				6.31E-04						1.04E-01											
14	Sol	20	8.34							3.15E-01	(2.25E-01	4.50E-01	2.12E-01	1.00E-01	(9.01E-00				0.29E-01					
33	Sol	30	8.38							(2.25E-01	(2.25E-01	(2.25E-01	3.92E-01	2.04E-01	1.53E-01	(2.25E-01	(2.25E-01	(2.25E-01	3.29E-01					
62	Sol	30	8.29				1.02E-06			(2.25E-01	(2.25E-01	(2.25E-01	(9.01E-00	(9.01E-00	(9.01E-00	(2.25E-01	NC	NC	7.21E-01			7.38E-00		
119	Sol	25	8.19							(2.25E-01	(2.25E-01	(2.25E-01	1.04E-01	1.62E-01	1.56E-01	3.15E-01	(2.25E-01							
147	Sol	10	8.13																					
174	Sol	250	8.33				2.83E-00			(2.25E-01	(2.25E-01	(2.25E-01	(9.01E-00	(9.01E-00	(9.01E-06	(2.25E-01	NC	NC	1.49E-01			3.35E-01		
174	Strip	300		6.71E-03			1.61E-05			(9.01E-02			(9.01E-00			(2.25E-01						1.00E-02		
174	Rinse	500					3.72E-04			(2.25E-01			(9.01E-00			(2.25E-01								
CYCLE 2																								
1	Sol	15	8.38										(9.01E-00											
7	Sol	15	8.00				1.07E-05						1.22E-01											
14	Sol	30	8.12							(2.25E-01	(2.25E-01	(2.25E-01	2.07E-01	(9.01E-00	2.48E-01	(2.25E-01	NC	NC	0.11E-00					
34	Sol	30	8.29							(2.25E-01	(2.25E-01	(2.25E-01	(9.01E-00	(9.01E-00	(9.01E-00	(2.25E-01	NC	NC						
62	Sol	20	8.25				3.00E-05			(2.25E-01	(4.50E-01		(9.01E-00	(9.01E-00		(1.35E-01	NC		1.17E-01			4.28E-02		
120	Sol	20	8.15				3.09E-05			4.95E-01	1.35E-01		(9.01E-00	(9.01E-00		(2.25E-01	NC		1.49E-01					
181	Sol	250	7.49				8.87E-04			(9.01E-02	(9.01E-02		(9.01E-00	(9.01E-00		(2.25E-01	NC		1.13E-03			1.29E-01		
181	Rinse	500					3.38E-03			(9.01E-02			(4.50E-00			(2.25E-01								
181	Strip	300		3.25E-02			2.39E-03			(9.01E-02			(4.50E-00			(1.35E-01								
CYCLE 3																								
97	Sol	250	7.92				3.50E-04							(9.01E-00					7.34E-02					

UNITS: In pCi/ml for all but Uranium, ug/ml for Uranium.

NC: Not counted because unfiltered fraction was less than detectable.

9 0 7 9 4 1 4 6 2

TABLE A.6. HBR/HD-85 (C5B-B) Cycles 1, 2 & 3 (pCi)

DAY	SAMPLE TYPE	VOLUME ml	pH	U UNFILTER	U 0.4 um	U 10 A	Pu-239-Pu-240 UNFILTER	Pu-239-Pu-240 0.4 um	Pu-239-Pu-240 10 A	Am-241-Pu-238 UNFILTER	Am-241-Pu-238 0.4 um	Am-241-Pu-238 10 A	Am-241 UNFILTER	Am-241 0.4 um	Am-241 10 A	Cm-244 UNFILTER	Cm-244 0.4 um	Cm-244 10 A	Cs-137 UNFILTER	Cs-137 0.4 um	Cs-137 10 A	Cs-134 UNFILTER	Cs-134 0.4 um	Cs-134 10 A
1	Sol	15	8.78	1.50E-02	1.20E-02	1.20E-02				Alpha(.45	Alpha(.45	Alpha(.45	(4.50E-01	(3.15E-01	(2.25E-01				5.77E-05	5.50E-05	5.35E-05	1.02E-04	1.75E-04	1.50E-04
7	Sol	15	8.35	8.00E-03	1.00E-02	1.00E-02	9.91E-02	9.01E-02	(2.25E-01	7.50E-01	7.00E-01	(2.25E-01	(4.50E-01	(4.50E-01	(2.25E-01	8.31E-01	4.95E-01	(2.25E-01	5.32E-06	5.45E-06	5.00E-06	1.02E-05	1.78E-05	1.65E-05
14	Sol	20	8.21	1.50E-02	1.40E-02	1.40E-02		1.00E-01	1.00E-01	Alpha(.45	9.00E-01	2.70E-01	(3.15E-01	(2.70E-01	(2.70E-01		(9.01E-02	(9.01E-02	8.93E-06	8.90E-06	8.33E-06	2.01E-05	2.99E-05	2.64E-05
33	Sol	30	8.20	5.00E-03	5.00E-03	4.00E-03	3.15E-01	1.35E-01	3.00E-01	5.05E-01	2.70E-01	5.05E-01	(5.75E-01	(5.75E-01	(5.75E-01	(2.25E-01	(4.50E-02	(2.25E-01	5.32E-07	5.10E-07	4.91E-07	1.09E-06	1.73E-06	1.50E-06
62	Sol	30	7.88	7.00E-03	7.00E-03	5.00E-03		1.00E-01	9.01E-02	Alpha(.32	3.60E-01	1.80E-01	(2.25E-01	(2.25E-01	(2.25E-01		(4.50E-02	(4.50E-02	1.37E-08	1.27E-08	1.54E-08	4.50E-06	4.45E-06	4.20E-06
119	Sol	25	7.76	9.00E-03	1.00E-02	8.00E-03	7.00E-01	(2.25E-01	(2.25E-01	2.93E-00	(2.25E-01	(2.25E-01	1.50E-00	(2.25E-01	(2.70E-01	9.45E-01	(2.25E-01	(2.25E-01	1.24E-08	1.23E-08	1.29E-08	4.00E-06	3.86E-06	3.82E-06
147	Sol	10	8.00	1.10E-02	8.00E-03		(2.25E-01	(2.25E-01		2.70E-01	(2.25E-01					(2.25E-01	(2.25E-01							
174	Sol	250	8.17	7.00E-03	7.00E-03	2.00E-03	2.25E-01			4.95E-01	Alpha(.23	Alpha(.23	(1.35E-01	(1.35E-01	(1.35E-01	1.35E-01			1.25E-08	1.25E-08	1.25E-08	3.84E-06	3.66E-06	3.57E-06
174	Strip	300		1.00E-02			2.12E-01			6.84E-01			1.67E-01			1.46E-01			1.51E-05			4.22E-03		
174	Rinse	600		3.10E-01	1.10E-01		1.62E-01	1.00E-01		4.32E-00	1.22E-00		2.03E-00	2.20E-01		1.35E-00	(9.01E-02		7.00E-05			2.12E-04		
CYCLE 2																								
1	Sol	15	8.31	3.00E-03	4.00E-03	3.00E-03	4.50E-02	4.50E-02	3.00E-01	1.00E-01	1.00E-01	1.17E-00	4.50E-01	4.95E-01	(1.35E-01	9.01E-02	9.01E-02	7.21E-01	8.95E-00	8.95E-00	8.65E-00	2.73E-05	2.53E-05	2.50E-05
7	Sol	15	8.02	3.00E-03	3.00E-03	3.00E-03	(9.01E-02		1.00E-01	1.00E-01	Alpha(.23	1.00E-01	(1.35E-01	(1.35E-01	(1.35E-01	9.01E-02		(9.01E-02	1.41E-07	1.41E-07	1.32E-07	4.12E-05	4.15E-05	3.89E-05
14	Sol	30	8.12	3.00E-03	3.00E-03	3.00E-03				Alpha(.27	Alpha(.27	Alpha(.23	(1.35E-01	(1.35E-01	(1.35E-01				1.57E-07	1.56E-07	1.60E-07	4.50E-05	4.45E-05	4.84E-05
34	Sol	30	8.05	2.00E-03	2.00E-03	2.00E-03				Alpha(.27	Alpha(.27	Alpha(.27	(1.35E-01	(3.60E-01	(4.50E-01				1.00E-07	1.70E-07	1.03E-07	4.02E-05	4.73E-05	4.77E-05
62	Sol	20	7.80	3.00E-03	2.00E-03					Alpha(.27	Alpha(.27		(1.35E-01	(1.35E-01					1.94E-07	1.91E-07		5.30E-05	5.27E-05	
120	Sol	20	7.97	1.00E-03	1.00E-03		9.01E-02			3.15E-01	Alpha(.32		1.00E-00	(2.25E-01		9.01E-02			1.25E-07	1.29E-07		3.57E-05	3.20E-05	
181	Sol	250	8.23	8.00E-03	8.00E-03		9.01E-02			3.15E-01	Alpha(.27		3.60E-01	(1.35E-01		1.35E-01			2.20E-07	2.28E-07		5.72E-05	5.60E-05	
181	Rinse	600		4.00E-03			1.35E-01			6.76E-01			2.70E-01			1.00E-01			2.17E-05			5.41E-03		
181	Strip	300		1.10E-02			8.11E-00			2.21E-01			8.11E-00			5.00E-00			7.52E-04			1.07E-03		
CYCLE 3																								
97	Sol	250	8.75	8.00E-03	9.00E-03		8.70E-01	9.01E-02		4.95E-00	7.00E-01		2.93E-00	(9.01E-02		2.52E-00	5.41E-01		2.05E-05	2.79E-06		8.17E-04	5.17E-04	

DAY	SAMPLE TYPE	VOLUME ml	pH	Co-60 UNFILTER	Co-60 0.4 um	Co-60 10 A	SrY-90 UNFILTER	SrY-90 0.4 um	SrY-90 10 A	Np-237 UNFILTER	Np-237 0.4 um	Np-237 10 A	Tc-99 UNFILTER	Tc-99 0.4 um	Tc-99 10 A	Sn-126 UNFILTER	Sn-126 0.4 um	Sn-126 10 A	C-14 UNFILTER	C-14 0.4 um	C-14 10 A	I-129 UNFILTER	I-129 0.4 um	I-129 10 A
1	Sol	15	8.78										(9.01E-00											
7	Sol	15	8.35				6.70E-02						2.01E-01											
14	Sol	20	8.21							(2.25E-01	(2.25E-01	(2.25E-01	1.17E-01	1.22E-01	1.70E-01				2.22E-02					
33	Sol	30	8.20							(2.25E-01	(2.25E-01	(2.25E-01	1.35E-01	(9.01E-00	1.35E-01	(2.25E-01	(2.25E-01	(2.25E-01	1.64E-02					
62	Sol	30	7.88				7.61E-04			(2.25E-01	9.01E-02	(2.25E-01	(9.01E-00	(9.01E-00	(9.01E-00	(2.25E-01	(2.25E-01	(2.25E-01	1.09E-02			2.20E-01		
119	Sol	25	7.76							(2.25E-01	(2.25E-01	(2.25E-01	1.20E-01	(9.01E-00	(9.01E-00	(2.25E-01	NC	NC						
147	Sol	10	8.00																					
174	Sol	250	8.17				3.47E-04			(2.25E-01	(2.25E-01	(2.25E-01	(9.01E-00	(9.01E-00	(9.01E-00	(2.25E-01	NC	NC	1.37E-03			1.90E-01		
174	Strip	300		1.14E-03			3.00E-03			(2.25E-01			(9.01E-00			(2.25E-01						4.00E-03		
174	Rinse	600					2.32E-04			(2.25E-01			2.03E-01	1.40E-01		(2.70E-01								
CYCLE 2																								
1	Sol	15	8.31										(9.01E-00											
7	Sol	15	8.02				3.44E-04						(9.01E-00											
14	Sol	30	8.12							(9.01E-02	(9.01E-02	(9.01E-02	(9.01E-00	(9.01E-00	(9.01E-00	(1.35E-01	NC	NC	1.05E-02					
34	Sol	30	8.05							(2.25E-01	(2.25E-01	(2.25E-01	2.00E-01	2.21E-01	(9.01E-00	(2.25E-01	NC	NC						
62	Sol	20	7.80				1.87E-04			(2.25E-01	(2.25E-01		(9.01E-00	(9.01E-00		(1.35E-01	NC		1.00E-02			1.12E-02		
120	Sol	20	7.97				6.02E-03			(2.25E-01	2.70E-01		2.00E-01	1.65E-01		(2.25E-01	NC		2.01E-02					
181	Sol	250	8.23				3.47E-04			(9.01E-02	(9.01E-02		(9.01E-00	(9.01E-00		(1.35E-01	NC		8.31E-02			4.01E-02		
181	Rinse	600					1.87E-03			(9.01E-02			(4.50E-00			(2.25E-01								
181	Strip	300		3.00E-02			1.92E-04			(9.01E-02			(4.50E-00			(1.35E-01								
CYCLE 3																								
97	Sol	250	8.75				7.30E-04							1.70E-01					3.15E-02					

UNITS: In pCi/ml for all but Uranium, ug/ml for Uranium.

NC: Not counted because unfiltered fraction was less than detectable.

90794 1463

TABLE A.7. HBR/UD-85 (C5B-A) Cycles 1, 2 & 3 (pCi)

DAY	SAMPLE TYPE	VOLUME ml	pH	U UNFILTER	U 0.4 um	U 10 A	Pu-239+Pu-240 UNFILTER	Pu-239+Pu-240 0.4 um	Pu-239+Pu-240 10 A	Am-241+Pu-238 UNFILTER	Am-241+Pu-238 0.4 um	Am-241+Pu-238 10 A	Am-241 UNFILTER	Am-241 0.4 um	Am-241 10 A	Cm-244 UNFILTER	Cm-244 0.4 um	Cm-244 10 A	Cs-137 UNFILTER	Cs-137 0.4 um	Cs-137 10 A	Cs-134 UNFILTER	Cs-134 0.4 um	Cs-134 10 A
1	Sol	15	8.49	1.20E-02	1.36E-02	1.40E-02	1.08E-01	1.08E-01		4.05E-01	2.78E-01	Alpha(.45	3.15E-01	8.11E-01	<4.50E-01	1.00E-01	9.01E-02		7.34E-03	7.34E-03	8.09E-03	2.04E-02	2.73E-02	2.41E-02
7	Sol	15	8.31	6.00E-03	7.00E-03	3.00E-03	2.70E-01	2.70E-01	4.50E-01	9.01E-01	8.56E-01	9.01E-01	<2.25E-01	<2.25E-01	<2.25E-01	2.70E-01	4.50E-01	2.25E-01	8.44E-03	6.63E-03	5.99E-03	2.29E-02	3.15E-02	1.41E-02
14	Sol	20	8.27	3.00E-03	3.00E-03	5.00E-03			2.70E-01	Alpha(.45	Alpha(.45	4.95E-01	<2.25E-01	<2.70E-01	<2.25E-01			<9.01E-02	8.71E-03	7.03E-03	8.34E-03	2.17E-02	2.43E-02	2.35E-02
33	Sol	30	8.22	5.00E-03	5.00E-03	8.00E-03	3.00E-01	<2.25E-01		5.41E-01	4.05E-01	Alpha(.45	<2.70E-01	<9.01E-01	<9.01E-01	<2.25E-01	<2.25E-01		9.23E-03	9.55E-03	8.51E-03	1.09E-02	1.65E-02	1.76E-02
62	Sol	30	7.74	7.00E-03	7.00E-03	7.00E-03	2.25E-01	2.25E-01		4.05E-01	3.60E-01	Alpha(.27	<1.35E-01	<1.35E-01	<2.25E-01	<9.01E-02	<9.01E-02		1.00E-04	9.59E-03	8.28E-03			
119	Sol	25	7.91	1.30E-02	1.50E-02	1.20E-02	4.50E-01	5.41E-01	2.70E-01	8.56E-01	1.08E-00	8.31E-01	2.25E-01	<2.25E-01	<2.25E-01	<2.25E-01	<2.25E-01	<2.25E-01	8.03E-03	8.94E-03	8.31E-03	1.81E-02	1.31E-02	<1.25E-02
147	Sol	10	8.36	1.30E-02	1.10E-02		4.05E-01	3.60E-01		8.11E-01	8.11E-01					<2.25E-01	<2.25E-01							
174	Sol	250	8.51	1.30E-02	1.30E-02	7.00E-03	3.15E-01		2.25E-01	5.86E-01	Alpha(.36	2.70E-01	<1.35E-01	<1.35E-01	<1.00E-01	9.01E-02		<1.35E-01	2.37E-04	2.13E-04	2.10E-04	6.04E-02	5.27E-02	5.95E-02
174	Strip	300		8.00E-03			2.61E-01			6.31E-01			1.17E-01			9.46E-00			4.77E-02					
174	Rinse	600		1.00E-03						Alpha(.27			3.15E-01						1.70E-03					
CYCLE 2																								
1	Sol	15	8.21	3.00E-03	2.00E-03	3.00E-03	4.50E-02			3.00E-01	Alpha(.27	Alpha(.23	<1.35E-01	<1.35E-01	<1.35E-01	1.35E-01			4.77E-03	4.01E-03	4.27E-03	1.07E-02	1.16E-02	
7	Sol	15	8.25	3.00E-03	3.00E-03	3.00E-03				Alpha(.27	Alpha(.27	Alpha(.27	<1.35E-01	<1.35E-01	<1.35E-01				5.30E-03	5.45E-03	5.09E-03	1.41E-02	<1.71E-02	1.22E-02
14	Sol	30	8.05	4.00E-03	4.00E-03	3.00E-03		1.35E-01		Alpha(.27	3.60E-01	Alpha(.37	<1.35E-01	<1.35E-01	<1.35E-01		<9.01E-02		5.45E-03	5.08E-03	5.45E-03		1.08E-02	
34	Sol	30	7.93	3.00E-03	3.00E-03	3.00E-03				Alpha(.27	Alpha(.23	Alpha(.23	<1.35E-01	<1.35E-01	<2.25E-01				2.71E-05	2.77E-05	2.55E-05	7.16E-03	7.40E-03	7.39E-03
62	Sol	5	7.98																4.01E-05			1.11E-04		
120	Sol	5	7.96																1.14E-05			2.92E-04		
181	Sol	250	7.48	8.00E-03	8.00E-03		8.56E-01	5.41E-01		1.05E-00	9.01E-01		<1.35E-01	<1.35E-01		9.01E-02	<9.01E-02		1.47E-05	1.47E-05		3.48E-04	3.52E-04	
181	Rinse	600		6.00E-03			9.01E-02			1.80E-01			2.70E-01			9.01E-02			8.84E-04			1.38E-03		
181	Strip	300		1.20E-02			2.43E-01			5.77E-01			9.01E-00			8.56E-00			9.69E-02					
CYCLE 3																								
97	Sol	250	8.29	8.00E-03	8.00E-03		1.08E-01	9.01E-02		1.13E-00	9.01E-01		1.68E-01	<9.01E-02		5.41E-01	5.86E-01		5.23E-07	5.18E-07		1.17E-06	1.18E-06	

DAY	SAMPLE TYPE	VOLUME ml	pH	Co-60 UNFILTER	Co-60 0.4 um	Co-60 10 A	SrY-90 UNFILTER	SrY-90 0.4 um	SrY-90 10 A	Np-237 UNFILTER	Np-237 0.4 um	Np-237 10 A	Tc-99 UNFILTER	Tc-99 0.4 um	Tc-99 10 A	Sn-126 UNFILTER	Sn-126 0.4 um	Sn-126 10 A	C-14 UNFILTER	C-14 0.4 um	C-14 10 A	I-129 UNFILTER	I-129 0.4 um	I-129 10 A
1	Sol	15	8.49	1.40E-02	2.05E-02	1.82E-02							<9.01E-00											
7	Sol	15	8.31				<4.50E-02						<9.01E-00											
14	Sol	20	8.27							<2.25E-01	<2.25E-01	<2.25E-01	<9.01E-00	<9.01E-00	<9.01E+00				8.35E-01					
33	Sol	30	8.22							<2.25E-01	<2.25E-01	<2.25E-01	1.17E-01	1.71E-01	<9.01E-00	<2.25E-01	<2.25E-01	<2.25E-01	1.49E-01					
62	Sol	30	7.74				1.35E-03			<2.25E-01	<2.25E-01	<2.25E-01	<9.01E-00	<9.01E-00	<9.01E-00	<2.25E-01	<2.25E-01	<2.25E-01	1.17E-01			1.25E-02		
119	Sol	25	7.91							<2.25E-01	<2.25E-01	<2.25E-01	1.71E-01	<9.01E-00	<9.01E-00	<2.25E-01	NC	NC						
147	Sol	10	8.36																					
174	Sol	250	8.51				1.31E-03			<2.25E-01	<2.25E-01	<2.25E-01	<9.01E-00	<9.01E-00	<9.01E-00	<2.25E-01	NC	NC	1.04E-01			1.11E-01		
174	Strip	300		1.16E-03			4.50E-02			<2.25E-01			<9.01E-00			<2.25E-01						8.18E-05		
174	Rinse	600					3.60E-02			<2.25E-01			<9.01E-00			<2.25E-01								
CYCLE 2																								
1	Sol	15	8.21										1.00E-01											
7	Sol	15	8.25				<9.01E-02						<9.01E-00											
14	Sol	30	8.05							<2.25E-01	<2.25E-01	<9.01E-02	<9.01E-00	<9.01E-00	<9.01E+00	<2.25E-01	NC	NC	4.05E-00					
34	Sol	30	7.93							<2.25E-01	<2.25E-01	<2.25E-01	1.44E-01	1.53E-01	2.34E-01	IS	IS	IS						
62	Sol	5	7.98																1.06E-01					
120	Sol	5	7.96																2.15E-01					
181	Sol	250	7.48				4.50E-02			1.35E-01	<9.01E-02		<9.01E-00	<9.01E-00		<1.35E-01	NC		<9.01E-00			3.39E-02		
181	Rinse	600					<4.05E-02			2.70E-01			<4.50E-00			<2.25E-01								
181	Strip	300		1.42E-02			<3.60E-02			<9.01E-02			<4.50E-00			<1.35E-01								
CYCLE 3																								
97	Sol	250	8.29				2.52E-03							<9.01E-00					3.07E-01					

UNITS: In pCi/ml for all but Uranium, ug/ml for Uranium.

NC: Not counted because unfiltered fraction was less than detectable.
IS: Insufficient sample

90794 1464

TABLE A.7. HBR/UD-85 (C5B-A) Cycles 1, 2 & 3 (pCi)

DAY	SAMPLE TYPE	VOLUME ml	pH	U UNFILTER	U 0.4 um	U 18 A	Pu-239+Pu-240 UNFILTER	Pu-239+Pu-240 0.4 um	Pu-239+Pu-240 18 A	Am-241+Pu-238 UNFILTER	Am-241+Pu-238 0.4 um	Am-241+Pu-238 18 A	Am-241 UNFILTER	Am-241 0.4 um	Am-241 18 A	Cm-244 UNFILTER	Cm-244 0.4 um	Cm-244 18 A	Cs-137 UNFILTER	Cs-137 0.4 um	Cs-137 18 A	Cs-134 UNFILTER	Cs-134 0.4 um	Cs-134 18 A
1	Sol	15	8.49	1.20E-02	1.38E-02	1.40E-02	1.00E-01	1.00E-01		4.05E-01	2.78E-01	Alpha(.45	3.15E-01	8.11E-01	(4.50E-01	1.00E-01	9.01E-02		7.34E-03	7.34E-03	8.00E-03	2.04E-02	2.73E-02	2.41E-02
7	Sol	15	8.31	6.00E-03	7.00E-03	3.00E-03	2.70E-01	2.70E-01	4.50E-01	9.01E-01	8.55E-01	9.01E-01	(2.25E-01	(2.25E-01	(2.25E-01	2.70E-01	4.50E-01	2.25E-01	6.44E-03	8.53E-03	5.99E-03	2.29E-02	3.15E-02	1.41E-02
14	Sol	29	8.27	3.00E-03	3.00E-03	6.00E-03			2.70E-01	Alpha(.45	Alpha(.45	4.95E-01	(2.25E-01	(2.70E-01	(2.25E-01			(9.01E-02	6.71E-03	7.03E-03	8.35E-03	2.17E-02	2.43E-02	2.36E-02
33	Sol	38	8.22	6.00E-03	5.00E-03	6.00E-03	3.60E-01	(2.25E-01		5.41E-01	4.05E-01	Alpha(.45	(2.70E-03	(9.01E-01	(9.01E-01	(2.25E-01	(2.25E-01		9.23E-03	9.55E-03	8.51E-03	1.09E-02	1.65E-02	1.75E-02
62	Sol	38	7.74	7.00E-03	7.00E-03	7.00E-03	2.25E-01	2.25E-01		4.05E-01	3.60E-01	Alpha(.27	(1.35E-01	(1.35E-01	(2.25E-01	(9.01E-02	(9.01E-02		1.00E-04	9.56E-03	8.29E-03			
119	Sol	25	7.91	1.30E-02	1.50E-02	1.20E-02	4.50E-01	5.41E-01	2.70E-01	8.55E-01	1.08E-00	8.31E-01	2.25E-01	(2.25E-01	(2.25E-01	(2.25E-01	(2.25E-01	(2.25E-01	8.05E-03	8.94E-03	8.31E-03	1.01E-02	1.31E-02	(1.25E-02
147	Sol	10	8.36	1.30E-02	1.10E-02		4.05E-01	3.60E-01		8.11E-01	8.11E-01					(2.25E-01	(2.25E-01							
174	Sol	250	8.51	1.30E-02	1.30E-02	7.00E-03	3.15E-01		2.25E-01	5.00E-01	Alpha(.36	2.70E-01	(1.35E-01	(1.35E-01	(1.00E-01	9.01E-02		(1.35E-01	2.37E-04	2.18E-04	2.18E-04	6.04E-02	5.27E-02	5.95E-02
174	Strip	300		8.00E-03			2.61E-01			6.31E-01			1.17E-01			9.46E-00			4.77E-02					
174	Rinse	600		1.00E-03						Alpha(.27			3.15E-03						1.70E-03					
CYCLE 2																								
1	Sol	15	8.21	3.00E-03	2.00E-03	3.00E-03	4.50E-02			3.00E-01	Alpha(.27	Alpha(.23	(1.35E-01	(1.35E-01	(1.35E-01	1.35E-01			4.77E-03	4.91E-03	4.27E-03	1.07E-02	1.16E-02	
7	Sol	15	8.25	3.00E-03	3.00E-03	3.00E-03				Alpha(.27	Alpha(.27	Alpha(.27	(1.35E-01	(1.35E-01	(1.35E-01				5.35E-03	5.45E-03	5.00E-03	1.41E-02	(1.71E-02	1.22E-02
14	Sol	30	8.05	4.00E-03	4.00E-03	3.00E-03		1.35E-01		Alpha(.27	3.00E-01	Alpha(.27	(1.35E-01	(1.35E-01	(1.35E-01		(9.01E-02		5.45E-03	5.68E-03	5.48E-03		1.00E-02	
34	Sol	38	7.93	3.00E-03	3.00E-03	3.00E-03				Alpha(.27	Alpha(.33	Alpha(.23	(1.35E-01	(1.35E-01	(2.25E-01				2.71E-05	2.77E-05	2.64E-05	7.16E-03	7.48E-03	7.39E-03
62	Sol	6	7.98																4.01E-05			1.11E-04		
120	Sol	5	7.96																1.14E-00			2.92E-04		
181	Sol	250	7.45	8.00E-03	8.00E-03		8.55E-01	5.41E-01		1.05E-00	9.01E-01		(1.35E-01	(1.35E-01		9.01E-02	(9.01E-02		1.47E-05	1.47E-05		3.48E-04	3.52E-04	
181	Rinse	600		8.00E-03			9.01E-02			1.80E-01			2.70E-01			9.01E-02			6.04E-04			1.80E-03		
181	Strip	300		1.20E-02			2.43E-01			5.77E-01			9.01E-00			8.55E-00			9.59E-02					
CYCLE 3																								
97	Sol	250	8.29	8.00E-03	8.00E-03		1.00E-01	9.01E-02		1.13E-00	9.01E-01		1.80E-01	(9.01E-02		5.41E-01	5.05E-01		5.23E-07	5.18E-07		1.17E-06	1.18E-06	

DAY	SAMPLE TYPE	VOLUME ml	pH	Co-60 UNFILTER	Co-60 0.4 um	Co-60 18 A	SrY-90 UNFILTER	SrY-90 0.4 um	SrY-90 18 A	Np-237 UNFILTER	Np-237 0.4 um	Np-237 18 A	Tc-99 UNFILTER	Tc-99 0.4 um	Tc-99 18 A	Sn-126 UNFILTER	Sn-126 0.4 um	Sn-126 18 A	C-14 UNFILTER	C-14 0.4 um	C-14 18 A	I-129 UNFILTER	I-129 0.4 um	I-129 18 A
1	Sol	15	8.49	1.49E-02	2.05E-02	1.82E-02							(9.01E-00											
7	Sol	15	8.31				(4.50E-02						(9.01E-00											
14	Sol	29	8.27							(2.25E-01	(2.25E-01	(2.25E-01	(9.01E-00	(9.01E-00	(9.01E-00				8.35E-01					
33	Sol	38	8.22							(2.25E-01	(2.25E-01	(2.75E-01	1.17E-01	1.71E-01	(9.01E-00	(2.25E-01	(2.25E-01	(3.75E-01	1.43E-01					
62	Sol	38	7.74				1.35E-03			(2.25E-01	(2.25E-01	(2.25E-01	(9.01E-00	(9.01E-00	(9.01E-00	(2.25E-01	(2.25E-01	(3.75E-01	1.17E-01			1.25E-02		
119	Sol	25	7.91							(2.25E-01	(2.25E-01	(2.25E-01	1.71E-01	(9.01E-00	(9.01E-00	(2.25E-01	NC	NC						
147	Sol	10	8.36																					
174	Sol	250	8.51				1.31E-03			(2.25E-01	(2.25E-01	(2.25E-01	(9.01E-00	(9.01E-00	(9.01E-00	(2.25E-01	NC	NC	1.04E-01			1.11E-01		
174	Strip	300		1.15E-03			4.50E-02			(2.25E-01			(9.01E-00			(2.25E-01						8.18E-05		
174	Rinse	600					3.00E-02			(2.25E-01			(9.01E-00			(2.25E-01								
CYCLE 2																								
1	Sol	15	8.21										1.00E-01											
7	Sol	15	8.25				(9.01E-02						(9.01E-00											
14	Sol	30	8.05							(2.25E-01	(2.25E-01	(9.01E-02	(9.01E-00	(9.01E-00	(9.01E-00	(7.25E-01	NC	NC	4.05E-00					
34	Sol	38	7.93							(2.25E-01	(2.25E-01	(2.25E-01	1.44E-01	1.53E-01	2.34E-01	IS	IS	IS						
62	Sol	6	7.98																1.00E-01					
120	Sol	5	7.96																2.10E-01					
181	Sol	250	7.45				4.50E-02			1.35E-01	(9.01E-02		(9.01E-00	(9.01E-00		(1.35E-01	NC		(9.01E-00			3.39E-02		
181	Rinse	600					(4.05E-02			2.70E-01			(4.50E-00			(2.25E-01								
181	Strip	300		1.42E-02			(3.00E-02			(9.01E-02			(4.50E-00			(1.35E-01								
CYCLE 3																								
97	Sol	250	8.29				2.52E-03							(9.01E-00					3.07E-01					

UNITS: In pCi/ml for all but Uranium, ug/ml for Uranium.

NC: Not counted because unfiltered fraction was less than detectable.
IS: Insufficient sample

9 0 7 9 4 1 4 6 5

A.3 RADIOCHEMISTRY ERROR ESTIMATES

The primary sources of error in the reported radiochemistry data are:

- Volume measurement errors incurred during sample aliquot preparations
- Recovery errors involved in radiochemical separations
- Counting statistics.

A summary of estimated error resulting from these factors is given below:

- $^{239+240}Pu$, ^{238}Pu + ^{241}Am, ^{244}Cm

Method: Direct plate followed by total alpha counting and alpha spectrometry

Volume Errors: ±2%

Recovery: 100% (no separation required)

Counting Statistics at $\pm 1\sigma$:

1 dpm/mL	(0.45 pCi/mL)	= ±60%
10 dpm/mL	(4.5 pCi/mL)	= ±8%
100 dpm/mL	(45 pCi/mL)	= ±2.5%
1,000 dpm/mL	(450 pCi/mL)	= ±1.5%

The counting statistics for 1, 10, and 100 dpm/mL are based on a 100-μL aliquot plate counted for 480 min with a background of 0.2 cpm. The 1,000 dpm/mL counting statistic is based on a 100-μL aliquot plate counted for 100 min with a background of 1 cpm. (Higher activity plates are counted on higher background counters, saving newer, lower-background counters for low-activity samples.)

90794 1466

- ^{241}Am

Method: Separation by anion exchange, plate, alpha count, and alpha spectrometry

Volume Errors: ±3%

Recovery: 97 ± 2%

Counting Statistics: Same as above for direct plate alpha, since the same volumes, counting times, and equipment are used

- ^{237}Np

Method: Separation by cation exchange and solvent extraction

Volume Errors: ±2%

Recovery: 98 ± 2%

Counting Statistics at ±1σ:

1 dpm/mL	(0.45 pCi/mL)	= ±30%
10 dpm/mL	(4.5 pCi/mL)	= ±6%
100 dpm/mL	(45 pCi/mL)	= ±4%
1,000 dpm/mL	(450 pCi/mL)	= ±1%

The ^{237}Np counting statistics for 1 and 10 dpm/mL are based on a 200-μL aliquot plate counted for 480 min with a background count of 0.2 cpm. Counting statistics for 100 and 1,000 dpm/mL are based on a 100-min count with a background of 1 cpm.

90794 1467

- ^{99}Tc

Method: Separation by cation exchange and solvent extraction followed by beta proportional counting

Volume Error: ±4%

Recovery: 94 ± 2%

Counting Statistics:

20 dpm/mL	(9 pCi/mL)	= Lower limit at 2σ
100 dpm/mL	(45 pCi/mL)	= ±11% at 1σ
1,000 dpm/mL	(450 pCi/mL)	= ±1.6% at 1σ

The ^{99}Tc counting statistics are based on a 500-μL aliquot extracted into 5 mL with 2 mL plated for beta counting. Counting time is 100 min with a background of 30 cpm.

- ^{137}Cs, ^{134}Cs, ^{60}Co

Method: Gamma spectrometry

Volume Errors: ±2%

Recovery: 100% (no separation required)

Counting Statistics at $\pm 1\sigma$:

1,000 dpm/mL	(450 pCi/mL)	= ±20%
10,000 dpm/mL	(4500 pCi/mL)	= ±8%
100,000 dpm/mL	(45,000 pCi/mL)	= ±2%
1,000,000 dpm/mL	(450,000 pCi/mL)	= ±1%

Based on 1-mL aliquot counted for 60 min

90794 1468

- Uranium

Method: Scintrex UA-3 uranium analyzer, laser-excited fluorescence

Overall error is estimated to be ±10% at 1σ when the instrument is operating in its optimum range. The lower limit is 0.001 μg/mL (±0.001 μg/mL) using a 100-μL sample aliquot.

A.4 REFERENCE

A1. Barner, J. O. 1984. Characterization of LWR Spent Fuel MCC-Approved Testing Material ATM-101. PNL-5109, Pacific Northwest Laboratory, Richland, Washington.

9 0 7 9 4 1 4 6 9

APPENDIX B

SOLUTION CHEMISTRY DATA

90794 1470

TABLE B.1. Solution Chemistry for the HBR/BF-25 (C5C-I) Test (0.4 μm filtered)

Species	Cycle 1 (μg/mL) Starting J-13 Water	33 Days	147 Days	174 Days	Cycle 2 (μg/mL) Starting J-13 Water	14 Days	34 Days	181 Days	Cycle 3 (μg/mL) Starting J-13 Water	20 Days	55 Days	97 Days
pH	8.00	8.44	7.77	7.95	7.74	8.31	8.15	8.04	8.12	8.01	7.78	7.92
Al	<0.075	0.077	<0.075	0.110	<0.075	<0.075	<0.075	<0.08	<0.08	0.200	0.080	0.850
B	0.288	0.051	0.194	0.170	0.160	0.183	0.170	0.160	0.200	0.240	0.180	0.200
Ca	15.04	12.65	12.42	11.00	14.00	10.87	10.00	12.30	13.30	15.10	12.90	12.70
Cr	---	---	<0.01	<0.01	0.015	<0.010	0.016	<0.01	<0.01	0.040	<0.01	<0.01
Fe	<0.01	0.13	0.03	0.05	<0.1	<0.01	<0.01	<0.01	<0.01	0.02	<0.01	<0.01
K	3.66	8.20	4.03	6.40	4.20	5.48	5.60	6.24	6.64	8.02	3.92	9.20
Mg	2.83	1.92	1.78	2.10	2.00	2.10	2.00	1.95	2.17	2.23	2.10	2.19
Mo	0.041	0.152	0.262	0.270	0.200	0.037	0.058	0.070	0.040	0.080	0.040	0.080
Na	41.52	41.04	46.85	47.00	47.00	46.29	45.00	45.10	48.20	44.60	59.40	34.00
Nd	<0.15	<0.15	<0.15	<0.15	<0.15	<0.15	<0.15	<3.0	<3.0	<3.0	<3.0	<3.0
Ni	---	---	0.260	0.280	0.041	0.049	0.064	0.080	0.050	0.080	0.040	0.060
Pd	<0.12	<0.12	<0.12	<0.12	<0.12	<0.12	<0.12	<2.4	<2.4	<2.4	<2.4	<2.4
Ru	<0.12	<0.12	<0.12	<0.12	<0.12	<0.12	<0.12	<2.4	<2.4	<2.4	<2.4	<2.4
Si	37.78	30.61	35.28	33.00	31.00	33.31	30.00	29.70	32.60	33.90	30.90	32.20
Sr	0.046	0.135	0.107	0.100	0.047	0.054	0.053	0.050	0.040	0.050	0.050	0.070
Zr	<0.010	0.016	<0.010	0.016	0.011	<0.010	0.013	<0.01	<0.01	0.030	<0.01	0.160
Cl	7.00	7.15	7.50	7.06	6.50	7.00	6.80	7.42	7.09	7.57	7.84	7.63
F	2.10	2.02	2.10	2.80	1.30	2.60	2.22	2.28	2.30	2.29	2.36	2.30
PO_4	---	1.30	---	---	---	---	---	---	---	---	---	---
NO_3	7.90	10.80	10.70	8.42	7.70	15.10	7.20	6.00	7.64	19.50	17.40	15.30
SO_4	18.00	24.10	18.80	20.90	15.80	22.40	19.70	18.70	17.20	20.20	19.50	19.60
HCO_3	125.6	121.0	122.5	121.0	122.5	113.4	120.5	118.9	123.0	112.3	111.8	113.4
Inorg C	24.70	23.80	24.10	23.80	24.10	22.30	23.70	23.40	24.20	22.10	22.00	22.30
Org C	---	---	1.40	---	---	---	---	0.24	---	---	---	---
Total C	25.60	25.10	25.50	25.20	25.50	23.60	23.75	---	25.00	---	---	---

90794 14711

TABLE B.2. Solution Chemistry for the TP/BF-85 (F6-2B) Test (0.4 μm filtered)

	Cycle 1 (μg/mL)				Cycle 2 (μg/mL)				Cycle 3 (μg/mL)			
Species	Starting J-13 Water	33 Days	147 Days	174 Days	Starting J-13 Water	14 Days	34 Days	181 Days	Starting J-13 Water	20 Days	55 Days	97 Days
pH	8.00	8.19	8.02	8.07	7.74	7.95	8.10	8.30	8.12	8.21	8.28	8.33
Al	<0.075	0.226	<0.075	<0.075	<0.075	<0.075	0.240	<0.08	<0.08	0.150	0.120	0.880
B	0.288	0.106	0.197	0.190	0.160	0.187	0.180	0.160	0.200	0.250	0.140	0.190
Ca	15.04	6.84	1.62	1.10	14.00	10.82	10.00	8.70	13.30	12.10	9.80	9.25
Cr	---	---	0.150	0.210	0.015	0.038	0.035	0.060	<0.01	0.080	0.110	0.150
Fe	<0.01	0.14	<0.01	<0.01	<0.10	<0.01	<0.01	<0.01	<0.01	0.010	<0.01	<0.01
K	3.66	6.61	7.11	7.50	4.20	1.73	3.00	7.03	6.64	9.40	5.09	11.90
Mg	2.83	1.23	0.23	0.20	2.00	1.82	1.66	1.10	2.17	1.91	1.49	1.20
Mo	0.041	0.184	0.711	1.000	0.200	0.090	0.160	0.440	0.040	0.100	0.150	0.230
Na	41.52	41.56	45.71	42.00	47.00	48.59	47.00	45.20	48.20	46.90	58.30	96.20
Nd	<0.15	<0.15	<0.15	<0.15	<0.15	<0.15	<0.36	<3.0	<3.0	<3.0	<3.0	<3.0
Ni	---	---	0.030	0.021	0.041	0.042	0.051	0.040	0.050	0.060	0.040	0.040
Pd	<0.12	<0.12	<0.12	<0.12	<0.12	<0.12	<0.29	<2.4	<2.4	<2.4	<2.4	<2.4
Ru	<0.12	<0.12	<0.12	<0.12	<0.12	<0.12	<0.12	<2.4	<2.4	<2.4	<2.4	<2.4
Si	37.78	17.06	7.36	5.90	31.00	30.90	28.00	24.80	32.60	32.40	28.70	27.00
Sr	0.046	0.058	0.019	0.014	0.047	0.061	0.070	0.060	0.040	0.050	0.040	0.060
Zr	<0.010	<0.010	<0.010	0.015	0.011	0.015	0.290	<0.01	<0.01	0.010	<0.01	0.160
Cl	7.00	7.29	7.30	6.67	6.50	7.00	6.80	7.46	7.09	7.64	7.62	7.62
F	2.10	1.96	1.60	1.61	1.30	2.40	2.21	2.15	2.30	2.29	2.27	2.26
PO_4	---	1.00	---	---	---	---	---	---	---	---	---	---
NO_3	7.90	5.15	5.80	5.01	7.70	2.20	2.60	4.26	7.64	4.56	4.77	4.66
SO_4	18.00	31.70	23.60	25.10	15.80	25.70	27.80	26.00	17.20	19.50	20.10	19.80
HCO_3	125.6	92.0	68.6	65.1	122.5	105.7	106.7	79.8	123.0	108.3	100.1	97.1
Inorg C	24.70	18.10	13.50	12.80	24.10	20.80	21.00	15.70	24.20	21.30	19.70	19.10
Org C	---	---	1.80	---	---	---	---	2.56	---	---	---	---
Total C	25.60	21.80	15.30	14.50	25.50	24.00	21.65	---	25.00	---	---	---

9 0 7 9 4 1 4 7 2

TABLE B.3. Solution Chemistry for the HBR/BF-85 (C5C-K) Test (0.4 μm filtered)

Species	Cycle 1 (μg/mL) Starting J-13 Water	33 Days	147 Days	174 Days	Cycle 2 (μg/mL) Starting J-13 Water	14 Days	34 Days	181 Days	Cycle 3 (μg/mL) Starting J-13 Water	20 Days	55 Days	97 Days
pH	8.00	8.24	7.87	7.92	7.74	8.33	8.34	8.17	8.12	8.19	8.11	8.35
Al	<0.075	0.389	<0.075	0.150	<0.075	<0.075	0.087	<0.08	<0.08	0.210	0.100	0.840
B	0.288	0.074	0.185	0.160	0.160	0.198	0.190	0.180	0.200	0.230	0.150	0.210
Ca	15.04	5.70	4.09	3.50	14.00	11.55	10.00	6.30	13.30	11.00	7.85	7.59
Cr	---	---	<0.01	<0.01	0.015	0.042	0.020	0.030	<0.01	0.080	0.070	0.070
Fe	<0.01	0.14	0.45	0.03	<0.10	<0.01	<0.01	<0.01	<0.01	0.02	<0.01	<0.01
K	3.66	5.08	1.42	7.20	4.20	5.05	6.70	5.65	6.64	7.74	4.39	9.87
Mg	2.83	1.06	0.70	0.76	2.00	1.79	1.61	0.76	2.17	1.60	1.19	1.02
Mo	0.041	0.206	1.780	2.300	0.200	0.101	0.120	0.370	0.040	0.160	0.220	0.370
Na	41.52	45.25	61.41	47.00	47.00	48.28	49.00	41.80	48.20	45.20	57.50	38.80
Nd	<0.15	<0.15	<0.15	<0.15	<0.15	<0.15	<0.15	<3.0	<3.0	<3.0	<3.0	<3.0
Ni	---	---	0.110	0.063	0.041	0.032	0.056	0.020	0.050	0.050	0.020	0.070
Pd	<0.12	<0.12	<0.12	<0.12	<0.12	<0.12	<0.12	<2.4	<2.4	<2.4	<2.4	<2.4
Ru	<0.12	<0.12	<0.12	<0.12	<0.12	<0.12	<0.12	<2.4	<2.4	<2.4	<2.4	<2.4
Si	37.78	15.13	22.56	18.00	31.00	30.53	25.00	15.80	32.60	28.70	23.60	24.20
Sr	0.046	0.060	0.050	0.034	0.047	0.121	0.110	0.060	0.040	0.040	0.040	0.050
Zr	<0.010	0.036	<0.010	0.014	0.011	<0.010	0.014	<0.01	<0.01	0.030	<0.01	0.150
Cl	7.00	7.84	9.10	8.18	6.50	6.90	6.80	7.09	7.09	7.57	7.61	7.47
F	2.10	2.02	2.00	1.82	1.30	2.40	2.22	1.74	2.30	2.21	2.13	2.12
PO_4	---	1.10	---	---	---	---	---	---	---	---	---	---
NO_3	7.90	7.31	1.10	0.10	7.70	2.00	16.50	3.34	7.64	3.84	4.09	4.10
SO_4	18.00	33.60	31.40	32.00	15.80	29.20	27.00	21.30	17.20	19.40	19.40	19.30
HCO_3	125.6	84.4	96.1	94.0	122.5	106.7	104.5	79.8	123.0	104.2	97.6	94.0
Inorg C	24.70	16.60	18.90	18.50	24.10	21.00	20.68	15.70	24.20	20.50	19.20	18.50
Org C	---	---	4.80	---	---	---	---	1.09	---	---	---	---
Total C	25.60	20.50	23.70	20.70	25.50	24.00	23.25	---	25.00	---	---	---

9 0 7 9 4 1 4 7 3

TABLE B.4. Solution Chemistry for the HBR/SD-85 (C5B-D) Test (0.4 μm filtered)

	Cycle 1 (μg/mL)				Cycle 2 (μg/mL)				Cycle 3 (μg/mL)	
Species	Starting J-13 Water	33 Days	147 Days	174 Days	Starting J-13 Water	14 Days	34 Days	181 Days	Starting J-13 Water	97 Days
pH	8.00	8.38	8.13	8.33	7.74	8.12	8.20	7.49	8.12	7.92
Al	<0.075	0.166	<0.075	0.090	<0.075	<0.075	<0.075	<0.08	<0.08	0.850
B	0.288	0.032	0.156	0.160	0.160	0.176	0.160	0.130	0.200	0.180
Ca	15.04	9.71	9.86	8.40	14.00	10.09	11.00	2.44	13.30	1.88
Cr	---	---	0.035	0.050	0.015	0.018	0.017	<0.01	<0.01	0.060
Fe	<0.01	<0.01	<0.01	<0.01	<0.10	<0.01	<0.01	<0.01	<0.01	<0.01
K	3.66	5.61	6.31	5.30	4.20	<0.50	8.00	5.85	6.64	11.20
Mg	2.83	1.51	1.11	1.20	2.00	1.77	1.65	0.36	2.17	0.20
Mo	0.041	0.025	0.029	0.058	0.200	0.048	0.043	0.510	0.040	0.050
Na	41.52	42.40	46.52	49.00	47.00	44.58	50.00	17.90	48.20	89.50
Nd	<0.15	<0.15	<0.15	<0.15	<0.15	<0.15	<0.15	<3.0	<3.0	<3.0
Ni	---	---	0.06	0.034	0.041	0.022	0.029	0.030	0.050	0.040
Pd	<0.12	<0.12	<0.12	<0.12	<0.12	<0.12	<0.12	<2.4	<2.4	<2.4
Ru	<0.12	<0.12	<0.12	<0.12	<0.12	<0.12	<0.12	<2.4	<2.4	<2.4
Si	37.78	24.06	30.13	27.00	31.00	29.72	29.00	5.12	32.60	11.40
Sr	0.046	0.045	0.086	0.077	0.047	0.046	0.048	0.010	0.040	0.010
Zr	<0.010	<0.010	<0.010	<0.01	0.011	<0.010	<0.010	<0.01	<0.01	0.160
Cl	7.00	6.76	7.20	6.47	6.50	6.40	6.70	6.46	7.09	7.28
F	2.10	2.03	2.00	1.91	1.30	2.00	2.24	0.64	2.30	1.97
PO_4	---	1.20	---	---	---	---	---	---	---	---
NO_3	7.90	2.82	2.90	2.54	7.70	1.60	1.00	1.92	7.64	4.53
SO_4	18.00	30.00	23.90	24.50	15.80	24.10	26.60	8.44	17.20	19.40
HCO_3	125.6	99.6	105.2	101.7	122.5	105.7	106.2	33.4	123.0	73.7
Inorg C	24.70	19.60	20.70	20.00	24.10	20.80	20.90	6.57	24.20	14.50
Org C	---	---	3.70	---	---	---	---	1.96	---	---
Total C	25.60	24.90	24.40	22.80	25.50	24.30	22.15	---	25.00	---

20794 1474

TABLE B.5. Solution Chemistry for the HBR/HD-85 (C5B-B) Test (0.4 μm filtered)

	Cycle 1 (μg/mL)				Cycle 2 (μg/mL)				Cycle 3 (μg/mL)	
Species	Starting J-13 Water	33 Days	147 Days	174 Days	Starting J-13 Water	14 Days	34 Days	181 Days	Starting J-13 Water	97 Days
pH	8.00	8.20	8.00	8.17	7.74	8.12	8.05	8.23	8.12	8.75
Al	<0.075	0.085	<0.075	<0.075	<0.075	<0.075	<0.075	<0.08	<0.08	0.890
B	0.288	0.057	0.125	0.140	0.160	0.172	0.150	0.140	0.200	0.150
Ca	15.04	4.63	2.00	1.60	14.00	7.17	3.40	3.05	13.30	11.60
Cr	---	---	0.100	0.140	0.015	0.016	0.030	0.160	<0.01	0.140
Fe	<0.01	0.03	<0.01	<0.01	<0.10	<0.01	<0.01	<0.01	<0.01	<0.01
K	3.66	8.91	7.44	7.20	4.20	3.89	8.50	6.64	6.64	11.64
Mg	2.83	0.78	0.24	0.27	2.00	1.06	0.41	0.23	2.17	0.76
Mo	0.041	0.021	0.028	0.082	0.200	0.032	0.033	0.050	0.040	0.050
Na	41.52	43.22	47.56	48.00	47.00	46.54	47.00	48.50	48.20	99.20
Nd	<0.15	<0.15	<0.15	<0.15	<0.15	<0.15	<0.15	<3.0	<3.0	<3.0
Ni	---	---	<0.02	<0.02	0.041	<0.020	0.027	0.020	0.050	0.070
Pd	<0.12	<0.12	<0.12	<0.12	<0.12	<0.12	<0.12	<2.4	<2.4	<2.4
Ru	<0.12	<0.12	<0.12	<0.12	<0.12	<0.12	<0.12	<2.4	<2.4	<2.4
Si	37.78	12.20	6.92	5.80	31.00	23.42	10.00	6.99	32.60	18.50
Sr	0.046	0.016	0.008	0.010	0.047	0.032	0.017	0.010	0.040	0.060
Zr	<0.010	<0.010	<0.010	0.010	0.011	<0.010	<0.010	<0.01	<0.01	0.160
Cl	7.00	7.04	7.50	6.72	6.50	6.90	6.70	7.96	7.09	7.55
F	2.10	1.78	2.00	1.92	1.30	2.30	1.95	2.40	2.30	2.21
PO_4	---	1.10	---	---	---	---	---	---	---	0.46
NO_3	7.90	2.59	2.60	2.95	7.70	1.40	0.87	3.16	7.64	3.64
SO_4	18.00	32.70	24.80	28.10	15.80	25.10	26.20	26.50	17.20	20.50
HCO_3	125.6	82.3	75.2	72.7	122.5	92.5	82.6	75.2	123.0	96.6
Inorg C	24.70	16.20	14.80	14.30	24.10	18.20	16.25	14.80	24.20	19.00
Org C	---	---	3.70	---	---	---	---	2.30	---	---
Total C	25.60	20.90	18.50	17.60	25.50	22.00	18.50	---	25.00	---

90794 1475

TABLE B.6. Solution Chemistry for the HBR/UD-85 (C5B-A) Test (0.4 μm filtered)

	Cycle 1 (μg/mL)				Cycle 2 (μg/mL)				Cycle 3 (μg/mL)	
Species	Starting J-13 Water	33 Days	147 Days	174 Days	Starting J-13 Water	14 Days	34 Days	181 Days	Starting J-13 Water	97 Days
pH	8.00	8.22	8.36	8.51	7.74	8.05	7.93	7.46	8.12	8.29
Al	<0.075	0.123	<0.075	0.130	<0.075	<0.075	<0.075	<0.08	<0.08	0.860
B	0.288	0.053	0.145	0.140	0.160	0.189	0.170	0.150	0.200	0.180
Ca	15.04	7.07	2.44	4.10	14.00	8.04	8.30	1.19	13.30	15.50
Cr	---	---	0.060	0.110	0.015	0.023	0.026	0.050	<0.01	0.030
Fe	<0.01	<0.01	<0.01	<0.01	<0.10	0.01	0.04	0.03	<0.01	<0.01
K	3.66	5.49	8.11	5.90	4.20	1.22	4.50	5.45	6.64	11.90
Mg	2.83	1.28	0.28	0.48	2.00	1.28	1.10	0.22	2.17	1.87
Mo	0.041	0.025	0.037	0.180	0.200	0.074	0.073	0.030	0.040	0.040
Na	41.52	40.12	48.37	45.00	47.00	47.51	46.00	12.60	48.20	101.00
Nd	<0.15	<0.15	<0.15	<0.15	<0.15	<0.15	<0.15	<3.0	<3.0	<3.0
Ni	---	---	<0.02	<0.02	0.041	0.021	0.044	0.040	0.050	0.050
Pd	<0.12	<0.12	<0.12	<0.12	<0.12	<0.12	<0.12	<2.4	<2.4	<2.4
Ru	<0.12	<0.12	<0.12	<0.12	<0.12	<0.12	<0.12	<2.4	<2.4	<2.4
Si	37.78	23.01	8.69	8.00	31.00	24.21	20.00	2.52	32.60	39.30
Sr	0.046	0.030	0.009	0.015	0.047	0.038	0.036	<0.01	0.040	0.100
Zr	<0.010	<0.010	<0.010	0.010	0.011	0.014	0.017	<0.01	<0.01	0.160
Cl	7.00	7.51	7.40	6.72	6.50	6.30	6.70	5.90	7.09	7.82
F	2.10	2.22	1.90	1.98	1.30	2.20	2.18	0.57	2.30	2.71
PO_4	---	1.40	---	---	---	---	---	---	---	---
NO_3	7.90	5.65	2.80	2.41	7.70	2.00	1.30	1.87	7.64	2.82
SO_4	18.00	76.90	25.60	27.50	15.80	22.80	24.10	5.50	17.20	21.20
HCO_3	125.6	88.4	73.7	79.8	122.5	101.7	103.2	20.9	123.0	124.4
Inorg C	24.70	17.40	14.50	15.70	24.10	20.00	20.30	4.12	24.20	24.40
Org C	---	---	3.40	---	---	---	---	1.90	---	---
Total C	25.60	23.50	17.90	19.00	25.50	22.20	23.30	6.02	25.00	---

90794 14476

APPENDIX C

X-RAY DIFFRACTION INDEXING DATA

90794 1477

TABLE C.1. Indexing for HBR/BF-85 Cycle 2 Rinse Filter XRD Pattern

Sample Pattern			Matched Line			
Deg. 2θ	d (Å)	I %	d (Å)	I %	Phase	JCPDS No.
5.49	16.090	55.9				
9.51	9.296	1.1	9.30	100	H	13-118
11.22	7.881	25.7	7.88	100	UP	8-442
11.92	7.418	1.8				
12.31	7.184	2.3				
13.43	6.586	14.8	6.61	40	UP	8-442
16.35	5.417	4.8	5.42	40	UP	8-442
18.52	4.786	2.9	4.76	50	UP	8-442
22.55	3.940	12.6	3.94	90	UP	8-442
24.74	3.596	4.6	3.60	40	UP	8-442
25.49	3.491	1.7	3.51	40	UP	8-442
26.91	3.310	1.0				
28.27	3.154	100.0	3.154	100	U	5-550
29.88	2.988	6.6	2.99	80	UP	8-442
30.69	2.911	4.9	2.91	80	UP	8-442
32.75	2.732	19.5	2.735	48	U	5-550
34.03	2.632	5.0	2.63	50	UP	8-442
35.02	2.560	2.2	2.57	20	UP	8-442
37.31	2.408	0.3	2.40	10	UP	8-442
40.97	2.201	6.2	2.20	40	UP	8-442
43.04	2.100	1.3	2.10	50	UP	8-442
44.03	2.055	2.2	2.06	20	UP	8-442
45.91	1.975	2.1	1.969	70	UP	8-442
46.28	1.960	2.3				
46.94	1.934	27.5	1.934	49	U	5-550
48.68	1.869	0.7				
51.56	1.771	0.8				
55.62	1.651	20.9	1.649	47	U	5-550
58.35	1.580	9.3	1.579	13	U	5-550
60.15	1.537	0.5				
68.53	1.368	2.5	1.368	9	U	5-550
75.65	1.256	7.2	1.255	18	U	5-550
78.00	1.224	4.9	1.223	15	U	5-550

U = UO_2
UP = uranophane
H = haiweeite

90794 1478

TABLE C.2. Indexing for TP/BF-85 Cycle 1 Rinse Filter XRD Pattern

Sample Pattern			Matched Line			
Deg. 2θ	d (Å)	I %	d (Å)	I %	Phase	JCPDS No.
5.49	16.082	5.9				
9.46	9.346	27.5	9.30	100	H	13-118
25.53	3.357	19.5	3.34	30	H	13-118
25.53	3.357	19.5	3.34	80	S	26-1392
28.20	3.162	100.0	3.154	100	U	5-550
28.58	3.121	22.0	3.04	30	H	13-118
28.58	3.121	22.0	3.035	100	C	5-586
32.67	2.738	13.2	2.735	48	U	5-550
46.83	1.938	17.5	1.934	49	U	5-550
55.61	1.651	12.6	1.649	47	U	5-550
57.03	1.613	3.1				
62.18	1.492	2.7				
64.83	1.437	4.3				
65.37	1.426	3.8				
73.64	1.285	5.0	1.255	18	U	5-550
75.59	1.257	8.9	1.223	15	U	5-550

U = UO_2
H = hatweeite
S = soddyite
C = calcite

90794 1479

TABLE C.2. Indexing for TP/BF-85 Cycle 1 Rinse Filter XRD Pattern

Sample Pattern			Matched Line			
Deg. 2θ	d (Å)	I %	d (Å)	I %	Phase	JCPDS No.
5.49	16.097	1.1				
9.47	9.327	6.0	9.30	100	H	13-118
11.88	7.910	2.7	7.88	100	UP	8-442
13.37	6.619	1.7	6.61	40	UP	8-442
28.18	3.164	100.0	3.154	100	U	5-550
28.63	3.115	11.8	3.09	10	UP	8-442
29.78	2.998	1.8	2.99	80	UP	8-442
32.67	2.738	12.0	2.375	48	U	5-550
46.87	1.937	22.0	1.934	49	U	5-550
48.63	1.871	1.1	1.867	30	UP	8-442
55.59	1.652	17.2	1.649	47	U	5-550
58.32	1.581	9.2	1.579	13	U	5-550
59.79	1.546	0.2				
68.44	1.370	2.4	1.37	9	U	5-550
70.44	1.336	1.5				
75.58	1.257	7.3	1.255	18	U	5-550
77.91	1.225	4.2	1.223	15	U	5-550

U = UO_2
UP = uranophane
H = haiweeite
C = calcite

90794 1480

APPENDIX D

PROCEDURES

90794 1481

APPENDIX D

PROCEDURES

Cycle 1 of the Series 3 tests was started February 19, 1986, and Cycle 3 was terminated May 18, 1987. Chemical analyses of Cycle 3 terminal samples were completed by September 1987. Principal procedure revisions used in the Series 3 tests that were in effect during this time are identified in this appendix. Principal radiochemical procedures are also summarized in this appendix. Other identified procedures are summarized in the report text or relate to operation of commercial analytical instruments for which manuals apply. Many of the procedures were revised in format only for a September 1986 compilation of WHC procedures in support of geological repositories. For these procedures, the revision containing only format changes is omitted from the following procedure listings. A record of revised pages is contained in each procedure. Copies of the following identified procedure revisions are included in the Series 3 tests data package.

D.1 SPECIMEN PREPARATION

At the time the Series 3 specimens were prepared, instructions were provided by memoranda. The instructional memorandum for the Series 3 specimen preparation was approved under Engineering Data Transmittal EDT A-12109.

Reference Memorandum, C. N. Wilson to J. M. Lott, Subject: "Preparation of NNWSI Series 3 Spent Fuel Leach Tests Specimens," dated July 31, 1985. (Formally transmitted by EDT A-12109, approved August 5, 1985.)

D.2 CYCLE START

- SFL-3-5, Rev 0, "NNWSI Series 3 Spent Fuel Leaching/Dissolution Tests: Cycle Start."

90794 1482

D.3 CYCLE TERMINATION

- SFL-3-6, Rev 0, "NNWSI Series 3 Spent Fuel Leaching/Dissolution Tests: Cycle-Termination."

D.4 SOLUTION SAMPLING

- SFL-3-7, Rev 0, "NNWSI Series 3 Spent Fuel Leaching/Dissolution Tests: Solution Sampling."

D.5 URANIUM

- HTA-4-16, Revs 0 and 2, "Solutions Analysis: Uranium by Laser-Excited Fluorescence."

Uranium is determined using a Scintrex[a] Model UA-3 uranium analyzer. Diluted aqueous solutions containing a buffered complexing reagent are excited by a UV-emitting nitrogen pulsed laser, and the green uranium fluorescence emitted from the solution is measured. An increase in signal from the addition of a known uranium-containing standard solution to the diluted test solution is used to calculate uranium concentration. The method gives reproducible results for sample uranium concentrations down to 1 ppb.

D.6 RADIOCHEMICAL SOURCE PREPARATION AND COUNTING

- HTA-4-22, Rev 2, "Solutions Analysis: Preparation of Alpha Sources by Direct Evaporation."
- HTA-4-23, Rev 2, "Solutions Analysis: Preparation of Beta Sources by Direct Evaporation."
- HTA-4-4, Rev 3, "Solutions Analysis: Liquid Scintillation."
- HTA-4-5, Rev 3, "Solutions Analysis: Alpha Spectrometry."
- HTA-4-6, Rev 3, "Solutions Analysis: Alpha Counting."
- HTA-4-8, Rev 3, "Solutions Analysis: Beta Counting."
- HTA-4-9, Rev 3, "Solutions Analysis: Gamma Spectrometry."

(a) Scintrex Ltd, Concord, Ontario, Canada.

9 0 7 9 4 1 4 8 3

D.7 $^{239+240}Pu$ AND ^{244}Cm

These radionuclides were counted on source disks prepared from unseparated solution aliquots using the following procedures. An accurately measured quantity (i.e., 100 to 500 μL $\pm$ 1 μL) of solution was evaporated onto a stainless steel source disk (HTA-4-22) which was then counted for total alpha activity (HTA-4-6) and analyzed by alpha energy spectrometry (HTA-4-5). The alpha spectrometry results were used to calculate the portions of the total alpha counts originating from each alpha energy peak. Three significant alpha spectrometry peaks generally resulted: $^{239+240}Pu$, ^{238}Pu + ^{241}Am, and ^{244}Cm. Results for all three alpha activities were reported.

D.8 ^{241}Am

- HTA-4-13, Revs 2 and 4, "Separation of Americium-241 and Curium-244 by Anion Exchange Prior to Measurement by Alpha Counting."

Since ^{241}Am and ^{238}Pu have similar alpha decay energies, a separation is required for ^{241}Am analysis (HTA-4-13). A 500-mL solution sample is reacted with 200 μL of 5 M hydroxylamine hydrochloride and 100 mL of 8 M HNO_3 and is passed through an anion exchange resin. The plutonium is loaded onto the resin while the americium passes through the resin. The ^{241}Am is then measured by alpha counting (HTA-4-6) and alpha spectrometry (HTA-4-5) after being evaporated onto a stainless steel source disk (HTA-4-22) that has been heated to dull red by flame from the bottom side to burn off organic and volatile residues.

D.9 ^{237}Np

- HTA-4-14, Revs 2 and 4, "Separation of Neptunium by Cation Exchange and Solvent Extraction Prior to Measurement by Alpha Counting."

Since ^{247}Np activity in the spent fuel tested is much lower than other alpha-emitting isotopes and is interfered with by ^{234}U alpha decay, a separation is required. Neptunium is separated by cation exchange of NpO_2^+ followed by solvent extraction of Np^{+4} into thenoyltrifluoracetone in xylene. The ^{237}Np activity is then evaporated onto a stainless steel source (HTA-4-22)

90794 1484

disk that is heated to "a high heat" on a hot plate to burn off organic residues. The ^{237}Np is counted using alpha counting (HTA-4-6) and alpha spectrometry (HTA-4-5).

D.10 ^{137}Cs, ^{134}Cs, AND ^{60}Co

^{137}Cs and ^{134}Cs were measured in nearly all samples by gamma spectrometry (HTA-4-9). ^{60}Co was also measured in many samples by gamma spectrometry. Quantitative gamma counting data were calculated from gamma energy peaks based on daily measurement of control standards of ^{241}Am, ^{137}Cs, and ^{60}Co mixtures run under the same geometry as the test samples.

D.11 ^{99}Tc

- HTA-4-12, Revs 1 and 3, "Separation of Technetium by Cation Exchange and Solution Extraction Prior to Measurement by Beta Counting."

Since ^{99}Tc decays solely by beta decay, spectrometry methods are not applicable and the ^{99}Tc must be separated from other beta emitters to be counted. The technetium is oxidized to TcO_4^- with sodium dichromate and separated from most other radioactive species that adsorb onto a cation exchange resin. Technetium is then extracted from the cation exchange effluent into hexone as tetraphenylarsonium pertechnate. A measured portion of the hexone is evaporated onto a stainless steel source disc under a heat lamp. The ^{99}Tc activity is then counted using a gas flow beta proportional counter.

D.12 ^{90}Sr

- HTA-4-11, Revs 1 and 3, "Separation of Strontium-90 by Cation Exchange Prior to Measurement by Beta Counting."

Since ^{90}Sr is a beta emitter, separation is required. The ^{90}Sr is separated from other radioactive species by selective elution from a cation exchange resin using 2-methyllactic acid. Following separation, the growth of ^{90}Y is measured by beta counting. The ^{90}Sr is then calculated, based on the growth of the ^{90}Y daughter over a measured period of time. The technique of Roberts (1961) is used.[D1]

9 0 7 9 4 1 4 8 5

D.13 ^{126}Sn

- HTA-4-21, Revs 0 and 2, "Separation of Tin-126 by Anion Exchange Prior to Measurement by Gamma Counting."

The test solution is mixed with bromine-saturated 2 M HCl and passed through a cation exchange resin to remove essentially all cations. Tin is then loaded onto an anion exchange resin and is washed free of other anions with dilute hydrochloric acid. Tin is eluted with dilute nitric acid and tin-126 is measured using a GeLi well gamma spectrometer (see GeLi well portion of Procedure HTA-4-9).

D.14 ^{14}C

- HTA-4-17, Revs 0 and 2, "Solutions Analysis: Carbon-14 by Distillation Separation Prior to Measurement by Liquid Scintillation Counting."

Carbon-14 is separated from other radioactive species by distillation of carbon dioxide from an acidic oxidizing solution. The carrier gas (air) is passed through Ascarite II[a] to remove carbon dioxide. The distilled ^{14}C dioxide is trapped in a liquid scintillation cocktail made basic with sodium hydroxide. The ^{14}C activity is then measured by the liquid scintillation Procedure HTA-4-4.

D.15 ^{129}I

Because of its low concentration and long half-life (17,000,000 yr), ^{129}I activity in spent fuel leach solutions is generally too low to detect by direct counting methods after separation. Therefore, a neutron activation analysis (NAA) procedure (performed by PNL) is used for ^{129}I. The ^{129}I analyses were performed by Robert Strebin of PNL, and a WHC technical procedure was not written for these analyses. The methods used are summarized below.

(a) Ascarite II is a registered trademark of Arthur H. Thomas Co., Philadelphia, Pennsylvania.

9 0 7 9 4 1 4 8 6

A measured volume of test solution and a "spike" solution containing ^{125}I are absorbed into quartz wool in a gas phase separation column. The sample is evaporated from the quartz wool by flaming the outside of the column while flowing air through the column. The oxidized iodine vapor species are trapped by absorption onto activated charcoal. The column is then evacuated, the charcoal trap valved off from the vacuum, and the charcoal trap is heated, reducing the iodine to I_2. The I_2 vaporizes from the heated charcoal trap and is condensed in a liquid N_2 cold trap. The column is sealed off above the liquid N_2 cold trap creating a glass ampoule containing the separated I_2. The ampoules are then activated by neutron irradiation in a nuclear reactor (Hanford N Reactor for Cycles 1 and 2; Washington State University Reactor for Cycle 3 samples). The irradiated ampoules are then broken in CCl_4, in which I_2 is soluble. ^{126}I and ^{130}I decay are then counted by gamma spectrometry over several ^{130}I half-lives (12.4 hours), and the original preirradiation ^{129}I is calculated.

D.16 OTHER SOLUTIONS ANALYSES

- HTA-4-1, Revs 1 and 3, "Solutions Analysis: Cations by ICP Spectrometry."
- ICP spectrometry was performed using an ARL[a] model 3510 sequential ICP spectrometer.
- HTA-4-2, Revs 1 and 3, "Solutions Analysis: Anions by Ion Chromatography."
- Ion chromatography was performed using a Dionex[b] Model 2110i ion chromatograph.
- HTA-4-3, Revs 1 and 3, "Solutions Analysis: Carbon."

Inorganic, organic, and total carbon measurements were made using a Dohrman[c] DC80 total organic carbon analyzer. Inorganic carbon was of primary interest since it was used to calculate the bicarbonate values reported.

(a) ARL Co., Sunland, California.
(b) Dionex Corporation, Sunnyvale, California.
(c) XERTEX-Dohrman, Santa Clara, California.

9 0 7 9 4 1 4 8 7

D.17 SOLIDS CHARACTERIZATION

- HTA-3-1, Rev 3, "Solids Analysis: Scanning Electron Microscopy."
- HTA-3-3, Rev 2, "Solids Analysis: X-Ray Diffraction Analysis."

D.18 BURNUP AND RADIONUCLIDE INVENTORY

Burnup and ^{244}Cm, ^{241}Am, $^{239+240}Pu$, ^{237}Np, ^{137}Cs, ^{99}Tc, and ^{14}C inventories were measured on H fuel samples. Carbon-14 was also measured on H. B. Robinson cladding samples. The fuel sample was dissolved and inventories for ^{244}Cm, ^{241}Am, $^{239+240}Pu$, ^{137}Cs, and ^{99}Tc measured on the resulting solution using the applicable procedures given above. Special procedures listed below were used for ^{237}Np and ^{14}C in the fuel and cladding. The addition procedures used were:

- HTA-4-24, Rev 0, "Samples Preparation: Dissolution of LWR Fuel Samples."
- HTA-4-25, Rev 1, "Burnup Analysis: Neodymium-148 Method."
- HTA-4-26, Rev 1, "Sample Preparation: LWR Fuel Solutions."
- HTA-4-27, Rev 1, "Measurement of Neptunium-237 in Dissolved Fuel Solutions."
- HTA-4-28, Rev 1, "Measurement of Carbon-14 in Irradiated UO_2 Fuel."
- HTA-4-30, Rev 1, "Measurement of Carbon-14 in Zircaloy Cladding."

D.19 REFERENCE

D1. F. P. Roberts. 1961. The Determination of Radiostrontium by Ion Exchange, HW-69511, General Electric, Richland, Washington.

90794 1488

APPENDIX E

SURFACE AREA

90794 14489

9079 4 1490

APPENDIX E

SURFACE AREA

Geometric surface areas were estimated for the H. B. Robinson ATM-101 and Turkey Point fuels by determining the distribution of particle weights in the HBR/BF-25 (C5C-I) and TP/BF-85 (F6-2B) fuel specimens and assuming a uniform particle shape. The specimens were spread out on one gallon "ice cream" carton lids and stirred to obtain a uniform distribution of particle sizes across the carton lid surface. Photographs of the specimens on the carton lids with cm scale labels are shown in Figure E.1. Particles were knifed to the sides of the carton lids leaving a center strip of particles approximately 3 cm wide across the carton lid undisturbed. All of the particles remaining in the center strip were weighed to obtain a representative distribution of the particle weights in each of the two archival fuel specimens. The particle weights measured for the C5C-I and F6-2B specimens are tabulated in Tables E.1 and E.2.

Most of particles in the spent fuel specimens exhibited near-equiaxed dimensions with the most common particle shape appearing to be a wedge. A right-angle wedge with dimensions L x L x hL shown in Figure E.2 was assumed to represent the average particle shape for the purpose of calculating geometric surface areas. Geometric surface area of such a regular shape is proportional to the particle weight raised to the 2/3 power (Equation E.1).

$$\text{Area} = k \times \text{Weight}^{2/3} \qquad \text{(E.1)}$$

Surface areas were calculated for each particle using equation E.1 and three different values for the constant k. Values used for the constant k (1.683, 1.576 and 1.501 cm^2/g) assumed proportional wedge height values (h in Figure E.2) of 0.5, 0.67 and 1.0, respectively, and particle density of 10.083 g/cm^3 (92% of theoretical). Average geometric surface areas were calculated by dividing the sum of the particle areas by the sum of the particle weights. The resulting calculated geometric surface areas are given in Table E.3. The

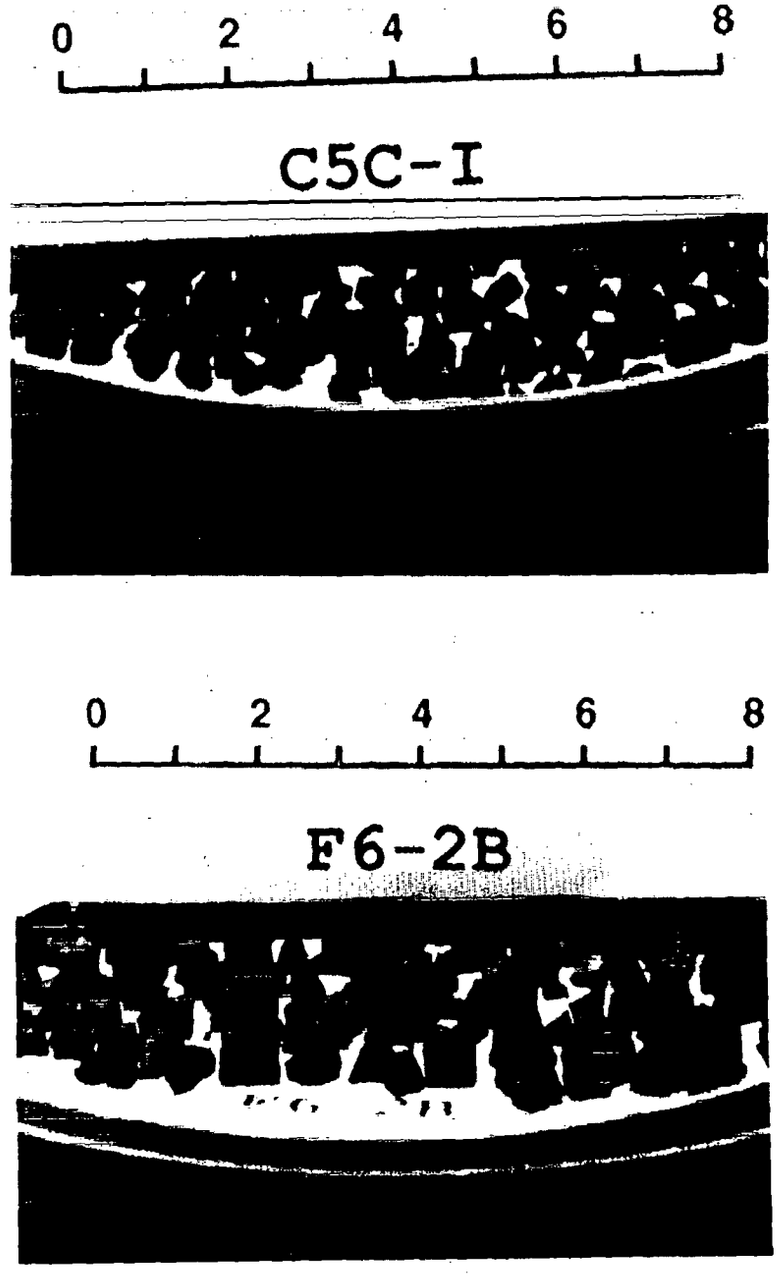

FIGURE E.1. HBR (C5C-I) and TP (F6-2B) Spent Fuel Specimens (scale shown is in cm)

90794 1491

TABLE E.1. C5C-I Particle Weights (g)

Weight	Weight	Weight
0.4842	0.1476	0.0101
0.4140	0.5181	0.0105
0.0224	0.1631	0.0054
0.0465	0.3161	0.0090
0.3672	0.5420	0.0032
0.2415	0.2185	0.0012
0.2865	0.3311	0.0720
0.1542	0.1834	0.4142
0.0734	0.3420	0.6736
0.1130	0.0065	0.1440
0.2364	0.0008	0.2796
0.2548	0.4427	0.1901
0.0282	0.5780	0.1154
0.2080	0.1746	0.1388
0.2973	0.3857	0.4811
0.1660	0.2400	0.0976
0.0822	0.5781	0.3102
0.1102	0.1229	0.1802
0.1259	0.2100	0.1388
0.1758	0.2414	0.2313
0.4329	0.1872	0.2973
0.1497	0.0156	0.6713
0.0201	0.4006	0.2884
0.1745	0.4942	0.1703
0.2151	0.1732	0.1547
0.3849	0.3538	0.1452
0.5674	0.3314	0.2297
0.0040	0.4207	0.1637
0.0034	0.2615	0.1389
0.0024	0.3501	0.0987
0.0042	0.1253	0.0491
0.0069	0.4066	0.0034
0.2457	0.1779	0.0011
0.0151	0.5985	0.0022
0.0018	0.1643	0.0020
0.1629	0.0165	

9 0 7 9 4 1 4 9 2

TABLE E.2. F6-2B Particle Weights (g)

Weight	Weight	Weight
0.8413	0.0843	0.3286
0.6579	0.3745	0.3127
1.2066	0.1901	0.0507
0.8870	0.3419	0.0262
0.5222	0.1571	0.0398
0.3863	0.5609	0.0239
0.3216	0.3059	0.0220
0.4485	0.3725	0.0795
0.3177	0.2810	0.0228
0.6688	0.2190	0.0113
0.3591	0.2394	0.0110
0.2388	0.1146	0.0134
0.2415	0.3512	0.0200
0.1938	0.3703	0.0090
0.1901	0.4720	0.0087
0.3863	0.2988	0.0072
0.4199	0.2417	0.0112
0.4871	0.4535	0.0153
0.2564	0.5624	0.0048
0.2160	0.2204	0.0051
0.6069	0.1728	0.0077
0.3150	0.6309	0.0045
0.3630	0.4941	0.0050
0.2422	0.4951	0.0138
0.1648	0.2985	0.0040
0.0765	0.2668	0.0034
0.4626	0.4342	0.0011
0.1591	0.2198	0.0027
0.1583	0.2732	0.0145
0.2471	0.2340	

90794 1493

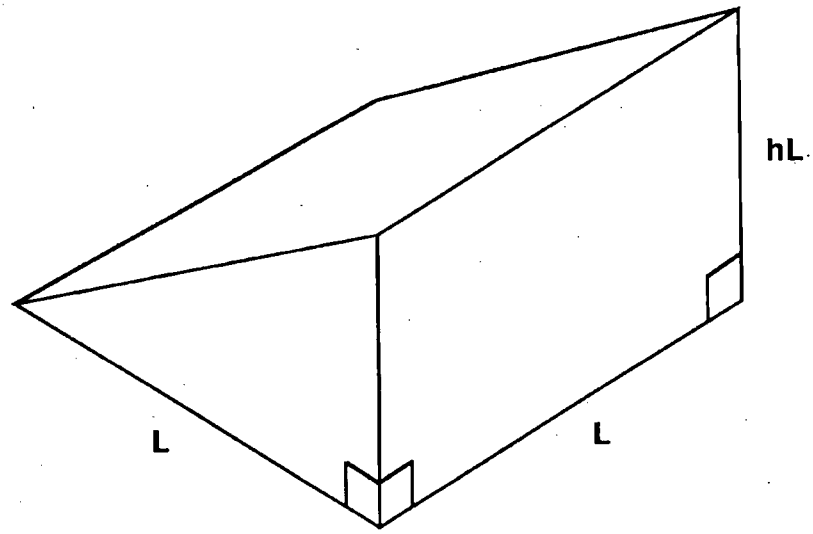

FIGURE E.2. Right-Angle Wedge Shape (L x L x hL) Assumed for Calculation of Spent Fuel Particle Geometric Surface Areas

TABLE E.3. Calculated Geometric Surface Areas (cm^2/g) Assuming L x L x hL Wedge-Shape Particles

Fuel	h = 0.50	h = 0.67	h = 1.00
HBR	2.57	2.40	2.29
TP	2.37	2.21	2.11

HBR fuel had a slightly smaller average particle size resulting in a slightly greater geometric surface area in comparison to the TP fuel. Geometric surface areas for the test specimens may be estimated by multiplying the values given in Table E.3 times the specimen weights given in Table 2.1 of the main text.

Due to the effects grain boundaries and other porosity, the actual effective specimen surface areas needed to calculate surface area normalized dissolution rates that are independent of particle size and morphology, would likely be greater than the geometric surface areas tabulated in Table E.3. However, based on currently available data, estimates of actual effective wettable surface area of the test specimens would be speculative. If one were to assume cube-shaped grains, and that grain surfaces perpendicular to the

90794 1494

particle exterior surface are exposed to a depth of one grain as a result of initial grain boundary dissolution, the exposed surface area would be five times the geometric surface area. However, the slow kinetics of diffusing species into and out of grain boundaries probably results in much lower dissolution rates along grain boundaries than from external particle surfaces. The observation that ^{99}Tc and ^{137}Cs dissolution rates did not significantly increase during test cycles suggests that increasing effective surface area as a result of progressive grain boundary dissolution was not an important factor during the Series 3 tests. The surface area added by the approximate 10 mg of fuel grains estimated to have been released from the fuel particles as a result of grain boundary dissolution during the test cycles (and collected on specimen rinse filters) would increase the specimen geometric surface areas by only a few percent.

The implications of potential increases in surface area as a result of fuel degradation are quite significant. For the purpose of establishing an upper bound for the potential rate of fuel dissolution, one could assume that the fuel is degraded to individual grains, all of which are exposed to water. Assuming that a matrix dissolution rate of about 5×10^{-4} per year occurred in the 85°C Series 3 tests, and that an average 4 mm particle size in the test specimens is degraded to 6 μm grains with similar shape (a 667 fold increase in geometric surface area), the implied fractional dissolution rate for the grains would be about 0.33 per year.

9079414 95

DISTRIBUTION

No. of Copies

OFFSITE

12 DOE/Office of Scientific and Technical Information

10 DOE Office of Civilian Radioactive Waste Management
Forrestal Building
Washington, DC 20585
ATTN: S. Rousso, RW-1
D. H. Alexander, RW-332
A. Berusch, RW-222
J. C. Bresee, RW-10
S. J. Brocoum, RW-221
T. H. Isaacs, RW-40
J. Hale, RW-222
G. Parker, RW-333
F. G. Peters, RW-10
R. Stein, RW-30

22 DOE Nevada Operations Office
Yucca Mountain Project Office
P.O. Box 98518
Las Vegas, NV 89193-8518
ATTN: C. P. Gertz, MS-523 (5)
T. H. Beall (12)
M. Blanchard
M. Cloninger
P. K. Fitzsimmons
L. Little
C. L. West

D. J. Bales
DOE/Office of Scientific and Technical Information
Science and Technology Division
P.O. Box 62
Oak Ridge, TN 37831

2 DOE Chicago Operations Office
9800 South Cass Avenue
Argonne, IL 60439
ATTN: M. Ferrigan
S. Mann

No. of Copies

2 Argonne National Laboratory
Chemical Technology Division
9700 S. Cass Avenue, Bldg. 205
Argonne, IL 60439
ATTN: J. Bates
E. Veleckis

B. Chin
Department of Mechanical Engineering
Auburn Univerity
Auburn, AL 36849

OWNI Library
Battelle Columbus Laboratory
505 King Avenue
Columbus, OH 43201

D. Schweitzer
Brookhaven National Laboratory
Associated Universities, Inc.
Upton, NY 11973

Comprehensive Planning Dept
Clark County
225 Bridger Avenue, 7th Floor
Las Vegas, NV 89155

J. Fordham
Water Resources Center
Desert Research Institute
P.O. Box 60220
Reno, NV 89506

C. M. Case
Desert Research Institute
7010 Dandini Blvd.
Reno, NV 89512

9 0 7 9 4 1 4 9 6

No. of
Copies

M. Mifflin
Water Resources Center
Desert Research Institute
2505 Chandler Avenue, Suite 1
Las Vegas, NV 89120

E. Ezra
YMP GIS Project
EG&G Energy Measurements, Inc.
P.O. Box 1912, MS H-02
Las Vegas, NV 89125

R. L. Bullock
Fenix & Scisson, Inc.
101 Cenvention Center Drive,
Suite P250, MS-403
Las Vegas, NV 89109

J. C. Calovini
Holmes & Narver, Inc.
101 Convention Center Drive,
Suite 860
Las Vegas, NV 89109

2 Lawrence Berkeley Laboratory
Berkeley, CA 94720
ATTN: E. P. Binnall,
Bldg 50B/4235
H. Nitsche, MS 70A-1115

42 Lawrence Livermore National
Laboratory
P.O. Box 808
Livermore, CA 94550
ATTN: R. Aines, L-219
L. Ballou, L-206
W. Bourcier, L-219
S. Bradley, L-204
C. Bruton, L-219
W. Clarke, L-202
J. Delany, L-219
W. Glassley, L-204

No. of
Copies

ATTN: K. Jackson, L-219
L. Jardine, L-204
D. Kiraly, L-204 (3)
K. Knauss, L-202
H. Lieder, L-325
W. Lin, L-201
W. McKenzie, L-209
W. O'Connell, L-195
S. Nguyen, L-396
V. Oversby, L-310
C. Poppe, L-47
M. Revelli, L-206
H. Shaw, L-204
R. Silva, L-396
R. Stout, L-201
M. ten Brink, L-202
R. Van Konynenburg,
L-370
B. Viani, L-219
H. Weed, L-201
T. Wolery, L-219
L. Younker, L-208
J. Yow, L-206
NWM Library, L-204 (10)

4 R. J. Herbst
Los Alamos National Laboratory
P.O. Box 1663, N-5, MS J-521
Los Alamos, NM 87545

H. N. Kalia
Los Alamos National Laboratory
101 Convention Center Drive,
Suite P230, MS-527
Las Vegas, NV 89109

R. E. Lowder
MAC Technical Services
101 Convention Center Drive
Suite P113
Las Vegas, NV 89109

9 0 7 9 4 1 4 9 7

No. of
Copies

E. Anderson
Mountain West Research-
Southwest, Inc.
432 North 44th Street
Suite 400
Phoenix, AZ 85008

3 National Institute of
Standards and Technology
Division 450
Gaithersburg, MD 20899
ATTN: J. Harris,
Bldg 223/Rm B-254
C. Interrante,
Bldg 223/Rm A-245
J. Ruspi,
Bldg 223/Rm B-254

Planning Department
Nye County
P.O. Box 153
Tonopah, NV 89049

D. Roy
Materials Research Laboratory
Pennsylvania State University
University Park, PA 16802

R. F. Pritchett
Reynolds Electrical and
Engineering Co., Inc.
P.O. Box 98521, MS-615
Las Vegas, NV 89193-8521

2 Roy F. Weston, Inc.
955 L'Enfant Plaza SW
Suite 800
Washington, DC 20024
ATTN: E. Benz
Technical Information
Center

No. of
Copies

7 Sandia National Laboratories
P.O. Box 5800
Albuquerque, NM 87185
ATTN: T. O. Hunter,
Org 6310 (5)
R. W. Lynch, Org 6300
S. Sinnock

2 Savannah River Laboratory
Aiken, SC 29808
ATTN: B. G. Kitchen,
Bldg 773-41A
J. Plodinec,
Bldg 773-A, Rm B-120

5 Science Applications
International Corporation
101 Convention Center Drive
Suite 407
Las Vegas, NV 89109
ATTN: J. H. Nelson
R. Morissette
D. Stahl
SAIC-T&MSS Library (2)

2 Southwest Research Institute
6220 Culebra Road
P.O. Drawer 28510
San Antonio, TX 78228
ATTN: H. K. Manaktala
P. K. Nair

T. Hay
Office of the Governor
State of Nevada
Capitol Complex
Carson City, NV 89710

9 0 7 9 4 1 4 9 8

No. of
Copies

4 State of Nevada
Nuclear Waste Project Office
Evergreen Center, Suite 252
1802 N. Carson Street
Carson City, NV 89701
ATTN: C. H. Johnson
R. R. Loux Jr. (3)

R. Moler
Systems Support Inc.
P.O. Box 1432
Manassas, VA 22110

T. H. Pigford
Department of Nuclear Engineering
University of California
Berkeley, CA 94720

L. Statler
202 Nuclear Science Center
University of Florida
Gainsville, FL 32611

C. G. Bell, Jr.
Civil and Mechanical Engineering Department
University of Nevada, Las Vegas
4505 South Maryland Parkway
Las Vegas, NV 89154

R. E. Ewing
Univesity of New Mexico
Department of Geology
Albuquerque, NM 87131

C. F. Costa
Nuclear Radiation Assessment Division
U.S. Environmental Protection Agency
Environmental Monitoring Systems Laboratory
P.O. Box 93478
Las Vegas, NV 89193-3478

No. of
Copies

8 U.S. Geological Survey
P.O. Box 25046
421 Federal Center
Denver, CO 80225
ATTN: K. W. Causseaux
L. R. Hayes (6)
R. V. Watkins

V. M. Glanzman
U.S. Geological Survey
P.O. Box 25046
913 Federal Center
Denver, CO 80225

J. F. Divine
U.S. Geological Survey
106 National Center
12201 Sunrise Valley Drive
Reston, VA 22092

5 U.S. Nuclear Regulatory Commission
Division of Waste Management
Washington, DC 20555
ATTN: M. Bell, MS WFI-4-H-3
S. Coplan, MS 4-H-3
NRC Document Control Clerk
Repository Licensing and Quality Assurance, Project Directorate
Senior Project Manager for Yucca Mountain, Repository Project Branch

P. T. Prestholt
U.S. Nuclear Regulatory Commission
1050 East Flamingo Road
Suite 319
Las Vegas, NV 89119

9 0 7 9 4 1 4 9 9

No. of
Copies

J. Pope
Process Technology & Testing
West Valley Nuclear Services
Co, Inc.
P.O. Box 191
West Valley, NY 14171-0191

2 Yale University
210 Kline Geology Lab
New Haven, CT 06511
ATTN: A. Lasaga
K. Turekian

J. Bastin
Nuclear Waste Technology
Westinghouse
P.O. Box 3912
Pittsburgh, PA 15230

FOREIGN

8 Whiteshell
Nuclear Research Establishment
Atomic Energy of Canada Ltd.
Pinawa, Manitoba ROE 1LO,
CANADA
ATTN: C. Davison, FWT Branch
N. Garisto, FWT Branch
L. Johnson, FWT Branch
F. P. Sargent, AECL
D. Shoesmith, RC Branch
S. Stroes-Gascoyne,
FWT Branch
S. Sunder, RC Branch
J. Tait, RC Branch

2 AERE Harwell Laboratory
Materials Development Division
Oxfordshire OX11 ORA
ENGLAND
ATTN: J. E. Bennett, Bldg 393
R. Williamson,
Bldg 338.4

No. of
Copies

K. A. Simpson
Berkeley Nuclear Laboratories
Berkeley, Gloucestershire
GL 13 9PB
ENGLAND

B. Grambow
Kernforschungszentrum
Karlsruhe GmbH
Institut für Nukleare
Entsorgungstechnik (INE)
P.O. Box 3640, D-7500
Karlsruhe 1
FEDERAL REPUBLIC OF GERMANY

R. Guillaumont
Laboratoire de Radiochimie
Institut de Physique Nucleaire
B.P. No 1-91406 Orsay
FRANCE

R. Odoj
Institut für Chemische
Technologie
Der Nuklearen Entsorgung
Kernforschungsanlage
Ict. Postfach 1913
5170 Julich
FEDERAL REPUBLIC OF GERMANY

K. Ollila
Technical Research Centre of
Finland
Reactor Laboratory
Otakaari 3 A, SF-02150
ESPOO 15
FINLAND

J. Bruno
Royal Institute of Technology
Department of Inorganic
Chemistry
S-100 44 Stockholm 70
SWEDEN

9 0 7 9 4 1 5 0 0

No. of
Copies

R. W. Forsyth
Studsvik AB
S-611 82 Nyköping
SWEDEN

L. Werme
Svensk Karnbranslehantering AB
Box 5864
S-10248 Stockholm
SWEDEN

ONSITE

4 DOE/Richland Operations Office

M. J. Lawrence, A7-50
D. C. Langstaff, A5-90
D. H. Dahlen, A5-10
Public Reading Room, A1-65

5 Westinghouse Hanford Co.

H. R. Brager, L5-03
R. L. Knecht, L5-59
M. K. Korenko, H5-59
BWIP Library, H9-16 (2)

55 Pacific Northwest Laboratories

M. J. Apted, K6-88
R. C. Arthur, K6-81
B. O. Barnes, P7-14
C. E. Beyer, P8-10
H. C. Burkholder, P7-41

No. of
Copies

M. E. Cunningham, P8-10
P. G. Doctor, K6-96
R. E. Einziger, P7-14
E. R. Gilbert, P8-34
W. J. Gray, P7-14
R. J. Guenther, P8-10
L. S. Kellogg, P7-20
M. R. Kreiter, K6-35
K. M. Krupka, BWO
W. L. Kuhn, K2-03
J. L. McElroy, P7-46
B. P. McGrail, K2-38
G. B. Mellinger, P7-18
J. E. Mendel, P7-38
Y. Onishi, K6-88
D. Rai, K6-81
R. J. Serne, K6-81
J. W. Shade, K2-38
H. D. Smith, P7-14
D. M. Strachan, K2-44
L. E. Thomas, P8-13
A. E. VanLuik, BWO
J. H. Westsik, P7-44
E. J. Wheelwright, P7-25
C. N. Wilson, P7-14 (20)
Publishing Coordination
Technical Report Files (5)

90794 1501